Elastodynamics with Hysteretic Damping

Elastodynamics with Hysteretic Damping

Proefschrift

ter verkrijging van de graad van doctor
aan de Technische Universiteit Delft
op gezag van de Rector Magnificus prof.dr.ir. J.T. Fokkema,
voorzitter van het College voor Promoties,
in het openbaar te verdedigen op donderdag 13 juni 2002 om 16.00 uur

door Carlos Juán CORNEJO CÓRDOVA

civiel ingenieur
geboren te Lima, Perú

Dit proefschrift is goedgekeurd door de promotor: Prof.dr.ir. A. Verruijt

Samenstelling promotiecommissie:

Rector Magnificus,	voorzitter
Prof.dr.ir. A. Verruijt,	Technische Universiteit Delft, promotor
Prof.dr.ir. F.B.J. Barends,	Technische Universiteit Delft
Prof.dr.ir. C.P.A. Wapenaar,	Technische Universiteit Delft
Prof.ir. A.C.W.M. Vrouwenvelder,	Technische Universiteit Delft
Prof.dr.ir. G. Degrande,	Katholieke Universiteit Leuven
Dr.ir. W.T. van Horssen,	Technische Universiteit Delft
Dr.ir. P. Hölscher,	GeoDelft

Published and distributed by: DUP Science

DUP Science is an imprint of
Delft University Press
P.O.Box 98
2600 MG Delft
The Netherlands
Telephone: +31 15 27 85 678
Telefax: +31 15 27 85 706
Email: Info@Library.TUDelft.NL

ISBN 90-407-2303-6

Keywords: soil dynamics, hysteretic damping, moving loads

Copyright © 2002 by C.J. Cornejo Córdova

All rights reserved. No part of the material protected by this copyright notice may be reproduced or utilised in any form or by any means, electronic of mechanical, including photocopying, recording or by any information storage and retrieval system, without permission from the publisher: Delft University Press.

Printed in the Netherlands

Acknowledgements

This research has been principally made possible with the permanent advice and guidance of Prof.Dr. A. Verruijt and Dr. P. Hölscher, in particular for the interest and the spent time during this research.

I would greatly like to thank the Geotechnical Laboratory of the Delft University of Technology for the realization of this research project. This research was financially supported by the Delft Interfaculty Research Center (DIOC) at the Delft University of Technology. I am indebted to the institute GeoDelft for allowing the performance of free vibration torsion test. I wish to thank Bob Woldringh for the information and participation of the No-Recess research program, carried out in 's-Gravendeel, The Netherlands. This program stands for new options for rapid and easy construction of embankments on soft soils. I would like to thank Dr. M. Bakker and Prof.Dr. A. de Hoop for their valuable suggestions on the development of part of the thesis. I gratefully thank Prof.Dr. A. Molenaar, Tony Visser, Robin van Dijk and Joop van Leeuwen for the collaboration of tests at the Geotechnical Laboratory, and the Road and Railroad Laboratory of the Delft University of Technology.

It is with a great feeling of pride and enormous satisfaction that I could learn from Prof.Dr. A. Verruijt a great variety of topics on the theory of elasticiteit and mathematics. Furthermore, Prof.Dr. A. Verruijt gave me the opportunity to lecture on solid dynamics at the University. I am most grateful to Dr. W. van Horssen and Prof. Dr. Degrande for helpful commentaries on this thesis.

I would especially like to thank my parents, and my brothers Mario and Raúl for their complete and tremendous support during my whole education at the Delft University of Technology. Without the aid of them this thesis could certainly never have been finished. I would like to express my gratitude to Alexander Bode for reviewing of the language of this thesis.

Carlos Cornejo

Abstract

A study of elastic wave motion in a dissipative medium, generated by surface forces is carried out in the present thesis. The main characteristic of the medium considered here, is that the dissipation of energy due to dynamic loads is not linearly proportional to the frequency. The purpose of this study is to describe the dynamic analysis of soils in terms of a linear elastic medium with hysteretic damping, which is a particular case of the Kelvin-Voigt damping with frequency dependent viscosity. Hysteretic damping is denoted using the damping ratio ζ. With the aid of the Fourier transformation and the Hankel transformation the governing wave equations of motion of the material are solved. Various cases are developed for the prediction of the behaviour of waves in an elastic medium with hysteretic damping. These cases can be applied to railways for high-speed trains and vibrations of foundations.

In general the solutions to the problems considered in this thesis are given in terms of the stress field, the displacements and the dynamic amplification factor of the vertical displacement. The influence of the hysteretic damping as a function of the damping factor on the magnitude of the results is presented.

Vibration loads on the surface of a half-space and on the surface of a half-plane are examined, including the case of a rigid circular plate on a half-space. The influence of the frequency of vibration of the load on the response is obtained.

A closed-form solution is given for the problem of a half-plane loaded by a moving load on its surface. Solutions for the subsonic, transonic and supersonic cases are found. Results indicate that for small values of the damping, such as $\zeta < 0.1$, the displacements and stresses are very large, compared to the elastostatic solution. For values of the velocity of the moving load in the vicinity of the Rayleigh wave velocity results are shown. The response of a moving load on a layer and on a layered half-plane are also obtained. For the case of dynamic interaction of a layer and a half-plane the influence of the relative stiffness of layer and half-plane is found. For very small values of the damping ratio a simple approximation of the location of the two peaks generated by a moving load at supersonic velocities is given.

For vertical loads on the surface of an elastic half-space with hysteretic damping an approximate method of solution is developed. The method is based on the assumption that the horizontal displacements are disregarded. With the aid of this method the vibration load and the moving load problems are also solved. The solutions to these problems are compared with the elastic solutions. For Poisson's values between 0 and 0.4, the response functions of the displacements below a uniform vibration load over circular area give an acceptable approximation of the elastic solution.

A moving transient line load on a half-space is examined using the approximate

method. In this case, hysteretic damping of the medium is not considered. In order to obtain analytic, closed-form expressions for the vertical displacements and vertical stresses, the problem is solved with the aid of the Cagniard-de Hoop method. Both the subsonic and supersonic cases are also studied.

For small deformations sand specimens have been tested in free vibration torsion in the laboratory of GeoDelft in The Netherlands to determine the magnitude of the damping ratio. For different polar mass moments of inertia of the attached mass to the top of the specimen, relationships between the shear stress and the shear strain are given. From the test results it is observed that the damping ratio of the specimens varied moderately with the magnitude of the deformations.

C. J. Cornejo Córdova, Elastodynamics with Hysteretic Damping, PhD Thesis, Delft University Technology, 2002.

Contents

Acknowledgements **v**

Abstract **vii**

List of symbols **xi**

1 Introduction **1**
1.1 High-speed trains 1
1.2 Outline of this study 3

2 Theory of elastodynamics **5**
2.1 Equations of motion 8
2.2 Elastic wave propagation 10
2.2.1 Helmholtz's decomposition 11
2.2.2 Helmholtz's equation 12
2.2.3 Equations in terms of potentials 12
2.3 Rayleigh surface waves 13
2.4 Linear Viscoelastic material 16
2.4.1 Kelvin-Voigt model 16
2.4.2 Linear viscoelasticity in three dimensions 17
2.4.3 Representation by Fourier transformation 18
2.5 Hysteretic damping 19

3 Vibrating load on an elastic half-space with hysteretic damping **21**
3.1 Axially symmetric system 21
3.2 Vibrating load on a half-space 23
3.3 Uniform load over circular area 24
3.3.1 Displacements at the surface 27
3.3.2 Quasi-static solution 28
3.3.3 Vertical displacement at the origin 31
3.3.4 Point load 31
3.3.5 Numerical integration 32
3.3.6 Average displacement 33
3.4 Uniform load over a rigid circular plate 35
3.5 Vibrating load on an elastic half-plane 38
3.5.1 Vibrating strip load 39

3.5.2 Vibrating point load 43

4 Moving loads on an elastic half-plane with hysteretic damping 45
4.1 Basic equations 45
4.2 Moving loads on a half-plane 46
4.2.1 Moving point load 47
4.2.2 Stress components 51
4.2.3 Displacements 59

5 Moving loads on an elastic plane layer with hysteretic damping 67
5.1 Basic equations 67
5.2 Moving loads on a plane layer 68
5.2.1 Moving point load 69
5.2.2 Stress components 73
5.2.3 Displacement components 78

6 Moving loads on a layer on a half-plane with hysteretic damping 81
6.1 Basic equations 82
6.2 Moving loads on a single layer on a half-plane 83
6.2.1 Moving point load 84
6.2.2 Stress components 89

7 Material with horizontal constraints 95
7.1 Uniform load over circular area 96
7.2 Moving loads on a half-plane 103

8 The Cagniard-de Hoop technique for a material with horizontal constraints 109
8.1 Line pulse 110
8.2 Moving line load 114
8.2.1 Vertical stress 121
8.3 The inclusion of the Voigt viscosity mechanism 124

9 Determination of damping in soils 125
9.1 Introduction 125
9.2 Testing procedure 126
9.3 Test results and interpretations 127

10 Conclusions 131

Bibliography 133

Samenvatting 143

Resumen 145

About the author 147

List of symbols

γ_{ij}	components of shear strains.
δ_{ij}	Kronecker's delta symbol.
ε_{ij}	components of the strain tensor.
ζ	damping ratio.
λ	Lamé constant.
λ_c	wavelength.
μ	Lamé constant.
ξ	dimensionless wave number.
ν	Poisson's ratio.
σ_{ij}	components of the stress tensor.
ρ	mass density.
ϕ	scalar potential.
χ	scalar potential.
ψ_{ij}	components of the vector potential.
$\boldsymbol{\psi}$	vector potential.
ω	angular frequency or circular frequency.
ω_{ij}	components of the infinitesimal rotation.
Θ	sum of the normal stresses.
c	wave velocity or phase velocity.
c_p	velocity of distorsion waves.
c_r	velocity of Rayleigh wave.
c_s	velocity of dilatation waves.
e	sum of the normal strains.
f	frequency.
h	thickness.
k_p	wave number related to c_p.
k_s	wave number related to c_s.
l	length.

p_0	amplitude of the vertical stress.
r_0	radius of a circular area.
t_0	arrival time.
t_r	relaxation time.
u_i	component of the displacement vector.
$\mathbf{u}$	vector displacement.
t	time.
v	velocity.
x_0	half length of a strip load.
D	damping ratio.
E	modulus of elasticity or Young's modulus.
G	modulus of rigidity or shear modulus.
K	modulus of volume expansion or bulk modulus.
M_p	dimensionless velocity related to c_p.
M_r	dimensionless velocity related to c_r.
M_s	dimensionless velocity related to c_s.
P	point force.
P	line force per unit length.
Q	line force per unit of length multiplied by time.
T	period.
$\mathbf{X}$	body force vector per unit volume.
X_i	components of the body force vector per unit volume.
$\Re$	real.
$\Im$	imaginary.
∇	gradient.
$\nabla\times$	curl.
∇^2	Laplace operator or Laplacian.
Δu_i	differential displacement in i-direction.
u_{id}/u_{is}	dynamic amplification factor of the displacement in i-direction.
(x, y, z)	Cartesian (rectangular) coordinates.
(x, z, θ)	polar coordinates.
(x_1, z_1)	moving coordinates.

Chapter 1

Introduction

Estimation of the dynamic response of a structure under the application of mechanical time-dependent loads such as earthquakes, explosions or machines requires knowledge of the dynamic properties of the medium under the structure and the structure itself. As a result of these loads the deformations and stresses are varying in time. Consequently, stress-strain relationships, tensile strength and cyclic behaviour are essentially significant in the analysis of dynamic response. Illustrative examples serving to clarify the time-dependent response of a structure are the railway track of a high-speed train and the dynamic loads that are transmitted to a structure that supports oscillating machinery. Furthermore, many applications in seismology, mining and geophysics can also be mentioned as examples.

For the study of ground vibrations a good understanding of the physical and mathematical analysis is required. Applying the basic laws of physics to dynamic systems, with restoring loads, mainly leads to partial differential equations. The solutions of these equations are used to describe dynamic systems. In all of the research activities of the dynamic behaviour of a structure a study of wave propagation under the structure is an aspect of great significance.

Another important aspect of ground vibrations is to take into account the energy dissipation or damping. This damping can be caused by the internal friction when the soil is deformed. The typical representation of this deformation is hysteretic damping. Therefore, the objective of this present study is to develop the dynamical theory of linear elasticity of a material with hysteretic damping. Topics of elastodynamic theory with hysteretic damping can be applied to railways for high-speed trains and vibrations of foundations.

1.1 High-speed trains

Quite a few investigations concerning ground vibration generated by high-speed trains have been done in various European countries, Japan and United States. Results of these investigations are given in terms of displacements and stresses.

The investigation of dynamic soil properties is essential for the design and the construction of the foundation of structures which can support dynamic loads. Railways for high-speed trains are a typical case, in particular when the trains move over rela-

tively soft soils. These trains generate waves that are propagated in the track and in the subsoil. Each type of soil has a different wave-velocity of propagation; this velocity is often smaller than the critical velocity of a moving train. The critical velocity is defined as the smallest load velocity at which the dynamic amplification factor of the track vibrations under the moving train reaches a maximum. Metrikine and Dieterman [1997] studied the three-dimensional vibrations of a beam on an elastic half-space.

One of the first studies of the dynamic behaviour of the railway in The Netherlands was formulated by de Nie [1949] who analyzed the track Oudewater-Gouda of the railway between Utrecht to Rotterdam and The Hague. He observed the possible implications of the dynamic behaviour of the track-ground system. It appeared that waves were generated along the railway. Results of this study also showed that the magnitude of the waves are much larger if the speed of the trains increases.

> *"Het tweede euvel, dat werd waargenomen, was de z.g. baangolving, dat is een op- en neergaande beweging van de gehele baan t.o.v. de omgeving gedurende het passeren van treinen. Deze golving neemt met de snelheid der treinen toe, en treedt vooral daar op, waar het baanlichaam een geringe dikte heeft,...". de Nie [1949], pp. 210.*

A study of high-speed trains in The Netherlands was given by Esveld *et al.* [1995]. They found that relatively large dynamic amplifications occur in the dynamic response of the rail-embankment-ground system as the train speed approaches a critical train speed. Dieterman [1996] formulated that high-speed trains on soft soils could lead to a similar problem to that produced by supersonic jets. High-speed trains mainly generate a large increase in vibration level if the train speed exceeds the velocity of Rayleigh surface waves in the ground. In the Netherlands, the velocity of Rayleigh surface waves in soft soils can be around 30 - 50 m/s. TNO [1997] measured ground vibration from a test railway site in Amsterdam to Utrecht in The Netherlands, where trains travel at velocities of up to 60 m/s (200 km/h) resulting in increasing amplitudes of the vibrations. Branderhorst [1997] examined three models for the prediction of ground response to high-speed trains.

For the design of the project High Speed Link - South (HSL-S) between Amsterdam and Brussels, a No-Recess research program was developed in 1999. The purpose of this research was to test the suitability of various embankment construction methods for a railway, see Woldringh and New [1999], Arcadis Trischler and Partner [1999], and Fugro Ingenieursbureau B.V. [1999].

Various studies have been developed for the modelling of train-induced ground vibration accounting for the embankment: Kaynia *et al.* [2000], Lombaert and Degrande [2001], Eijgenraam *et al.* [2001], Sun [2001], Degrande and Shillemans [2001], Kaynia [2001], and Metrikine *et al.* [2001].

The main characteristic of hysteretic damping, considered in this thesis, is that the damping ratio in each full cycle of loading is independent of the frequency of the loading. This is in agreement with the results of Hardin [1965], on the basis of an extensive study of the properties of soils when subjected to dynamic loading.

1.2 Outline of this study

This study contains several applications of elastodynamic theory. With the aid of these applications the phenomenon of wave propagation in an elastic material with incorporation of energy dissipation in the material is investigated. Major emphasis is placed on models and techniques for describing the dynamic response of a railway track to high-speed trains and the propagation of vibrations into a material caused by dynamic loadings.

In general, it is attempted to find close-form solutions to the problems considered in this thesis. The mathematical techniques used to solve the considered problems are principally developed with the aid of the Fourier transformation. Other aspects of interest in relation to the subject of discussion are the advantages of each solution relative to other solution techniques. In the present study some calculations of transient wave propagation are found by using the Cagniard-de Hoop method, see de Hoop [1960].

The determination of vertical normal displacements and stresses caused by a vertical normal load on the surface of a half-space can be calculated using an approximate method of solution by assuming that the horizontal displacements may be disregarded, so that the only actual displacement is the vertical displacement. An elastic solution based on conditions of this type has been attributed to Westergaard [1938]. Several contributions to this subject from elastodynamics theory are examined in this study.

A brief survey of the basic principles of elastodynamics theory is presented in Chapter 2. The relationship between stress, strain and time in terms of the material parameters, and the strain components in terms of displacements are given. These in turn represent the deformation of a body. The governing wave equations of motion of the material are derived. Furthermore, an introduction to linear viscoelastic stress analysis is introduced. The concept of hysteretic damping is also explained.

In Chapter 3 the problem considered consists of a vibrating load on a circular area on the surface of an elastic half-space with hysteretic damping. The case of a rigid circular plate on the surface is also examined. In addition the case of a vibrating load on a half-plane is analyzed.

A closed-form solution of the displacements and stresses caused by loads moving over the surface of an elastic half-plane with hysteretic damping is found in Chapter 4, see Verruijt and Cornejo Córdova [2001]. The influence of hysteretic damping in terms of the damping factor on the magnitude of the results is presented. The dynamic amplification of stresses and displacements becomes very large if the velocity of the load approaches the Rayleigh wave velocity or supersonic waves velocities.

In Chapter 5 and 6 moving loads on an elastic plane layer and on an elastic single layer on a half-plane with hysteretic damping are studied. The equations related to phase velocities and wave numbers are derived, and the dispersion curves are shown. The reflections caused by a rigid base of a layer or the interface of two different materials are illustrated.

In problems of an elastic half-space in which vertical loads on the surface are applied only, an approximate method of solution formulated by Westergaard [1938] is developed in Chapter 7. The solutions of the considered problems are compared with the solutions of the problems in Chapter 3 and 4.

The moving line problem is studied in Chapter 8. The transient wave case is solved with the aid of Cagniard-de Hoop method, see de Hoop [1960, 2001] and Cornejo Córdova [2002]. A closed-form solution of the vertical displacement for a vertical moving line load acting on the surface of a half-space is obtained in Chapter 7, using the approximate method.

In Chapter 9 a laboratory study of soil dynamic response is presented. A free vibration torsion test was performed on soil cylindrical specimen at GeoDelft in The Netherlands. The objective of this test is to quantify the magnitude of damping of the sand with shearing strain amplitudes smaller than 5×10^{-4}. Results from this test also provide insight into shear-strain behaviour

Conclusions of the present study are given in Chapter 10.

Chapter 2

Theory of elastodynamics

As a preparation for the applications of the theory the basic principles of elastodynamics are discussed in this chapter, with a short review of essential concepts and assumptions. It will be assumed that the material is homogeneous, continuous and isotropic. This implies that the elastic properties are the same in all directions at each point.

When a body is under the action of external forces, internal forces are generated in the body. If it is assumed that these internal forces are continuously distributed over a cross-sectional area, the concept of stress can be defined as the total force F divided by the area A. The direction of the force indicates also the direction of the stress. The direction of the force is generally inclined to the area, signifying the presence of a normal stress perpendicular to the area, and shear stress acting in the plane of the area.

A body is deformed, or strained, when the mutual positions of points in the body are changed. The theory of strain studies these deformations of the body. Throughout this thesis only infinitesimal small deformations will be considered, as a first approximation. The body B in the deforming region R is shown in Figure 2.1. The point P_1 moves

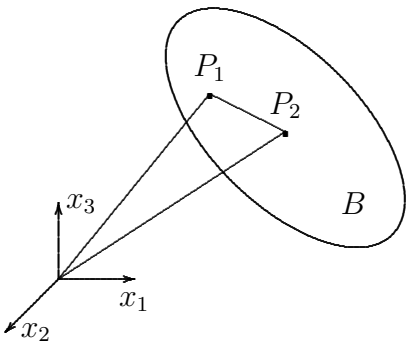

Figure 2.1: Points P_1 and P_2 in the body B.

to the position P_2. The stresses will be denoted by σ_{ij}. The first subscript denotes the direction of normal to the plane on which the stress is occurring and the second indicates the direction of the stress component. The sign convention is such that tension

is considered positive, and compression is considered negative. The normal strain ε_{11} is defined as the change in length per unit length in the direction x_1. The shear strain is usually expressed by γ_{ij}. The directions of the shear strain are denoted by the same subscripts as for the shear stress. This implies that the subscripts i and j denotes the directions x_i and x_j, respectively. Hence,

$$\gamma_{ij} = \partial_{x_i} u_j + \partial_{x_j} u_i, \tag{2.1}$$

where u_i and u_j are the displacements in x_i and x_j directions, respectively. The shear strain γ_{ij} describes the change of the right angle between the x_i and x_j directions. The definitions of strain can be unified by introducing the strain tensor ε_{ij} as:

$$\varepsilon_{ij} = \frac{1}{2}(\partial_{x_i} u_j + \partial_{x_j} u_i). \tag{2.2}$$

or, using another notation,

$$\varepsilon_{ij} = \frac{1}{2}(\partial_i u_j + \partial_j u_i). \tag{2.3}$$

The rotation of an infinitesimal element $dx_i dx_j$ is given by

$$\omega_{ij} = \frac{1}{2}(\partial_{x_i} u_j - \partial_{x_j} u_i). \tag{2.4}$$

The rotation can also be defined as a vector ω_k, such that $\omega_k = \omega_{ij}$. The rotation is skew-symmetric, or antisymmetric, because $\omega_{ij} = -\omega_{ji}$. It may also be mentioned

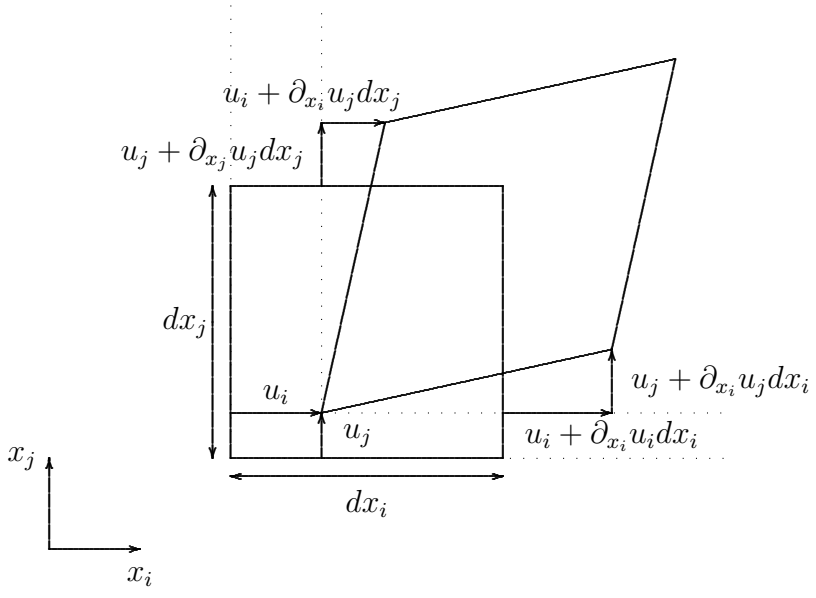

Figure 2.2: Deformation and rotation of the element $dx_i dx_j$.

that ω_k describes the rotation of a rigid element if ε_{ij} vanishes. The infinitesimal deformation and rotation of the rectangular element $dx_i dx_j$ are shown in Figure 2.2.

Linear stress-strain relations are considered and these are credited to Robert Hooke in 1676. When a bar is submitted to the action of a normal stress, it is assumed that the stress is a linear function of the strain, $\sigma_{11} = E\varepsilon_{11}$, where E is the modulus of elasticity or Young's modulus. The elongation of the element also produces a lateral contraction in the other two directions,

$$\varepsilon_{22} = \varepsilon_{33} = -\frac{\nu}{E}\sigma_{11} \tag{2.5}$$

where ν is a constant called Poisson's ratio. This represents the ratio of the lateral strain to the longitudinal strain. The negative sign indicates that an axial extension usually causes a lateral contraction.

If an infinitesimal parallelepiped element with surfaces parallel to the coordinate planes is submitted to the simultaneous action of normal stresses σ_{11}, σ_{22} and σ_{33}, the strains can be expressed in terms of the above stresses,

$$\varepsilon_{11} = \frac{1}{E}(\sigma_{11} - \nu(\sigma_{22} + \sigma_{33})). \tag{2.6}$$

In some cases it is useful to introduce the sum of the normal strains e and the sum of the normal stresses Θ. These are related by

$$e = \frac{\Delta V}{V} = \varepsilon_{11} + \varepsilon_{22} + \varepsilon_{33}, \tag{2.7}$$

$$\Theta = \sigma_{11} + \sigma_{22} + \sigma_{33}, \tag{2.8}$$

where the relation between e, the volume expansion or volume dilatation, and Θ, the sum of the normal stresses, is

$$e = \frac{\Delta V}{V} = \frac{(1-2\nu)}{E}\Theta, \tag{2.9}$$

with V and ΔV denoting volume and change of volume, respectively. In the special case of a uniform hydrostatic pressure of magnitude p, the normal stresses are

$$\sigma_{11} = \sigma_{22} = \sigma_{33} = -p, \tag{2.10}$$

and the shear stresses are equal to zero. The relation between e and p is now

$$e = -\frac{p}{K}, \tag{2.11}$$

in which the modulus of volume expansion K, also called the bulk modulus or the modulus of compression, is defined as

$$K = \frac{E}{3(1-2\nu)}. \tag{2.12}$$

The normal stresses may be related to the normal strains by the inverse form of Hooke's law,

$$\sigma_{11} = \lambda e + 2\mu\varepsilon_{11} \tag{2.13}$$

where the constants λ and μ are called Lamé's constants (Lamé, 1852). These are defined as

$$\lambda = \frac{\nu E}{(1+\nu)(1-2\nu)} \quad \text{and} \quad \mu = \frac{E}{2(1+\nu)}. \tag{2.14}$$

The relation between the shear stress and the shear strain depends upon the shear modulus or the modulus of rigidity, G,

$$\sigma_{ij} = 2G\varepsilon_{ij} = G\gamma_{ij}. \tag{2.15}$$

The shear modulus G is equivalent to Lamé's coefficient μ, and the bulk modulus K can also be given as $K = \lambda + 2/3\mu$. If Poisson's ratio is equal to $1/4$, then $\lambda = \mu$.

The complete form of Hooke's law, valid for any stress or strain component in an isotropic material, now is

$$\sigma_{ij} = \lambda e\delta_{ij} + 2\mu\varepsilon_{ij}, \tag{2.16}$$

where δ_{ij} is Kronecker's delta symbol,

$$\delta_{ij} = \begin{cases} 1, & \text{if } i = j, \\ 0, & \text{if } i \neq j. \end{cases}$$

This incorporates both the behaviour in normal strain and in shear strain.

2.1 Equations of motion

The motion of a material body is assumed to satisfy conservation of mass, meaning that the mass of the body is the same at all times. Furthermore, the mass density ρ is defined at every point in the body as the mass divided by the volume.

In general, the forces acting on a body can be divided into body forces and surface forces. The body force at an internal point P is defined as the force exerted on the body from an external source to the body, divided by the infinitesimal body element of volume at P. An example of a body force is the gravitational force, given as ρg_3 in which g_3 is the gravitational acceleration in the direction x_3. A surface force is the force acting across any surface of the body, in particular on its boundary, divided by the (infinitesimal) area of the surface element.

The equations of motion of an element in the interior of a body can be derived by considering an infinitesimal parallelepiped with surfaces parallel to the coordinate planes x_1, x_2 and x_3, see Figure 2.3. If it is assumed that the dimensions of the parallelepiped can be taken so small that the moments of the normal stresses vanish, then equilibrium of moments of the element requires that the shear stresses components be equal in pairs, $\sigma_{12} = \sigma_{21}$, $\sigma_{23} = \sigma_{32}$ and $\sigma_{31} = \sigma_{13}$.

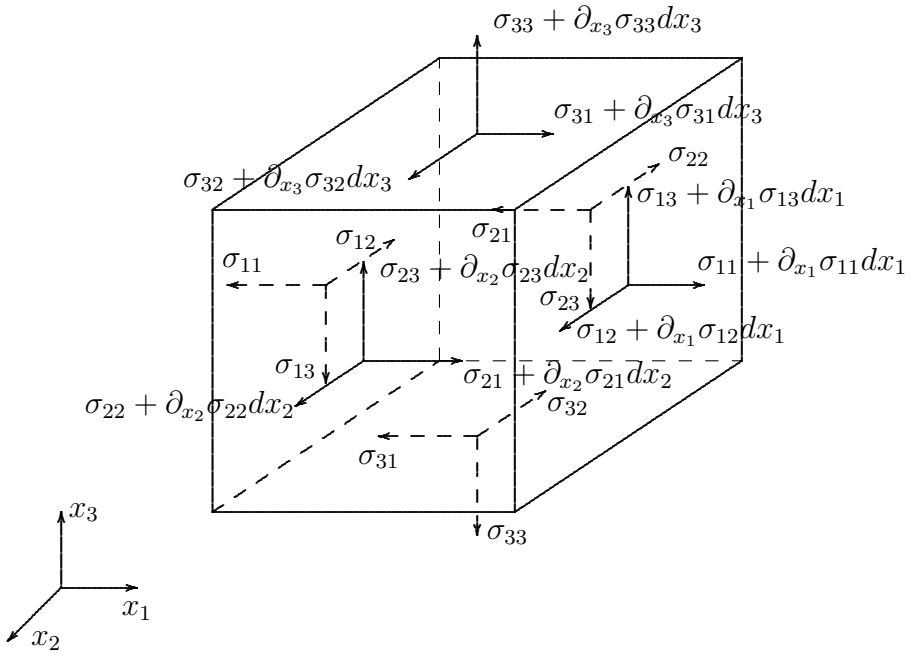

Figure 2.3: Stress components on an infinitesimal parallelepiped.

The equation of motion in the x_1-direction at a given time t is found by adding all the forces acting on the volume element $\Delta V = dx_1dx_2dx_3$, and setting it equal to the increment of the impulse of the mass, $\rho\Delta V\partial_{tt}^2 u_1$, where u_1 is the displacement in x_1-direction and the density ρ is considered as constant at every point. It follows that

$$\partial_{x_1}\sigma_{11} + \partial_{x_2}\sigma_{21} + \partial_{x_3}\sigma_{31} + \rho X_1 = \rho\partial_{tt}^2 u_1, \tag{2.17}$$

where X_1 is the body force per unit volume in x_1-direction. In the same manner the equations of motion in the directions of x_2 and x_3 can be obtained, yielding

$$\partial_{x_1}\sigma_{12} + \partial_{x_2}\sigma_{22} + \partial_{x_3}\sigma_{32} + \rho X_2 = \rho\partial_{tt}^2 u_2, \tag{2.18}$$

$$\partial_{x_1}\sigma_{13} + \partial_{x_2}\sigma_{23} + \partial_{x_3}\sigma_{33} + \rho X_3 = \rho\partial_{tt}^2 u_3, \tag{2.19}$$

where u_2 and u_3 are the displacements in the directions of x_2 and x_3, respectively. The particle velocities and accelerations are defined as $\partial_t u_1$ and $\partial_{tt}^2 u_1$, in x_1-direction.

Using the generalized form of Hooke's law (2.16), the equations of motion can be expressed in terms of the displacement components (Navier's equation),

$$(\lambda + \mu)\partial_{x_1} e + \mu\nabla^2 u_1 + \rho X_1 = \rho\partial_{tt}^2 u_1, \tag{2.20}$$

$$(\lambda + \mu)\partial_{x_2} e + \mu\nabla^2 u_2 + \rho X_2 = \rho\partial_{tt}^2 u_2, \tag{2.21}$$

$$(\lambda + \mu)\partial_{x_3} e + \mu\nabla^2 u_3 + \rho X_3 = \rho\partial_{tt}^2 u_3, \tag{2.22}$$

where $e = \varepsilon_{11} + \varepsilon_{22} + \varepsilon_{33}$ and the Laplace operator ∇^2 is defined as

$$\nabla^2 = \partial^2_{x_1x_1} + \partial^2_{x_2x_2} + \partial^2_{x_3x_3}. \tag{2.23}$$

or, using another notation

$$\nabla^2 = \partial^2_{11} + \partial^2_{22} + \partial^2_{33}.$$

The equations of motion can be written in vector form as

$$(\lambda + \mu)\nabla e + \mu\nabla^2(u_1, u_2, u_3) + \rho(X_1, X_2, X_3) = \rho\partial^2_{tt}(u_1, u_2, u_3), \tag{2.24}$$

where $\nabla = (\partial_{x_1}, \partial_{x_2}, \partial_{x_3})$ is the gradient vector.

The equation of motion can be written in another form by introducing the rotation vector

$$(\omega_1, \omega_2, \omega_3) = \frac{1}{2}\nabla \times (u_1, u_2, u_3), \tag{2.25}$$

in which $\nabla \times (u_1, u_2, u_3) = (\partial_{x_2}u_3 - \partial_{x_3}u_2, \partial_{x_3}u_1 - \partial_{x_1}u_3, \partial_{x_1}u_2 - \partial_{x_2}u_1)$ is the curl of the displacement vector. With the aid of the property

$$\nabla^2(u_1, u_2, u_3) = \nabla(\nabla \cdot (u_1, u_2, u_3)) - \nabla \times \nabla \times (u_1, u_2, u_3), \tag{2.26}$$

and introducing the vector displacement $\mathbf{u} = (u_1, u_2, u_3)$ and the body force vector per unit volume $\mathbf{X} = (X_1, X_2, X_3)$, the equation of motion can also be written as

$$(\lambda + 2\mu)\nabla(\nabla \cdot \mathbf{u}) - \mu\nabla \times \nabla \times \mathbf{u} + \rho\mathbf{X} = \rho\partial^2_{tt}\mathbf{u}. \tag{2.27}$$

This expression is a linear system of hyperbolic partial differential equations for the dependent variables u_1, u_2 and u_3. One advantage of the vector form is that it facilitates the expression of the equations in other coordinate systems. Since the equations of motion are linear, the superposition principle can be applied. In many cases the weight of the body element is frequently considered as the only body force. This implies that two components of the vector $\rho\mathbf{X}$ are equal to zero and the third component is equal to ρg, in which g is the gravitational acceleration.

2.2 Elastic wave propagation

The concept of waves is fundamental to elastodynamics, as it provides a convenient way to describe the mathematics and the physics of the transmission of energy, including energy adsorption. The propagation of waves was studied fundamentally by Poisson, Navier, Cauchy and Lamé. Poisson established two types of waves which, at great distances from the sources of disturbance, are almost longitudinal and transversal. Poisson's work formulated a class of particular solutions to the displacement equation of motion, for the case that the displacement vector $\mathbf{u}$ can be written as the gradient of a potential function. Poisson in 1829 also asserted that the solution of the displacement equation of motion can be described by the sum of two components, a dilatational and an equivoluminal motion, with two different wave speeds. Later, in 1852 Lamé used the property that every displacement vector field can be expressed in terms of a scalar and vector potential.

2.2.1 Helmholtz's decomposition

Expressing the displacement field as a combination of two simpler fields facilitates the analysis of solutions of the elastodynamic equations. With the aid of Helmholtz's theorem the vector $\mathbf{u}$ can be expressed as the sum of the gradient of a scalar potential ϕ and the curl of a vector potential $\boldsymbol{\psi}$, resulting in

$$\mathbf{u} = \nabla\phi + \nabla \times \boldsymbol{\psi}, \tag{2.28}$$

where both potentials are everywhere continuous and differentiable at interior points where $\mathbf{u}$ is also continuous. The gradient term is sometimes denoted as the longitudinal component, since it points in the direction of the greatest rate of change of the scalar potential. The curl term is also denoted as the transverse component. The condition $\nabla \cdot \boldsymbol{\psi} = 0$ may be assumed without loss of generality. This is also known as the gauge condition.

Helmholtz's decomposition is valid for an infinite domain on the condition that $\mathbf{u} = O(r^{-2})$, i.e., provided that the absolute value of $\mathbf{u}$, $|\mathbf{u}|$ decreases to zero at very large distances r from the origin at least as rapidly as a constant times r^{-2}. Introducing (2.28) into (2.26) and using (2.27), the latter reduces to

$$\nabla(\rho\partial_{tt}^2\phi - (\lambda + 2\mu)\nabla^2\phi) + \nabla \times (\rho\partial_{tt}^2\boldsymbol{\psi} - \mu\nabla^2\boldsymbol{\psi}) = 0, \tag{2.29}$$

provided that $\mathbf{X} = 0$. It follows from (2.29), by taking the divergence and the curl of this equation, respectively, and noting that the condition $\nabla.\boldsymbol{\psi} = 0$ holds,

$$\nabla^2\nabla^2\phi = \frac{1}{c_p^2}\partial_{tt}^2\nabla^2\phi \quad \text{and} \quad \nabla^2\nabla^2\boldsymbol{\psi} = \frac{1}{c_s^2}\partial_{tt}^2\nabla^2\boldsymbol{\psi}. \tag{2.30}$$

Important particular solutions of this equation can be obtained if the potentials ϕ and $\boldsymbol{\psi}$ satisfy the wave equations

$$\nabla^2\phi = \frac{1}{c_p^2}\partial_{tt}^2\phi \quad \text{and} \quad \nabla^2\boldsymbol{\psi} = \frac{1}{c_s^2}\partial_{tt}^2\boldsymbol{\psi}, \tag{2.31}$$

where c_p is the velocity of dilatation waves, in which the deformation consists of dilatation or volume change and c_s is the velocity of distortional waves, in which the deformation consists of shear and rotation but no volume change. Waves of these two types are also frequently denoted as irrotational, compressional or primary P and equivoluminal, shear or secondary S. They are defined by

$$c_p = \sqrt{\frac{\lambda + 2\mu}{\rho}} \quad \text{and} \quad c_s = \sqrt{\frac{\mu}{\rho}}. \tag{2.32}$$

Setting Lamé's constant $\mu = 0$ in the equations of linear elasticity results in equations for an elastic medium that cannot support shear stresses. These types of equations are sometimes denoted as the equations of sound propagation, or the acoustic equations. In that case the displacement equation (2.27) reduces to

$$\lambda\nabla(\nabla \cdot \mathbf{u}) = \rho\partial_{tt}^2\mathbf{u}. \tag{2.33}$$

This displacement vector can also be given in terms of a scalar potential ϕ, $\mathbf{u} = \nabla\phi$. Hence,

$$\nabla^2\phi = \frac{1}{c^2}\partial_{tt}^2\phi, \tag{2.34}$$

where $c = \sqrt{\lambda/\rho}$ is the speed of propagation of the acoustic medium.

2.2.2 Helmholtz's equation

A wave is frequently considered as a periodic disturbance, that travels with finite velocity through a medium. In general waves are governed by a second-order linear partial equation of the following type

$$\nabla^2\eta = \frac{1}{c^2}\partial_{tt}^2\eta, \tag{2.35}$$

where $\eta = \eta(\mathbf{x}, t)$ describes the disturbance traveling with the speed of propagation c and $\mathbf{x}$ is a vector with three orthogonal components. Considering the Fourier transformation of both sides of the equation, and defining

$$\tilde{\eta}(\mathbf{x}, \omega) = \int_{-\infty}^{\infty} \eta(\mathbf{x}, t)\exp(-i\omega t)dt, \tag{2.36}$$

this gives, substituting in (2.35), the time-independent wave equation

$$\nabla^2\tilde{\eta} + k_c^2\tilde{\eta} = 0, \tag{2.37}$$

where $k_c = \omega/c = 2\pi/\lambda_c$ is the wave number. λ_c is the wavelength and ω is the circular frequency (angular frequency) of the wave. This equation is known as Helmholtz's equation. The period of the wave is $T = 2\pi/\omega$ and $f = 1/T$ is the frequency.

2.2.3 Equations in terms of potentials

In general, the vector displacement may be represented by a scalar potential ϕ and the vector potential $\boldsymbol{\psi}$, with components ψ_1, ψ_2 and ψ_3 in terms of x_1, x_2, x_3 and t. Hence, it is useful to define $\mathbf{u} = (u_1, u_2, u_3)$ as

$$u_1 = \partial_{x_1}\phi + \partial_{x_2}\psi_3 - \partial_{x_3}\psi_2, \tag{2.38}$$

$$u_2 = \partial_{x_2}\phi + \partial_{x_3}\psi_1 - \partial_{x_1}\psi_3, \tag{2.39}$$

$$u_3 = \partial_{x_3}\phi + \partial_{x_1}\psi_2 - \partial_{x_2}\psi_1. \tag{2.40}$$

It follows that the equation of motion can be satisfied by potentials ϕ and $\boldsymbol{\psi}$ that satisfy the wave equations

$$\nabla^2\phi = \frac{1}{c_p^2}\partial_{tt}^2\phi, \tag{2.41}$$

$$\nabla^2\psi_n = \frac{1}{c_s^2}\partial_{tt}^2\psi_n, \quad n = 1, 2, 3. \tag{2.42}$$

The stresses can be expressed into the potentials by the following relations,

$$\sigma_{11} = \lambda\nabla^2\phi + 2\mu(\partial_{x_1x_1}^2\phi + \partial_{x_1}(\partial_{x_2}\psi_3 - \partial_{x_3}\psi_2)), \tag{2.43}$$

$$\sigma_{22} = \lambda\nabla^2\phi + 2\mu(\partial_{x_2x_2}^2\phi + \partial_{x_2}(\partial_{x_3}\psi_1 - \partial_{x_1}\psi_3)), \tag{2.44}$$

$$\sigma_{33} = \lambda\nabla^2\phi + 2\mu(\partial_{x_3x_3}^2\phi + \partial_{x_3}(\partial_{x_1}\psi_2 - \partial_{x_2}\psi_1)), \tag{2.45}$$

$$\sigma_{12} = \mu[2\partial_{x_1x_2}\phi + \partial_{x_1}(\partial_{x_3}\psi_1 - \partial_{x_1}\psi_3) + \partial_{x_2}(\partial_{x_2}\psi_3 - \partial_{x_3}\psi_2)], \tag{2.46}$$

$$\sigma_{23} = \mu[2\partial_{x_2x_3}\phi + \partial_{x_2}(\partial_{x_1}\psi_2 - \partial_{x_2}\psi_1) + \partial_{x_3}(\partial_{x_3}\psi_1 - \partial_{x_1}\psi_3)], \tag{2.47}$$

$$\sigma_{31} = \mu[2\partial_{x_3x_1}\phi + \partial_{x_3}(\partial_{x_2}\psi_3 - \partial_{x_3}\psi_2) + \partial_{x_1}(\partial_{x_1}\psi_2 - \partial_{x_2}\psi_1)]. \tag{2.48}$$

2.3 Rayleigh surface waves

Waves propagated over the surface of a medium were investigated by Lord Rayleigh in 1887. A surface wave can be considered as a wave that propagates in a direction tangential to a surface, while the amplitude of the wave decreases in the normal direction. A property of these surface waves, or Rayleigh waves, is that the amplitude decays with the distance from the surface. For more detailed information the text of Achenbach [1973] can be referred to.

The case of Rayleigh waves for the two-dimensional problem of plane waves for plane strain conditions is presented. Consider the propagation of Rayleigh waves in a half-plane occupying the region $x_3 \geq 0$, as given in Figure 2.4. Assuming that the

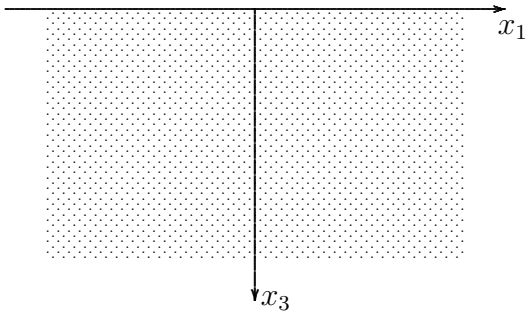

Figure 2.4: Rayleigh surface waves for a half-plane.

displacement $u_2 = 0$ and the displacements u_1 and u_3 can be expressed in terms of the scalar potentials $\phi = \phi(x_1, x_3, t)$ and $\psi = \psi(x_1, x_3, t)$. These are related by

$$u_1 = \partial_{x_1}\phi - \partial_{x_3}\psi, \tag{2.49}$$

$$u_3 = \partial_{x_3}\phi + \partial_{x_1}\psi, \tag{2.50}$$

and the stress components are

$$\sigma_{11} = \lambda(\partial^2_{x_1x_1}\phi + \partial^2_{x_3x_3}\phi) + 2\mu(\partial^2_{x_1x_1}\phi - \partial_{x_1}\partial_{x_3}\psi), \tag{2.51}$$

$$\sigma_{33} = \lambda(\partial^2_{x_1x_1}\phi + \partial^2_{x_3x_3}\phi) + 2\mu(\partial^2_{x_3x_3}\phi + \partial_{x_1}\partial_{x_3}\psi), \tag{2.52}$$

$$\sigma_{13} = \mu(2\partial_{x_1}\partial_{x_3}\phi + \partial^2_{x_1x_1}\psi - \partial^2_{x_3x_3}\psi). \tag{2.53}$$

These potentials satisfy the wave equations $c_p^2\nabla^2\phi = \partial^2_{tt}\phi$ and $c_s^2\nabla^2\psi_n = \partial^2_{tt}\psi_n$. The plane waves are propagated in the direction of x_1 in the plane boundary surface, $x_3 = 0$. Besides, it is considered that the surface waves can be represented by a function of the form $f(x_3)\exp(-ik(x_1 - ct))$, where the function $f(x_3)$ depends on x_3 only. It is now furthermore assumed that plane Rayleigh waves can be described by

$$\phi = A\exp(-kax_3)\exp(-ik(x_1 - ct)), \tag{2.54}$$

$$\psi = B\exp(-kbx_3)\exp(-ik(x_1 - ct)), \tag{2.55}$$

with

$$a = \sqrt{1 - \alpha^2}; \quad \alpha = c/c_p, \tag{2.56}$$

$$b = \sqrt{1 - \beta^2}; \quad \beta = c/c_s. \tag{2.57}$$

The values of a and b are assumed to be real and positive, and the wave velocity or the phase velocity c is $0 < c < c_s < c_p$. A and B are arbitrary constants. The amplitude of the waves decays with increasing x_3, and tends to zero as $x_3 \to \infty$.

The boundary conditions on the free surface, $x_3 = 0$ are $\sigma_{33} = 0$ and $\sigma_{31} = 0$. From (2.52) and (2.53), yielding

$$(b^2 + 1)A + i2bB = 0, \tag{2.58}$$

$$i2aA - (b^2 + 1)B = 0. \tag{2.59}$$

A trivial solution for this system of equations occurs when $A = B = 0$. The condition for a non-trivial solution is found when the determinant of the coefficients of A and B vanishes, which means

$$(b^2 + 1)^2 - 4ab = 0.$$

From (2.56) and (2.57), this results in

$$(2 - \beta^2)^4 = 16(1 - \beta^2/m^2)(1 - \beta^2),$$

with

$$m = \frac{c_p^2}{c_s^2} = \frac{2(1-\nu)}{1-2\nu}.$$

Disregarding the trivial value $c = 0$, the so-called Rayleigh wave equation is

$$\beta^6 - 8\beta^4 + \beta^2(24 - 16/m^2) - 16(1 - 1/m^2) = 0. \tag{2.60}$$

For an incompressible medium $c_p \to \infty$, $m \to \infty$, yielding

$$\beta^6 - 8\beta^4 + 24\beta^2 - 16 = 0.$$

It follows that $\beta = 0.95538$, the other solutions are complex values which do not describe surface waves. The velocity of the Rayleigh wave is denoted by $c_r = c < c_s$, this implies that for this case $c_r = 0.9554c_s$. For a material with Poisson's ratio equal to zero, $m = 2.0$ the velocity of Rayleigh wave $c_r = 0.874032c_s$.

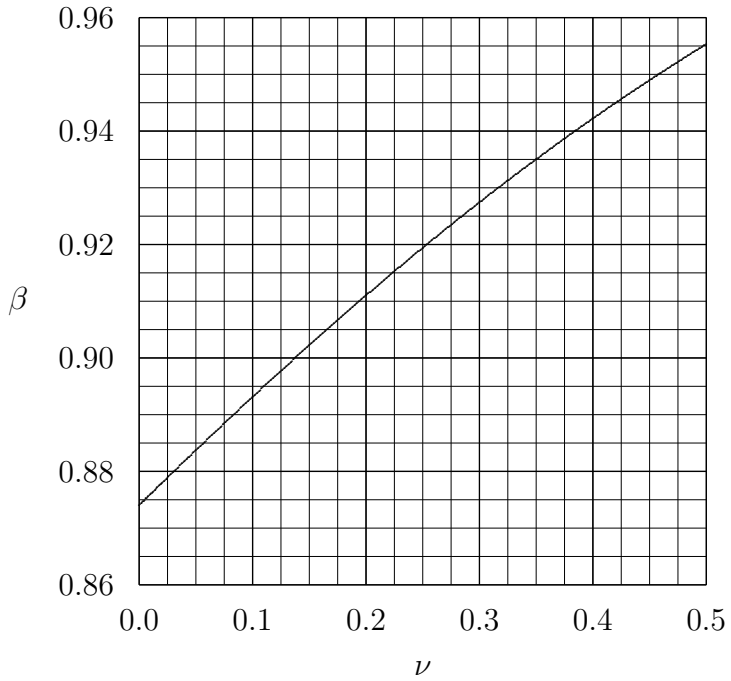

Figure 2.5: Rayleigh surface wave velocity, $\beta = c_r/c_s$ as in terms of Poisson's ratio ν.

Figure 2.5 shows values of β in function of Poisson's ratio, calculated by Knopoff in 1954. The following is an approximation expression for c_r,

$$c_r = \frac{0.87 + 1.12\nu}{1+\nu}.$$

An extensive study of Rayleigh waves is presented in the text of Viktorov [1967].

2.4 Linear Viscoelastic material

A material is considered to be linearly viscoelastic if the stress σ is proportional to the strain ϵ at a given time t, and the linear superposition principle is satisfied. These conditions are described by $\epsilon(C\sigma(t)) = C\epsilon(\sigma(t))$, where C is a constant, and $\epsilon(\sigma_1(t_1) + \sigma_2(t_1 - t_2)) = \epsilon(\sigma_1(t_1)) + \epsilon(\sigma_2(t_1 - t_2))$.

The concepts of creep and relaxation are useful for describing the mechanic properties of a viscoelastic material. Creep is a slow continuous deformation of a material under constant stress. In viscoelastic materials subjected to a constant strain, the stress will gradually reduce in a process called relaxation. The effects of creep and relaxation may occur at the same time under combined loading. Bland [1960], Hunter [1960], Flügge [1975], Findley *et al.* [1976], and Ben-Menahem and Singh [1981] can be given as reference texts.

2.4.1 Kelvin-Voigt model

One of the simplest types of stress-strain relation for linear viscoelastic materials is the Kelvin-Voigt model. This is illustrated in Figure 2.6, where a linear spring element and a linear dashpot element are connected in parallel. Stress-strain relations are represented by the spring

$$\sigma_1 = \mathrm{R}\epsilon, \tag{2.61}$$

and by the dashpot

$$\sigma_2 = \eta \frac{d\epsilon}{dt}, \tag{2.62}$$

where R is the linear spring constant or the Young's modulus. This spring exhibits instantaneous elasticity recovery. The constant η is the coefficient of viscosity. The

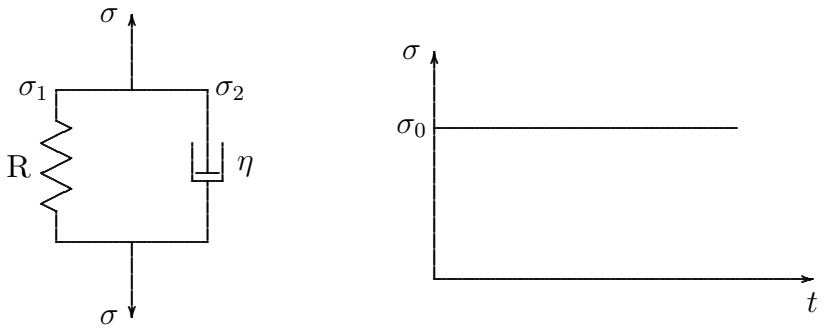

Kelvin-Voigt model Creep

Figure 2.6: Behaviour of Kelvin-Voigt model

strain rate $d\epsilon/dt$ is proportional to the stress σ. This implies that the dashpot will be

deformed continuously at a constant rate when it is subjected to a step of constant stress.

The total stress is

$$\sigma = \sigma_1 + \sigma_2. \tag{2.63}$$

By elimination of σ_1 and σ_2 among these equations the relation stress-strain becomes

$$\sigma = \mathrm{R}\epsilon + \eta\frac{d\epsilon}{dt}. \tag{2.64}$$

For the case of creep under a constant stress σ_0 applied at $t = 0$, the solution of this equation is

$$\epsilon = \frac{\sigma_0}{\mathrm{R}}(1 - \exp(-\mathrm{R}t/\eta)). \tag{2.65}$$

It is observed that the strain increases with a reducing rate and approaches the value of σ_0/R asymptotically when t tends to infinity. The initial strain rate at $t = 0+$ is finite, $d\epsilon(0+)/dt = \sigma_0/\eta$, and the strain rate approaches the value $\epsilon(\infty) = 0$ asymptotically when t tends to infinity.

2.4.2 Linear viscoelasticity in three dimensions

The Kelvin-Voigt model can be generalized to the three-dimensional stress-strain relation, given in (2.16). In order to relate these parameters with the theory of elasticity the respective analogies with the Lamé constants are given by

$$\mu \to \mu + \mu'\partial_t. \tag{2.66}$$

$$\lambda \to \lambda + \lambda'\partial_t. \tag{2.67}$$

Ewing *et al.* [1957], and Ben-Menahem and Singh [1981] gave this type of notation. A complete description of the viscoelastic behaviour of materials is given by Christensen [1982]. The complete form of the stress-strain relations for a Kelvin-Voigt solid can be written as

$$\sigma_{ij} = (\lambda + \lambda'\partial_t)e\delta_{ij} + 2(\mu + \mu'\partial_t)\varepsilon_{ij}, \tag{2.68}$$

where δ_{ij} is Kronecker's delta symbol,

$$\delta_{ij} = \begin{cases} 1, & \text{if } i = j, \\ 0, & \text{if } i \neq j. \end{cases}$$

This includes both the normal and shear stress-strain relation. Substitution of (2.66) and (2.67) into (2.20) - (2.22), the equations of motion for a Kelvin-Voigt solid can be expressed by

$$(\lambda + \mu + (\lambda' + \mu')\partial_t)\partial_{x_n}e + (\mu + \mu'\partial_t)\nabla^2 u_n = \rho\partial_{tt}^2 u_n, \quad n = 1, 2, 3, \tag{2.69}$$

provided that $X_n = 0$.

In a similar way, the wave equations (2.41) and (2.42) can be given by

$$\left(1 + \frac{(\lambda' + 2\mu')}{(\lambda + 2\mu)}\partial_t\right)\nabla^2\phi = \frac{1}{c_p^2}\partial_{tt}^2\phi, \tag{2.70}$$

$$\left(1 + \frac{\mu'}{\mu}\partial_t\right)\nabla^2\psi_n = \frac{1}{c_s^2}\partial_{tt}^2\psi_n, \quad n = 1, 2, 3. \tag{2.71}$$

2.4.3 Representation by Fourier transformation

In general the representation of the properties of a viscoelastic material are denoted much simpler by using the Fourier transformation. This leads directly to the complex modulus description of the mechanical properties of a viscoelastic material. Consider Young's modulus $E \to E + E'\partial_t$ and the relation stress-strain

$$\sigma = E\varepsilon + E'\partial_t\varepsilon,$$

applying the exponential Fourier transformation, and defining $\tilde{\sigma}$ and $\tilde{\varepsilon}$ as

$$\tilde{\sigma}(\omega) = \int_{-\infty}^{\infty}\sigma(t)\exp(-i\omega t)dt \quad \text{and} \quad \tilde{\varepsilon}(\omega) = \int_{-\infty}^{\infty}\varepsilon(t)\exp(-i\omega t)dt, \tag{2.72}$$

the stress-strain relation in terms of the circular frequency ω is given by

$$\tilde{\sigma}(\omega) = E(1 + i\omega E'/E)\tilde{\varepsilon}(\omega). \tag{2.73}$$

Similarly, the potentials ϕ and ψ_n can be transformed into $\tilde{\phi}$ and $\tilde{\psi}_n$ in terms of ω, yielding

$$\left(1 + i\omega\frac{(\lambda' + 2\mu')}{(\lambda + 2\mu)}\right)\nabla^2\tilde{\phi} = -\frac{\omega^2}{c_p^2}\tilde{\phi}, \tag{2.74}$$

$$\left(1 + i\omega\frac{\mu'}{\mu}\right)\nabla^2\tilde{\psi}_n = -\frac{\omega^2}{c_s^2}\tilde{\psi}_n, \quad n = 1, 2, 3, \tag{2.75}$$

where

$$\tilde{\phi} = \int_{-\infty}^{\infty}\phi(t)\exp(-i\omega t)dt \quad \text{and} \quad \tilde{\psi}_n = \int_{-\infty}^{\infty}\psi(t)\exp(-i\omega t)dt. \tag{2.76}$$

The Lamé parameters (2.66) and (2.67) are rewritten as $\lambda \to \lambda + i\omega\lambda'$ and $\mu \to \mu + i\omega\mu'$.

2.5 Hysteretic damping

Many studies of the mechanical behaviour of materials are frequently described with the Kelvin-Voigt model. This model considers that the damping is proportional to the frequency. A variation of this model was introduced by Hardin [1965]. Hardin assumed that the viscosity decreases with the frequency such that the ratio viscosity to shear modulus remains constant with the frequency. Theodersen and Garrick [1940] were the first to propose the frequency-independent structural damping model. Later, Bishop [1955] introduced the label constant hysteretic model.

Inaudi and Kelly [1995] formulated that the Hilbert transform gives a time-domain expression for the concept of linear hysteretic damping. An analysis of the causal hysteretic element is given by Makris [1997], and Makris and Zhang [2000]. The behaviour of soils with hysteretic damping is studied in Verruijt [1999].

Hysteretic damping or structural damping denotes internal damping. Usually, the Lamé constants in the frequency domain are given by

$$\mu \rightarrow \mu(1 + i2\zeta sign(\omega)), \tag{2.77}$$

$$\lambda \rightarrow \lambda(1 + i2\zeta sign(\omega)), \tag{2.78}$$

where $sign(\omega)$ denotes the sign of ω and ζ is the damping ratio (correspondence principle). More information can be found in the texts of Wolf [1988, 1994].

The damping ratio is commonly expressed as D in geotechnical engineering. This is a measure of the attenuation or energy dissipation. Richart *et al.* [1970] defined the

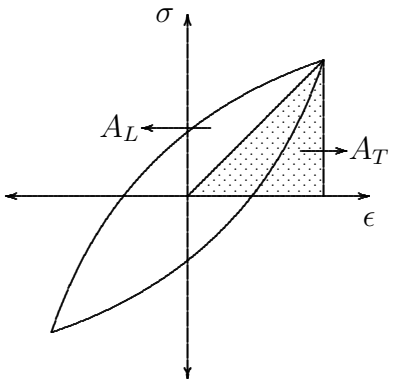

Figure 2.7: The loop of stress-strain relation, damping ratio.

damping ratio as the ratio of the energy dissipated per cycle of harmonic excitation in a certain volume to the peak elastic energy stored in the same volume. It is given by

$$\mathsf{D} = \frac{A_L}{4\pi A_T}. \tag{2.79}$$

where A_L indicates the strain energy represented by area under the hysteretic loop and A_T indicates the triangular area, as depicted in Figure 2.7.

The damping ratio of the Kelvin-Voigt model is proportional to the frequency and can be expressed as

$$\mathsf{D}_\mu = 0.5\frac{\omega\mu'}{\mu} \quad \text{and} \quad \mathsf{D}_\lambda = 0.5\frac{\omega\lambda'}{\lambda}, \tag{2.80}$$

where D_μ and D_λ denote the damping ratios for the Lamé constants. Figure 2.8 shows the physical variation of the damping ratio ζ with the circular frequency ω.

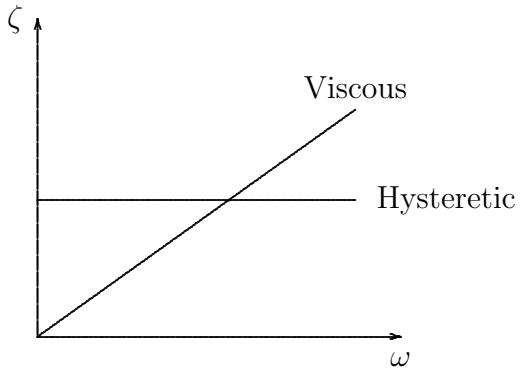

Figure 2.8: Viscous damping and hysteretic damping in terms of the circular frequency.

Chapter 3

Vibrating load on an elastic half-space with hysteretic damping

The objective of this chapter is to examine the effects of vibrating loads on an elastic material with hysteretic damping. Another objective is to determine the effects of Poisson's ratio and frequency of vibration. Analytical solutions for the propagation of waves in an elastic medium due to vibrating loads on the surface of a half-space have been studied by many researchers. Important contributions were made by Lamb [1904], Reissner [1936], Miller and Pursey [1954, 1955], Arnold *et al.* [1955], Ewing *et al.* [1957], Lysmer *et al.* [1966]. and Karasudhi *et al.* [1968]. A study of the dynamic response of circular footings was presented by Luco *et al.* [1971]. Vibrations of rigid bodies on elastic media when the bodies are excited at high frequency were studied by Awojobi [1965, 1971], with special emphasis on materials in which the stiffness increases linearly with the depth. Kausel and Roësset [1975] examined the effects of internal damping, layer depth, Poisson's ratio, and embedment on the stiffness functions of circular footings due to dynamic forces. Kausel and Roësset [1981] presented a transfer matrix method for wave amplification through layered media. Impedance functions for foundations embedded in a half-space medium were examined by Luco and Wong [1986], Apsel and Luco [1987], and de Barros and Luco [1995]. Traffic-induced ground vibrations were analyzed by Hao and Ang [1998]. The static solution had been obtained by Boussinesq [1885] and Love [1924].

Here, the problem of waves due to a vibrating load on the surface of an isotropic elastic half-space with hysteretic damping is examined.

3.1 Axially symmetric system

An axially symmetric system is considered and the vertical z-axis is the axis of symmetry, see Figure 3.1. A method for solving this axially symmetric system is to use the Hankel transformation. The basic equations of motion in three dimensions in cylindrical coordinates (r, θ, z) are

$$\partial_r \sigma_{rr} + \partial_z \sigma_{rz} + \frac{1}{r}(\sigma_{rr} - \sigma_{\theta\theta}) = \rho \partial_{tt}^2 u_r, \tag{3.1}$$

$$\partial_r \sigma_{rz} + \partial_z \sigma_{zz} + \frac{1}{r}\sigma_{rz} = \rho \partial_{tt}^2 u_z, \tag{3.2}$$

where u_r and u_z are the displacements in the r and z directions, with $r \geq 0$ and $z \geq 0$, and σ_{ij} are the stresses with $i, j = r, \theta$ and z. Because of the axial symmetry

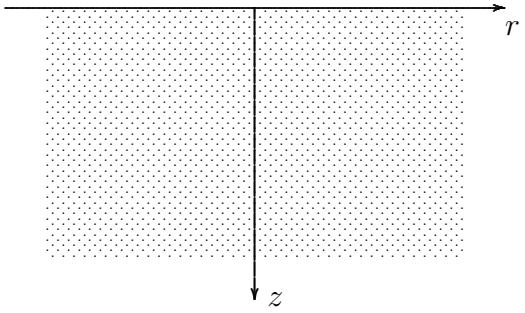

Figure 3.1: Half-space.

with respect to the z-axis, the displacements $u_r = u_r(r, z, t)$ and $u_z = u_z(r, z, t)$ are only expressed in terms of the coordinates r and z, and time t. In this case, the displacement $u_\theta = 0$ and the partial derivatives with respect to θ are zero, $\partial_\theta = 0$. The displacements can also be written using the potential functions $\phi = \phi(r, z, t)$ and $\psi = \psi(r, z, t)$ (Eringen and Suhubi [1975]),

$$u_r = \partial_r \phi + \partial_r \partial_z \psi, \tag{3.3}$$

$$u_z = \partial_z \phi - \partial_{rr}^2 \psi - \frac{1}{r}\partial_r \psi. \tag{3.4}$$

The components of the stress field of the system in terms of ϕ and ψ are, assuming that the material is isotropic elastic, with viscous damping,

$$\sigma_{rr} = \lambda \nabla^2 \phi + \lambda t_r \partial_t \nabla^2 \phi + 2\mu(\partial_{rr}^2 \phi + \partial_{rr}^2 \partial_z \psi) + 2\mu t_r \partial_t (\partial_{rr}^2 \phi + \partial_{rr}^2 \partial_z \psi), \tag{3.5}$$

$$\sigma_{\theta\theta} = \lambda \nabla^2 \phi + \lambda t_r \partial_t \nabla^2 \phi + 2\mu \frac{1}{r}(\partial_r \phi + \partial_r \partial_z \psi) + 2\mu \frac{1}{r} t_r \partial_t (\partial_r \phi + \partial_r \partial_z \psi), \tag{3.6}$$

$$\begin{aligned} \sigma_{zz} = {} & \lambda \nabla^2 \phi + \lambda t_r \partial_t \nabla^2 \phi + 2\mu \left(\partial_{zz}^2 \phi - \partial_{rr}^2 \partial_z \psi - \frac{1}{r}\partial_r \partial_z \psi \right) \\ & + 2\mu t_r \partial_t \left(\partial_{zz}^2 \phi - \partial_{rr}^2 \partial_z \psi - \frac{1}{r}\partial_r \partial_z \psi \right), \end{aligned} \tag{3.7}$$

$$\begin{aligned} \sigma_{rz} = {} & \mu \left(2\partial_r \partial_z \phi + \partial_r \partial_{zz}^2 \psi - \partial_{rrr}^3 \psi + \frac{1}{r^2}\partial_r \psi - \frac{1}{r}\partial_{rr}^2 \psi \right) \\ & + \mu t_r \partial_t \left(2\partial_r \partial_z \phi + \partial_r \partial_{zz}^2 \psi - \partial_{rrr}^3 \psi + \frac{1}{r^2}\partial_r \psi - \frac{1}{r}\partial_{rr}^2 \psi \right), \end{aligned} \tag{3.8}$$

where t_r is the response time of the material, describing the effect of viscous damping, and the Laplacian ∇^2 is defined as

$$\nabla^2 = \partial_{rr}^2 + \frac{1}{r}\partial_r + \partial_{zz}^2. \tag{3.9}$$

Introducing (3.5) - (3.8) into (3.1) and (3.2) shows that the basic equations can be satisfied if the potentials are solutions of

$$\nabla^2\phi + t_r\partial_t\nabla^2\phi = \frac{1}{c_p^2}\partial_{tt}^2\phi, \tag{3.10}$$

$$\nabla^2\psi + t_r\partial_t\nabla^2\psi = \frac{1}{c_s^2}\partial_{tt}^2\psi, \tag{3.11}$$

where c_p and c_s are defined by $c_p^2 = (\lambda + 2\mu)/\rho$ and $c_s^2 = \mu/\rho$.

3.2 Vibrating load on a half-space

The case of a half-space, which supports a uniform vibrating load on the surface $z = 0$ will be studied in detail (Miller and Pursey [1954]), see Figure 3.2. The load has a constant circular frequency ω in time, with $\omega > 0$. Therefore, the potential functions can be considered to be of the following form

$$\phi(r, z, t) = \breve{\phi}(r, z)\exp(i\omega t), \tag{3.12}$$

$$\psi(r, z, t) = \breve{\psi}(r, z)\exp(i\omega t), \tag{3.13}$$

where $\breve{\phi}$ and $\breve{\psi}$ are functions in terms of r and z and $\exp(i\omega t)$ is a time factor. Hence,

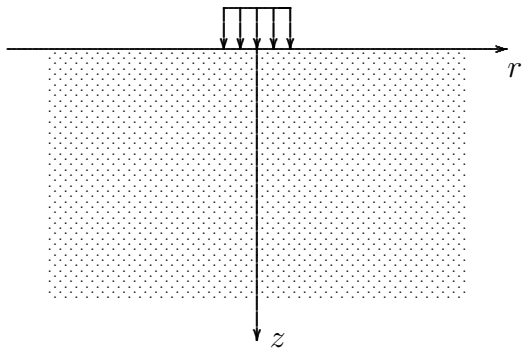

Figure 3.2: Vibrating load on a half-space.

the expressions of the basic potential functions (3.10) and (3.11) can be rewritten as

$$\nabla^2\breve{\phi} + \frac{k_p^2}{1 + i\omega t_r}\breve{\phi} = 0, \tag{3.14}$$

$$\nabla^2 \breve{\psi} + \frac{k_s^2}{1 + i\omega t_r} \breve{\psi} = 0, \tag{3.15}$$

where the positive parameters k_p and k_s are related to the frequency ω by

$$k_p = \frac{\omega}{c_p} \quad \text{and} \quad k_s = \frac{\omega}{c_s}. \tag{3.16}$$

Substitution of (3.12) and (3.13) into (3.5) - (3.8) leads to the following expressions for the stress components

$$\breve{\sigma}_{rr} = \lambda(1 + i\omega t_r)\nabla^2 \breve{\phi} + 2\mu(1 + i\omega t_r)(\partial_{rr}^2 \breve{\phi} + \partial_{rr}^2 \partial_z \breve{\psi}), \tag{3.17}$$

$$\breve{\sigma}_{\theta\theta} = \lambda(1 + i\omega t_r)\nabla^2 \breve{\phi} + 2\mu(1 + i\omega t_r)\frac{1}{r}(\partial_r \breve{\phi} + \partial_r \partial_z \breve{\psi}), \tag{3.18}$$

$$\breve{\sigma}_{zz} = \lambda(1 + i\omega t_r)\nabla^2 \breve{\phi} + 2\mu(1 + i\omega t_r)\left(\partial_{zz}^2 \breve{\phi} - \partial_{rr}^2 \partial_z \breve{\psi} - \frac{1}{r}\partial_r \partial_z \breve{\psi}\right), \tag{3.19}$$

$$\breve{\sigma}_{rz} = \mu(1 + i\omega t_r)\left(2\partial_r \partial_z \breve{\phi} + \partial_r \partial_{zz}^2 \breve{\psi} - \partial_{rrr}^3 \breve{\psi} + \frac{1}{r^2}\partial_r \breve{\psi} - \frac{1}{r}\partial_{rr}^2 \breve{\psi}\right). \tag{3.20}$$

The displacements are given by

$$u_r(r, z, t) = \breve{u}_r(r, z)\exp(i\omega t), \tag{3.21}$$

$$u_z(r, z, t) = \breve{u}_z(r, z)\exp(i\omega t). \tag{3.22}$$

3.3 Uniform load over circular area

In order to represent a uniform normal circular load at a surface which has a radius r_0, it is assumed that the boundary conditions on the free surface $z = 0$ are given by

$$z = 0 \ : \ \sigma_{rz} = 0, \tag{3.23}$$

$$z = 0 \ : \ \sigma_{zz} = \begin{cases} -p_0 \exp(i\omega t), & r < r_0, \\ 0, & r > r_0, \end{cases} \tag{3.24}$$

where p_0 is the amplitude of the vertical stress over the circular area. By application of the method of Hankel transformations of order zero, the transformed potentials $\breve{\phi}$ and $\breve{\psi}$, become

$$\tilde{\phi}(\xi, z) = \int_0^\infty \breve{\phi}(r, z) r J_0(\xi r)\, dr, \tag{3.25}$$

$$\tilde{\psi}(\xi, z) = \int_0^\infty \breve{\psi}(r, z) r J_0(\xi r)\, dr, \tag{3.26}$$

where ξ is the radial wave number. The inverse Hankel transformations are defined as

$$\breve{\phi}(r, z) = \int_0^\infty \tilde{\phi}(\xi, z) \xi J_0(\xi r)\, d\xi, \tag{3.27}$$

$$\breve{\psi}(r, z) = \int_0^\infty \tilde{\psi}(\xi, z) \xi J_0(\xi r)\, d\xi. \tag{3.28}$$

Introducing (3.25) and (3.26) into (3.14) and (3.15) leads to the following equations

$$\partial^2_{zz}\tilde{\phi} - a^2\tilde{\phi} = 0, \tag{3.29}$$

$$\partial^2_{zz}\tilde{\psi} - b^2\tilde{\psi} = 0, \tag{3.30}$$

where the wave numbers a and b are expressed as

$$a^2 = \xi^2 - \frac{k_p^2}{1 + i\omega t_r} = R_p^2 \exp(i2\vartheta_p), \tag{3.31}$$

$$b^2 = \xi^2 - \frac{k_s^2}{1 + i\omega t_r} = R_s^2 \exp(i2\vartheta_s), \tag{3.32}$$

in which R_p, R_s, and the angles ϑ_p and ϑ_s are defined by

$$R_p^4 = \frac{(\xi^2 - k_p^2)^2 + \xi^4(\omega t_r)^2}{1 + (\omega t_r)^2}, \tag{3.33}$$

$$R_s^4 = \frac{(\xi^2 - k_s^2)^2 + \xi^4(\omega t_r)^2}{1 + (\omega t_r)^2}, \tag{3.34}$$

$$\vartheta_p = \frac{1}{2}\arctan\left(\frac{k_p^2 \omega t_r}{\xi^2(1 + (\omega t_r)^2) - k_p^2}\right); \quad 0 \le \vartheta_p < \pi/2, \tag{3.35}$$

$$\vartheta_s = \frac{1}{2}\arctan\left(\frac{k_s^2 \omega t_r}{\xi^2(1 + (\omega t_r)^2) - k_s^2}\right); \quad 0 \le \vartheta_s < \pi/2. \tag{3.36}$$

The solutions of (3.29) and (3.30) which are finite for very large z are now

$$\tilde{\phi}(\xi, z) = \tilde{A}(\xi) \exp(-az), \tag{3.37}$$

$$\tilde{\psi}(\xi, z) = \tilde{B}(\xi) \exp(-bz), \tag{3.38}$$

where the arbitrary complex functions $\tilde{A}$ and $\tilde{B}$ are given in terms of the radial wave number ξ. It is assumed that the wave numbers a and b have the property that their real and imaginary parts are always positive if the response time $t_r \neq 0$. The values of ϑ_p and ϑ_s lie in the interval $[0, \pi/2)$. This assumption is needed because it is required that for $z \to \infty$, and waves propagating in positive z-direction, $\tilde{\phi}$ and $\tilde{\psi}$ must vanish. These solutions satisfy the radiation condition, see Sommerfeld [1949].

Introducing (3.37) and (3.38) into (3.19) and (3.20), the expressions for $\breve{\sigma}_{zz}$ and $\breve{\sigma}_{rz}$ are found after application of the inverse Hankel transformations,

$$\breve{\sigma}_{zz}(r,z) = (1+i\omega t_r)\int_0^\infty ((-\lambda\xi^2 + a^2(\lambda+2\mu))\tilde{A}\exp(-az) - b2\mu\xi^2\tilde{B}\exp(-bz))\xi J_0(\xi r)\,d\xi, \tag{3.39}$$

$$\breve{\sigma}_{rz}(r,z) = (1+i\omega t_r)\mu\int_0^\infty (2a\xi\tilde{A}\exp(-az) - (b^2\xi+\xi^3)\tilde{B}\exp(-bz))\xi J_1(\xi r)\,d\xi, \tag{3.40}$$

with the aid of the properties of the Bessel functions (Abramowitz and Stegun [1964]),

$$\frac{dJ_0(\xi r)}{dr} = -\xi J_1(\xi r), \tag{3.41}$$

$$\frac{d^2J_0(\xi r)}{dr^2} + \frac{1}{r}\frac{dJ_0(\xi r)}{dr} = -\xi^2 J_0(\xi r), \tag{3.42}$$

$$-\frac{d^3J_0(\xi r)}{dr^3} + \frac{1}{r^2}\frac{dJ_0(\xi r)}{dr} - \frac{1}{r}\frac{d^2J_0(\xi r)}{dr^2} = -\xi^3 J_1(\xi r). \tag{3.43}$$

By application of the Hankel transformation in the boundary conditions (3.23) and (3.24), and using (3.39) and (3.40) for $z = 0$, the following system of equations arises

$$2a\tilde{A} - (\xi^2 + b^2)\tilde{B} = 0, \tag{3.44}$$

$$(\lambda(a^2-\xi^2) + 2\mu a^2)\tilde{A} - 2b\mu\xi^2\tilde{B} = -p_0 r_0 \frac{J_1(\xi r_0)}{\xi(1+i\omega t_r)}. \tag{3.45}$$

The solution of this system is

$$\tilde{A}(\xi) = -\frac{p_0 r_0}{\mu}\frac{1}{(1+i\omega t_r)}(\xi^2+b^2)\frac{J_1(\xi r_0)}{\xi\Delta}, \tag{3.46}$$

$$\tilde{B}(\xi) = -\frac{p_0 r_0}{\mu}\frac{1}{(1+i\omega t_r)}2a\frac{J_1(\xi r_0)}{\xi\Delta}, \tag{3.47}$$

where the determinant of the system Δ is defined as

$$\Delta = (\xi^2 + b^2)^2 - 4ab\xi^2. \tag{3.48}$$

It may be verified that the determinant is never equal to zero in the damped case for a real ξ. This determinant is also called Rayleigh's function $R(\xi)$ (Ewing *et al.* [1957]), when the value of t_r is equal to zero, it gives

$$R(\xi) = (2\xi^2 - k_s^2)^2 - 4(\xi^2 - k_s^2/m)^{1/2}(\xi^2 - k_s^2)^{1/2}\xi^2, \tag{3.49}$$

where the dimensionless parameter m is defined as

$$m = \frac{k_s^2}{k_p^2} = \frac{c_p^2}{c_s^2} = \frac{2(1-\nu)}{1-2\nu}. \tag{3.50}$$

In order to find the free annular Rayleigh waves, the vertical stress σ_{zz} on the surface may be assumed to be equal to zero. A solution for this case is possible only for values of ξ which satisfy the equation $R(\xi) = 0$. As mentioned before there are no zeros if the response time $t_r > 0$. Returning to the solutions (3.46) and (3.47), the potentials $\breve{\phi}$ and $\breve{\psi}$ are obtained after application of the respective inverse Hankel transformations,

$$\breve{\phi}(r,z) = -\frac{p_0 r_0}{\mu}\frac{1}{(1+i\omega t_r)}\int_0^\infty \exp(-az)\frac{(\xi^2+b^2)}{\Delta}J_1(\xi r_0)J_0(\xi r)\,d\xi, \tag{3.51}$$

$$\breve{\psi}(r,z) = -\frac{p_0 r_0}{\mu}\frac{1}{(1+i\omega t_r)}\int_0^\infty \exp(-bz)\frac{2a}{\Delta}J_1(\xi r_0)J_0(\xi r)\,d\xi. \tag{3.52}$$

Next, the expressions for $\breve{u}_r$ and $\breve{u}_z$ are

$$\breve{u}_r(r,z) = \frac{p_0 r_0}{\mu}\frac{1}{(1+i\omega t_r)}\int_0^\infty (\exp(-az)(\xi^2+b^2) - \exp(-bz)2ab)\frac{\xi}{\Delta} J_1(\xi r_0)J_1(\xi r)\,d\xi, \tag{3.53}$$

$$\breve{u}_z(r,z) = \frac{p_0 r_0}{\mu}\frac{1}{(1+i\omega t_r)}\int_0^\infty (\exp(-az)(\xi^2+b^2) - \exp(-bz)2\xi^2)\frac{a}{\Delta} J_1(\xi r_0)J_0(\xi r)\,d\xi. \tag{3.54}$$

3.3.1 Displacements at the surface

The vertical and radial displacements at the surface $z = 0$ are expressed by

$$\breve{u}_r(r,0) = \frac{p_0 r_0}{\mu}\frac{1}{(1+i\omega t_r)}\int_0^\infty (\xi^2+b^2-2ab)\frac{\xi}{\Delta}J_1(\xi r_0)J_1(\xi r)\,d\xi, \tag{3.55}$$

$$\breve{u}_z(r,0) = -\frac{p_0 r_0}{\mu}\frac{k_s^2}{(1+i\omega t_r)^2}\int_0^\infty \frac{a}{\Delta}J_1(\xi r_0)J_0(\xi r)\,d\xi. \tag{3.56}$$

In order to calculate $\breve{u}_z(r,0)$ as a function of the radial distance and of the time, it is useful to introduce the dimensionless parameters $d = r/r_0$, $\alpha = k_s r_0 = \omega r_0/c_s$ and $\beta = \xi/k_s$ into the right hand side of (3.56). Therefore,

$$\breve{u}_z(r,0) = -\frac{p_0 r_0}{\mu}\frac{1}{(1+i\omega t_r)^2}\int_0^\infty F(\beta)J_1(\alpha\beta)J_0(d\alpha\beta)\,d\beta, \tag{3.57}$$

with

$$F(\beta) = \frac{a_a}{(\beta^2+b_b^2)^2 - 4a_a b_b \beta^2}, \tag{3.58}$$

where the dimensionless wave numbers a_a and b_b are related by

$$a_a^2 = \frac{a^2}{k_s^2} = \beta^2 - \frac{1}{m(1+i\omega t_r)}, \tag{3.59}$$

$$b_b^2 = \frac{b^2}{k_s^2} = \beta^2 - \frac{1}{(1+i\omega t_r)}. \tag{3.60}$$

The real and imaginary parts of a_a and b_b must be positive if the response time of the material $t_r \neq 0$. The parameters d and α represent the dimensionless radial distance and circular frequency, respectively.

3.3.2 Quasi-static solution

The quasi-static solution of the vertical displacement on the surface $u_z(r,0,t)$ means here the limiting behaviour of $\breve{u}_z(r,0)$ for the case $\alpha = \omega r_0/c_s \to 0$. Introducing a new variable of integration $\kappa_0 = \alpha\beta$ in (3.57), yields

$$\begin{aligned} u_z(r,0,t) &= -\frac{p_0 r_0}{\mu}\frac{\exp(i\omega t)}{\alpha(1+i\omega t_r)^2}\int_0^\infty F(\kappa_0/\alpha)J_1(\kappa_0)J_0(d\kappa_0)\,d\kappa_0 \\ &= -\frac{p_0 r_0}{\mu}\frac{m}{2(m-1)}\frac{\exp(i\omega t)}{(1+i\omega t_r)}\int_0^\infty \frac{J_1(\kappa_0)J_0(d\kappa_0)}{\kappa_0}\,d\kappa_0. \end{aligned} \tag{3.61}$$

It may be noted that this expression is identical for the case of a static uniform load over a circular area on the surface, given by Timoshenko and Goodier [1951], except for the factors $\exp(i\omega t)$ and $(1+i\omega t_r)$, which represent for the first factor the fluctuation of the load, and for the second factor a reduction of the amplitude by damping.

In order to calculate the quasi-static solution at the origin, the parameter d can be taken as $d = 0$, the dynamic amplification factor u_z/u_{zs} and the quasi-static vertical displacement amplitude at the origin u_{zs}, given as reference, are introduced. These expressions are defined by

$$\frac{u_z}{u_{zs}} = h\exp(i\omega t), \tag{3.62}$$

where

$$u_{zs} = \frac{p_0 r_0}{\mu} \frac{m}{2(m-1)} \frac{1}{(1+i\omega t_r)} = \frac{p_0 r_0}{\mu} \frac{1}{(1+i\omega t_r)}(1-\nu), \tag{3.63}$$

and the complex function $h = h_1 + ih_2$ is the response function of the surface, which can now be expressed as

$$h = -\frac{1}{(1-\nu)(1+i\omega t_r)} I(\alpha), \tag{3.64}$$

with the integral I defined by

$$I(\alpha) = \int_0^\infty F(\beta) J_1(\alpha\beta) J_0(d\alpha\beta)\, d\beta. \tag{3.65}$$

The value of the integral I will be evaluated numerically. This evaluation is possible for the case of a damped problem, since there is no singularity for all values of β if a non-zero damping is considered. The numerical solution for very small values of the circular frequency will be compared with the static solution (Boussinesq problem).

The hysteretic damping of the material is described by the damping factor ζ. It is assumed to be a constant material property, and independent of the circular frequency ω. It is defined as

$$\zeta = \frac{1}{2}\omega t_r. \tag{3.66}$$

Next, R_p, R_s, ϑ_p and ϑ_s are rewritten as

$$R_p^4 = \frac{(\xi^2 - k_p^2)^2 + 4\xi^4\zeta^2}{1+4\zeta^2}, \tag{3.67}$$

$$R_s^4 = \frac{(\xi^2 - k_s^2)^2 + 4\xi^4\zeta^2}{1+4\zeta^2}, \tag{3.68}$$

$$\vartheta_p = \frac{1}{2}\arctan\left(\frac{2k_p^2\zeta}{\xi^2(1+4\zeta^2) - k_p^2}\right); \quad 0 \le \vartheta_p < \pi/2, \tag{3.69}$$

$$\vartheta_s = \frac{1}{2}\arctan\left(\frac{2k_s^2\zeta}{\xi^2(1+4\zeta^2) - k_s^2}\right); \quad 0 \le \vartheta_s < \pi/2. \tag{3.70}$$

The undamped case can be considered to be the limiting case for $\zeta \to 0$. The denominator of the function $F(\beta)$ in the integrand of (3.65) has a minimum for a value of β slightly larger than 1. This corresponds to the Rayleigh wave singularity in the undamped case. For a damping ratio $\zeta > 0$ there will be no singularities of the integrand, although the integrand may become very large for small values of ζ and a critical value of β, slightly larger than 1. Using Simpson's integration method,

the integral in (3.65) is calculated by subdividing the interval of integration $[0, \beta_{max}]$ into a number of sections, where β_{max} is the upper limit of the numerical integral. Furthermore, each section is subdivided into intervals. In the first intervals, in which the variation of the integrand is the largest, the subdivision has been taken finer.

The dynamic amplification factor u_z/u_{zs} is shown in Figure 3.3 for a very small value of the dimensionless frequency $\alpha = \omega r_0/c_s = 0.01$, the dimensionless radial parameter $d = r/r_0$, and β_{max}. Results for this case are similar to the static solution, given by Timoshenko and Goodier [1951], and are shown in the figure by dots. The agreement with the present quasi-static solution appears to be very good.

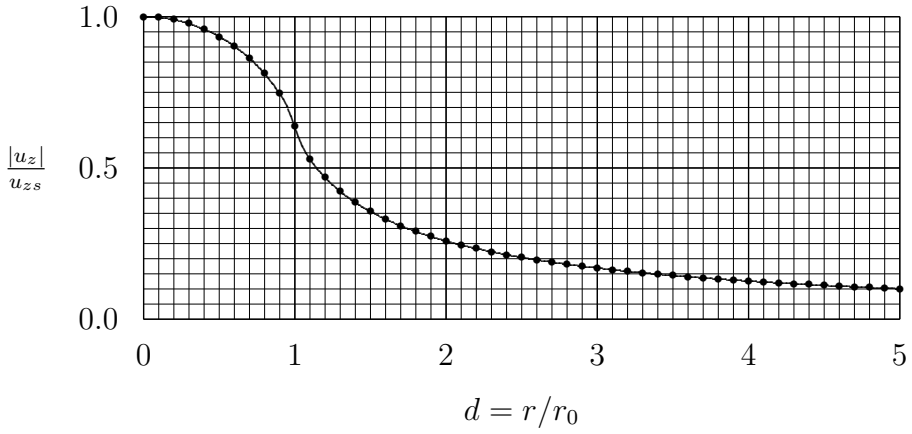

Figure 3.3: Static and quasi-static: $\nu = 0$, $\alpha = 0.01$, $\beta_{max} = 5000$.

The amplitude of the displacement for a higher circular frequency $\alpha = 1$ is shown in Figure 3.4, for two values of the damping ratio, $\zeta = 0.01$ and 0.1. It may be noted that the displacements are smaller for greater value of ζ, and that they decrease rapidly at small distances from the loaded area. In general, it can be seen that the influence of ζ is small, however. For soft soils a practical value for the damping ratio ζ can be considered to be 0.1.

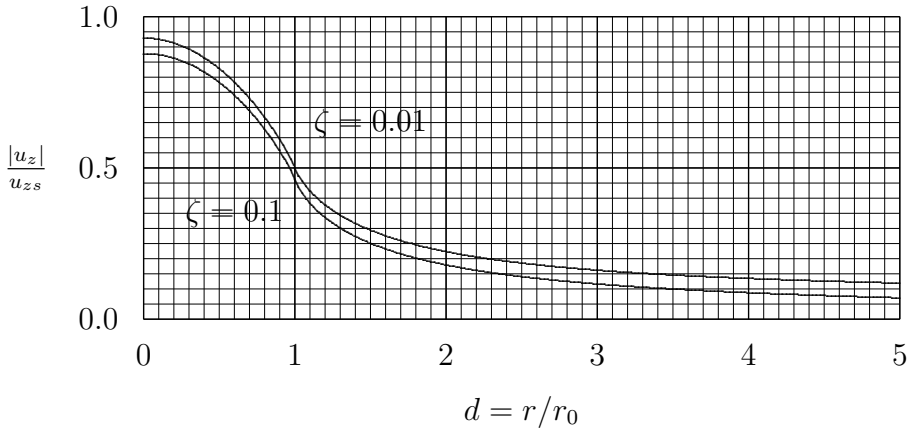

Figure 3.4: Vibrating circle: $\nu = 0$, $\alpha = 1$, $\beta_{max} = 10000$.

3.3.3 Vertical displacement at the origin

The vertical displacement at the origin u_{z0} is determined when the value of I is calculated for the case of $d = 0$. Using (3.57), it follows that

$$u_{z0} = -\frac{p_0 r_0}{\mu} \frac{\exp(i\omega t)}{(1 + i2\zeta)^2} I_0(\alpha), \tag{3.71}$$

in which the integral I_0 is given by

$$I_0(\alpha) = \int_0^\infty F(\beta) J_1(\alpha\beta)\, d\beta. \tag{3.72}$$

The dynamic amplification factor for the displacement at the origin u_{z0}/u_{zs} can be expressed by

$$\frac{u_{z0}}{u_{zs}} = f \exp(i\omega t), \tag{3.73}$$

where $f = f_1 + if_2$ is the response function at the origin, as already introduced by Reissner [1936] for an undamped material $t_r = 0$. For a damped material, it results in

$$f = -\frac{1}{(1 - \nu)(1 + i2\zeta)} I_0. \tag{3.74}$$

Using Simpson's numerical integration method the values of f_1, f_2 and the absolute value $|f|$ will be calculated in terms of the parameter $\alpha = \omega r_0/c_s$.

3.3.4 Point load

The case of a concentrated constant load P on the surface can be obtained when the radius of the circular load r_0 is very small or $r_0 \to 0$ and $p_0 \to \infty$, so that the vertical normal stress σ_{zz} at $z = 0$ can be considered as $p_0 = P/\pi r_0^2$. Therefore, using (3.56) the vertical displacement on the surface $z = 0$ is found to be

$$u_z(r, 0, t) = -\frac{P}{2\pi\mu} \frac{k_s^2 \exp(i\omega t)}{(1 + i2\zeta)^2} \int_0^\infty \frac{\xi a}{\Delta} J_0(\xi r)\, d\xi, \tag{3.75}$$

in which the function $J_1(\xi r_0) \approx \xi r_0/2$ if the radius of the loading area r_0 is supposed to be very small. In order to calculate the dynamic amplification factor on the surface, the response function on the surface $g = g_1 + ig_2$ and the static displacement for a point load u_{zs} on the surface are used. Hence,

$$\frac{u_z(r, 0, t)}{u_{zs}} = g \exp(i\omega t), \tag{3.76}$$

where g is defined as

$$g = -\frac{1}{(1 - \nu)(1 + i2\zeta)} G(\kappa), \tag{3.77}$$

and the integral G is given by

$$G(\kappa) = \int_0^\infty \beta\kappa F(\beta) J_0(\kappa\beta)\, d\beta, \tag{3.78}$$

in which the dimensionless radial distance factor, $\kappa = k_s r = \omega r/c_s$ is introduced. It may be noted that the integral in (3.78) represents the Hankel transformation of order zero of the function $F(\beta)$, multiplied by the factor κ.

3.3.5 Numerical integration

For the calculation of the dynamic amplification factor Simpson's numerical integration

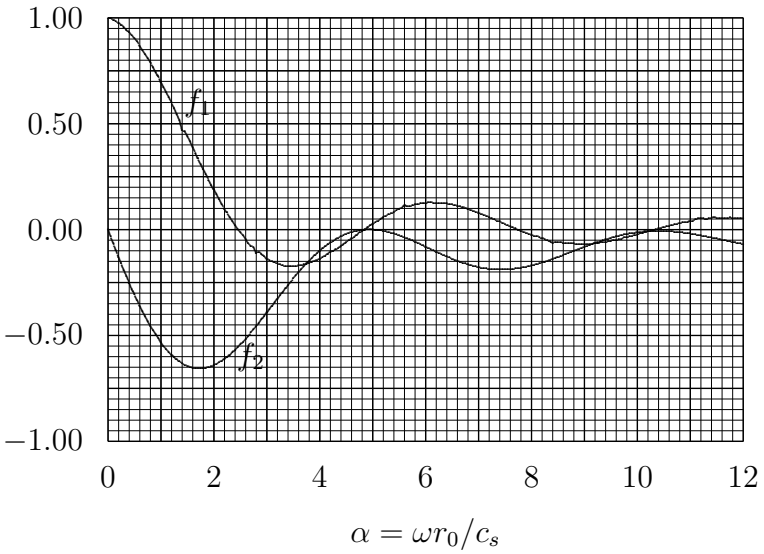

Figure 3.5: Real and imaginary values of the displacement at origin, $d = 0$: $\nu = 0$, $\zeta = 0.1$, $\beta_{max} = 10000$.

method will be used, since this integral is not singular for all values of β. The factor $F(\beta)/(1 + i2\zeta)$ is given by

$$\frac{F(\beta)}{1 + i2\zeta} = \frac{a_a(1 - i2\zeta)}{\Delta_\beta(1 + 4\zeta^2)}, \tag{3.79}$$

where

$$a_a^2 = \beta^2 - \frac{1}{m(1 + i2\zeta)}, \tag{3.80}$$

$$b_b^2 = \beta^2 - \frac{1}{(1 + i2\zeta)}, \tag{3.81}$$

$$\Delta_\beta = (\beta^2 + b_b^2)^2 - 4a_a b_b \beta^2. \tag{3.82}$$

The real and imaginary parts of f are given in Figure 3.5. It can be seen from this figure that f_1 and f_2 are practically equal to zero for certain values of α, and that these zeros are almost the same. For other values of ν, it can be observed that f_1 and f_2 are practically equal to zero for certain values of α, but these zeros are not always the same. It may be also added that the response functions remain almost unchanged if ζ is taken to be a factor 10 smaller or larger. Figure 3.6 shows the absolute value $|f|$. It can be seen from this figure that the dynamic amplitude is always smaller than the quasi-static amplitude, obtained when the load vibrates at a very small circular frequency ω. For values of $|f| \approx 0$ then the dynamic amplification factor $u_{z0}/u_{zs} \approx 0$.

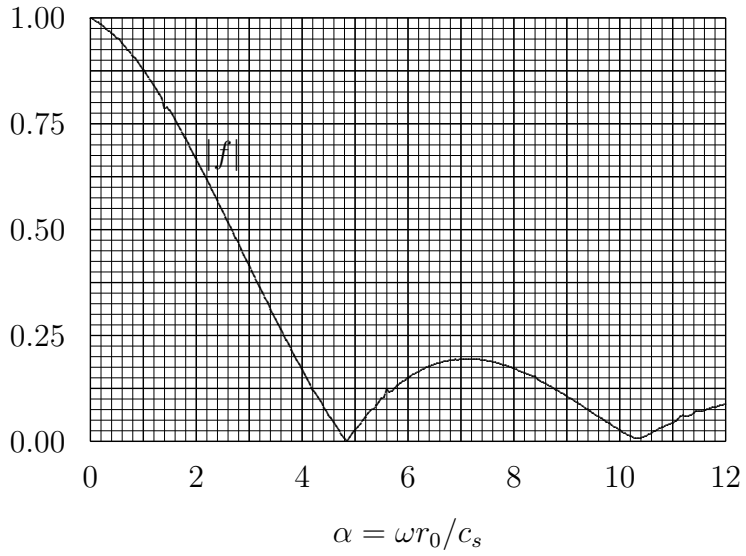

Figure 3.6: Absolute value of the displacement at origin, $d = 0$: $\nu = 0$, $\zeta = 0.1$, $\beta_{max} = 10000$.

3.3.6 Average displacement

A particular quantity is the average vertical displacement of the loaded area on the surface $\overline{u}_z$, see Miller and Pursey [1954]. This is defined as

$$\overline{u}_z = \frac{1}{\pi r_0^2} \int_0^{2\pi} \int_0^{r_0} u_z(r,0) r \, dr d\theta = \frac{2}{r_0^2} \int_0^{r_0} u_z(r,0) r \, dr. \tag{3.83}$$

Using (3.56), the time factor $\exp(i\omega t)$ and the property of Bessel functions from Abramowitz & Stegun [1964],

$$\int_0^{r_0} J_0(\xi r) r \, dr = \frac{r_0}{\xi} J_1(r_0 \xi), \tag{3.84}$$

in (3.83), the expression for $\overline{u}_z$ becomes

$$\begin{aligned} \overline{u}_z &= -\frac{2p_0}{\mu} \frac{k_s^2 \exp(i\omega t)}{(1+i2\zeta)^2} \int_0^{\infty} \frac{a}{\Delta} \frac{J_1^2(r_0\xi)}{\xi} \, d\xi \\ &= -\frac{2p_0 r_0}{\mu} \frac{\exp(i\omega t)}{(1+i2\zeta)^2} \int_0^{\infty} F(\beta) \frac{J_1^2(\alpha\beta)}{\alpha\beta} \, d\beta. \end{aligned} \tag{3.85}$$

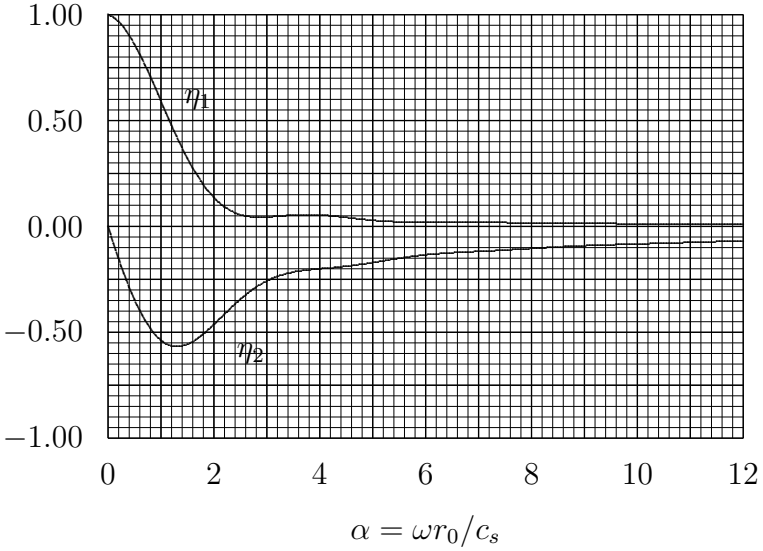

Figure 3.7: Real and imaginary values of the average displacement: $\nu = 0$, $\zeta = 0.1$, $\beta_{max} = 10000$.

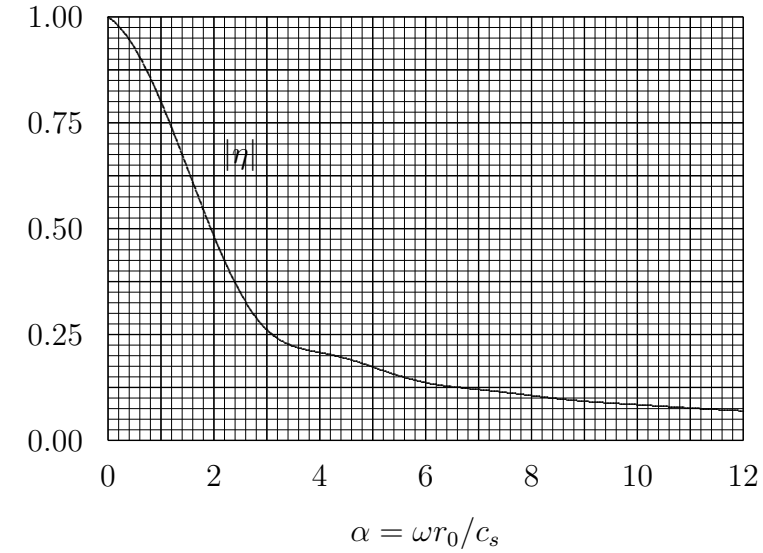

Figure 3.8: Absolute value of the average displacement: $\nu = 0$, $\zeta = 0.1$, $\beta_{max} = 10000$.

On the other hand, the amplitude of the average vertical displacement in the quasi-static case $\overline{u}_{zs}$ is

$$\overline{u}_{zs} = \frac{4p_0 r_0}{3\pi\mu} \frac{m}{(m-1)(1+i2\zeta)} = \frac{8p_0 r_0}{3\pi\mu} \frac{(1-\nu)}{(1+i2\zeta)}, \tag{3.86}$$

where the effect of the damping on the quasi static response has been included in the factor $(1 + i2\zeta)$. In order to calculate (3.86) it has been necessary to use the solution of a uniform static load over the circular area, see Timoshenko and Goodier [1951] and the relation of Struve's integral (Watson [1962], section 13.33),

$$\int_0^\infty \frac{J_1^2(t)}{t^2}\, dt = \frac{4}{3\pi}. \tag{3.87}$$

The dynamic amplification factor $\overline{u}_z/\overline{u}_{zs}$ is expressed as

$$\frac{\overline{u}_z}{\overline{u}_{zs}} = \eta \exp(i\omega t), \tag{3.88}$$

where the complex response factor $\eta = \eta_1 + i\eta_2$. The value η is given by

$$\eta = -\frac{N(\alpha)}{(1-\nu)(1+i2\zeta)}, \tag{3.89}$$

with

$$N(\alpha) = \frac{3\pi}{4} \int_0^\infty \frac{F(\beta) J_1^2(\alpha\beta)}{\alpha\beta}\, d\beta. \tag{3.90}$$

The value of N has been determined numerically. The integral in (3.90) is reduced to the quasi-static case for the limiting case of $\alpha = \omega r_0/c_s \to 0$.

The response functions η_1 and η_2 are shown in Figure 3.7, as a function of the dimensionless parameter α. Compared to the response functions at the origin f_1 and f_2 in Figure 3.5, the oscillations have almost disappeared.

Figure 3.8 shows the amplitude of the dynamic amplification factor of the average displacement $|\eta|$. This figure shows that the maximum displacement occurs in the quasi-static case $\alpha = 0$ and that the average displacement diminishes almost monotonically with increasing angular frequency. For other values of ν, it can be verified that the influence of ν on the average displacement is small. Furthermore, it may also be verified that the influence of ζ on the average displacement is relatively small.

3.4 Uniform load over a rigid circular plate

In the case of a rigid circular plate, it is assumed that there is no friction between the base of the plate and the medium (Das [1983]). The stress distribution below the plate has been assumed to be the same as in the static case (Timoshenko and Goodier [1951]). It follows that the boundary conditions on the surface $z = 0$ are assumed to be

$$z = 0 \ : \ \sigma_{rz} = 0, \tag{3.91}$$

$$z = 0 \ : \ \sigma_{zz} = \begin{cases} -\frac{1}{2} p_0 r_0 (r_0^2 - r^2)^{-1/2} \exp(i\omega t), & r < r_0, \\ 0, & r > r_0, \end{cases} \tag{3.92}$$

In order to solve this case Hankel transformation method will be applied again. After using the Hankel transformations of the potentials and the respective stresses, the inverse Hankel transformations give

$$\breve{\phi}(r,z) = -\frac{p_0 r_0}{2\mu} \frac{1}{(1+i\omega t_r)} \int_0^\infty \exp(-az) \frac{(\xi^2 + b^2)}{\Delta} \sin(\xi r_0) J_0(\xi r)\, d\xi, \tag{3.93}$$

$$\breve{\psi}(r,z) = -\frac{p_0 r_0}{2\mu} \frac{1}{(1+i\omega t_r)} \int_0^\infty \exp(-bz) \frac{2a}{\Delta} \sin(\xi r_0) J_0(\xi r)\, d\xi. \tag{3.94}$$

It can be seen that the only difference between these results and (3.51) and (3.52) is the factor $J_1(\xi r_0)$. This factor has been replaced by the factor $\sin(\xi r_0)/2$. It implies that the vertical displacement of the surface $z = 0$ is, in dimensionless form

$$u_z(r,0,t) = -\frac{p_0 r_0}{2\mu} \frac{\exp(i\omega t)}{(1+i\omega t_r)^2} \int_0^\infty F(\beta) \sin(\alpha\beta) J_0(d\alpha\beta)\, d\beta, \tag{3.95}$$

with

$$F(\beta) = \frac{a_a}{(\beta^2 + b_b^2)^2 - 4 a_a b_b \beta^2}.$$

Taking $d = 0$, the displacement at the origin is

$$u_{z0} = -\frac{p_0 r_0}{2\mu} \frac{\exp(i\omega t)}{(1+i\omega t_r)^2} \int_0^\infty F(\beta) \sin(\alpha\beta)\, d\beta. \tag{3.96}$$

Introducing $\kappa_0 = \alpha\beta$ as variable of integration and the damping ratio ζ, defined in (3.66), and using the approximation

$$F(\kappa_0/\alpha) \approx -(1-\nu)(1+i2\zeta)\alpha/\kappa_0,$$

which is valid for small values of α, it follows that for the quasi-static case

$$u_{zs} = \frac{p_0 r_0 (1-\nu)}{2\mu(1+i2\zeta)} \int_0^\infty \frac{\sin(\kappa_0)}{\kappa_0}\, d\kappa_0 = \frac{\pi p_0 r_0 (1-\nu)}{4\mu(1+i2\zeta)}. \tag{3.97}$$

The dynamic amplification factor at the origin u_{z0}/u_{zs} is

$$\frac{u_{z0}}{u_{zs}} = -\frac{2\exp(i\omega t)}{\pi(1-\nu)(1+i2\zeta)} \int_0^\infty F(\beta) \sin(\alpha\beta)\, d\beta. \tag{3.98}$$

Similarly, the average displacement of the plate $\overline{u}_z$ is determined by

$$\overline{u}_z = -\frac{p_0 r_0 \exp(i\omega t)}{\mu(1+i2\zeta)^2} \int_0^\infty F(\beta) \frac{\sin(\alpha\beta) J_1(\alpha\beta)}{\alpha\beta}\, d\beta. \tag{3.99}$$

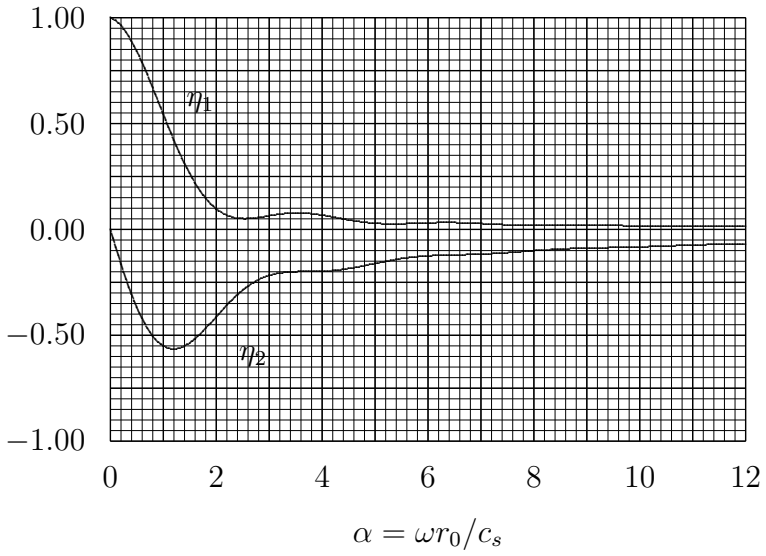

Figure 3.9: Real and imaginary values of the average displacement: $\nu = 0$, $\zeta = 0.1$, $\beta_{max} = 10000$.

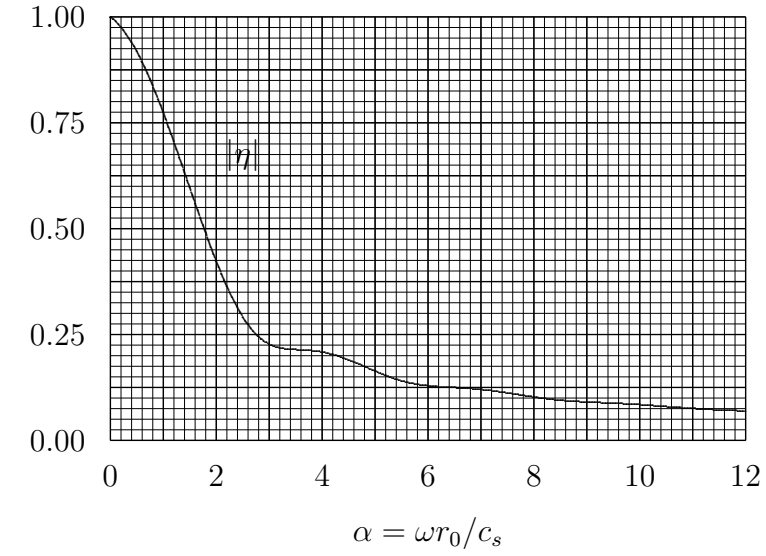

Figure 3.10: Absolute value of the average displacement: $\nu = 0$, $\zeta = 0.1$, $\beta_{max} = 10000$.

The dynamic amplification factor of the average displacement of the plate $\overline{u}_z/\overline{u}_{zs}$ is

$$\frac{\overline{u}_z}{\overline{u}_{zs}} = \eta \exp(i\omega t), \tag{3.100}$$

where the complex response factor $\eta = \eta_1 + i\eta_2$. This is given by

$$\eta = -\frac{4}{\pi(1-\nu)(1+i2\zeta)} \int_0^\infty \frac{F(\beta)\sin(\alpha\beta)J_1(\alpha\beta)}{\alpha\beta}\, d\beta.$$

The quasi-static case can be found when the limit of u_{z0} is calculated for $\alpha \to 0$, then $J_1(\alpha\beta) \to \alpha\beta/2$. For this quasi-static case, the expressions u_{zs} and $\overline{u}_{zs}$ are equal. The response functions η_1 and η_2 are depicted in Figure 3.9, as a function of the dimensionless parameter α. The comparison between these results and Figure 3.7 shows that they are very similar.

Figure 3.10 illustrates the amplitude of the dynamic amplification factor of the average displacement $|\eta|$. For very large values of the dimensionless parameter α the factor $\overline{u}_z/\overline{u}_{zs}$ is very small, compared to the quasi-static case $\alpha \to 0$.

3.5 Vibrating load on an elastic half-plane

Two-dimensional problems may be solved easier than their three-dimensional equivalents. This is due to the fact that the fundamental field equations in two-dimensions can be transformed to scalar wave equations, instead of the one scalar and one vector wave equation of three-dimensional theory. The text of Ewing *et al.* [1957] can be given as literature in this field. The case of propagation waves in an elastic half-plane is presented in this section, see Figure 3.11. The z-axis is considered as the axis of

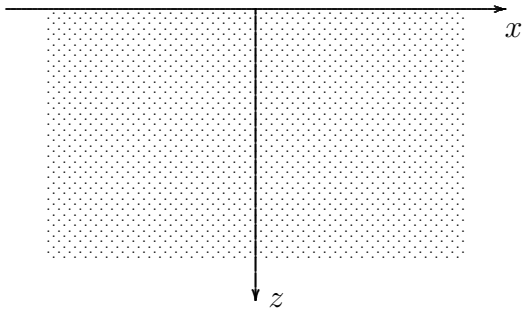

Figure 3.11: Half-plane.

symmetry. The basic equations of motion in two-dimensions take the following form

$$\partial_x \sigma_{xx} + \partial_z \sigma_{zx} = \rho \partial_{tt}^2 u_x, \tag{3.101}$$

$$\partial_x \sigma_{xz} + \partial_z \sigma_{zz} = \rho \partial_{tt}^2 u_z, \tag{3.102}$$

where $u_x(x,z,t)$ and $u_z(x,z,t)$ are the components of the displacements in the x and z directions, respectively. The displacements can be written in terms of the potential functions $\phi(x,z,t)$ and $\psi(x,z,t)$,

$$u_x = \partial_x\phi - \partial_z\psi, \tag{3.103}$$

$$u_z = \partial_z\phi + \partial_x\psi. \tag{3.104}$$

The stress components are also written as function of ϕ and ψ,

$$\begin{aligned}\sigma_{xx} &= \lambda(\partial^2_{xx}\phi + \partial^2_{zz}\phi) + \lambda t_r\partial_t(\partial^2_{xx}\phi + \partial^2_{zz}\phi)\\ &\quad + 2\mu(\partial^2_{xx}\phi - \partial_x\partial_z\psi) + 2\mu t_r\partial_t(\partial^2_{xx}\phi - \partial_x\partial_z\psi),\end{aligned} \tag{3.105}$$

$$\begin{aligned}\sigma_{zz} &= \lambda(\partial^2_{xx}\phi + \partial^2_{zz}\phi) + \lambda t_r\partial_t(\partial^2_{xx}\phi + \partial^2_{zz}\phi)\\ &\quad + 2\mu(\partial^2_{zz}\phi + \partial_x\partial_z\psi) + 2\mu t_r\partial_t(\partial^2_{zz}\phi + \partial_x\partial_z\psi),\end{aligned} \tag{3.106}$$

$$\sigma_{xz} = \mu(2\partial_x\partial_z\phi + \partial^2_{xx}\psi - \partial^2_{zz}\psi) + \mu t_r\partial_t(2\partial_x\partial_z\phi + \partial^2_{xx}\psi - \partial^2_{zz}\psi), \tag{3.107}$$

Substituting (3.103) - (3.107) into (3.101) and (3.102) shows that the basic equations can be satisfied if the potentials are solutions of

$$\partial^2_{xx}\phi + \partial^2_{zz}\phi + t_r\partial_t(\partial^2_{xx}\phi + \partial^2_{zz}\phi) = \frac{1}{c_p^2}\partial^2_{tt}\phi, \tag{3.108}$$

$$\partial^2_{xx}\psi + \partial^2_{zz}\psi + t_r\partial_t(\partial^2_{xx}\psi + \partial^2_{zz}\psi) = \frac{1}{c_s^2}\partial^2_{tt}\psi. \tag{3.109}$$

3.5.1 Vibrating strip load

The case of a vibrating strip load with circular frequency $\omega > 0$ on the surface $z = 0$ will be considered (Miller and Pursey [1954]), see Figure 3.12. The boundary conditions have the following form

$$z = 0 \ : \ \sigma_{xz} = 0, \tag{3.110}$$

$$z = 0 \ : \ \sigma_{zz} = \begin{cases} -p_0\exp(i\omega t), & |x| < x_0,\\ 0, & |x| > x_0,\end{cases} \tag{3.111}$$

where x_0 is the half length of the strip load. It is assumed that ϕ and ψ are

$$\phi(x,z,t) = \breve{\phi}(x,z)\exp(i\omega t), \tag{3.112}$$

$$\psi(x,z,t) = \breve{\psi}(x,z)\exp(i\omega t), \tag{3.113}$$

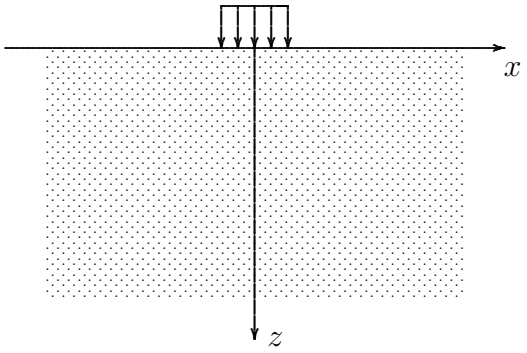

Figure 3.12: Vibrating load on a half-plane.

where $\breve{\phi}$ and $\breve{\psi}$ are functions in terms of x and z, and $\exp(i\omega t)$ is a time factor. Therefore, expressions (3.108) and (3.109) are rewritten as

$$\nabla^2\breve{\phi} + \frac{k_p^2}{1+i\omega t_r}\breve{\phi} = 0, \tag{3.114}$$

$$\nabla^2\breve{\psi} + \frac{k_s^2}{1+i\omega t_r}\breve{\psi} = 0, \tag{3.115}$$

where the Laplacian ∇^2 and the positive parameters k_p and k_s are defined as

$$\nabla^2 = \partial_{xx}^2 + \partial_{zz}^2, \tag{3.116}$$

$$k_p = \omega/c_p \quad \text{and} \quad k_s = \omega/c_s. \tag{3.117}$$

Introducing (3.112) and (3.113) into (3.105) - (3.107) leads to the following expressions for the stress components

$$\breve{\sigma}_{xx} = \lambda(1+i\omega t_r)\nabla^2\breve{\phi} + 2\mu(1+i\omega t_r)(\partial_{xx}^2\breve{\phi} - \partial_x\partial_z\breve{\psi}), \tag{3.118}$$

$$\breve{\sigma}_{zz} = \lambda(1+i\omega t_r)\nabla^2\breve{\phi} + 2\mu(1+i\omega t_r)(\partial_{zz}^2\breve{\phi} + \partial_x\partial_z\breve{\psi}), \tag{3.119}$$

$$\breve{\sigma}_{xz} = \mu(1+i\omega t_r)(2\partial_x\partial_z\breve{\phi} + \partial_{xx}^2\breve{\psi} - \partial_{zz}^2\breve{\psi}). \tag{3.120}$$

Using the exponential Fourier transformation over the x-coordinate in the potential functions $\breve{\phi}$ and $\breve{\psi}$, it follows that

$$\tilde{\phi}(k,z) = \int_{-\infty}^{\infty} \breve{\phi}(x,z)\exp(-ikx)\,dx, \tag{3.121}$$

$$\tilde{\psi}(k,z) = \int_{-\infty}^{\infty} \breve{\psi}(x,z)\exp(-ikx)\,dx. \tag{3.122}$$

The partial differential wave equations (3.114) and (3.105) are transformed into

$$\partial_{zz}^2\tilde{\phi} - a^2\tilde{\phi} = 0, \tag{3.123}$$

$$\partial_{zz}^2\tilde{\psi} - b^2\tilde{\psi} = 0, \tag{3.124}$$

where the wave numbers a and b are

$$a^2 = k^2 - \frac{k_p^2}{(1+i\omega t_r)} = R_p^2 \exp(i2\vartheta_p), \tag{3.125}$$

$$b^2 = k^2 - \frac{k_s^2}{(1+i\omega t_r)} = R_s^2 \exp(i2\vartheta_s), \tag{3.126}$$

in which R_p, R_s, the angles ϑ_p and ϑ_s are

$$R_p^4 = \frac{(k^2-k_p^2)^2 + k^4(\omega t_r)^2}{1+(\omega t_r)^2}, \tag{3.127}$$

$$R_s^4 = \frac{(k^2-k_s^2)^2 + k^4(\omega t_r)^2}{1+(\omega t_r)^2}, \tag{3.128}$$

$$\vartheta_p = \frac{1}{2}\arctan\left(\frac{k_p^2\omega t_r}{k^2(1+(\omega t_r)^2) - k_p^2}\right); \quad 0 \le \vartheta_p < \pi/2, \tag{3.129}$$

$$\vartheta_s = \frac{1}{2}\arctan\left(\frac{k_s^2\omega t_r}{k^2(1+(\omega t_r)^2) - k_s^2}\right); \quad 0 \le \vartheta_s < \pi/2. \tag{3.130}$$

It is assumed that the solutions of (3.123) and (3.124) are finite for very large values of z. This results in

$$\tilde{\phi} = \tilde{A}(k)\exp(-az), \tag{3.131}$$

$$\tilde{\psi} = \tilde{B}(k)\exp(-bz), \tag{3.132}$$

where the complex parameters $\tilde{A}$ and $\tilde{B}$ are given in terms of the horizontal wave number k. It is assumed that the real and imaginary parts of a and b are positive and the values of θ_p and θ_s lie in the interval $[0, \pi/2)$ if the response time $t_r \neq 0$. These assumptions are needed because it is required that for $z \to \infty$ and waves propagating in the positive z-direction, $\tilde{\phi}$ and $\tilde{\psi}$ must vanish. These solutions satisfy the radiation condition, see Rayleigh [1894].

By application of the Fourier transformation in the boundary conditions (3.110) and (3.111), it follows that

$$-i2(1+i\omega t_r)ka\tilde{A} + (k_s^2 - 2(1+i\omega t_r)k^2)\tilde{B} = 0, \tag{3.133}$$

$$(-k_s^2 + 2(1+i\omega t_r)k^2)\tilde{A} - i2(1+i\omega t_r)kb\tilde{B} = -\frac{p_0}{\mu}\frac{2\sin(kx_0)}{k}. \tag{3.134}$$

The solution of this system of equations is

$$\tilde{A} = \frac{p_0}{\mu}\frac{2\sin(kx_0)}{k}\frac{(k_s^2 - 2(1+i\omega t_r)k^2)}{\Delta}, \tag{3.135}$$

$$\tilde{B} = \frac{p_0}{\mu}\frac{2\sin(kx_0)}{k}\frac{(i2(1+i\omega t_r)ka)}{\Delta}, \tag{3.136}$$

where the determinant Δ of the system of equations is

$$\Delta = (k_s^2 - 2(1+i\omega t_r)k^2)^2 - 4k^2ab(1+i\omega t_r)^2. \tag{3.137}$$

Substitution of (3.135) and (3.136) into (3.131) and (3.132), the expressions for $\breve{\phi}$ and $\breve{\psi}$ are obtained after application of the inverse Fourier transformations,

$$\breve{\phi} = \frac{p_0}{\mu}\frac{2}{\pi}\int_0^\infty \frac{\sin(kx_0)}{k}\frac{(k_s^2 - 2(1+i\omega t_r)k^2)}{\Delta}\exp(-az)\cos(kx)\,dk, \tag{3.138}$$

$$\breve{\psi} = -\frac{p_0}{\mu}\frac{2}{\pi}\int_0^\infty \frac{\sin(kx_0)}{k}\frac{(2(1+i\omega t_r)ka)}{\Delta}\exp(-bz)\sin(kx)\,dk. \tag{3.139}$$

Introducing the elastic parameter m and using the damping factor ζ to represent the hysteretic damping, defined in (3.66), then the expression (3.137) is rewritten as

$$\Delta = (k_s^2 - 2(1+i2\zeta)k^2)^2 - 4k^2ab(1+i2\zeta)^2, \tag{3.140}$$

with

$$\zeta = \frac{1}{2}\omega t_r. \tag{3.141}$$

It can be verified that if the damping ratio $\zeta \neq 0$ then the determinant $\Delta \neq 0$. For the damping ratio $\zeta = 0$ Rayleigh's function $R(k)$ is found. This function is defined by

$$R(k) = (2k^2 - k_s^2)^2 - 4k^2(k^2 - k_s^2/m)^{1/2}(k^2 - k_s^2)^{1/2}, \tag{3.142}$$

with

$$m = \frac{k_s^2}{k_p^2} = \frac{c_p^2}{c_s^2} = \frac{2(1-\nu)}{(1-2\nu)}. \tag{3.143}$$

Using (3.104), (3.138) and (3.139) the solution of the vertical displacement at the surface in $z = 0$ can be determined as

$$u_z(x,0,t) = -\frac{p_0}{\mu}\frac{2k_s^2\exp(i\omega t)}{\pi(1+i2\zeta)^2}\int_0^\infty \frac{\sin(kx_0)}{k}\frac{a\cos(kx)}{((k^2+b^2)^2 - 4k^2ab)}\,dk. \tag{3.144}$$

3.5.2 Vibrating point load

The case of a point load P can be described when the length of the strip load $2x_0$ is very small or $x_0 \to 0$ and $p_0 \to \infty$, so that the vertical normal stress σ_{zz} at $z = 0$ can be considered as $p_0 = P/2x_0$, yielding

$$u_z(x,0,t) = -\frac{P}{\mu}\frac{k_s^2 \exp(i\omega t)}{\pi(1+i2\zeta)^2}\int_0^\infty \frac{a}{((k^2+b^2)^2 - 4k^2ab)}\cos(kx)\,dk. \tag{3.145}$$

In order to calculate $u_z(x,0,t)$, it is useful to introduce the dimensionless parameters $\kappa_x = k_s x = \omega x/c_s$ and $\beta_x = k/k_s$ into the right hand side of (3.145). It follows that,

$$u_z(x,0,t) = -\frac{P}{\mu}\frac{\exp(i\omega t)}{\pi(1+i2\zeta)^2}\int_0^\infty F(\beta_x)\cos(\kappa_x\beta_x)\,d\beta_x, \tag{3.146}$$

where the function $F(\beta_x)$ is given by

$$F(\beta_x) = \frac{a_a}{((\beta_x^2+b_b^2)^2 - 4\beta_x^2 a_a b_b)}, \tag{3.147}$$

with the dimensionless wave numbers a_a and b_b,

$$a_a^2 = \frac{a^2}{k_s^2} = \beta_x^2 - \frac{1}{m(1+i2\zeta)}, \tag{3.148}$$

$$b_b^2 = \frac{b^2}{k_s^2} = \beta_x^2 - \frac{1}{(1+i2\zeta)}. \tag{3.149}$$

The values of R_p, R_s, ϑ_p and ϑ_s are rewritten as

$$R_p^4 = \frac{(k^2-k_p^2)^2 + 4k^4\zeta^2}{1+4\zeta^2}, \tag{3.150}$$

$$R_s^4 = \frac{(k^2-k_s^2)^2 + 4k^4\zeta^2}{1+4\zeta^2}, \tag{3.151}$$

$$\vartheta_p = \frac{1}{2}\arctan\left(\frac{2k_p^2\zeta}{k^2(1+4\zeta^2)-k_p^2}\right);\quad 0 \le \vartheta_p < \pi/2, \tag{3.152}$$

$$\vartheta_s = \frac{1}{2}\arctan\left(\frac{2k_s^2\zeta}{k^2(1+4\zeta^2)-k_s^2}\right);\quad 0 \le \vartheta_s < \pi/2. \tag{3.153}$$

A particular way for representing the displacement is by considering a differential displacement Δu_z. This is defined as

$$\Delta u_z = u_z(x,0,t) - u_z(x+l,0,t), \tag{3.154}$$

where l is given non-zero length. Substitution of (3.146) into (3.154) leads to

$$\frac{\mu \Delta u_z}{P} = -\frac{\exp(i\omega t)}{\pi(1+i2\zeta)^2} I_l, \tag{3.155}$$

where the dimensionless parameter $\kappa_l = k_s l = \omega l / c_s$. The integral I_l is given as

$$I_l = \int_0^\infty F(\beta_x)(\cos(\kappa_l \beta_x x/l) - \cos(\kappa_l \beta_x (x/l+1)))\, d\beta_x. \tag{3.156}$$

The absolute value $|\Delta u_z|$ is shown in Figure 3.13, for a small value of $\kappa_l = 0.01$ and $\zeta = 0.001$. In order to evaluate I_l in (3.156) the integral has been calculated until an upper limit of the integration β_{xmax}. Next, the integral is evaluated using Simpson's integration method. The results for the static case are illustrated in the figure by dots.

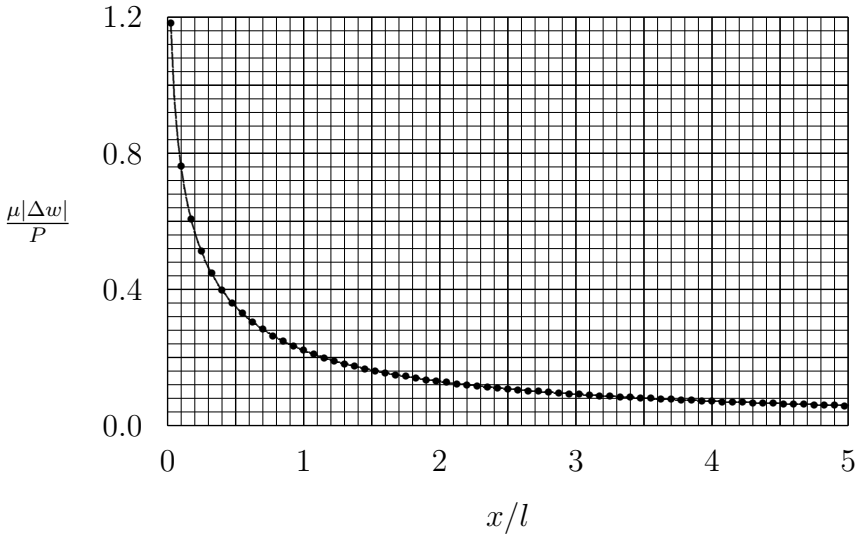

Figure 3.13: Absolute value of the differential displacement $|\Delta u_z|$: $\nu = 0$, $\zeta = 0.001$, $\kappa_l = 0.01$, $\beta_{xmax} = 100000$.

It can be seen that both results are very similar in this case. The static solution Δu_s is obtained when the value of $k_s \to 0$. This gives

$$\frac{\mu \Delta u_s}{P} = -\frac{(1-\nu)}{\pi} \log\left(\frac{x/l}{x/l+1}\right). \tag{3.157}$$

This expression was also given by Harr [1966].

Chapter 4

Moving loads on an elastic half-plane with hysteretic damping

The ground response of a moving load on an elastic medium over the upper boundary of a half-plane is presented in this chapter. The study of the generation of vibrations under the action of moving loads has been a subject of notable consideration in applied mechanics in the past, due to its interest to the theory of wave propagation. Sneddon [1952] only studied the subsonic case of a moving load at a constant speed along its surface. Furthermore, Cole and Huth [1958] obtained the solutions for the transonic and supersonic cases. The solution for a moving load on a half-plane can also be found in the books of Fung [1965] and Frýba [1972]. The case of an oblique moving load on the boundary of a half-plane has been analyzed in Eringen and Suhubi [1975] and Georgiadis and Barber [1993].

The influence of the hysteretic damping on the magnitude of the displacements and stresses will be examined for a moving load at a constant velocity along the surface of a half-plane, see Verruijt and Cornejo Córdova [2001].

4.1 Basic equations

The basic equations of motion in two dimensions are

$$\partial_x \sigma_{xx} + \partial_z \sigma_{zx} = \rho \partial_{tt}^2 u_x, \tag{4.1}$$

$$\partial_x \sigma_{xz} + \partial_z \sigma_{zz} = \rho \partial_{tt}^2 u_z, \tag{4.2}$$

where $u_x(x, z, t)$ and $u_z(x, z, t)$ are the components of the displacements in the x and z directions, respectively. These displacements can also be written in terms of the potential functions $\phi(x, z, t)$ and $\psi(x, z, t)$, as follows

$$u_x = \partial_x \phi - \partial_z \psi, \tag{4.3}$$

$$u_z = \partial_z \phi + \partial_x \psi. \tag{4.4}$$

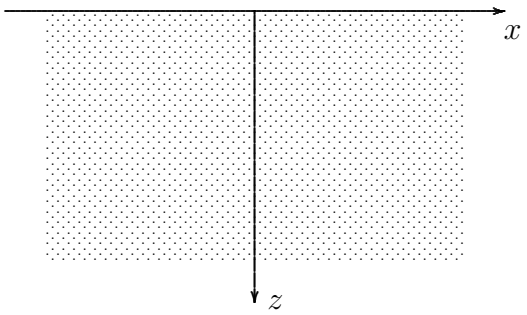

Figure 4.1: Half-plane.

Figure 4.1 shows a half-plane with coordinates $-\infty < x < \infty$ and $z \geq 0$. The stress components can also be expressed as function of ϕ and ψ,

$$\begin{aligned}\sigma_{xx} =&\lambda(\partial^2_{xx}\phi + \partial^2_{zz}\phi) + \lambda t_r \partial_t(\partial^2_{xx}\phi + \partial^2_{zz}\phi) \\ &+ 2\mu(\partial^2_{xx}\phi - \partial_x\partial_z\psi) + 2\mu t_r\partial_t(\partial^2_{xx}\phi - \partial_x\partial_z\psi),\end{aligned} \tag{4.5}$$

$$\begin{aligned}\sigma_{zz} =&\lambda(\partial^2_{xx}\phi + \partial^2_{zz}\phi) + \lambda t_r \partial_t(\partial^2_{xx}\phi + \partial^2_{zz}\phi) \\ &+ 2\mu(\partial^2_{zz}\phi + \partial_x\partial_z\psi) + 2\mu t_r\partial_t(\partial^2_{zz}\phi + \partial_x\partial_z\psi),\end{aligned} \tag{4.6}$$

$$\sigma_{xz} = \mu(2\partial_x\partial_z\phi + \partial^2_{xx}\psi - \partial^2_{zz}\psi) + \mu t_r\partial_t(2\partial_x\partial_z\phi + \partial^2_{xx}\psi - \partial^2_{zz}\psi), \tag{4.7}$$

where t_r is the relaxation time. It is assumed that the relaxation time for the two fundamental forms of deformation, shear and compression, are equal. In order to represent the hysteretic damping the value of t_r should be inversely proportional to the frequency of the load. Applying (4.3) - (4.7) into (4.1) and (4.2) shows that the basic equations can be satisfied if the potentials are solutions of

$$\partial^2_{xx}\phi + \partial^2_{zz}\phi + t_r\partial_t(\partial^2_{xx}\phi + \partial^2_{zz}\phi) = \frac{1}{c_p^2}\partial^2_{tt}\phi, \tag{4.8}$$

$$\partial^2_{xx}\psi + \partial^2_{zz}\psi + t_r\partial_t(\partial^2_{xx}\psi + \partial^2_{zz}\psi) = \frac{1}{c_s^2}\partial^2_{tt}\psi. \tag{4.9}$$

where $c_s^2 = \mu/\rho$ and $c_p^2 = (\lambda + 2\mu)/\rho$.

4.2 Moving loads on a half-plane

The propagation of the waves in a half-plane (two-dimensional) is considered in this section. A particular case is the moving of a load on a half-plane, for $z \geq 0$. The velocity v of the load is considered to be constant. Introducing a moving coordinate system (x_1, z_1),

$$x_1 = x - vt; \quad -\infty < x_1 < \infty \ \text{ and } \ z_1 = z; \quad z_1 \geq 0, \tag{4.10}$$

and substitution of (4.10) into (4.5) - (4.9), gives

$$\frac{\sigma_{xx}}{\mu} = (M_s^2 - 2M_p^2 + 2)\partial^2_{x_1x_1}\phi - 2\partial_{x_1}\partial_{z_1}\psi - 2vt_r\partial_{x_1}(\partial^2_{x_1x_1}\phi - \partial_{x_1}\partial_{z_1}\psi), \tag{4.11}$$

$$\frac{\sigma_{zz}}{\mu} = (M_s^2 - 2)\partial^2_{x_1x_1}\phi + 2\partial_{x_1}\partial_{z_1}\psi + 2vt_r\partial_{x_1}(\partial^2_{x_1x_1}\phi - \partial_{x_1}\partial_{z_1}\psi), \tag{4.12}$$

$$\frac{\sigma_{xz}}{\mu} = 2\partial_{x_1}\partial_{z_1}\phi - (M_s^2 - 2)\partial^2_{x_1x_1}\psi - 2vt_r\partial_{x_1}(\partial_{x_1}\partial_{z_1}\phi + \partial^2_{x_1x_1}\psi), \tag{4.13}$$

where the dimensionless parameters M_p and M_s, the so-called Mach numbers, are related to the velocity v by

$$M_p = \frac{v}{c_p} \quad \text{and} \quad M_s = \frac{v}{c_s}. \tag{4.14}$$

These parameters define the speed range of motion: subsonic ($v < c_s$), transonic ($c_s < v < c_p$) and supersonic ($v > c_p$). Similarly, the expressions of the basic potential equations (4.8) and (4.9) can also be written as

$$\partial^2_{x_1x_1}\phi + \partial^2_{z_1z_1}\phi - vt_r\partial_{x_1}(\partial^2_{x_1x_1}\phi + \partial^2_{z_1z_1}\phi) = M_p^2\partial^2_{x_1x_1}\phi, \tag{4.15}$$

$$\partial^2_{x_1x_1}\psi + \partial^2_{z_1z_1}\psi - vt_r\partial_{x_1}(\partial^2_{x_1x_1}\psi + \partial^2_{z_1z_1}\psi) = M_s^2\partial^2_{x_1x_1}\psi. \tag{4.16}$$

The solution of (4.15) and (4.16) will be found when the boundary conditions are given.

4.2.1 Moving point load

In order to describe the case of a moving point load, it can be supposed that the boundary conditions have the following form

$$z_1 = 0 \ : \ \sigma_{xz} = 0, \tag{4.17}$$

$$z_1 = 0 \ : \ \sigma_{zz} = -P\delta(x - vt) = -P\delta(x_1), \tag{4.18}$$

where $\delta(x_1)$ is the delta function and P is a perpendicular line force per unit length, see Figure 4.2. Applying the exponential Fourier transformation over the x_1 coordinate, the transformed potential functions become

$$\tilde{\phi}(k, z_1) = \int_{-\infty}^{\infty} \phi(x_1, z_1)\exp(-ikx_1)\,dx_1, \tag{4.19}$$

$$\tilde{\psi}(k, z_1) = \int_{-\infty}^{\infty} \psi(x_1, z_1)\exp(-ikx_1)\,dx_1, \tag{4.20}$$

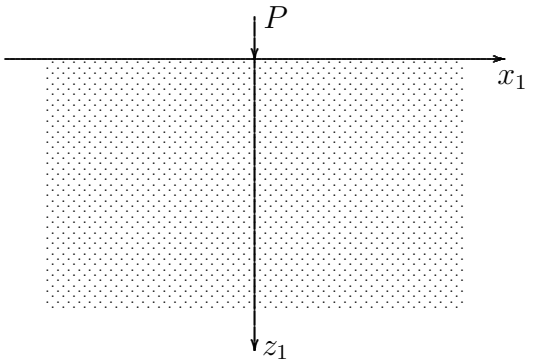

Figure 4.2: Moving load on a half-plane.

where k is the horizontal wave number. After taking the Fourier transformation of (4.15) and (4.16), it follows that

$$\partial^2_{z_1 z_1}\tilde{\phi} - k^2 \frac{(1 - M_p^2 + (vt_r k)^2 - ivt_r k M_p^2)}{1 + (vt_r k)^2}\tilde{\phi} = 0, \tag{4.21}$$

$$\partial^2_{z_1 z_1}\tilde{\psi} - k^2 \frac{(1 - M_s^2 + (vt_r k)^2 - ivt_r k M_s^2)}{1 + (vt_r k)^2}\tilde{\psi} = 0. \tag{4.22}$$

It is assumed that the solutions of (4.21) and (4.22) have the following form

$$\tilde{\phi}(k, z_1) = A(k)\exp(-a|k|z_1), \tag{4.23}$$

$$\tilde{\psi}(k, z_1) = B(k)\exp(-b|k|z_1), \tag{4.24}$$

where a and b are wave numbers. One also assumes that their real parts are positive and that their imaginary parts are negative, so that for $z_1 \to \infty$ waves propagate in positive z-direction, and the potentials $\tilde{\phi}$ and $\tilde{\psi}$ must vanish. The arbitrary complex coefficients A and B are determined from the boundary conditions. The wave numbers a and b can be expressed as

$$a^2 = R_p^2 \exp(-i2\vartheta_p), \tag{4.25}$$

$$b^2 = R_s^2 \exp(-i2\vartheta_s), \tag{4.26}$$

where R_p, R_s and the angles ϑ_p and ϑ_s are given by

$$R_p = \sqrt[4]{\frac{(1 - M_p^2 + (vt_r k)^2)^2 + (vt_r k M_p^2)^2}{(1 + (vt_r k)^2)^2}}, \tag{4.27}$$

$$R_s = \sqrt[4]{\frac{(1 - M_s^2 + (vt_r k)^2)^2 + (vt_r k M_s^2)^2}{(1 + (vt_r k)^2)^2}}, \tag{4.28}$$

$$\vartheta_p = \frac{1}{2}\arctan\left(\frac{vt_r k M_p^2}{1 - M_p^2 + (vt_r k)^2}\right); \quad 0 \leq \vartheta_p < \pi/2, \tag{4.29}$$

$$\vartheta_s = \frac{1}{2}\arctan\left(\frac{vt_r k M_s^2}{1 - M_s^2 + (vt_r k)^2}\right); \quad 0 \leq \vartheta_s < \pi/2. \tag{4.30}$$

Because only outgoing waves occur in this case, meaning that the values of ϑ_s and ϑ_p lie in the interval $[0, \pi/2)$, these solutions satisfy the radiation condition, formulated by Rayleigh [1894]. In a similar way, using (4.19) and (4.20) the stress components (4.11) - (4.13) are

$$\frac{\tilde{\sigma}_{xx}}{\mu} = -k^2(M_s^2 - 2M_p^2 + 2 - i2vt_r k)\tilde{\phi} - i2k(1 - ivt_r k)\partial_{z_1}\tilde{\psi}, \tag{4.31}$$

$$\frac{\tilde{\sigma}_{zz}}{\mu} = -k^2(M_s^2 - 2 + i2vt_r k)\tilde{\phi} + i2k(1 - ivt_r k)\partial_{z_1}\tilde{\psi}, \tag{4.32}$$

$$\frac{\tilde{\sigma}_{xz}}{\mu} = i2k(1 - ivt_r k)\partial_{z_1}\tilde{\phi} + k^2(M_s^2 - 2 + i2vt_r k)\tilde{\psi}. \tag{4.33}$$

From (4.17), (4.18), (4.32) and (4.33) for $z = 0$, it follows that

$$-i2(1 - ivt_r k)a|k|A + k(M_s^2 - 2 + i2vt_r k)B = 0, \tag{4.34}$$

$$-k^2(M_s^2 - 2 + i2vt_r k)A - i2k(1 - ivt_r k)b|k|B = -\frac{P}{\mu}. \tag{4.35}$$

This system of equations has the complex determinant Δ. This is given as

$$\Delta = k^3 D, \tag{4.36}$$

where the complex parameter D is written as

$$D = (M_s^2 - 2 + i2vt_r k)^2 - 4(1 - ivt_r k)^2 ab, \tag{4.37}$$

and

$$A = \frac{P}{\mu}\frac{k(M_s^2 - 2 + i2vt_r k)}{\Delta}, \tag{4.38}$$

$$B = i\frac{P}{\mu}\frac{2|k|(1 - ivt_r k)a}{\Delta}. \tag{4.39}$$

Rayleigh surface waves will be found when the value of t_r in (4.37) is equal to zero. The development of this case has been examined by Ewing *et al.* [1957]. Surface waves on viscoelastic half-space are studied in the texts of Christensen [1982], and Caviglia

and Morro [1992]. The propagation of waves due to moving loads on a viscoelastic half-space are also analyzed by Christensen. Introducing (4.38) and (4.39) into (4.23) and (4.24), yields

$$\tilde{\phi}(k, z_1) = \frac{P}{\mu} \frac{k(M_s^2 - 2 + i2vt_r k)}{\Delta} \exp(-a|k|z_1), \tag{4.40}$$

$$\tilde{\psi}(k, z_1) = i\frac{P}{\mu} \frac{2|k|(1 - ivt_r k)a}{\Delta} \exp(-b|k|z_1). \tag{4.41}$$

In order to describe the behaviour of the material supporting a moving load, hysteretic damping is used. This technique has been discussed by Verruijt [1999] who formulated that for soils it can be expected that the damping will be the same, regardless of the frequency of the load. This can be possible by assuming that the factor $vt_r k$ is constant. This means that the apparent viscosity of the medium is small for high frequencies, and large for low frequencies, so that this factor remains constant. Defining the damping ratio ζ as

$$\zeta = \frac{vt_r k}{2} sign(k), \tag{4.42}$$

where $|\zeta|$ is assumed to be constant and $sign(k)$ denotes the sign of k. This representation of hysteretic damping has been presented in the text of Wolf [1988]. Hardin [1965] proposed that the behaviour of dry soils (sand) subjected to small deformations can be represented by hysteretic damping. The damping ratio ζ is also considered to be an independent material parameter. Problems of moving loads on an elastic medium with hysteretic damping have also been investigated by de Barros and Luco [1994], Lefeuve-Mesgouez [1999], Sheng *et al.* [1999], Jones *et al.* [2000], Degrande and Lombaert [2000], and Kaynia *et al.* [2000].

Replacing (4.42) into (4.40) and (4.41), it follows that

$$\tilde{\phi}(k, z_1) = \frac{P}{\mu} \frac{(M_s^2 - 2 + i4\zeta)}{k^2 D} \exp(-a|k|z_1), \tag{4.43}$$

$$\tilde{\psi}(k, z_1) = i\frac{P}{\mu} \frac{2|k|(1 - i2\zeta)a}{k^3 D} \exp(-b|k|z_1), \tag{4.44}$$

where D is rewritten as

$$D = (M_s^2 - 2 + i4\zeta)^2 - 4(1 - i2\zeta)^2 ab, \tag{4.45}$$

and R_p, R_s, ϑ_p and ϑ_s are given by

$$R_p = \sqrt[4]{\frac{(1 - M_p^2)^2 + 4\zeta^2}{1 + 4\zeta^2}}, \tag{4.46}$$

$$R_s = \sqrt[4]{\frac{(1-M_s^2)^2+4\zeta^2}{1+4\zeta^2}}, \tag{4.47}$$

$$\vartheta_p = \frac{1}{2}\arctan\left(\frac{2\zeta M_p^2}{1-M_p^2+4\zeta^2}\right); \quad 0 \le \vartheta_p < \pi/2, \tag{4.48}$$

$$\vartheta_s = \frac{1}{2}\arctan\left(\frac{2\zeta M_s^2}{1-M_s^2+4\zeta^2}\right); \quad 0 \le \vartheta_s < \pi/2. \tag{4.49}$$

4.2.2 Stress components

The horizontal stress is obtained by using the respective Fourier transformation in (4.31), it then becomes

$$\begin{aligned}\frac{\tilde{\sigma}_{xx}}{P} =& -(M_s^2-2+i4\zeta)(M_s^2-2M_p^2+2-i4\zeta)\frac{1}{D}\exp(-a|k|z_1)\\ &-4(1-i2\zeta)^2 ab\frac{1}{D}\exp(-b|k|z_1).\end{aligned} \tag{4.50}$$

Therefore, using the inverse Fourier transformation, yields

$$\begin{aligned}\frac{2\pi\sigma_{xx}}{P} =& -\int_{-\infty}^{\infty}(M_s^2-2+i4\zeta)(M_s^2-2M_p^2+2-i4\zeta)\frac{1}{D}\\ &\qquad\times\exp(-a|k|z_1)\exp(ikx_1)\,dk\\ &-\int_{-\infty}^{\infty}4(1-i2\zeta)ab\frac{1}{D}\exp(-b|k|z_1)\exp(ikx_1)\,dk\\ =&\int_{\infty}^{0}\overline{C}_1\exp(-\overline{a}kz_1)\exp(-ikx_1)\,dk\\ &-\int_{0}^{\infty}C_1\exp(-akz_1)\exp(ikx_1)\,dk\\ &+\int_{\infty}^{0}\overline{C}_2\exp(-\overline{b}kz_1)\exp(-ikx_1)\,dk\\ &-\int_{0}^{\infty}C_2\exp(-bkz_1)\exp(ikx_1)\,dk,\end{aligned} \tag{4.51}$$

where $\overline{a}$ and $\overline{b}$ are the conjugates of a and b, respectively. The complex constants C_1 and C_2 are given by

$$C_1 = (M_s^2-2+i4\zeta)(M_s^2-2M_p^2+2-i4\zeta)\frac{1}{D}, \tag{4.52}$$

$$C_2 = 4(1 - i2\zeta)^2 ab \frac{1}{D}, \tag{4.53}$$

$$a = R_p \exp(-i\vartheta_p) = p_p - iq_p, \tag{4.54}$$

$$b = R_s \exp(-i\vartheta_s) = p_s - iq_s. \tag{4.55}$$

Expression (4.51) leads to

$$\begin{aligned}\frac{\pi\sigma_{xx}}{P} =& -\Re(C_1)\frac{p_p z_1}{(x_1 + q_p z_1)^2 + (p_p z_1)^2} + \Im(C_1)\frac{x_1 + q_p z_1}{(x_1 + q_p z_1)^2 + (p_p z_1)^2} \\ & - \Re(C_2)\frac{p_s z_1}{(x_1 + q_s z_1)^2 + (p_s z_1)^2} + \Im(C_2)\frac{x_1 + q_s z_1}{(x_1 + q_s z_1)^2 + (p_s z_1)^2},\end{aligned} \tag{4.56}$$

with $\Re$ is real and $\Im$ is imaginary. The horizontal stresses for different values of M_s are shown in Figure 4.3. It appears that for the supersonic case $M_s = 2.0$ the stresses in front of the load are practically equal to zero. For $M_s = 0.8$ and $M_s = 2.0$ the maximum peaks are located behind the load.

For relatively small values of the damping ratio, $\zeta < 0.02$, the response of the horizontal stresses is substantially increased. This is illustrated in Figure 4.4 when the load moves with the velocity of Rayleigh waves, $M_s = 0.874032$, in an elastic medium for Poisson's ratio $\nu = 0$. By varying the value of the damping ratio ζ it can be seen that the peaks of the horizontal stresses are approximately inversely proportional to ζ. These become infinitely large when the damping ratio ζ tends to zero and would be located at $x_1/z_1 = -0.25$ and 0.25.

In a similar way the vertical stress can be found. It follows that

$$\frac{\tilde{\sigma}_{zz}}{P} = -(M_s^2 - 2 + i4\zeta)^2 \frac{1}{D}\exp(-a|k|z_1) + 4(1 - i2\zeta)^2 ab\frac{1}{D}\exp(-b|k|z_1). \tag{4.57}$$

Therefore, this results in

$$\begin{aligned}\frac{2\pi\sigma_{zz}}{P} =& -\int_{-\infty}^{\infty}(M_s^2 - 2 + i4\zeta)^2\frac{1}{D}\exp(-a|k|z_1)\exp(ikx_1)\,dk \\ & + \int_{-\infty}^{\infty} 4(1 - i2\zeta)^2 ab\frac{1}{D}\exp(-b|k|z_1)\exp(ikx_1)\,dk \\ =& \int_{\infty}^{0}\overline{C}_3\exp(-\overline{a}kz_1)\exp(-ikx_1)\,dk \\ & - \int_{0}^{\infty} C_3\exp(-akz_1)\exp(ikx_1)\,dk \\ & - \int_{\infty}^{0}\overline{C}_2\exp(-\overline{b}kz_1)\exp(-ikx_1)\,dk \\ & + \int_{0}^{\infty} C_2\exp(-bkz_1)\exp(ikx_1)\,dk,\end{aligned} \tag{4.58}$$

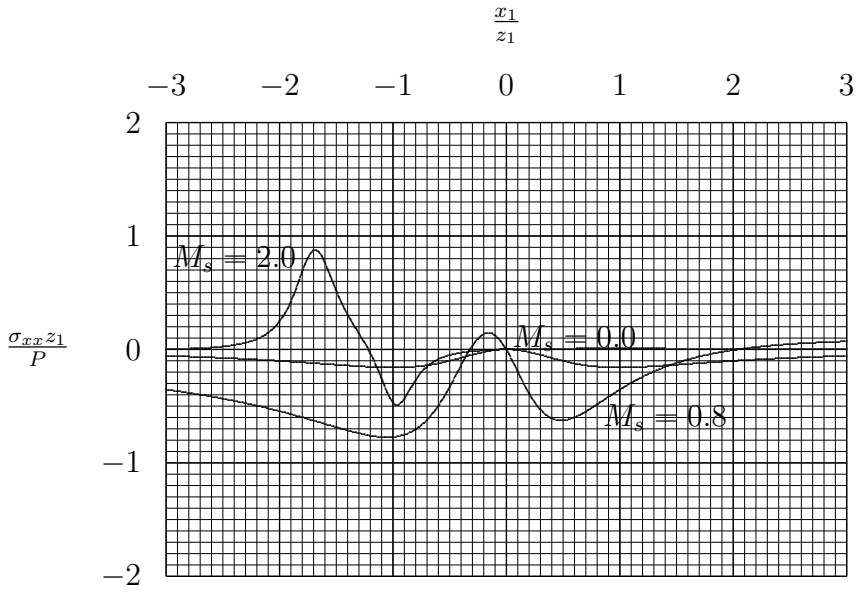

Figure 4.3: Moving load on a half-plane, horizontal stress for different M_s: $\nu = 0$, $\zeta = 0.1$.

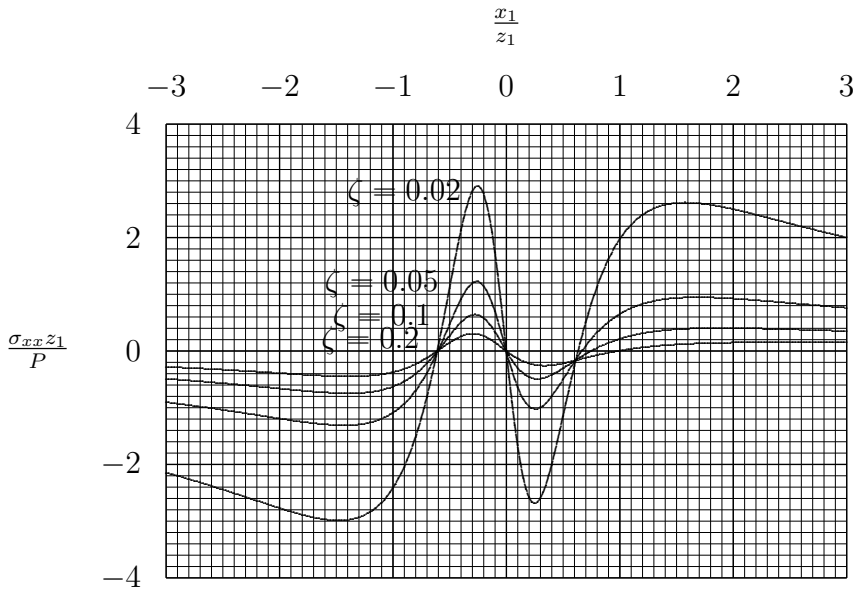

Figure 4.4: Moving load on a half-plane, horizontal stress for different ζ: $\nu = 0$, $M_s = 0.874032$.

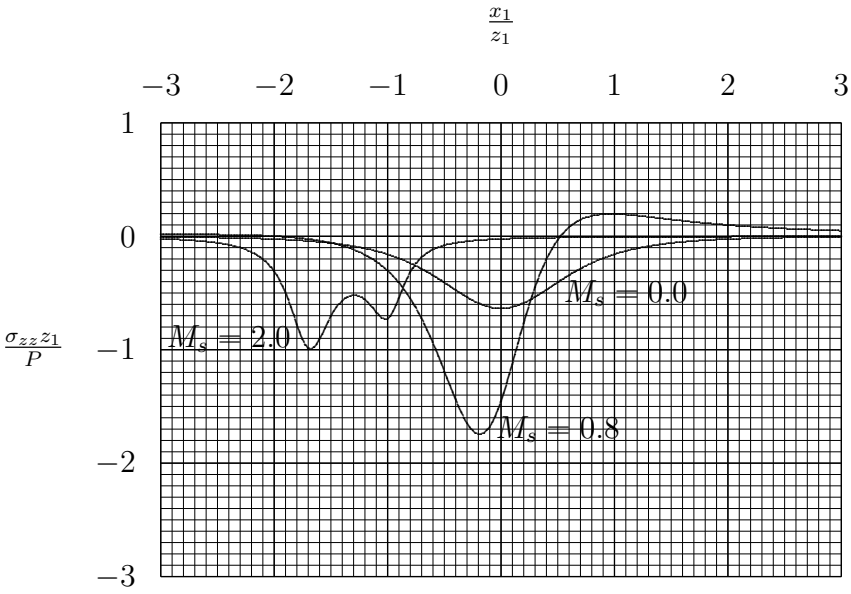

Figure 4.5: Moving load on a half-plane, vertical stress for different M_s: $\nu = 0$, $\zeta = 0.1$.

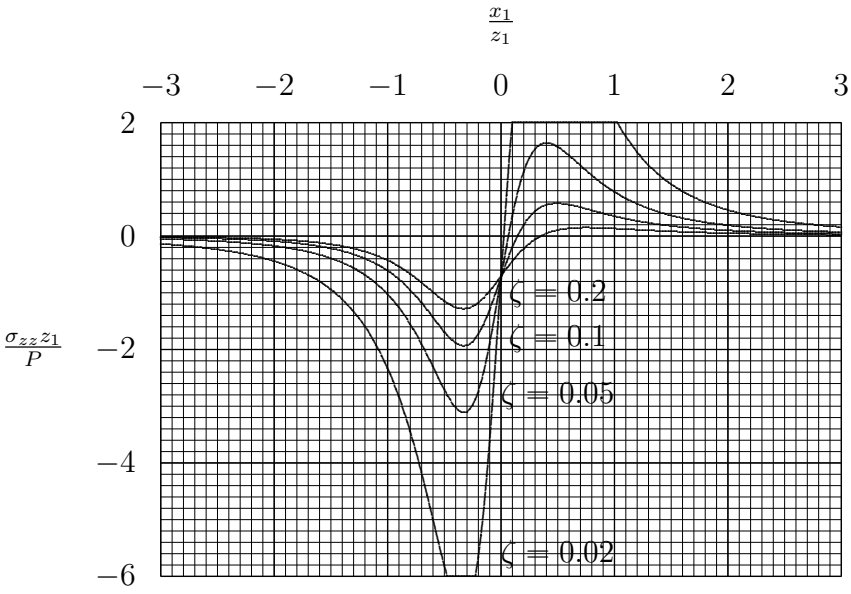

Figure 4.6: Moving load on a half-plane, vertical stress for different ζ: $\nu = 0$, $M_s = 0.874032$.

where the complex constant C_3 is given by

$$C_3 = (M_s^2 - 2 + i4\zeta)^2 \frac{1}{D}. \tag{4.59}$$

After calculating (4.58), the following result is obtained

$$\begin{aligned}\frac{\pi\sigma_{zz}}{P} =& -\Re(C_3)\frac{p_p z_1}{(x_1+q_p z_1)^2+(p_p z_1)^2} + \Im(C_3)\frac{x_1+q_p z_1}{(x_1+q_p z_1)^2+(p_p z_1)^2} \\ &+ \Re(C_2)\frac{p_s z_1}{(x_1+q_s z_1)^2+(p_s z_1)^2} - \Im(C_2)\frac{x_1+q_s z_1}{(x_1+q_s z_1)^2+(p_s z_1)^2}.\end{aligned} \tag{4.60}$$

Figure 4.5 shows the distribution of the vertical stresses for different values of M_s. The static response is found for $M_s = 0$. For the subsonic case $M_s = 0.8$ the maximum stress is observed behind the load at $x_1/z_1 = -0.19$. For the supersonic case $M_s = 2.0$ the results show the location of the two peaks at $x_1/z_1 = -1.68$ and -1.03. These peaks are approximately inversely proportional to the damping ratio ζ.

The increase of the response of the vertical stresses for different values of the damping ratio ζ is illustrated in Figure 4.6, when the load travels with the velocity of Rayleigh waves in an elastic medium with the Poisson's ratio $\nu = 0$. It can be seen that the vertical stresses are very large for smaller values of ζ. The peaks of the maximum vertical stress are approximately inversely proportional to the damping ratio ζ. For

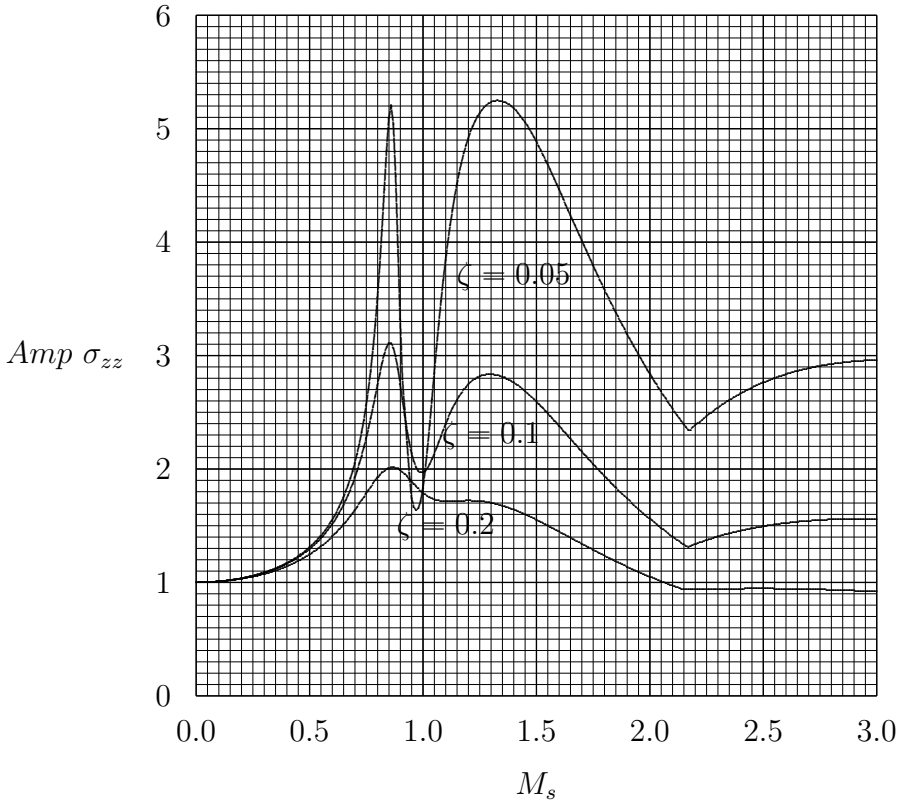

Figure 4.7: Moving load on a half-plane, amplification factor of the maximum vertical stress for different ζ: $\nu = 0$.

very small values of the damping ratio, $\zeta < 0.001$, the results are not shown. These peaks would become very large.

The amplification factor of the maximum vertical stress, *Amp* σ_{zz}, is shown in Figure 4.7, as a function of M_s, for different values of the damping ratio ζ. Here, the maximum static value of the vertical stress σ_{zz} is used as a reference value. The influence of damping is again observed to be very large. If the value of the damping ratio is larger than 0.2, then the response is significantly reduced. For values of M_s smaller than 0.5 the influence of the damping ratios on the results is not significant. For values of the damping ratio smaller than 0.001 the results are not shown. The maximum value of *Amp* σ_{zz} would be obtained for $M_s = 0.874032$ (the velocity of Rayleigh waves in an elastic medium with Poisson's ratio $\nu = 0$).

The shear stress is given by

$$\begin{aligned}\frac{\tilde{\sigma}_{xz}}{P} =& - i2(M_s^2 - 2 + i4\zeta)a|k|(1 - i2\zeta)\frac{1}{kD}\exp(-a|k|z_1) \\ &+ i2|k|(1 - i2\zeta)a(M_s^2 - 2 + i4\zeta)\frac{1}{kD}\exp(-b|k|z_1).\end{aligned} \tag{4.61}$$

Solving in the same way as the horizontal stress, gives

$$\begin{aligned}\frac{2\pi\sigma_{xz}}{P} =& - i\int_{-\infty}^{\infty} 2(M_s^2 - 2 + i4\zeta)a|k|(1 - i2\zeta)\frac{1}{kD} \\ &\qquad \times \exp(-a|k|z_1)\exp(ikx_1)\,dk \\ &+ i\int_{-\infty}^{\infty} 2|k|(1 - i2\zeta)a(M_s^2 - 2 + i4\zeta)\frac{1}{kD} \\ &\qquad \times \exp(-b|k|z_1)\exp(ikx_1)\,dk \\ =& - i\int_{\infty}^{0} \overline{C}_4(\exp(-\overline{a}kz_1) - \exp(-\overline{b}kz_1))\exp(-ikx_1)\,dk \\ &- i\int_{0}^{\infty} C_4(\exp(-akz_1) - \exp(-bkz_1))\exp(ikx_1)\,dk,\end{aligned} \tag{4.62}$$

where the complex constant C_4 is given by

$$C_4 = 2(M_s^2 - 2 + i4\zeta)a(1 - i2\zeta)\frac{1}{D}. \tag{4.63}$$

Expression (4.62) can be reduced to the following

$$\begin{aligned}\frac{\pi\sigma_{xz}}{P} =& + \Im(C_4)\frac{p_p z_1}{(x_1 + q_p z_1)^2 + (p_p z_1)^2} + \Re(C_4)\frac{x_1 + q_p z_1}{(x_1 + q_p z_1)^2 + (p_p z_1)^2} \\ &- \Im(C_4)\frac{p_s z_1}{(x_1 + q_s z_1)^2 + (p_s z_1)^2} - \Re(C_4)\frac{x_1 + q_s z_1}{(x_1 + q_s z_1)^2 + (p_s z_1)^2}.\end{aligned} \tag{4.64}$$

Figure 4.8 shows the shear stresses for different values of M_s. In general, the stresses for the case $M_s = 0.8$ are greater than for the case $M_s = 2.0$.

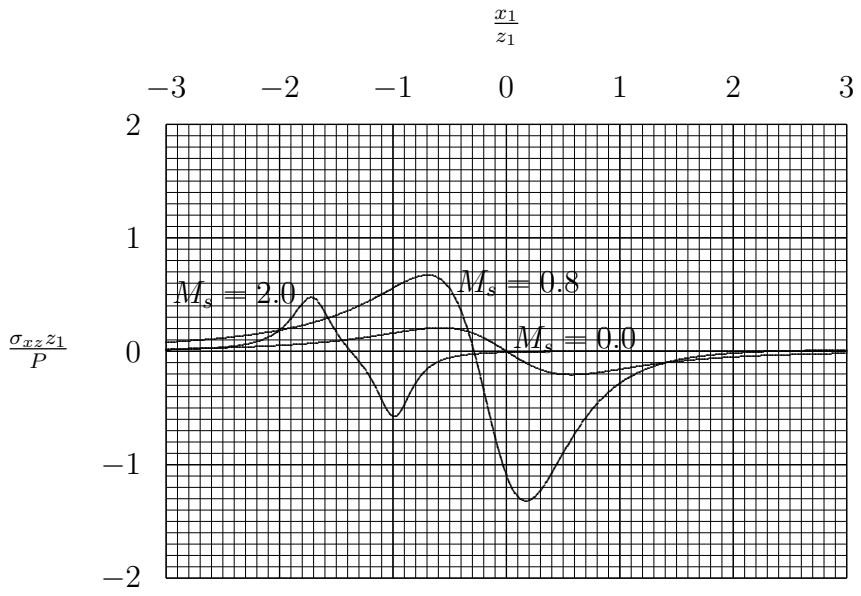

Figure 4.8: Moving load on a half-plane, shear stress for different M_s: $\nu = 0$, $\zeta = 0.1$.

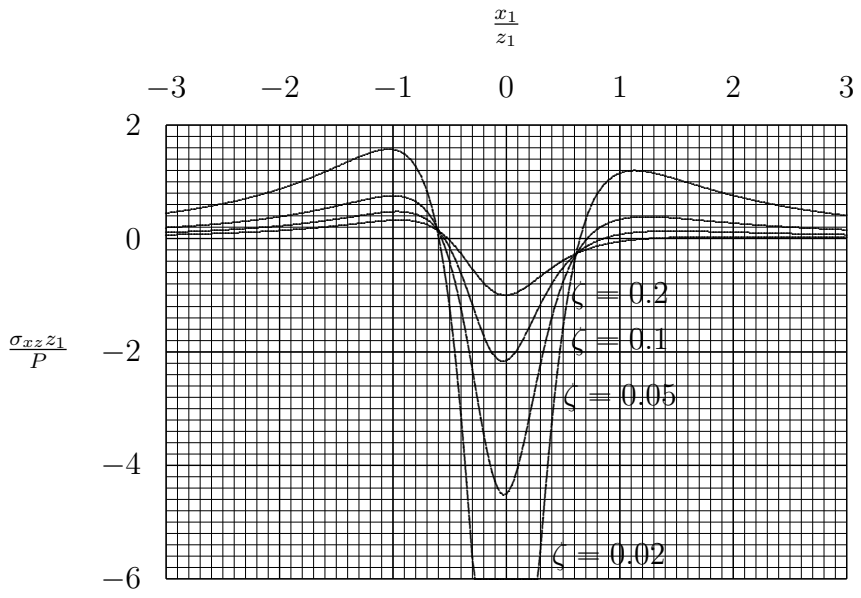

Figure 4.9: Moving load on a half-plane, shear stress for different ζ: $\nu = 0$, $M_s = 0.874032$.

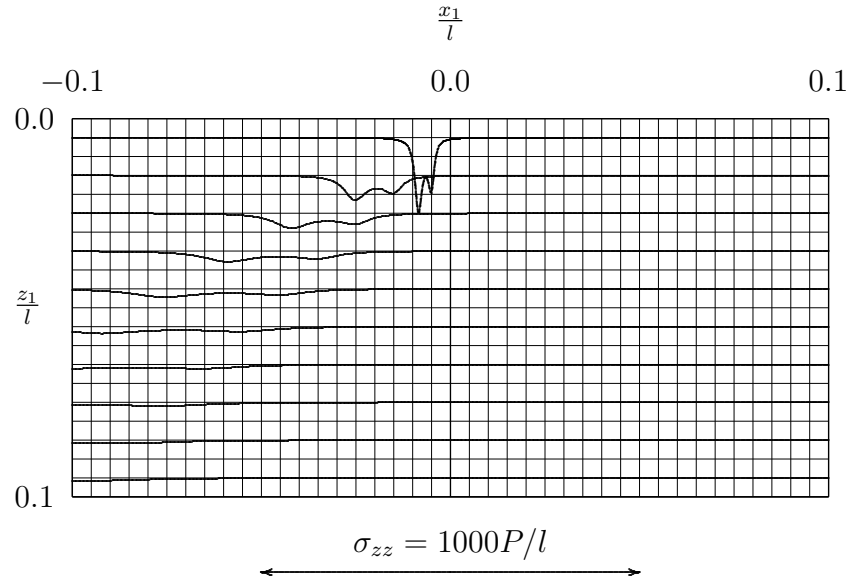

Figure 4.10: Moving load on a half-plane, vertical stress: $\nu = 0$, $\zeta = 0.1$, $M_s = 2.0$.

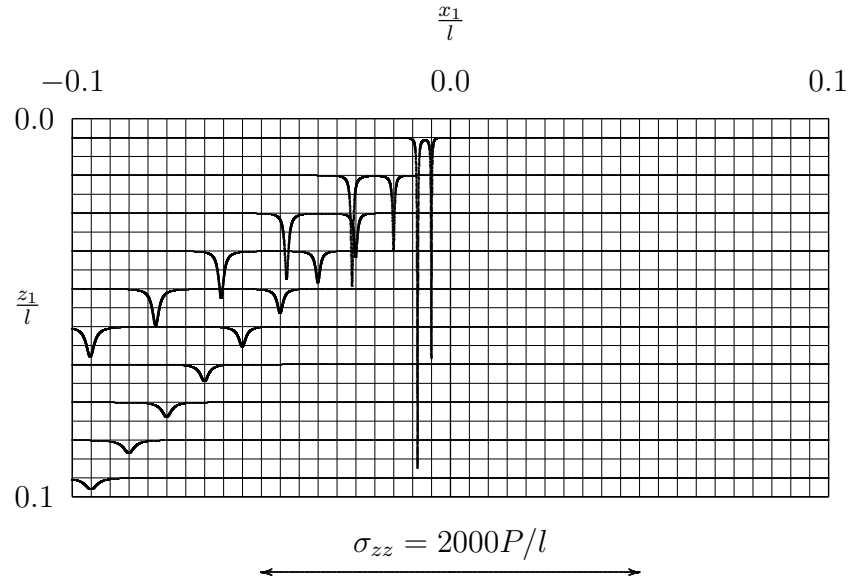

Figure 4.11: Moving load on a half-plane, vertical stress: $\nu = 0$, $\zeta = 0.01$, $M_s = 2.0$.

The influence of hysteretic damping on the magnitude of the shear stresses is illustrated in Figure 4.9. In this case, the velocity of the load equals the velocity of Rayleigh waves in an elastic medium with $\nu = 0$. The results clearly indicate that the very large shear stresses for smaller values of ζ are much decreased if the damping ratio increases.

The stress components (4.56), (4.60) and (4.64) can also be expressed as

$$\begin{aligned}\frac{\pi\sigma_{xx}z_1}{P} =& -\Re(C_1)\frac{p_p}{(x_1/z_1+q_p)^2+p_p^2}+\Im(C_1)\frac{x_1/z_1+q_p}{(x_1/z_1+q_p)^2+p_p^2}\\ &-\Re(C_2)\frac{p_s}{(x_1/z_1+q_s)^2+p_s^2}+\Im(C_2)\frac{x_1/z_1+q_s}{(x_1/z_1+q_s)^2+p_s^2},\end{aligned} \tag{4.65}$$

$$\begin{aligned}\frac{\pi\sigma_{zz}z_1}{P} =& -\Re(C_3)\frac{p_p}{(x_1/z_1+q_p)^2+p_p^2}+\Im(C_3)\frac{x_1/z_1+q_p}{(x_1/z_1+q_p)^2+p_p^2}\\ &+\Re(C_2)\frac{p_s}{(x_1/z_1+q_s)^2+p_s^2}-\Im(C_2)\frac{x_1/z_1+q_s}{(x_1/z_1+q_s)^2+p_s^2},\end{aligned} \tag{4.66}$$

$$\begin{aligned}\frac{\pi\sigma_{xz}z_1}{P} =& +\Im(C_4)\frac{p_p}{(x_1/z_1+q_p)^2+p_p^2}+\Re(C_4)\frac{x_1/z_1+q_p}{(x_1/z_1+q_p)^2+p_p^2}\\ &-\Im(C_4)\frac{p_s}{(x_1/z_1+q_s)^2+p_s^2}-\Re(C_4)\frac{x_1/z_1+q_s}{(x_1/z_1+q_s)^2+p_s^2}.\end{aligned} \tag{4.67}$$

It may be noted that the solution of the field stress is not symmetric with respect to $x_1 = 0$ when the damping is not equal to zero. It is observed that there is singularity below the load. This effect is due to the presence of the point load.

The static solution can be found when the velocity of the load is very small; this case is the so-called Flamant problem. The solution of Cole and Huth [1958] for the subsonic case $M_s < 1$ is determined when the value of the damping is equal to zero. For this case the solutions of the horizontal and vertical stress are symmetric with respect to $x_1 = 0$.

A different way to represent the vertical stresses for $M_s = 2.0$ and $\zeta = 0.1$ is shown in Figure 4.10. It appears that the influence of the damping, $\zeta = 0.1$ in relation to $\zeta = 0.01$ (see Figure 4.11) is notably decreased. It should be observed that the scale in Figure 4.10 is a factor 2 smaller than in Figure 4.11. The two peaks in Figure 4.10 and Figure 4.11 indicate the wave fronts by a moving load at supersonic velocity. Note that for $x_1/l > 0$ the stresses vanish.

4.2.3 Displacements

In order to calculate the horizontal displacement u_x, expression (4.1) is rewritten as

$$\partial_{x_1}\sigma_{xx} + \partial_{z_1}\sigma_{zx} = \rho v^2 \partial^2_{x_1x_1} u_x. \tag{4.68}$$

Integrating with respect to x_1 twice gives

$$\int \sigma_{xx}\, dx_1 + \int\int \partial_{z_1}\sigma_{zx}\, dx_1 dx_1 = M_s^2 \mu u_x. \tag{4.69}$$

Therefore, using (4.56) and (4.64) leads to the following expression

$$\begin{aligned}\frac{\pi\mu}{P}u_x = &-\Re[C_5]\arctan\left(\frac{x_1+q_pz_1}{p_pz_1}\right) + \Im[C_5]\log\sqrt{((x_1+q_pz_1)^2+(p_pz_1)^2}\\ &-\Re[C_6b]\arctan\left(\frac{x_1+q_sz_1}{p_sz_1}\right) + \Im[C_6b]\log\sqrt{(x_1+q_sz_1)^2+(p_sz_1)^2}\\ &+K_xx + L_x,\end{aligned} \tag{4.70}$$

where K_x and L_x are integration constants. To be in agreement with the undamped case for the subsonic case $M_s < 1$ in Cole and Huth [1958] K_x and L_x are zero. The complex constants C_5 and C_6 are given by

$$C_5 = (M_s^2 - 2 + i4\zeta)\frac{1}{D} \quad \text{and} \quad C_6 = 2a(1 - i2\zeta)\frac{1}{D}. \tag{4.71}$$

It appears that the horizontal displacement for the undamped and damped cases are not antisymmetric with respect to x_1. Expression (4.70) can be rewritten as

$$\frac{\pi\mu}{P}u_x = \Im[C_5\log(\xi_p) + C_6b\log(\xi_s)], \tag{4.72}$$

where $\xi_p = r_p\exp(-i\beta_p)$, $\xi_s = r_s\exp(-i\beta_s)$, and r_p, r_s, β_p, β_s are given by

$$r_p = \sqrt{(x_1+q_pz_1)^2+(p_pz_1)^2} \quad \text{and} \quad \beta_p = \arctan\left(\frac{x_1+q_pz_1}{p_pz_1}\right), \tag{4.73}$$

$$r_s = \sqrt{(x_1+q_sz_1)^2+(p_sz_1)^2} \quad \text{and} \quad \beta_s = \arctan\left(\frac{x_1+q_sz_1}{p_sz_1}\right). \tag{4.74}$$

A particular case is the value of the horizontal displacement at the surface u_{xd}. This is expressed as

$$u_{xd} = \frac{P}{\pi\mu}\Im[(C_5 + C_6b)(\log|x_1| - i\pi/2)]. \tag{4.75}$$

Using (4.75), the static displacement at the surface u_{xs} can be found. This is obtained when the value of $M_s \to 0$ and the damping ratio $\zeta = 0$, yielding

$$u_{xs} = -\frac{P}{4\mu}\frac{1}{(m-1)} = -\frac{P}{4\mu}(1-2\nu), \tag{4.76}$$

where m is a dimensionless parameter. This is defined as

$$m = \frac{2(1-\nu)}{1-2\nu} = \frac{\lambda+2\mu}{\mu} = \frac{c_p^2}{c_s^2} = \frac{M_s^2}{M_p^2}. \tag{4.77}$$

This solution was also given by Harr [1966]. The dynamic amplification factor u_{xd}/u_{xs} at the surface is

$$\frac{u_{xd}}{u_{xs}} = -\frac{4(m-1)}{\pi}(\Im[C_5 + C_6 b]\log|x_1| - \Re[C_5 + C_6 b]\pi/2). \tag{4.78}$$

For determination of the vertical displacement u_z the basic equation of motion (4.2) is used. This is rewritten as

$$\partial_{x_1}\sigma_{xz} + \partial_{z_1}\sigma_{zz} = \rho v^2 \partial^2_{x_1 x_1} u_z. \tag{4.79}$$

Integrating with respect to x_1 twice gives

$$\int \sigma_{xz}\, dx_1 + \int\int \partial_{z_1}\sigma_{zz}\, dx_1 dx_1 = M_s^2 \mu u_z. \tag{4.80}$$

Therefore, introducing (4.60) and (4.64) into (4.80) leads to the following expression

$$\begin{aligned}\frac{\pi\mu}{P}u_z =& \Im[C_5 a]\arctan\left(\frac{x_1 + q_p z_1}{p_p z_1}\right) + \Re[C_5 a]\log\sqrt{(x_1 + q_p z_1)^2 + (p_p z_1)^2} \\ &+ \Im[C_6]\arctan\left(\frac{x_1 + q_s z_1}{p_s z_1}\right) + \Re[C_6]\log\sqrt{(x_1 + q_s z_1)^2 + (p_s z_1)^2} \\ &+ K_z x + L_z,\end{aligned} \tag{4.81}$$

where K_z and L_z are integration constants. Again $K_w = L_w = 0$ is needed to be in agreement with Cole and Huth [1958]. It follows that

$$\frac{\pi\mu}{P}u_z = \Re[C_5 a\log(\xi_p) + C_8\log(\xi_s)]. \tag{4.82}$$

A special case is the vertical displacement at the surface u_{zd}. It follows that

$$u_{zd} = \frac{P}{\pi\mu}M_s^2\Re\left[\frac{a}{D}(\log|x_1| - i\pi/2)\right]. \tag{4.83}$$

Therefore, the static vertical displacement at the surface u_{zs} can be obtained when the value of $M_s \to 0$ and the damping ratio $\zeta = 0$, yielding

$$u_{zs} = \frac{P}{\pi\mu}\frac{m}{2(m-1)}\log|x| = \frac{P}{\pi\mu}(1-\nu)\log|x|. \tag{4.84}$$

For the case of $x_1 = 0$, expression (4.82) becomes

$$\frac{\pi\mu}{P}u_z = \Re[C_5(\log(R_p z_1) - i\theta_p) + C_6 b(\log(R_s z_1) - i\theta_s)]. \tag{4.85}$$

Another way of denoting the vertical displacement is by using the differential displacement Δu_z. This is defined as

$$\Delta u_z = u_z(x_1, z_1) - u_z(x_1 + l, z_1), \tag{4.86}$$

where l is a given non-zero length. Substitution of (4.81) into (4.86) results in

$$\begin{aligned}\frac{\pi\mu}{P}\Delta u_z = &- \Im[C_5 a] \arctan\left(\frac{p_p z_1/l}{(p_p z_1/l)^2 + ((x_1 + q_p z_1)/l + 1/2)^2 - 1/4}\right) \\ &+ \Re[C_5 a] \log \sqrt{\frac{((x_1 + q_p z_1)/l)^2 + ((p_p z_1)/l)^2}{((x_1 + q_p z_1)/l + 1)^2 + ((p_p z_1)/l)^2}} \\ &- \Im[C_6] \arctan\left(\frac{p_s z_1/l}{(p_s z_1/l)^2 + ((x_1 + q_s z_1)/l + 1/2)^2 - 1/4}\right) \\ &+ \Re[C_6] \log \sqrt{\frac{((x_1 + q_s z_1)/l)^2 + ((p_s z_1)/l)^2}{((x_1 + q_s z_1)/l + 1)^2 + ((p_s z_1)/l)^2}}. \end{aligned} \tag{4.87}$$

The differential displacement at the surface Δu_{zd} is

$$\frac{\pi\mu}{P}\Delta u_{zd} = M_s^2 \Re\left[\frac{a}{D}\right] \log\left|\frac{x_1/l}{x_1/l + 1}\right|. \tag{4.88}$$

For the supersonic case $M_s = 2.0$ and a damping ratio $\zeta = 0.1$, the differential vertical displacement is illustrated in Figure 4.12. The figure indicates that two discontinuities are generated, however they are less pronounced. For larger values of the damping the results become progressively smoother and smoother. It is also observed that a small upward displacement in front of the load is present. This effect only appears if a relatively large value of the damping ratio is considered.

Figure 4.13 shows the almost undamped case, given by the damping $\zeta = 0.001$ and the supersonic case $M_s = 2.0$. It appears in this figure that two jumps are generated. The slopes of these two jumps correspond to the solution of the undamped case by

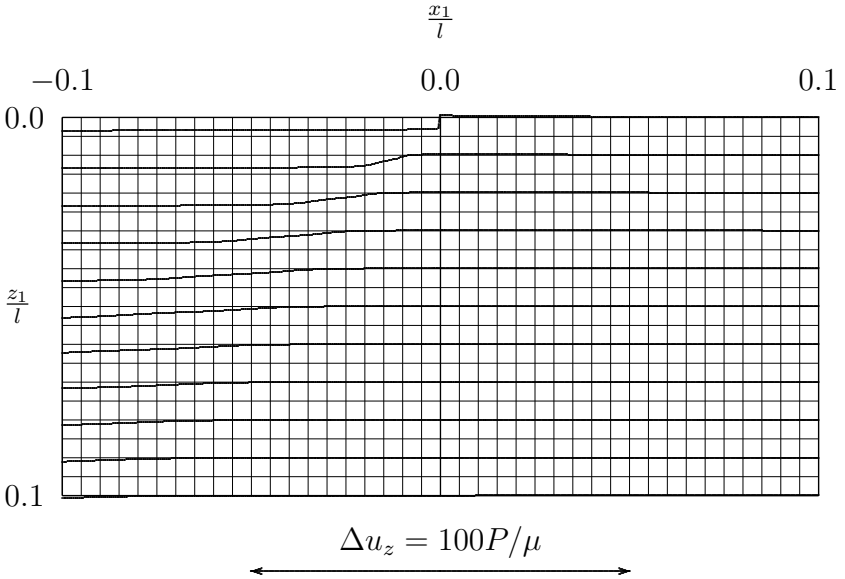

Figure 4.12: Moving load on a half-plane, differential displacement Δu_z: $\nu = 0$, $\zeta = 0.1$, $M_s = 2.0$.

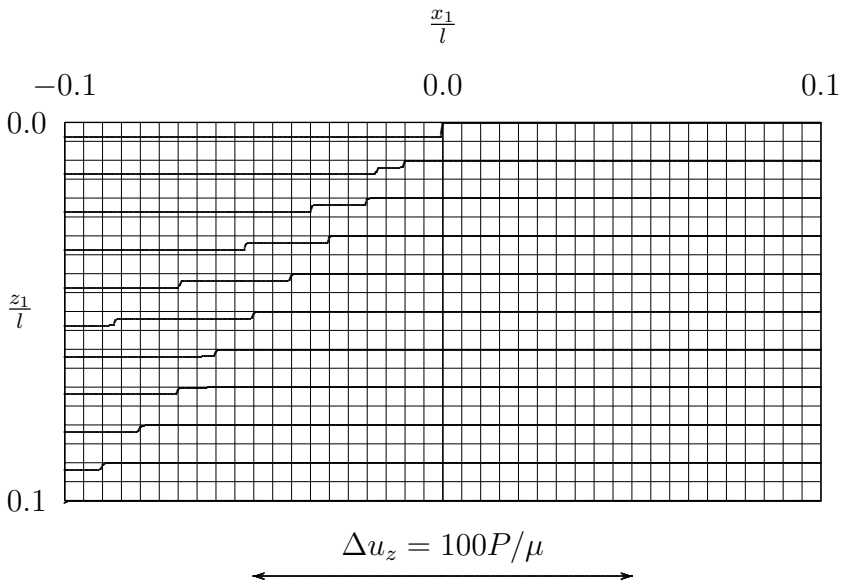

Figure 4.13: Moving load on a half-plane, differential displacement Δu_z: $\nu = 0$, $\zeta = 0.001$, $M_s = 2.0$.

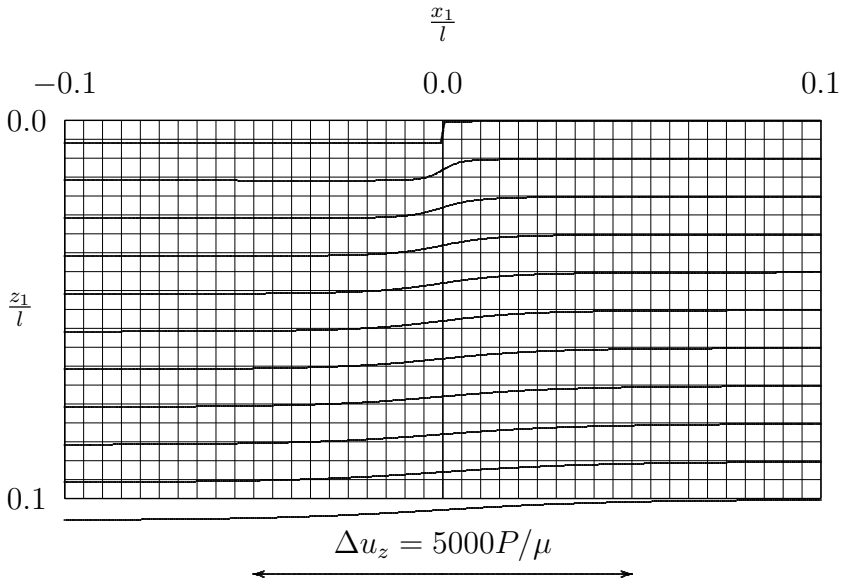

Figure 4.14: Moving load on a half-plane, differential displacement Δu_z: $\nu = 0$, $\zeta = 0.01$, $M_s = 0.874032$.

Cole and Huth [1958]. These jumps occur at $x_1 = -\sqrt{M_s^2 - 1}z_1 = -\sqrt{3}z_1$ and $x_1 = -\sqrt{M_p^2 - 1}z_1 = -z_1$, where $\nu = 0$ and $M_s = 2.0$. These slopes verify the wave fronts by a moving load at supersonic velocity, see the text of Fung [1965]. Similar results are obtained when the damping is smaller than 0.001, with the jumps becoming even sharper.

It is interesting to determine the case of the Rayleigh wave velocity in an elastic medium, $M_s = 0.874032$, if the value of Poisson's ratio is equal to zero. In this case the displacements are very large, and a strong jump appears just below the load, as shown in Figure 4.14. For this case the scale of the displacements is a factor 50 larger than in Figure 4.12 and Figure 4.13. These results confirm that the displacements are much larger for the Rayleigh wave velocity. The results of the classical solution for the point load on an elastic half-plane, known as Flamant's solution and given by the text of Timoshenko and Goodier [1951], can be approached when the load on the surface travels with a very small velocity.

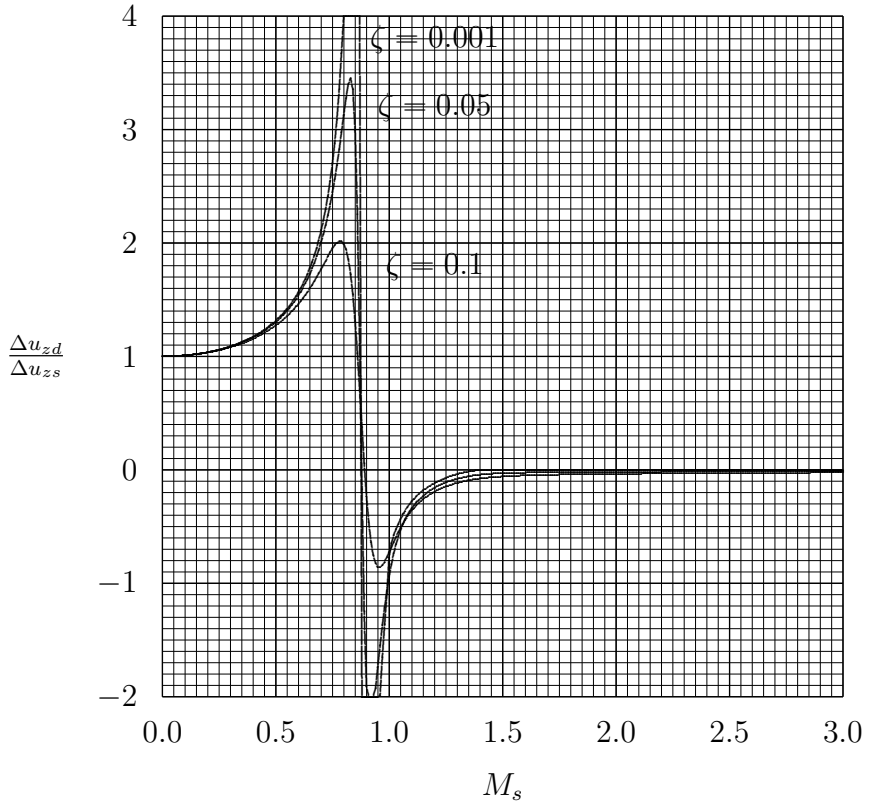

Figure 4.15: Moving load on a half-plane, amplitude of the dynamic amplification factor of the differential displacement at the surface $\Delta u_{zd}/\Delta u_{zs}$: $\nu = 0$.

The dynamic amplification factor of the differential displacement $\Delta u_{zd}/\Delta u_{zs}$ at the surface is defined as

$$\frac{\Delta u_{zd}}{\Delta u_{zs}} = \frac{M_s^2(1+4\zeta^2)}{(1-\nu)} \Re\left[\frac{a}{D}\right] \frac{\log\left|\frac{x_1/l}{x_1/l+1}\right|}{\log\left|\frac{x/l}{x/l+1}\right|}, \tag{4.89}$$

where the quasi-static differential displacement at the surface Δu_{zs} is

$$\frac{\pi\mu}{P}\Delta u_{zs} = \frac{(1-\nu)}{(1+i2\zeta)} \log\left|\frac{x/l}{x/l+1}\right|. \tag{4.90}$$

The factor $(1+i2\zeta)$ is a scaling factor, included to calculate the quasi-static case.

Figure 4.15 illustrates the amplitude of $\Delta u_{zd}/\Delta u_{zs}$ as a function of M_s, for three values of the damping ratio: $\zeta = 0.001,\ 0.05,\ 0.1$. For a very small value of ζ the undamped case can be approached. Note that a damping ratio of $\zeta = 0.1$ reduces the peak value to about two times the quasi-static value. It can also be seen that the influence of ζ on the peaks of the dynamic amplification factor is again very large. For values of $M_s > 2.0$ the amplitude of $\Delta u_{zd}/\Delta u_{zs}$ are very small.

Chapter 5

Moving loads on an elastic plane layer with hysteretic damping

The propagation of waves in a plane layer caused by surface forces is examined for an isotropic elastic medium with hysteretic damping. The wave motion corresponding to an elastic plane layer has been extensively discussed in several studies. Love [1911, 1926] investigated the dispersion of Rayleigh waves on the surface of a layer. A wide treatment of the study of waves in elastic plate is found in Lamb [1917]. A theory of flexural motions of elastic plates was formulated by Mindlin [1951]. The study of dispersion curves for several modes are given by Tolstoy and Usdin [1953] for the case of a layer on a very stiff elastic half-space. The case of a plate bounded by two parallel planes is given by Ewing *et al.* [1957]. Furthermore, detailed information on the dispersion curves for free waves is found. An analysis of the critical velocities of a harmonic point load moving along an elastic space layer is presented by Dieterman and Metrikine [1997]. A two-dimensional model of ground vibration of a visco-elastic layer, and two Euler-Bernoulli beams perturbed by a constant and harmonically varying moving point load is found by Metrikine and Vrouwenvelder [2000].

The case of propagation of waves in an elastic medium with hysteretic damping due to a moving load on the surface of a plane layer is presented in this chapter.

5.1 Basic equations

The basic equations of motion in two dimensions are given by

$$\partial_x \sigma_{xx} + \partial_z \sigma_{zx} = \rho \partial_{tt}^2 u_x, \tag{5.1}$$

$$\partial_x \sigma_{xz} + \partial_z \sigma_{zz} = \rho \partial_{tt}^2 u_z, \tag{5.2}$$

where $u_x(x,z,t)$ and $u_z(x,z,t)$ are the displacements in the x and z directions, with $-\infty < x < \infty$ and $-h \leq z \leq 0$. The displacements are expressed in terms of the potential functions $\phi(x,z,t)$ and $\psi(x,z,t)$, as follows

$$u_x = \partial_x \phi - \partial_z \psi, \tag{5.3}$$

$$u_z = \partial_z \phi + \partial_x \psi. \tag{5.4}$$

Figure 5.1 shows a plane layer with depth h. The stress components are also given in

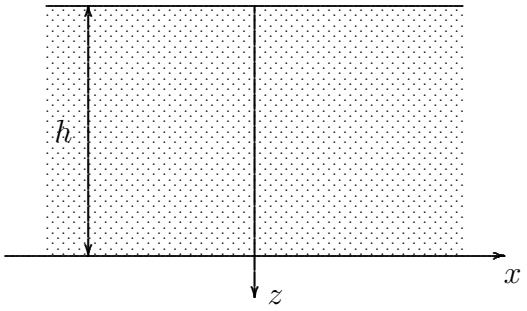

Figure 5.1: Plane layer.

terms of ϕ and ψ,

$$\sigma_{xx} = \lambda(1 + t_r\partial_t)(\partial^2_{xx}\phi + \partial^2_{zz}\phi) + 2\mu(1 + t_r\partial_t)(\partial^2_{xx}\phi - \partial_x\partial_z\psi), \tag{5.5}$$

$$\sigma_{zz} = \lambda(1 + t_r\partial_t)(\partial^2_{xx}\phi + \partial^2_{zz}\phi) + 2\mu(1 + t_r\partial_t)(\partial^2_{zz}\phi + \partial_x\partial_z\psi), \tag{5.6}$$

$$\sigma_{xz} = \mu(1 + t_r\partial_t)(2\partial_x\partial_z\phi + \partial^2_{xx}\psi - \partial^2_{zz}\psi), \tag{5.7}$$

where t_r is a relaxation time. In order to describe the hysteretic damping the value of t_r should be inversely proportional to the frequency of the load. Substitution expressions of (5.3) through (5.7) into (5.1) and (5.2) shows that the basic equations of motion can be satisfied if the potentials are solutions of

$$(1 + t_r\partial_t)(\partial^2_{xx}\phi + \partial^2_{zz}\phi) = \frac{1}{c_p^2}\partial^2_{tt}\phi, \tag{5.8}$$

$$(1 + t_r\partial_t)(\partial^2_{xx}\psi + \partial^2_{zz}\psi) = \frac{1}{c_s^2}\partial^2_{tt}\psi, \tag{5.9}$$

where $c_p^2 = (\lambda + 2\mu)/\rho$ and $c_s^2 = \mu/\rho$.

5.2 Moving loads on a plane layer

Plane waves in a fixed layer of uniform thickness h are studied. A moving load at constant velocity v along the surface of a layer is examined. The problem is solved with the aid of a moving coordinate system (x_1, z_1), with $-\infty < x_1 < \infty$ and $-h \le z_1 \le 0$,

$$x_1 = x - vt \quad \text{and} \quad z_1 = z. \tag{5.10}$$

Substituting (5.10) into (5.5) - (5.9), follows that

$$\frac{\sigma_{xx}}{\mu} = (M_s^2 - 2M_p^2 + 2)\partial^2_{x_1x_1}\phi - 2\partial_{x_1}\partial_{z_1}\psi - 2vt_r\partial_{x_1}(\partial^2_{x_1x_1}\phi - \partial_{x_1}\partial_{z_1}\psi), \tag{5.11}$$

$$\frac{\sigma_{zz}}{\mu} = (M_s^2 - 2)\partial^2_{x_1x_1}\phi + 2\partial_{x_1}\partial_{z_1}\psi + 2vt_r\partial_{x_1}(\partial^2_{x_1x_1}\phi - \partial_{x_1}\partial_{z_1}\psi), \tag{5.12}$$

$$\frac{\sigma_{xz}}{\mu} = 2\partial_{x_1}\partial_{z_1}\phi - (M_s^2 - 2)\partial^2_{x_1x_1}\psi - 2vt_r\partial_{x_1}(\partial_{x_1}\partial_{z_1}\phi + \partial^2_{x_1x_1}\psi), \tag{5.13}$$

with $M_s = v/c_s$ and $M_p = v/c_p$. In a similar way, the expressions for the basic equations (5.8) and (5.9) can be rewritten as

$$(1 - vt_r\partial_{x_1})(\partial^2_{x_1x_1}\phi + \partial^2_{z_1z_1}\phi) = M_p^2\partial^2_{x_1x_1}\phi, \tag{5.14}$$

$$(1 - vt_r\partial_{x_1})(\partial^2_{x_1x_1}\psi + \partial^2_{z_1z_1}\psi) = M_s^2\partial^2_{x_1x_1}\psi. \tag{5.15}$$

The solution of this system of equations will be determined when the boundary conditions are given.

5.2.1 Moving point load

For the case of a moving point load on a fixed layer, the boundary conditions at the surface $z = -h$ are free of shear stress and loaded with a constant line force P. At the bottom of the layer $z = 0$ the displacements vanish (see Figure 5.2). Udias [1999], and Kausel and Manolis [2000] can be given as reference texts for the study of a fixed layer bounded by a free surface. The boundary conditions are represented by

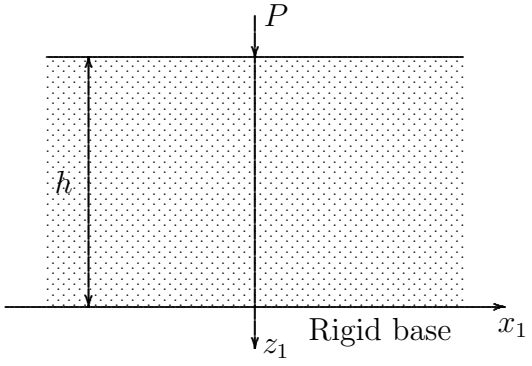

Figure 5.2: Moving load on a plane layer.

$$z_1 = -h \ : \ \sigma_{zz} = -P\delta(x - vt) = -P\delta(x_1), \tag{5.16}$$

$$z_1 = -h \ : \ \sigma_{xz} = 0, \tag{5.17}$$

$$z_1 = 0 \ : \ u_x = 0, \tag{5.18}$$

$$z_1 = 0 \ : \ u_z = 0, \tag{5.19}$$

where $\delta(x_1)$ is the Delta function. Using the exponential Fourier transformation over the x_1 coordinate the potential functions ϕ and ψ are transformed into

$$\tilde{\phi}(k, z_1) = \int_{-\infty}^{\infty} \phi(x_1, z_1) \exp(-ikx_1)\, dx_1, \tag{5.20}$$

$$\tilde{\psi}(k, z_1) = \int_{-\infty}^{\infty} \psi(x_1, z_1) \exp(-ikx_1)\, dx_1, \tag{5.21}$$

where k is the horizontal wave number. Introducing (5.20) and (5.21) into (5.14) and (5.15), yields

$$\partial^2_{z_1 z_1} \tilde{\phi} - k^2 \frac{(1 - M_p^2 + (vt_r k)^2 - ivt_r k M_p^2)}{1 + (vt_r k)^2} \tilde{\phi} = 0, \tag{5.22}$$

$$\partial^2_{z_1 z_1} \tilde{\psi} - k^2 \frac{(1 - M_s^2 + (vt_r k)^2 - ivt_r k M_s^2)}{1 + (vt_r k)^2} \tilde{\psi} = 0. \tag{5.23}$$

Assume that the solutions of (5.22) and (5.23) have the following form

$$\tilde{\phi}(k, z_1) = A_1(k) \exp(-akz_1) + A_2(k) \exp(akz_1), \tag{5.24}$$

$$\tilde{\psi}(k, z_1) = B_1(k) \exp(-bkz_1) + B_2(k) \exp(bkz_1), \tag{5.25}$$

where a and b are wave numbers. The complex coefficients A_1, A_2, B_1 and B_2 are obtained from the boundary conditions. The values of a and b can be written as

$$a^2 = R_p^2 \exp(-i2\vartheta_p), \tag{5.26}$$

$$b^2 = R_s^2 \exp(-i2\vartheta_s), \tag{5.27}$$

where R_p, R_s, and the angles ϑ_p and ϑ_s are given by

$$R_p = \sqrt[4]{\frac{(1 - M_p^2)^2 + (vt_r k)^2}{1 + (vt_r k)^2}}, \tag{5.28}$$

$$R_s = \sqrt[4]{\frac{(1 - M_s^2)^2 + (vt_r k)^2}{1 + (vt_r k)^2}}, \tag{5.29}$$

$$\vartheta_p = \frac{1}{2}\arctan\left(\frac{vt_r k M_p^2}{1 - M_p^2 + (vt_r k)^2}\right); \quad 0 \le \vartheta_p < \pi/2, \tag{5.30}$$

$$\vartheta_s = \frac{1}{2}\arctan\left(\frac{vt_r k M_s^2}{1 - M_s^2 + (vt_r k)^2}\right); \quad 0 \le \vartheta_s < \pi/2. \tag{5.31}$$

Using (5.20) and (5.21) the stress components (5.12) - (5.14), and the displacements (5.3) and (5.4) are transformed into

$$\frac{\tilde{\sigma}_{xx}}{\mu} = -k^2(M_s^2 - 2M_p^2 + 2 - i2vt_r k)\tilde{\phi} - i2k(1 - ivt_r k)\partial_{z_1}\tilde{\psi}, \tag{5.32}$$

$$\frac{\tilde{\sigma}_{zz}}{\mu} = -k^2(M_s^2 - 2 + i2vt_r k)\tilde{\phi} + i2k(1 - ivt_r k)\partial_{z_1}\tilde{\psi}, \tag{5.33}$$

$$\frac{\tilde{\sigma}_{xz}}{\mu} = i2k(1 - ivt_r k)\partial_{z_1}\tilde{\phi} + k^2(M_s^2 - 2 + i2vt_r k)\tilde{\psi}, \tag{5.34}$$

$$\tilde{u}_x = ik\tilde{\phi} - \partial_{z_1}\tilde{\psi}, \tag{5.35}$$

$$\tilde{u}_z = \partial_{z_1}\tilde{\phi} + ik\tilde{\psi}. \tag{5.36}$$

From (5.16) - (5.19) and (5.33) - (5.36) for $z = -h$ and 0, it follows that

$$\begin{bmatrix} d_{11}e^{a\xi} & d_{11}e^{-a\xi} & i2bd_{21}e^{b\xi} & -i2bd_{21}e^{-b\xi} \\ -i2ad_{21}e^{a\xi} & i2ad_{21}e^{-a\xi} & d_{11}e^{b\xi} & d_{11}e^{-b\xi} \\ i & i & b & -b \\ -a & a & i & i \end{bmatrix} \begin{bmatrix} A_1 \\ A_2 \\ B_1 \\ B_2 \end{bmatrix} = \begin{bmatrix} C \\ 0 \\ 0 \\ 0 \end{bmatrix}, \tag{5.37}$$

where the dimensionless wave number ξ, and the parameters C, d_{11} and d_{21} are

$$\xi = kh, \tag{5.38}$$

$$C = \frac{P}{\mu}\frac{h^2}{\xi^2}, \tag{5.39}$$

$$d_{11} = M_s^2 - 2 + i2vt_r k \quad \text{and} \quad d_{21} = 1 - ivt_r k. \tag{5.40}$$

The solution of the system of equations (5.37) is

$$\begin{bmatrix} A_1 \\ A_2 \\ B_1 \\ B_2 \end{bmatrix} = \begin{bmatrix} -2abd_{21}e^{-a\xi} + d_{11}(\sinh(b\xi) - ab\cosh(b\xi)) \\ -(2abd_{21}e^{-a\xi} + d_{11}(\sinh(b\xi) + ab\cosh(b\xi))) \\ ia(d_{11}e^{-b\xi} + 2d_{21}(\cosh(a\xi) - ab\sinh(a\xi))) \\ -ia(d_{11}e^{b\xi} + 2d_{21}(\cosh(a\xi) + ab\sinh(a\xi))) \end{bmatrix} \frac{2C}{\Delta}, \tag{5.41}$$

where Δ is the determinant of the system. The determinant is also known as the dispersion relation for a fixed plane layer when the relaxation time t_r in (5.42) is equal to zero. It follows that

$$\Delta = -4(4abd_{11}d_{21} + ab(d_{11}^2 + 4d_{21}^2)\cosh(b\xi)\cosh(a\xi) - (d_{11}^2 + 4a^2b^2d_{21}^2)\sinh(b\xi)\sinh(a\xi)). \tag{5.42}$$

It can also be verified that the determinant is not equal to zero for all values of the dimensionless wave number ξ and when the value of M_s lies between zero and the dimensionless parameter $M_r = c_r/c_s$. The Rayleigh wave velocity is denoted by c_r.

For different values of Poisson's ratio the relationship of the wave velocity M_s to the dimensionless wave number ξ is shown in Figure 5.3. It appears that for $\xi = 16$, the value of M_s approaches M_r. The velocity of the Rayleigh wave c_r is obtained when

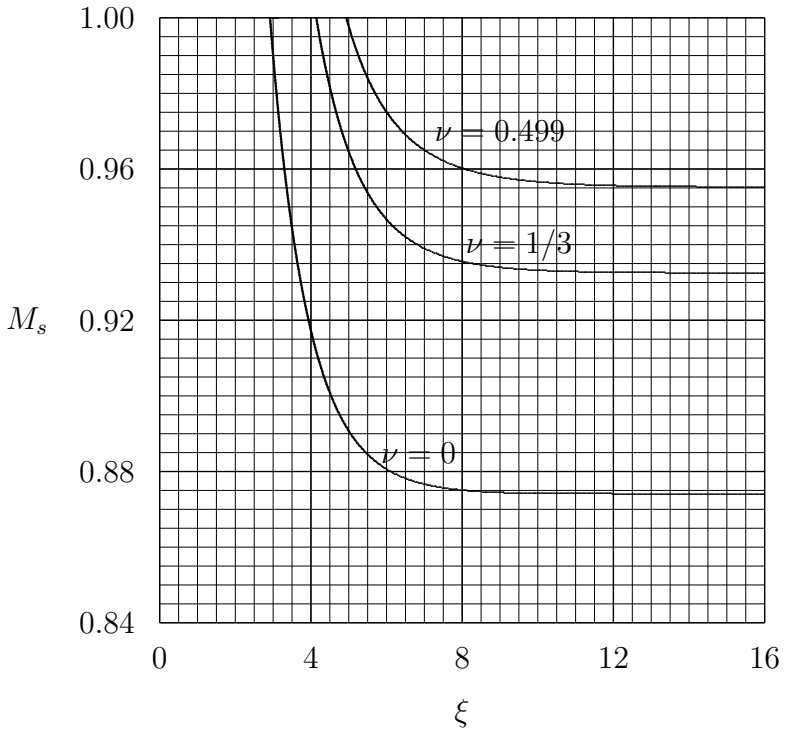

Figure 5.3: Moving load on a plane layer, dispersion curve.

the relaxation time t_r is considered to be zero. The Rayleigh wave equation is

$$(M_s^2 - 2)^2 - 4(1 - M_s^2)^{1/2}(1 - M_p^2)^{1/2} = 0. \tag{5.43}$$

Introducing (5.41) into (5.24) and (5.25), this becomes

$$\tilde{\phi} = -(2abd_{21}\cosh(a(1 + z_1/h)\xi) + d_{11}(\sinh(b\xi)\sinh(a\xi z_1/h) + ab\cosh(b\xi)\cosh(a\xi z_1/h)))\frac{4C}{\Delta}, \tag{5.44}$$

$$\tilde{\psi} = -ia(d_{11}\sinh(b(1 + z_1/h)\xi) + 2d_{21}(\cosh(a\xi)\sinh(b\xi z_1/h) + ab\sinh(a\xi)\cosh(b\xi z_1/h)))\frac{4C}{\Delta}. \tag{5.45}$$

The hysteretic damping is represented by the damping ratio ζ. This is given as

$$\zeta = \frac{vt_r k}{2} sign(k), \tag{5.46}$$

where $|\zeta|$ is considered to be a constant, and $sign(k)$ denotes the sign of k. Therefore, expressions (5.28) - (5.31) and (5.40) lead to

$$R_p = \sqrt[4]{\frac{(1-M_p^2)^2 + 4\zeta^2}{1+4\zeta^2}}, \tag{5.47}$$

$$R_s = \sqrt[4]{\frac{(1-M_s^2)^2 + 4\zeta^2}{1+4\zeta^2}}, \tag{5.48}$$

$$\vartheta_p = \frac{1}{2}\arctan\left(\frac{2\zeta M_p^2}{1-M_p^2+4\zeta^2}\right); \quad 0 \le \vartheta_p < \pi/2, \tag{5.49}$$

$$\vartheta_s = \frac{1}{2}\arctan\left(\frac{2\zeta M_s^2}{1-M_s^2+4\zeta^2}\right); \quad 0 \le \vartheta_s < \pi/2, \tag{5.50}$$

$$d_{11} = M_s^2 - 2 + i4\zeta \quad \text{and} \quad d_{21} = 1 - i2\zeta. \tag{5.51}$$

5.2.2 Stress components

The stress components are determined when the respective Fourier transformations are found. Substituting (5.44) and (5.45) into (5.32) - (5.34), gives

$$\begin{aligned}\frac{\tilde{\sigma}_{xx}}{P} = [&d_{31}(2abd_{21}\cosh(a(1+z_1/h)\xi) + d_{11}(\sinh(b\xi)\sinh(a\xi z_1/h) \\ &+ ab\cosh(b\xi)\cosh(a\xi z_1/h))) - 2abd_{21}(d_{11}\cosh(b(1+z_1/h)\xi) \\ &+ 2d_{21}(\cosh(a\xi)\cosh(b\xi z_1/h) + ab\sinh(a\xi)\sinh(b\xi z_1/h)))]\frac{4}{\Delta},\end{aligned} \tag{5.52}$$

$$\begin{aligned}\frac{\tilde{\sigma}_{zz}}{P} = [&d_{11}(2abd_{21}\cosh(a(1+z_1/h)\xi) + d_{11}(\sinh(b\xi)\sinh(a\xi z_1/h) \\ &+ ab\cosh(b\xi)\cosh(a\xi z_1/h))) + 2abd_{21}(d_{11}\cosh(b(1+z_1/h)\xi) \\ &+ 2d_{21}(\cosh(a\xi)\cosh(b\xi z_1/h)ab\sinh(a\xi)\sinh(b\xi z_1/h)))]\frac{4}{\Delta},\end{aligned} \tag{5.53}$$

$$\begin{aligned}\frac{\tilde{\sigma}_{xz}}{P} = -ia[&2d_{21}(2abd_{21}\sinh(a(1+z_1/h)\xi) + d_{11}(\sinh(b\xi)\cosh(a\xi z_1/h) \\ &+ ab\cosh(b\xi)\sinh(a\xi z_1/h))) + d_{11}(d_{11}\sinh(b(1+z_1/h)\xi) \\ &+ 2d_{21}(\cosh(a\xi)\sinh(b\xi z_1/h) + ab\sinh(a\xi)\cosh(b\xi z_1/h)))]\frac{4}{\Delta},\end{aligned} \tag{5.54}$$

where the parameter d_{31} is given as

$$d_{31} = M_s^2 - 2M_p^2 + 2 - i4\zeta. \tag{5.55}$$

Therefore, applying the inverse Fourier transformation with respect to the dimensionless wave number ξ to (5.52) - (5.54), one obtains the following expressions for the stresses

$$\begin{aligned}\frac{\pi\sigma_{xx}h}{4P} = \int_0^\infty \Re[[&d_{31}(2abd_{21}\cosh(a(1+z_1/h)\xi)\\ &+ d_{11}(\sinh(b\xi)\sinh(a\xi z_1/h) + ab\cosh(b\xi)\cosh(a\xi z_1/h)))\\ &- 2abd_{21}(d_{11}\cosh(b(1+z_1/h)\xi) + 2d_{21}(\cosh(a\xi)\cosh(b\xi z_1/h)\\ &+ ab\sinh(a\xi)\sinh(b\xi z_1/h)))]\exp(i\xi x_1/h)/\Delta]\,d\xi,\end{aligned} \tag{5.56}$$

$$\begin{aligned}\frac{\pi\sigma_{zz}h}{4P} = \int_0^\infty \Re[[&d_{11}(2abd_{21}\cosh(a(1+z_1/h)\xi)\\ &+ d_{11}(\sinh(b\xi)\sinh(a\xi z_1/h) + ab\cosh(b\xi)\cosh(a\xi z_1/h)))\\ &+ 2abd_{21}(d_{11}\cosh(b(1+z_1/h)\xi) + 2d_{21}(\cosh(a\xi)\cosh(b\xi z_1/h)\\ &+ ab\sinh(a\xi)\sinh(b\xi z_1/h)))]\exp(i\xi x_1/h)/\Delta]\,d\xi,\end{aligned} \tag{5.57}$$

$$\begin{aligned}\frac{\pi\sigma_{xz}h}{4P} = \int_0^\infty \Im[[&2d_{21}(2abd_{21}\sinh(a(1+z_1/h)\xi)\\ &+ d_{11}(\sinh(b\xi)\cosh(a\xi z_1/h) + ab\cosh(b\xi)\sinh(a\xi z_1/h)))\\ &+ d_{11}(d_{11}\sinh(b(1+z_1/h)\xi) + 2d_{21}(\cosh(a\xi)\sinh(b\xi z_1/h)\\ &+ ab\sinh(a\xi)\cosh(b\xi z_1/h)))]a\exp(i\xi x_1/h)/\Delta]\,d\xi.\end{aligned} \tag{5.58}$$

In order to calculate the stress field the integrals of the right hand side of (5.56) - (5.58) are evaluated numerically using Simpson's integration method.

Figure 5.4 shows the quasi-static vertical stresses at the bottom $z_1/h = 0$ when the value of M_s is very small and the damping ratio ζ tends to zero. For Poisson's ratio $\nu = 0.4999$ the results are in agreement with the solution for the case of Biot, given in the text of Harr [1966]. Margurerre [1931] also found that the influence of Poisson's ratio on the results is of little significance for the static case. For Poisson's ratio $\nu = 0$ the results are depicted by dots. For the supersonic case $M_s = 2.0$ and a damping ratio $\zeta = 0.1$, Figure 5.5 illustrates the vertical stresses in terms of the dimensionless

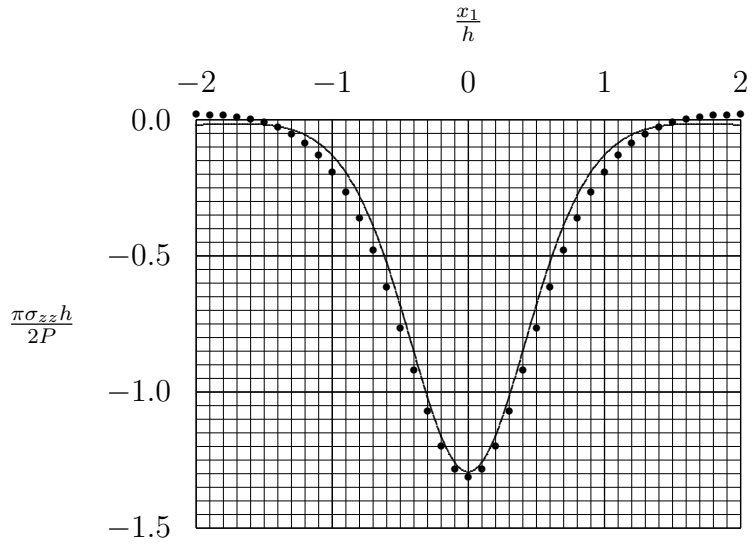

Figure 5.4: Moving load on a plane layer, quasi-static vertical stress at the bottom $z_1 = 0$.

depth z_1/h. Wave fronts by a moving load at supersonic velocity are shown. It can also be observed that two peaks are generated. The first peak corresponds to the compression wave and the second peak corresponds to the shear wave. Observe also that the distribution of the vertical stresses at $x_1/h = 2.0$ vanish. On account of the rigid base of the layer the vertical stresses behind the two peaks fluctuate substantially.

For a small value of the damping ratio $\zeta = 0.01$, Figure 5.6 shows influence on the magnitude of the vertical stresses. In this case the damping ratio is a factor 10 smaller. The results confirm clearly that the large stresses for small values of the damping ratio are reduced when the damping ratio increases. Furthermore, it can be observed that the scale is 10 times larger than in Figure 5.5. It can also be seen that two peaks are generated. For Poisson's ratio $\nu = 0$ and $M_s = 2.0$, the slope of the peak corresponding to the shear wave approaches the expression $x_1 = \sqrt{M_s^2 - 1}z_1 = \sqrt{3}z_1$; the second peak corresponding to the compression wave approaches the expression $x_1 = \sqrt{M_p^2 - 1}z_1 = z_1$. The fluctuations behind the two peaks are generated owing to the bottom of the layer. A simple approximation of the peaks of the reflections can be given by the following expressions: $x_1 = \sqrt{M_s^2 - 1}(z_1 - 1) = \sqrt{3}(z_1 - 1)$ and $x_1 = \sqrt{M_p^2 - 1}(z_1 - 1) = z_1 - 1$. For Poisson's ratio $\nu = 0$ and $M_s = 2.0$, the value of M_p equals $\sqrt{2}$.

The vertical stresses are shown in Figure 5.7 for the case of velocities close to the Rayleigh wave velocity, for Poisson's ratio $\nu = 0$ and damping ratio $\zeta = 0.01$. The dimensionless velocity is in this case $M_s = 0.874032$, which is approximately the Rayleigh wave velocity in an elastic medium if $\nu = 0$. It also appears that for values of $x_1/h > 0$ the vertical stresses vanish.

For a damping ratio $\zeta = 0.1$ and $M_s = 0.874032$, the influence of the damping ratio on the vertical stresses is seen in Figure 5.8. In this case the results are strongly reduced in comparison with Figure 5.7. In this figure the scale is 10 times smaller than in Figure 5.7. For values of $x_1/h > 0$ the vertical stresses vanish again.

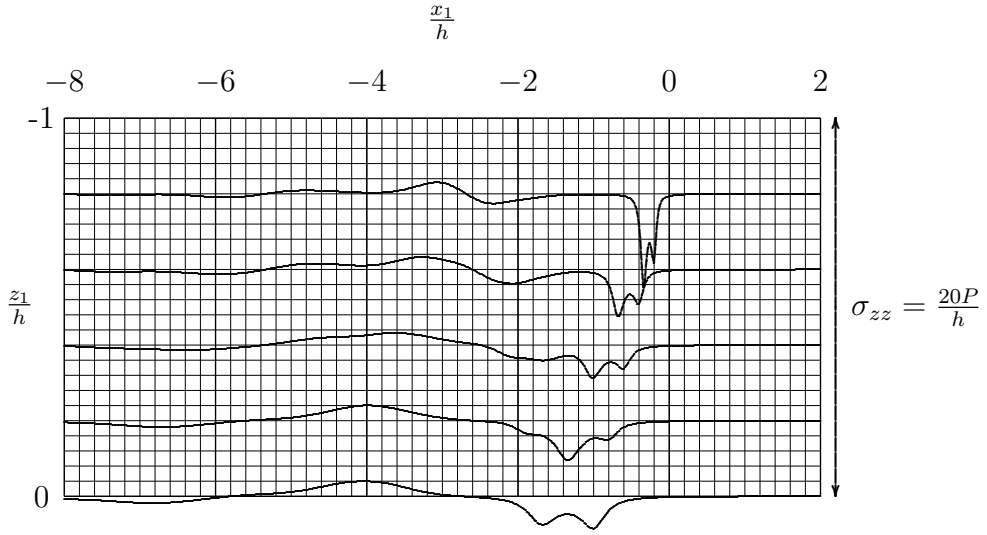

Figure 5.5: Moving load on a plane layer, vertical stress: $\nu = 0$, $\zeta = 0.1$, $M_s = 2.0$.

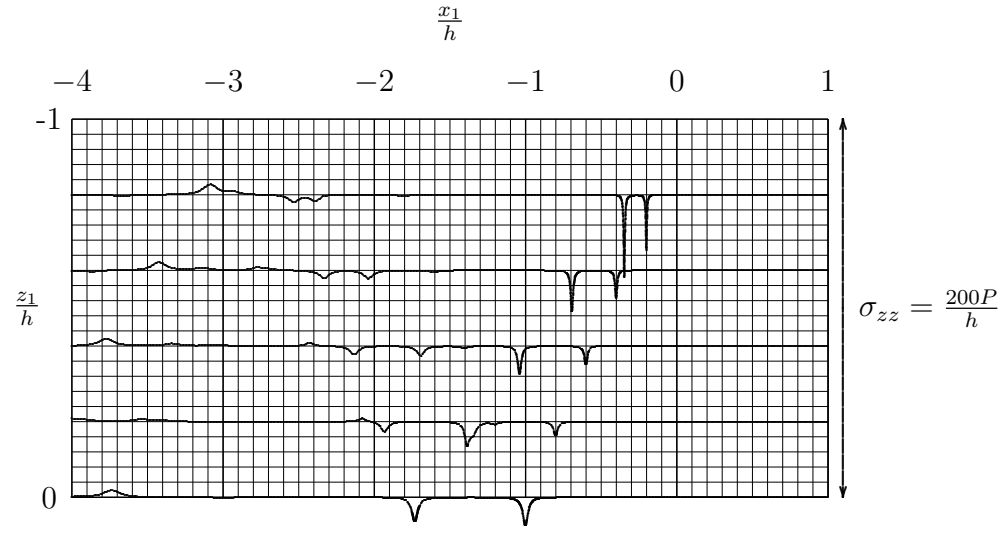

Figure 5.6: Moving load on a plane layer, vertical stress: $\nu = 0$, $\zeta = 0.01$, $M_s = 2.0$.

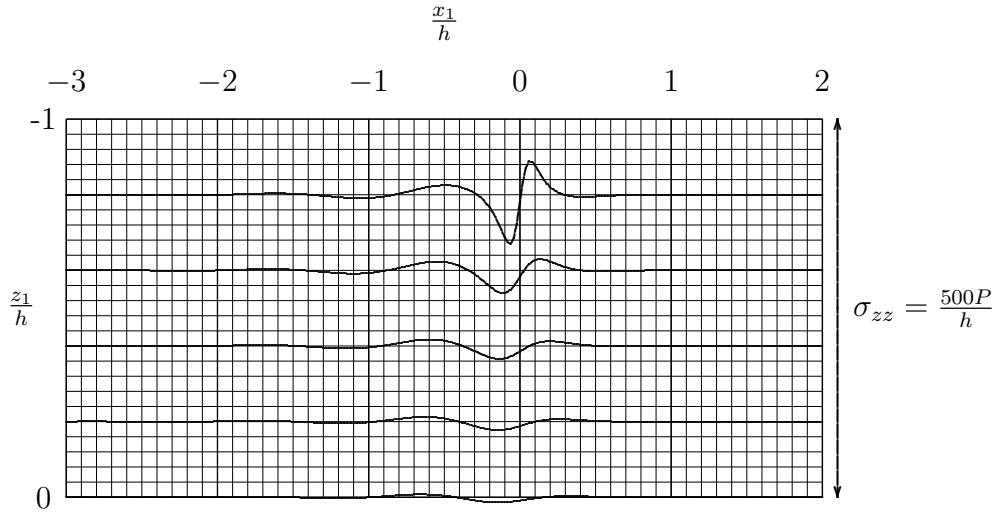

Figure 5.7: Moving load on a plane layer, vertical stress: $\nu = 0$, $\zeta = 0.01$, $M_s = 0.874032$.

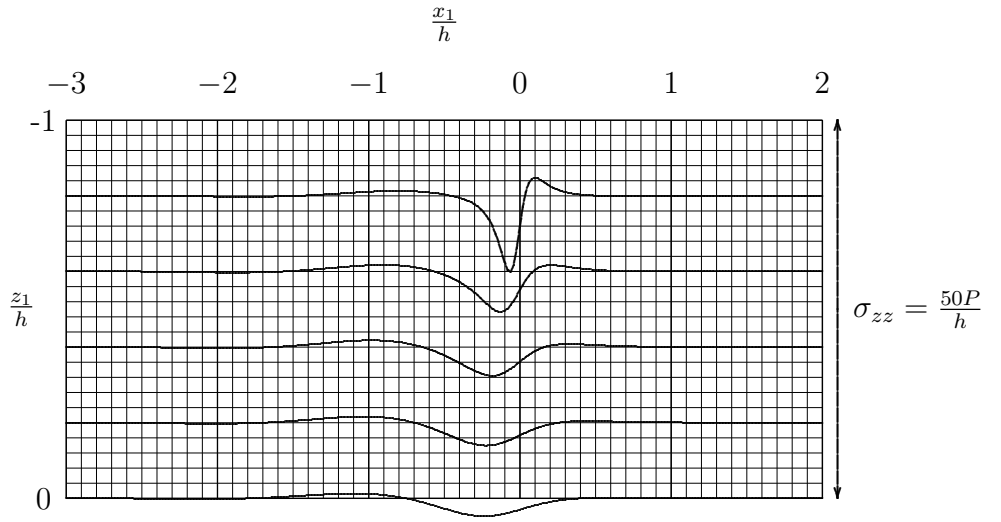

Figure 5.8: Moving load on a plane layer, vertical stress: $\nu = 0$, $\zeta = 0.1$, $M_s = 0.874032$.

5.2.3 Displacement components

Introducing (5.44) and (5.45) into (5.35) and using the inverse Fourier transformation, one obtains the horizontal displacement,

$$\begin{aligned}\frac{\pi\mu}{P}u_x = i2\int_{-\infty}^{\infty}[&-(2abd_{21}(\cosh(a(1+z_1/h)\xi)+d_{11}(\sinh(b\xi)\sinh(a\xi z_1/h)\\&+ab\cosh(b\xi)\cosh(a\xi z_1/h)))+ab(d_{11}\cosh(b(1+z_1/h)\xi)\\&+2d_{21}(\cosh(a\xi)\cosh(b\xi z_1/h)+ab\sinh(a\xi)\sinh(b\xi z_1/h)))]\\&\times\exp(i\xi x_1/h)/\left(\xi\Delta\right)d\xi,\end{aligned}\tag{5.59}$$

$$\begin{aligned}\frac{\pi\mu}{4P}u_x = -\int_0^{\infty}\Im[[&-(2abd_{21}(\cosh(a(1+z_1/h)\xi)\\&+d_{11}(\sinh(b\xi)\sinh(a\xi z_1/h)+ab\cosh(b\xi)\cosh(a\xi z_1/h)))\\&+ab(d_{11}\cosh(b(1+z_1/h)\xi)+2d_{21}(\cosh(a\xi)\cosh(b\xi z_1/h)\\&+ab\sinh(a\xi)\sinh(b\xi z_1/h)))]\exp(i\xi x_1/h)/\left(\xi\Delta\right)]\,d\xi.\end{aligned}\tag{5.60}$$

Introducing (5.44) and (5.45) into (5.36) and using the inverse Fourier transformation, one obtains the vertical displacement,

$$\begin{aligned}\frac{\pi\mu}{P}u_z = 2\int_{-\infty}^{\infty}[&-(2abd_{21}\sinh(a(1+z_1/h)\xi)+d_{11}(\sinh(b\xi)\cosh(a\xi z_1/h)\\&+ab\cosh(b\xi)\sinh(a\xi z_1/h)))+d_{11}\sinh(b(1+z_1/h)\xi)\\&+2d_{21}(\cosh(a\xi)\sinh(b\xi z_1/h)+ab\sinh(a\xi)\cosh(b\xi z_1/h))]\\&\times a\exp(i\xi x_1/h)/\left(\xi\Delta\right)d\xi,\end{aligned}\tag{5.61}$$

$$\begin{aligned}\frac{\pi\mu}{4P}u_z = \int_0^{\infty}\Re[[&-(2abd_{21}\sinh(a(1+z_1/h)\xi)+d_{11}(\sinh(b\xi)\cosh(a\xi z_1/h)\\&+ab\cosh(b\xi)\sinh(a\xi z_1/h)))+d_{11}\sinh(b(1+z_1/h)\xi)\\&+2d_{21}(\cosh(a\xi)\sinh(b\xi z_1/h)+ab\sinh(a\xi)\cosh(b\xi z_1/h))]\\&\times a\exp(i\xi x_1/h)/\left(\xi\Delta\right)]\,d\xi.\end{aligned}\tag{5.62}$$

The vertical displacement can also be expressed with the aid of the differential vertical displacement Δu_z, defined as

$$\Delta u_z = u_z(x_1, z_1) - u_z(x_1 + l, z_1), \tag{5.63}$$

where l is a given non-zero length. Therefore, it becomes

$$\begin{aligned}\frac{\pi\mu}{4P}\Delta u_z = \int_0^\infty \Re[[&-(2abd_{21}\sinh(a(1+z_1/h)\xi)\\ &+ d_{11}(\sinh(b\xi)\cosh(a\xi z_1/h) + ab\cosh(b\xi)\sinh(a\xi z_1/h)))\\ &+ d_{11}\sinh(b(1+z_1/h)\xi) + 2d_{21}(\cosh(a\xi)\sinh(b\xi z_1/h)\\ &+ ab\sinh(a\xi)\cosh(b\xi z_1/h))]\\ &\times a\exp(i\xi x_1/h)(1.0 - \exp(i\xi l/h))/\,(\xi\Delta)]\,d\xi.\end{aligned} \tag{5.64}$$

For very small values of M_s, Poisson's ratio $\nu = 0$ and very large values of the ratio $l/h = 1000$, the quasi-static differential vertical displacement is shown in Figure 5.9.

For Poisson's ratio $\nu = 0$ and damping ratio $\zeta = 0.1$ at the Rayleigh wave velocity $M_s = 0.874032$, the results obtained for Δu_z are given in Figure 5.10. It can also be seen in the figure that for $x_1/h > 1.0$ the differential vertical displacement Δu_z tends to zero.

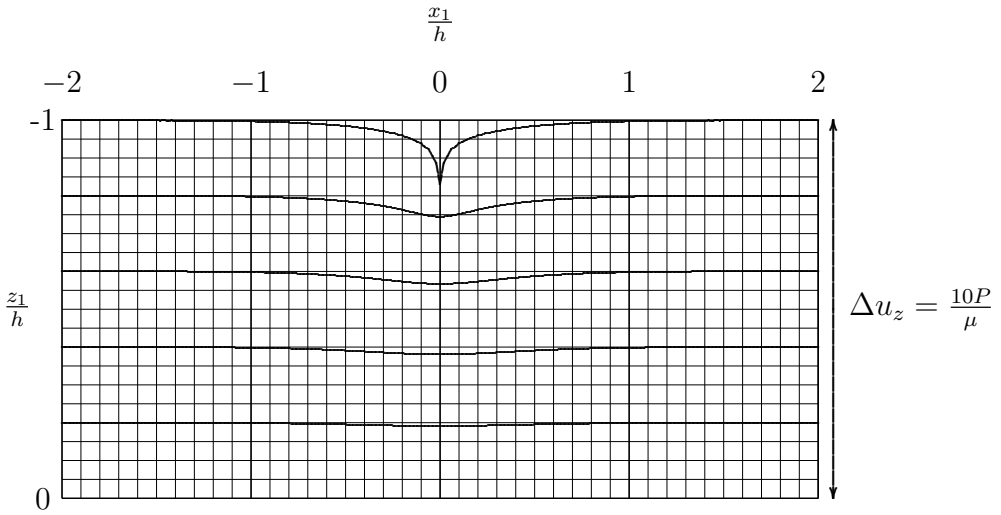

Figure 5.9: Moving load on a plane layer, quasi-static differential vertical displacement: $\nu = 0$, $l/h = 1000$.

For a damping ratio $\zeta = 0.01$ and $M_s = 0.874032$ Figure 5.11 shows the differential vertical displacement Δu_z. Comparison of Figure 5.10 and Figure 5.11 shows the influence of the damping ratio on the magnitude of results. Note that in Figure 5.11 the scale is a factor 5 larger than Figure 5.10. It can be seen that for $x_1/h > 1.0$ the differential vertical displacement Δu_z tends to zero again.

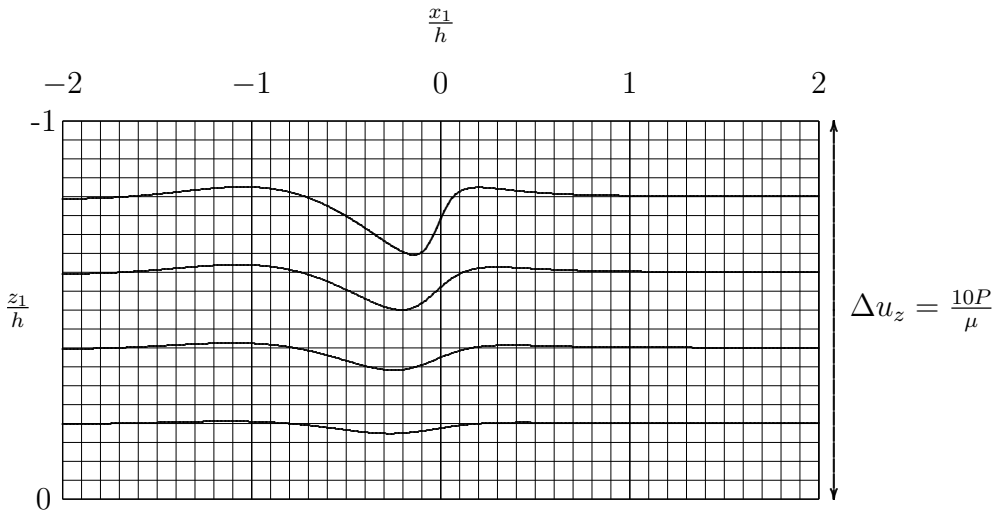

Figure 5.10: Moving load on a plane layer, differential vertical displacement: $\nu = 0$, $\zeta = 0.1$, $M_s = 0.874032$, $l/h = 1000$.

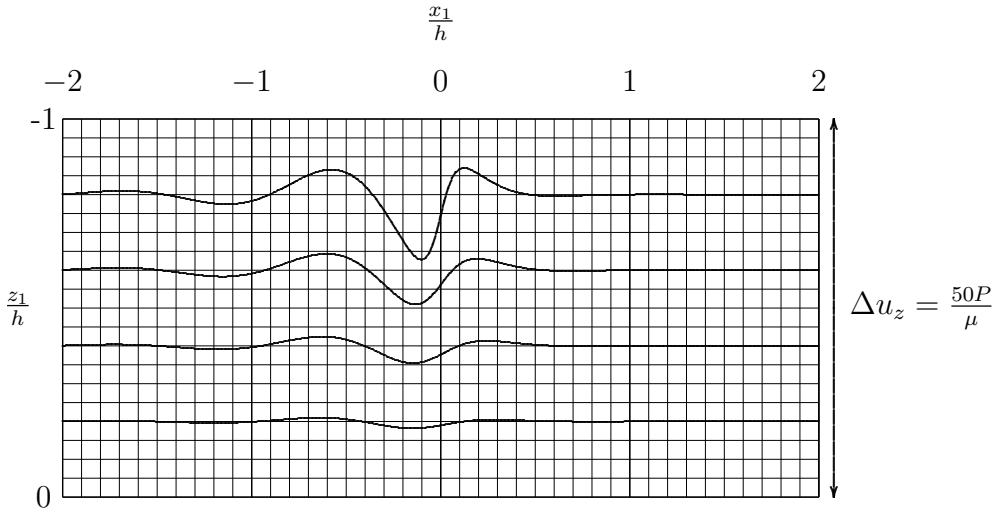

Figure 5.11: Moving load on a plane layer, differential vertical displacement: $\nu = 0$, $\zeta = 0.01$, $M_s = 0.874032$, $l/h = 1000$.

Chapter 6

Moving loads on a layer on a half-plane with hysteretic damping

A description of wave propagation induced in an elastic single layer on a half-plane due to moving loads on the surface is studied. The static problem of a line load acting at the surface of a layered system was investigated by Marguerre [1933]. Results of the vertical stress between a layer and a half-plane were presented by Egorov [1938]. Fox [1948] found the vertical stresses at any point on the vertical axis of a two-layer system. Several problems that are of interest in the theory of elastostatics are treated in the book of Poulos and Davis [1974].

The propagation behaviour of waves through a layered elastic medium is completely different than the propagation of waves in a homogeneous medium since the effects of interface between the media are present. Bromwich [1899] investigated the case of an elastic layer of uniform thickness joined to an elastic half-space. An extension of this work was given by Love [1911]. The problem of a disturbance in a two-layered liquid half-space was analyzed by Pekeris [1948]. Sezawa and Kanai [1935], Kanai [1951], Satô [1951], and Tolstoy and Usdin [1953] determined dispersion curves for several modes.

A study of the transmission of waves through a stratified solid medium is given by Thomson [1950]. A wide analysis of propagation of waves in a layered system is found by Ewing *et al.* [1957]. Miles [1966] studied the case of a two-layered, fluid half-plane to a point load moving over the surface. A discussion of this paper is given by Achenbach [1967]. Free waves traveling in a layer supported by a half-plane are obtained by Achenbach and Keshava [1967]. A study of the dynamic interaction of a layer and a half-space is presented by Achenbach and Epstein [1967]. The response to a moving load of an elastic layer supported by a half-plane is found by Sackman [1961] and Achenbach *et al.* [1967].

The influence of the damping on a layered half-space is studied. Luco and Apsel [1983], and Apsel and Luco [1983] developed a method to find the three-dimensional dynamic response of a layered half-space to an arbitrary buried source. They also formulated an integral representation for the displacement and stress fields in the layered medium. The numerical evaluation of the integrals were validated by comparison with previous results by others methods. Xu and Mal [1987] presented a procedure to calculate the Green's functions for a layered half-plane. The procedure is based on the

wavenumber integral representation. A model of a point load moving on the surface of a multi-layered viscoelastic half-space is presented by de Barros and Luco [1994]. The technique for solving this problem is based on an integral representation of the total response in terms of the wavenumber. Lefeuve-Mesgouez [1999] examined the problem of a rectangular strip vibrating load on a multilayered elastic medium with hysteretic damping.

The response to a moving load on the surface of an elastic layer in contact with an elastic half-plane with hysteretic damping is considered. The case of welded contact is only discussed. The dispersion curve is obtained when the velocity of the shear wave of the layer is larger than the velocity of the shear waves in the half-plane.

6.1 Basic equations

Using the subscript $j = 1$ to distinguish the layer and $j = 2$ to distinguish the half-plane, the basic field equations of motion for the two mediums are given by

$$\partial_x \sigma_{xxj} + \partial_z \sigma_{zxj} = \rho_j \partial_{tt}^2 u_{xj}, \tag{6.1}$$

$$\partial_x \sigma_{xzj} + \partial_z \sigma_{zzj} = \rho_j \partial_{tt}^2 u_{zj}, \tag{6.2}$$

where $u_{xj}(x, z, t)$ and $u_{zj}(x, z, t)$ are the components of the displacements in the x and z directions, with $-\infty < x < \infty$, and $-h \geq z \geq 0$ in the layer $j = 1$ and $z \geq 0$ in the half-plane $j = 2$. The single layer on a half-plane is depicted in Figure 6.1 where

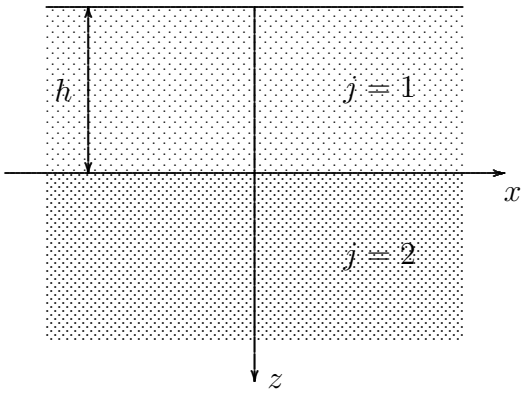

Figure 6.1: Single layer on a half-plane.

h is the depth of the layer. The displacements are written in terms of the potential functions $\phi_j(x, z, t)$ and $\psi_j(x, z, t)$,

$$u_{xj} = \partial_x \phi_j - \partial_z \psi_j, \tag{6.3}$$

$$u_{zj} = \partial_z \phi_j + \partial_x \psi_j. \tag{6.4}$$

The stress components are expressed as functions of ϕ_j and ψ_j,

$$\sigma_{xxj} = \lambda_j (1 + t_{rj} \partial_t)(\partial_{xx}^2 \phi_j + \partial_{zz}^2 \phi_j) + 2\mu_j (1 + t_{rj} \partial_t)(\partial_{xx}^2 \phi_j - \partial_x \partial_z \psi_j), \tag{6.5}$$

$$\sigma_{zzj} = \lambda_j(1 + t_{rj}\partial_t)(\partial^2_{xx}\phi_j + \partial^2_{zz}\phi_j) + 2\mu_j(1 + t_{rj}\partial_t)(\partial^2_{zz}\phi_j + \partial_x\partial_z\psi_j), \tag{6.6}$$

$$\sigma_{xzj} = \mu_j(1 + t_{rj}\partial_t)(2\partial_x\partial_z\phi_j + \partial^2_{xx}\psi_j - \partial^2_{zz}\psi_j), \tag{6.7}$$

where t_{rj} is a relaxation time. In order to describe the hysteretic damping the value of t_{rj} should be inversely proportional to the frequency of the load. The two forms of deformation, shear and compression, have been taken equal for reasons of simplicity. Substitution of (6.3) - (6.7) into (6.1) and (6.2) shows that the basic equations of motion can be satisfied if the potentials are solutions of

$$(1 + t_{rj}\partial_t)(\partial^2_{xx}\phi_j + \partial^2_{zz}\phi_j) = \frac{1}{c^2_{pj}}\partial^2_{tt}\phi_j, \tag{6.8}$$

$$(1 + t_{rj}\partial_t)(\partial^2_{xx}\psi_j + \partial^2_{zz}\psi_j) = \frac{1}{c^2_{sj}}\partial^2_{tt}\psi_j. \tag{6.9}$$

where $c^2_{pj} = (\lambda_j + 2\mu_j)/\rho_j$ and $c^2_{sj} = \mu_j/\rho_j$.

6.2 Moving loads on a single layer on a half-plane

The case of a moving load with constant velocity v on the surface of a single layer on a half-plane is analyzed. Introducing the moving coordinate system (x_1, z_1), with $-\infty < x_1 < \infty$ and $-h \leq z_1 \leq \infty$,

$$x_1 = x - vt \quad \text{and} \quad z_1 = z. \tag{6.10}$$

Introducing (6.10) into (6.5) - (6.9), gives

$$\begin{aligned}\frac{\sigma_{xxj}}{\mu_j} =&(M^2_{sj} - 2M^2_{pj} + 2)\partial^2_{x_1x_1}\phi_j - 2\partial_{x_1}\partial_{z_1}\psi_j \\ &- 2vt_{rj}\partial_{x_1}(\partial^2_{x_1x_1}\phi_j - \partial_{x_1}\partial_{z_1}\psi_j),\end{aligned} \tag{6.11}$$

$$\frac{\sigma_{zzj}}{\mu_j} = (M^2_{sj} - 2)\partial^2_{x_1x_1}\phi_j + 2\partial_{x_1}\partial_{z_1}\psi_j + 2vt_{rj}\partial_{x_1}(\partial^2_{x_1x_1}\phi_j - \partial_{x_1}\partial_{z_1}\psi_j), \tag{6.12}$$

$$\frac{\sigma_{xzj}}{\mu_j} = 2\partial_{x_1}\partial_{z_1}\phi_j - (M^2_{sj} - 2)\partial^2_{x_1x_1}\psi_j - 2vt_{rj}\partial_{x_1}(\partial_{x_1}\partial_{z_1}\phi_j + \partial^2_{x_1x_1}\psi_j), \tag{6.13}$$

where $M_{pj} = v/c_{pj}$ and $M_{sj} = v/c_{sj}$. Expressions (6.8) and (6.9) are rewritten as

$$(1 - vt_{rj}\partial_{x_1})(\partial^2_{x_1x_1}\phi_j + \partial^2_{z_1z_1}\phi_j) = M^2_{pj}\partial^2_{x_1x_1}\phi_j, \tag{6.14}$$

$$(1 - vt_{rj}\partial_{x_1})(\partial^2_{x_1x_1}\psi_j + \partial^2_{z_1z_1}\psi_j) = M^2_{sj}\partial^2_{x_1x_1}\psi_j. \tag{6.15}$$

Before solving (6.14) and (6.15) the boundary conditions will be given.

6.2.1 Moving point load

The contact between the layer and half-plane along the x_1-axis is considered to be a welded contact. It is also assumed that the boundary conditions can be represented by

$$z_1 = -h \ : \ \sigma_{zz1} = -P\delta(x - vt) = -P\delta(x_1), \tag{6.16}$$

$$z_1 = -h \ : \ \sigma_{xz1} = 0, \tag{6.17}$$

$$z_1 = 0 \ : \ \sigma_{zz1} = \sigma_{zz2}, \tag{6.18}$$

$$z_1 = 0 \ : \ \sigma_{xz1} = \sigma_{xz2}, \tag{6.19}$$

$$z_1 = 0 \ : \ u_{x1} = u_{x2}, \tag{6.20}$$

$$z_1 = 0 \ : \ u_{z1} = u_{z2}, \tag{6.21}$$

where P is the concentrated line force on the surface of the layer $z_1 = -h$ and $\delta(x_1)$ is the Dirac function. A moving load on a layered half-plane is illustrated in Figure 6.2. In order to solve this problem the exponential Fourier transformation with respect to

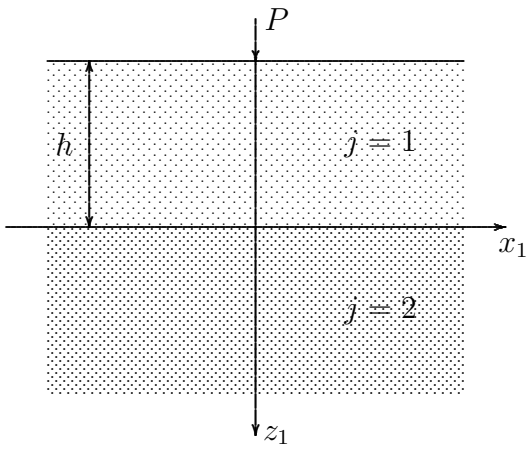

Figure 6.2: Moving load on a single layer on a half-plane.

the x_1 coordinate is used. The potential functions ϕ_j and ψ_j are transformed into

$$\tilde{\phi}_j(k, z_1) = \int_{-\infty}^{\infty} \phi_j(x_1, z_1) \exp(-ikx_1)\, dx_1, \tag{6.22}$$

$$\tilde{\psi}_j(k, z_1) = \int_{-\infty}^{\infty} \psi_j(x_1, z_1) \exp(-ikx_1)\, dx_1. \tag{6.23}$$

Replacing (6.22) and (6.23) into (6.14) and (6.15), gives

$$\partial^2_{z_1 z_1}\tilde{\phi}_j - k^2\frac{(1-M^2_{pj}+(vt_{rj}k)^2 - ivt_{rj}kM^2_{pj})}{1+(vt_{rj}k)^2}\tilde{\phi}_j = 0, \tag{6.24}$$

$$\partial^2_{z_1 z_1}\tilde{\psi}_j - k^2\frac{(1-M^2_{sj}+(vt_{rj}k)^2 - ivt_{rj}kM^2_{sj})}{1+(vt_{rj}k)^2}\tilde{\psi}_j = 0. \tag{6.25}$$

Assume that the solutions of (6.24) and (6.25) are expressed as

$$\tilde{\phi}_1(k,z_1) = A_{11}(k)\sinh(a_1 k z_1) + A_{21}(k)\cosh(a_1 k z_1), \tag{6.26}$$

$$\tilde{\psi}_1(k,z_1) = B_{11}(k)\sinh(b_1 k z_1) + B_{21}(k)\cosh(b_1 k z_1), \tag{6.27}$$

$$\tilde{\phi}_2(k,z_1) = A_{12}(k)\exp(-a_2|k|z_1), \tag{6.28}$$

$$\tilde{\psi}_2(k,z_1) = B_{12}(k)\exp(-b_2|k|z_1), \tag{6.29}$$

where a_1, a_2, b_1 and b_2 are wave numbers. Consider that the waves in the half-plane, $j = 2$, only propagate in the positive z_1-direction. This means that the real parts of a_2 and b_2 are positive and that their imaginary parts are negative, so that the solution of $\tilde{\phi}_2$ and $\tilde{\psi}_2$ must vanish for $z_1 \to \infty$. According to Rayleigh [1894], the radiation condition is satisfied. The arbitrary complex coefficients A_{11}, A_{21}, B_{11}, B_{21}, A_{12} and B_{12} are calculated with the aid of the boundary conditions. The wave numbers a_j and b_j are written as

$$a_j^2 = R_{pj}^2\exp(-i2\vartheta_{pj}), \tag{6.30}$$

$$b_j^2 = R_{sj}^2\exp(-i2\vartheta_{sj}), \tag{6.31}$$

where R_{pj}, R_{sj}, and the angles ϑ_{pj} and ϑ_{sj} are defined by

$$R_{pj} = \sqrt[4]{\frac{(1-M^2_{pj})^2+(vt_{rj}k)^2}{1+(vt_{rj}k)^2}}, \tag{6.32}$$

$$R_{sj} = \sqrt[4]{\frac{(1-M^2_{sj})^2+(vt_{rj}k)^2}{1+(vt_{rj}k)^2}}, \tag{6.33}$$

$$\vartheta_{pj} = \frac{1}{2}\arctan\left(\frac{vt_{rj}kM^2_{pj}}{1-M^2_{pj}+(vt_{rj}k)^2}\right); \quad 0 \le \vartheta_{pj} < \pi/2, \tag{6.34}$$

$$\vartheta_{sj} = \frac{1}{2}\arctan\left(\frac{vt_{rj}kM_{sj}^2}{1-M_{sj}^2+(vt_{rj}k)^2}\right);\quad 0 \le \vartheta_{sj} < \pi/2. \tag{6.35}$$

The stress components (6.11) - (6.13) and the displacements (6.3) and (6.4) are transformed into

$$\frac{\tilde{\sigma}_{xxj}}{\mu_j} = -k^2(M_{sj}^2 - 2M_{pj}^2 + 2 - i2vt_{rj}k)\tilde{\phi}_j - i2k(1-ivt_{rj}k)\partial_{z_1}\tilde{\psi}_j, \tag{6.36}$$

$$\frac{\tilde{\sigma}_{zzj}}{\mu_j} = -k^2(M_{sj}^2 - 2 + i2vt_{rj}k)\tilde{\phi}_j + i2k(1-ivt_{rj}k)\partial_{z_1}\tilde{\psi}_j, \tag{6.37}$$

$$\frac{\tilde{\sigma}_{xzj}}{\mu_j} = i2k(1-ivt_{rj}k)\partial_{z_1}\tilde{\phi}_j + k^2(M_{sj}^2 - 2 + i2vt_{rj}k)\tilde{\psi}_j, \tag{6.38}$$

$$\tilde{u}_{xj} = ik\tilde{\phi}_j - \partial_{z_1}\tilde{\psi}_j, \tag{6.39}$$

$$\tilde{u}_{zj} = \partial_{z_1}\tilde{\phi}_j + ik\tilde{\psi}_j. \tag{6.40}$$

The system of equations (6.16) and (6.21) is given in matrix form

$$\begin{bmatrix} -d_{11}sh(a_1\xi) & d_{11}ch(a_1\xi) & -i2b_1d_{21}ch(b_1\xi) & i2b_1d_{21}sh(b_1\xi) \\ i2a_1d_{21}ch(a_1\xi) & -i2a_1d_{21}sh(a_1\xi) & -d_{11}sh(b_1\xi) & d_{11}ch(b_1\xi) \\ 0 & d_{11}\xi & -i2b_1d_{21}\xi & 0 \\ i2a_1d_{21}\xi & 0 & 0 & d_{11}\xi \\ 0 & i\xi & -b_1\xi & 0 \\ a_1\xi & 0 & 0 & i\xi \end{bmatrix}$$

$$\begin{bmatrix} 0 & 0 \\ 0 & 0 \\ -d_{12}\xi/\varrho & -i2b_2d_{22}|\xi|/\varrho \\ i2a_2d_{22}|\xi|/\varrho & -d_{12}\xi/\varrho \\ -i\xi & -b_2|\xi| \\ a_2|\xi| & -i\xi \end{bmatrix} \begin{bmatrix} A_{11} \\ A_{21} \\ B_{11} \\ B_{21} \\ A_{12} \\ B_{12} \end{bmatrix} = \begin{bmatrix} C \\ 0 \\ 0 \\ 0 \\ 0 \\ 0 \end{bmatrix}, \tag{6.41}$$

where $sh = \sinh$, $ch = \cosh$ and the dimensionless wave number ξ is defined as

$$\xi = kh, \tag{6.42}$$

and the parameters C, ϱ, d_{11}, d_{21}, d_{12} and d_{22} are given by

$$C = \frac{P}{\mu_1}\frac{h^2}{\xi^2} \quad \text{and} \quad \varrho = \frac{\mu_1}{\mu_2}, \tag{6.43}$$

$$d_{11} = M_{s1}^2 - 2 + i2vt_{r1}k \quad \text{and} \quad d_{21} = 1 - ivt_{r1}k, \tag{6.44}$$

$$d_{12} = M_{s2}^2 - 2 + i2vt_{r2}k \quad \text{and} \quad d_{22} = 1 - ivt_{r2}k. \tag{6.45}$$

Next, the undamped case is examined, where the relaxation times t_1 and t_2 are assumed to be zero. The determinant of the system of equations Δ is defined as

$$\Delta = \begin{vmatrix} -d_{11}sh(a_1\xi) & d_{11}ch(a_1\xi) & -i2b_1ch(b_1\xi) & i2b_1sh(b_1\xi) & 0 \\ i2a_1ch(a_1\xi) & -i2a_1sh(a_1\xi) & -d_{11}sh(b_1\xi) & d_{11}ch(b_1\xi) & 0 \\ 0 & d_{11}\xi & -i2b_1\xi & 0 & -d_{12}\xi/\varrho \\ i2a_1\xi & 0 & 0 & d_{11}\xi & i2a_2|\xi|/\varrho \\ 0 & i\xi & -b_1\xi & 0 & -i\xi \\ a_1\xi & 0 & 0 & i\xi & a_2|\xi| \end{vmatrix} \begin{vmatrix} 0 \\ 0 \\ -i2b_2|\xi|/\varrho \\ -d_{12}\xi/\varrho \\ -b_2|\xi| \\ -i\xi \end{vmatrix}. \tag{6.46}$$

For welded contact of a stiff and heavy layer of thickness $2h$, Achenbach [1967] calculated the dispersion curve. Figure 6.3 shows the dispersion curve in agreement with Achenbach. The dispersion curve of the layer with thickness h is depicted by dashes.

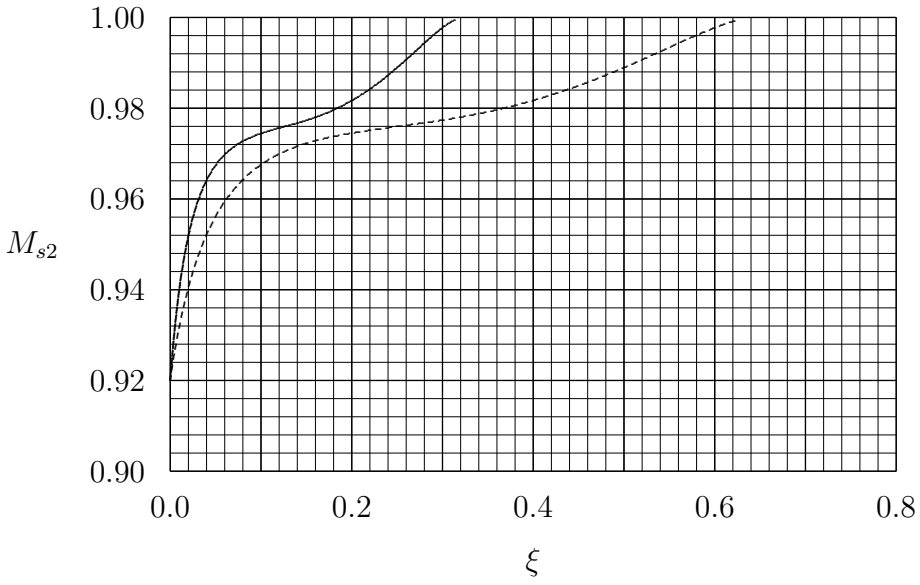

Figure 6.3: Dispersion curve for welded contact, layer with thickness $2h$ (Achenbach [1967]) and layer with thickness h: $\mu_1/\mu_2 = 8$, $\rho_1/\rho_2 = 1.44$, $\nu_1 = \nu_2 = 0.25$.

For the case of $\mu_1/\mu_2 = 10$, $\rho_1 = \rho_2$, $\nu_1 = \nu_2 = 0$ and layer with thickness h, the dispersion curve is shown in Figure 6.4

The damping ratio ζ_j is used to describe the hysteretic damping. This is defined as

$$\zeta_j = \frac{vt_{rj}k}{2} sign(k), \tag{6.47}$$

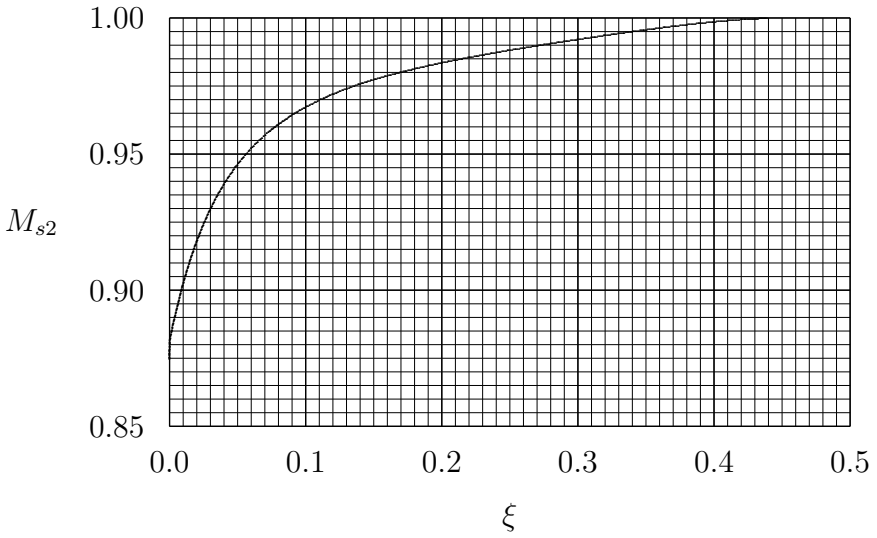

Figure 6.4: Dispersion curve for welded contact, stiff and heavy layer with thickness h: $\mu_1/\mu_2 = 10$, $\rho_1/\rho_2 = 1$, $\nu_1 = \nu_2 = 0$.

where $|\zeta_j|$ is considered to be a constant material parameter, and $sign(k)$ indicates the sign of k. Therefore,

$$R_{pj} = \sqrt[4]{\frac{(1 - M_{pj}^2)^2 + 4\zeta_j^2}{1 + 4\zeta_j^2}}, \tag{6.48}$$

$$R_{sj} = \sqrt[4]{\frac{(1 - M_{sj}^2)^2 + 4\zeta_j^2}{1 + 4\zeta_j^2}}, \tag{6.49}$$

$$\vartheta_{pj} = \frac{1}{2} \arctan\left(\frac{2\zeta_j M_{pj}^2}{1 - M_{pj}^2 + 4\zeta_j^2}\right); \quad 0 \leq \vartheta_{pj} < \pi/2, \tag{6.50}$$

$$\vartheta_{sj} = \frac{1}{2} \arctan\left(\frac{2\zeta_j M_{sj}^2}{1 - M_{sj}^2 + 4\zeta_j^2}\right); \quad 0 \leq \vartheta_{sj} < \pi/2, \tag{6.51}$$

$$d_{11} = M_{s1}^2 - 2 + i4\zeta_1 \quad \text{and} \quad d_{21} = 1 - i2\zeta_1, \tag{6.52}$$

$$d_{12} = M_{s2}^2 - 2 + i4\zeta_2 \quad \text{and} \quad d_{22} = 1 - i2\zeta_2. \tag{6.53}$$

With the aid of (6.48) - (6.53) the matrix (6.41) can be solved.

6.2.2 Stress components

Substitution of (6.26) - (6.29) into (6.36) - (6.39) and using the inverse Fourier transformation with respect to the dimensionless wave number ξ, the stress components are found. For the layer ($j = 1$):

$$\frac{\pi\sigma_{xx1}h}{P} = -\int_0^\infty \Re[(d_{31}(A_{11}sh(a_1\xi z_1/h) + A_{21}ch(a_1\xi z_1/h)) + i2b_1d_{21}(B_{11}ch(b_1\xi z_1/h) + B_{21}sh(b_1\xi z_1/h))) \times \exp(i\xi x_1/h)]\, d\xi, \tag{6.54}$$

$$\frac{\pi\sigma_{zz1}h}{P} = -\int_0^\infty \Re[(d_{11}(A_{11}sh(a_1\xi z_1/h) + A_{21}ch(a_1\xi z_1/h)) - i2b_1d_{21}(B_{11}ch(b_1\xi z_1/h) + B_{21}sh(b_1\xi z_1/h))) \times \exp(i\xi x_1/h)]\, d\xi, \tag{6.55}$$

$$\frac{\pi\sigma_{xz1}h}{P} = \int_0^\infty \Re[(i2a_1d_{21}(A_{11}ch(a_1\xi z_1/h) + A_{21}sh(a_1\xi z_1/h)) + d_{11}(B_{11}sh(b_1\xi z_1/h) + B_{21}ch(b_1\xi z_1/h))) \exp(i\xi x_1/h)]\, d\xi, \tag{6.56}$$

where

$$d_{31} = M_{s1}^2 - 2M_{p1}^2 + 2 - i4\zeta_1. \tag{6.57}$$

For the half-plane ($j = 2$):

$$\frac{\pi\sigma_{xx2}h}{P} = -\frac{1}{\varrho}\int_0^\infty \Re[(d_{32}A_{12}\exp(-a_2\xi z_1/h) - i2b_2d_{22}B_{12}\exp(-b_2\xi z_1/h)) \times \exp(i\xi x_1/h)]\, d\xi, \tag{6.58}$$

$$\frac{\pi\sigma_{zz2}h}{P} = -\frac{1}{\varrho}\int_0^\infty \Re[(d_{12}A_{12}\exp(-a_2\xi z_1/h) + i2b_2d_{22}B_{12}\exp(-b_2\xi z_1/h)) \times \exp(i\xi x_1/h)]\, d\xi, \tag{6.59}$$

$$\frac{\pi\sigma_{xz2}h}{P} = -\frac{1}{\varrho}\int_0^\infty \Re[(i2a_2d_{22}A_{12}\exp(-a_2\xi z_1/h) - d_{12}B_{12}\exp(-b_2\xi z_1/h)) \times \exp(i\xi x_1/h)]\, d\xi, \tag{6.60}$$

where

$$d_{32} = M_{s2}^2 - 2M_{p2}^2 + 2 - i4\zeta_2. \tag{6.61}$$

The integrals of the stress components will be calculated numerically, using Simpson's integration method.

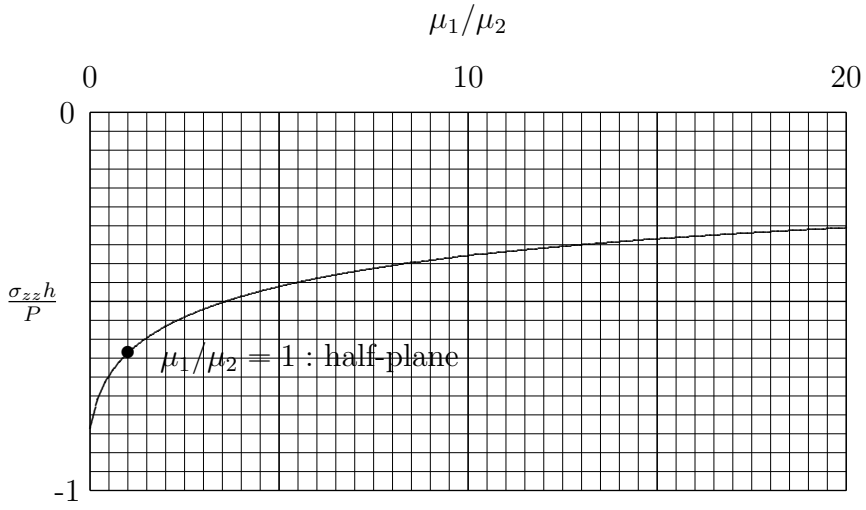

Figure 6.5: Moving load on a single layer on a half-plane, the quasi-static vertical stress at ($x_1 = 0$, $z_1 = 0$): $\rho_1/\rho_2 = 1$, $\nu_1 = \nu_2 = 0$.

The quasi-static vertical stress at the interface layer half-plane, $x_1 = 0$ and $z_1 = 0$, is calculated in terms of the parameter $\varrho = \mu_1/\mu_2$. Results are shown in Figure 6.5 for materials without damping when the velocity of the load is very small, using densities $\rho_1 = \rho_2$ and Poisson's ratios $\nu_1 = \nu_2 = 0$. For values of μ_1/μ_2 larger than 20 the stresses are almost independent of the stiffness.

Figure 6.6 shows the quasi-static vertical stress in terms of the relative depth z_1/h for undamped materials $\zeta_1 = \zeta_2 = 0$. For values of $\rho_1/\rho_2 = 1$ and $\nu_1 = \nu_2 = 0$ the Flamant problem with $\mu_1/\mu_2 = 1$ is shown on the left hand side of Figure 6.6. The stiff layer problem with $\mu_1/\mu_2 = 10$ is shown on the right hand side of Figure 6.6. It also appears that the results of the stiff layer problem are not much larger than the Flamant problem.

For small values of the damping ratios $\zeta_1 = \zeta_2 = 0.01$, and for supersonic velocities $M_{s1} = 2.0$, the results of a relative very stiff half-plane $\varrho = \mu_1/\mu_2 = 0.0001$ are given in Figure 6.7, see also Chapter 5.2.2 (Moving load on a fixed layer). The results generate two peaks in the layer $-1 < z_1/h \leq 0$. The slope of the first peak corresponding to the shear wave approaches the expression $x_1 = \sqrt{M_{s1}^2 - 1}z_1 = \sqrt{3}z_1$. The second peak, corresponding to the compression wave, approaches the expression $x_1 = \sqrt{M_{p1}^2 - 1}z_1 = z_1$, where Poisson's ratios $\nu_1 = \nu_2 = 0$ and $M_{s1} = 2.0$. In the layer, an approximation of the peaks of the reflections can be found in terms of the expressions $x_1 = \sqrt{M_{s1}^2 - 1}(z_1 - 1) = \sqrt{3}(z_1 - 1)$ and $x_1 = \sqrt{M_{p1}^2 - 1}(z_1 - 1) = z_1 - 1$, where $M_{p1} = \sqrt{2}$. In the half-plane, the vertical stresses are relatively much smaller than in the layer.

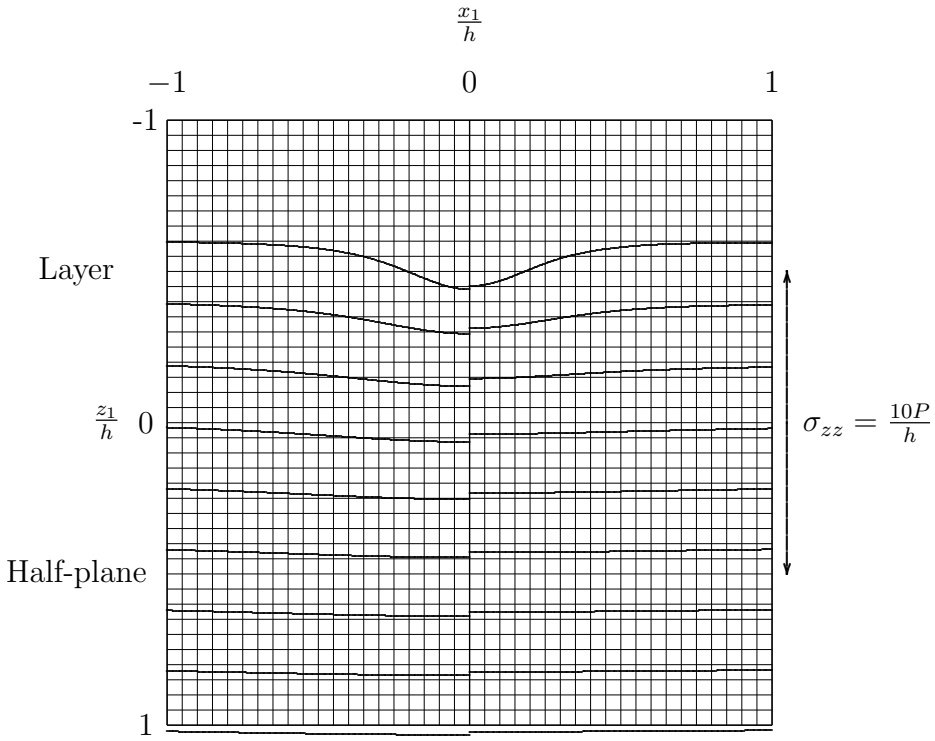

Figure 6.6: Moving load on a single layer on a half-plane, the quasi-static vertical stress: left hand side the Flamant problem, right hand side $\mu_1/\mu_2 = 10$, $\rho_1/\rho_2 = 1$, $\nu_1 = \nu_2 = 0$.

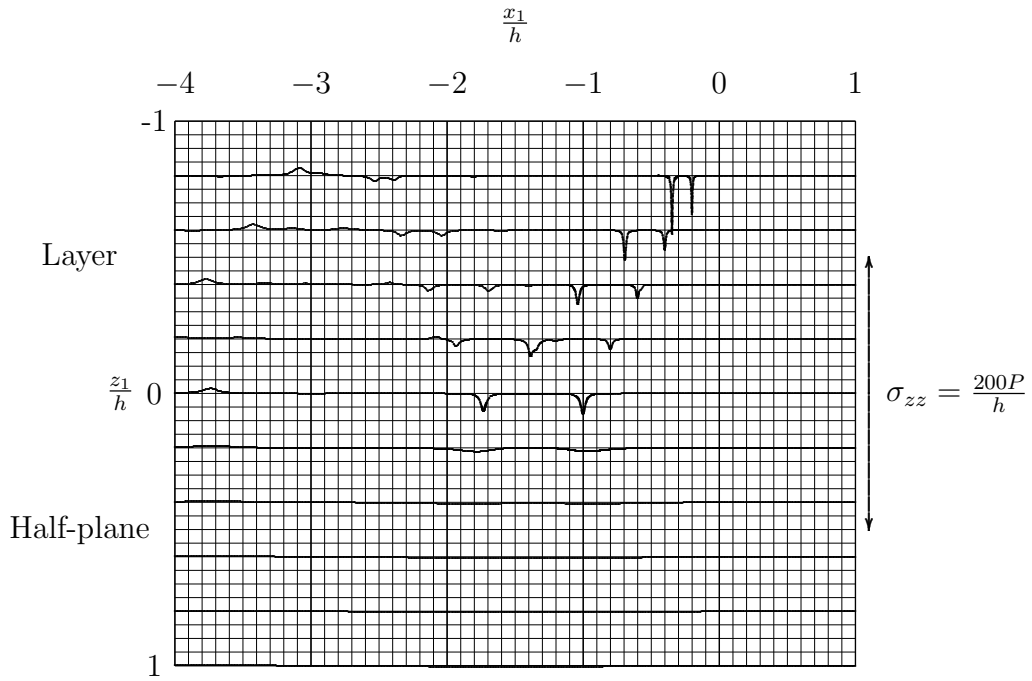

Figure 6.7: Moving load on a single layer on a half-plane, vertical stress: $\mu_1/\mu_2 = 0.0001$, $\rho_1/\rho_2 = 1$, $\nu_1 = \nu_2 = 0$, $\zeta_1 = \zeta_2 = 0.01$, $M_{s1} = 2.0$.

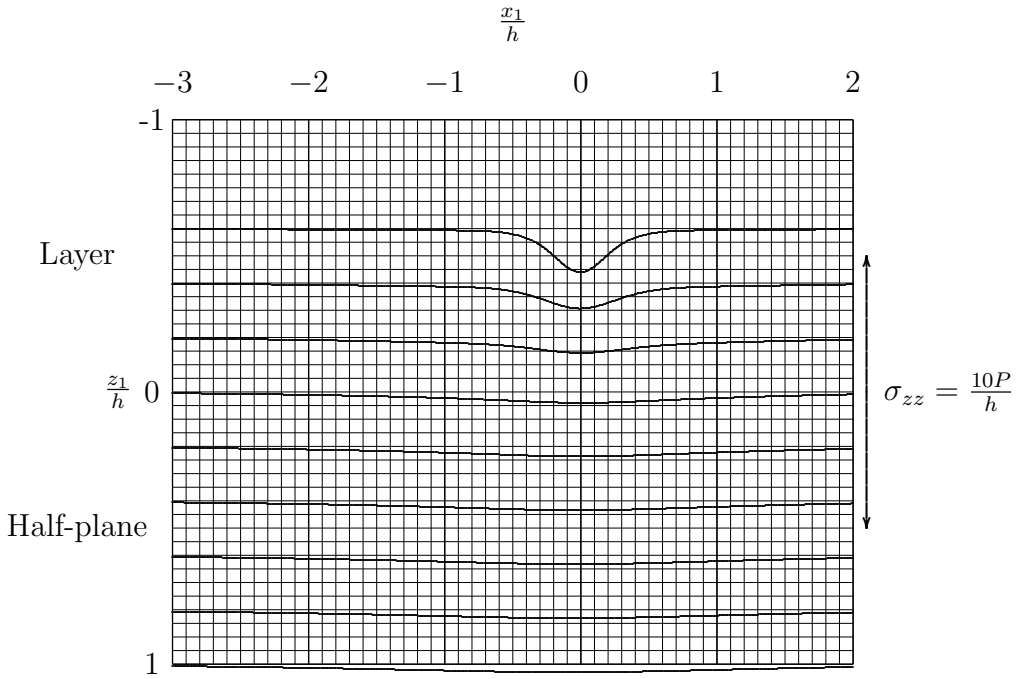

Figure 6.8: Moving load on a single layer on a half-plane, vertical stress: $\mu_1/\mu_2 = 10$, $\rho_1/\rho_2 = 1$, $\nu_1 = \nu_2 = 0$, $\zeta_1 = \zeta_2 = 0.1$, $M_{s2} = 0.874032$.

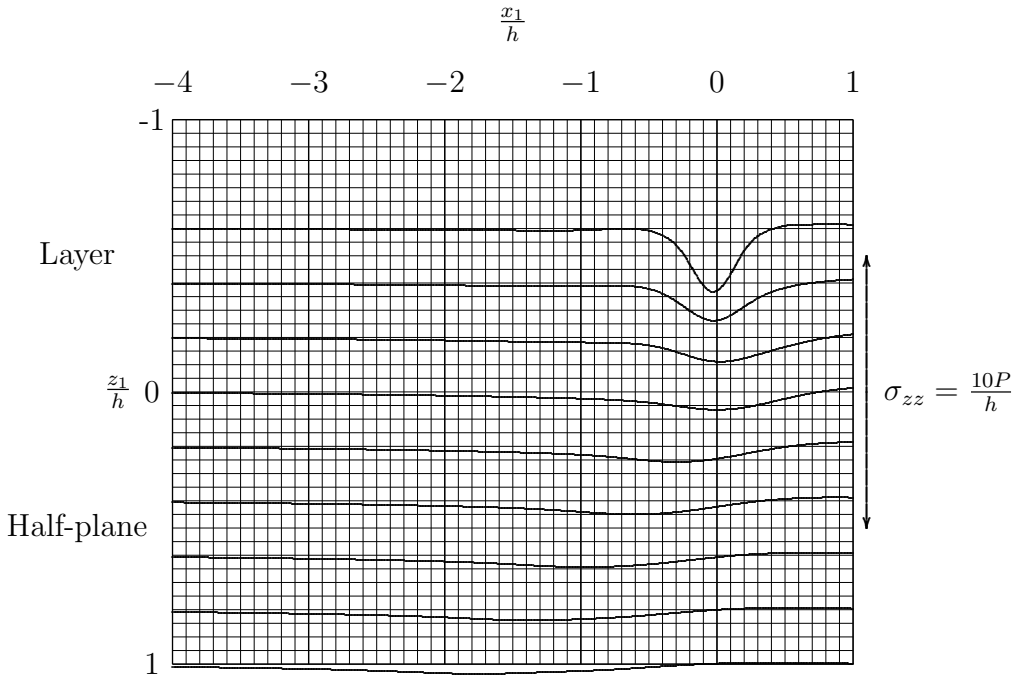

Figure 6.9: Moving load on a single layer on a half-plane, vertical stress: $\mu_1/\mu_2 = 10$, $\rho_1/\rho_2 = 1$, $\nu_1 = \nu_2 = 0$, $\zeta_1 = \zeta_2 = 0.1$, $M_{s2} = 2.0$.

For the particular case of velocities close to the Rayleigh wave velocity of the half-plane $M_{s2} = 0.874032$, and if Poisson's ratio $\nu_2 = 0$, the results are shown in Figure 6.8. It appears that for $\mu_1/\mu_2 = 10$ and damping ratios $\zeta_1 = \zeta_2 = 0.1$, the stresses in the half-plane are more or less uniformly distributed.

For the case $M_{s2} = 2.0$, $\mu_1/\mu_2 = 10$ and damping ratios $\zeta_1 = \zeta_2 = 0.1$, Figure 6.9 shows that the stresses in the half-plane are not distributed in the same manner at different depths z_1/h. It also appears that no peaks are generated in the half-plane. This occurs because the stiffness of the layer is 10 times larger than the stiffness of the half-plane. Furthermore, comparison with Figure 6.8 it can be seen that the results differ very little.

The amplification factor of the maximum vertical stress $Amp\ \sigma_{zz}$ along the layer half-plane interface $z_1/h = 0$ is presented in Figure 6.10 as a function of M_{s2}. The maximum static value of the vertical stress in $z_1 = 0$ is considered as a reference value. It appears that for damping ratios $\zeta_1 = \zeta_2 = 0.05$, Poisson's values $\mu_1 = \mu_2 = 0$ and densities $\rho_1 = \rho_2$, the influence of the dimensionless parameter $\varrho = \mu_1/\mu_2$ on the results is very notable.

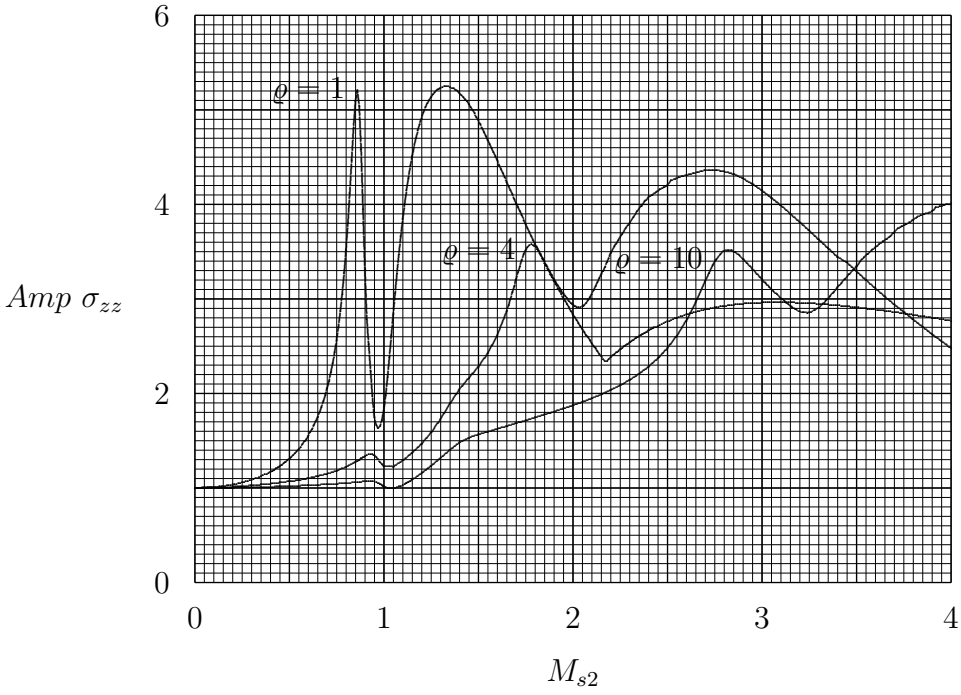

Figure 6.10: Moving point load on a single layer on a half-plane, amplification factor of the maximum vertical stress in $z_1 = 0$ for different $\varrho = \mu_1/\mu_2$: $\rho_1 = \rho_2$, $\zeta_1 = \zeta_2 = 0.05$, $\nu_1 = \nu_2 = 0$.

Chapter 7

Material with horizontal constraints

Problems consisting of an elastic half-space or an elastic half-plane, in which loads of vertical direction are applied on the surface only, it can be assumed that the vertical displacements are notably larger than the horizontal displacements. Therefore, an approximate method of solution can be developed. In this method, the horizontal displacements are disregarded, so that the only actual displacement is the vertical displacement. In order to obtain the solution of problems under these assumptions the medium is referred to as a material with horizontal constraints. Examples of this particular case are the vibrating load on an elastic half-space and the moving-load problem on an elastic half-plane, examined in Chapter 3 and 4, respectively. In 1938 Westergaard found the solution for materials satisfying these assumptions for Boussinesq problems. Fadum [1948] calculated the solution of a vertical line load of finite length acting at the surface. These solutions are given in the text of Harr [1966].

Consider the horizontal displacements u_x and u_y and the vertical displacement u_z of the vector displacement $\mathbf{u} = (u_x, u_y, u_z)$. Assume that only the vertical component of $\mathbf{u}$ is taken into account. It follows that the vector displacement is expressed as $\mathbf{u} = (0, 0, u_z)$. Therefore, the elastodynamic wave equation of motion is reduced to the scalar equation of motion of a material with horizontal constraints in z direction. This is the so-called Westergaard's equation of motion, which is formulated as

$$\mu(\partial_{xx}^2 u_z + \partial_{yy}^2 u_z) + (\lambda + 2\mu)\partial_{zz}^2 u_z = \rho\partial_{tt}^2 u_z. \tag{7.1}$$

Barends [1971], Verruijt [1996], Cornejo [1997] and de Hoop [2001] also used Westergaard's equation for solving elastodynamics problems. In a similar way the stress components on horizontal planes in terms of u_z are given by

$$\sigma_{zz} = (\lambda + 2\mu)\partial_z u_z, \tag{7.2}$$

$$\sigma_{zx} = \mu\partial_x u_z, \tag{7.3}$$

$$\sigma_{zy} = \mu\partial_y u_z. \tag{7.4}$$

Consequently, some problems of propagation of waves in a material with horizontal constraints and hysteretic damping will be treated. This means that the Lamé constants will be expressed as $\lambda \to \lambda(1 + t_r\partial_t)$ and $\mu \to \mu(1 + t_r\partial_t)$, where t_r is the relaxation time.

7.1 Uniform load over circular area

In order to describe an axially symmetric problem the cylindrical polar coordinates are used. Figure 7.1 shows the case of a vibrating load on a circular area on the surface of a half-space. The basic equation of motion for a material with hysteretic damping is written as

$$\mu(1+t_r\partial_t)\left(\partial_{rr}^2 u_z+\frac{1}{r}\partial_r u_z\right)+(\lambda+2\mu)(1+t_r\partial_t)\partial_{zz}^2 u_z=\rho\partial_{tt}^2 u_z, \tag{7.5}$$

where the vertical displacement $u_z = u_z(r,z,t)$. The vertical load causes a periodically

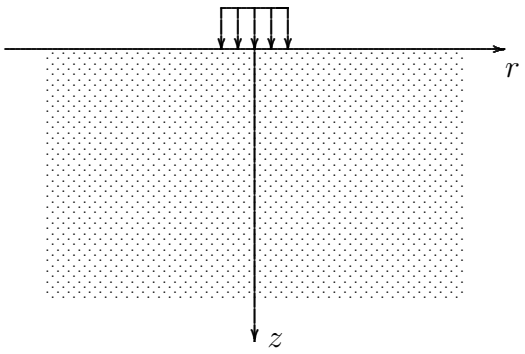

Figure 7.1: Vibrating circular load on half-space.

varying pressure on a circular area at the surface $z = 0$. The boundary condition for the vertical normal stress is given by

$$z=0\ :\ \sigma_{zz}=(\lambda+2\mu)(1+t_r\partial_t)\partial_z u_z\begin{cases}-p_0\exp(i\omega t), & r<r_0,\\ 0, & r>r_0,\end{cases} \tag{7.6}$$

where p_0 is the amplitude of the vertical stress over the circular area, r_0 is the radius of the loaded area, ω is the circular frequency of the periodic load. It should be observed that the vanishing of the shear stress $\sigma_{rz} = \mu(1+t_r\partial_t)\partial_r u_z$ on the surface cannot be satisfied in this case. This effect is caused by assuming that the horizontal displacements are negligible.

Considering the vertical displacement u_z to be

$$u_z(r,z,t)=\breve{u}_z(r,z)\exp(i\omega t), \tag{7.7}$$

where $\breve{u}_z$ is a function in terms of r and z, and $\exp(i\omega t)$ is a time factor, the basic equation of motion (7.5) results in

$$n^2\left(\partial_{rr}^2\breve{u}_z+\frac{1}{r}\partial_r\breve{u}_z\right)+\partial_{zz}^2\breve{u}_z=-\frac{k_p^2}{(1+i\omega t_r)}\breve{u}_z, \tag{7.8}$$

where $n^2 = \mu/(\lambda+2\mu) = c_s^2/c_p^2 = (1-2\nu)/(2(1-\nu))$, $c_s^2 = \mu/\rho$, $c_p^2 = (\lambda+2\mu)/\rho$ and the wave number $k_p = \omega/c_p$, referred to P-wave. Applying the Hankel transformation

of order zero to (7.8), the transformed vertical displacement $\breve{u}_z$ becomes

$$\tilde{u}_z(\xi, z) = \int_0^\infty \breve{u}_z(r, z) r J_0(\xi r)\, dr, \tag{7.9}$$

with the inverse Hankel transformation

$$\breve{u}_z(r, z) = \int_0^\infty \tilde{u}_z(\xi, z) \xi J_0(\xi r)\, d\xi, \tag{7.10}$$

where ξ is the radial wave number. Substituting (7.9) in (7.8) the differential partial equation is transformed into

$$\partial_{zz}^2 \tilde{u}_z - \left(n^2 \xi^2 - \frac{k_p^2}{(1 + i\omega t_r)} \right) \tilde{u}_z = 0. \tag{7.11}$$

Assuming that the solution of (7.11) has the form

$$\hat{u}_z(\xi, z) = A(\xi) \exp(-az), \tag{7.12}$$

where a is the wave number. It is assumed that its real and imaginary parts are always positive, so that for $z \to \infty$ waves propagate in the positive z-direction and the transformed displacement $\tilde{u}_z$ must vanish. This effect describes the radiation condition, credited by Rayleigh [1894]. With the aid of the boundary condition (7.6) the arbitrary complex coefficient A can be found. The wave number a is written as

$$a^2 = R^2 \exp(i2\vartheta), \tag{7.13}$$

where

$$R^4 = \frac{(n^2\xi^2 - k_p^2)^2 + n^4 \xi^4 (\omega t_r)^2}{1 + (\omega t_r)^2}, \tag{7.14}$$

$$\vartheta = \frac{1}{2} \arctan \left(\frac{k_p^2 \omega t_r}{n^2 \xi^2 (1 + (\omega t_r)^2) - k_p^2} \right); \quad 0 \le \vartheta < \pi/2. \tag{7.15}$$

For this problem only outgoing waves occur, which means that the value of ϑ lies in the interval $[0, \pi/2)$. Using (7.12) and the transformed expression (7.6), the solution of the transformed problem gives

$$\tilde{u}_z(\xi, z) = \frac{p_0 r_0}{(\lambda + 2\mu)} \frac{J_1(\xi r_0)}{a\xi(1 + i\omega t_r)} \exp(-az). \tag{7.16}$$

The inverse Hankel transformation of this expression is

$$\breve{u}_z(r, z) = \frac{p_0 r_0}{(\lambda + 2\mu)} \frac{1}{(1 + i\omega t_r)} \int_0^\infty \frac{J_1(\xi r_0) J_0(\xi r)}{a} \exp(-az)\, d\xi. \tag{7.17}$$

After introducing the dimensionless parameters $d = r/r_0$, $\alpha = k_s r_0 = \omega r_0/c_s$ and $\beta = \xi/k_s$ into the right hand side of (7.17), and taking $z = 0$ (on the surface), then $\breve{u}_z(r,0)$ is written as

$$\breve{u}_z(r,0) = \frac{p_0 r_0}{(\lambda+2\mu)} \frac{1}{(1+i\omega t_r)} \int_0^\infty \frac{J_1(\alpha\beta) J_0(d\alpha\beta)}{a_a}\, d\beta, \tag{7.18}$$

where the dimensionless wave number a_a is given by

$$a_a^2 = \frac{a^2}{k_s^2} = n^2 \left(\beta^2 - \frac{1}{(1+i\omega t_r)} \right). \tag{7.19}$$

The hysteretic damping of the material is represented by the damping ratio ζ. This is defined as

$$\zeta = \frac{1}{2}\omega t_r. \tag{7.20}$$

Therefore, R and ϑ are rewritten as

$$\frac{R^4}{n^4 k_s^4} = \frac{(\beta^2-1)^2 + 4\beta^4\zeta^2}{1+4\zeta^2}, \tag{7.21}$$

$$\vartheta = \frac{1}{2} \arctan\left(\frac{2\zeta}{\beta^2(1+4\zeta^2) - 1} \right); \quad 0 \le \vartheta < \pi/2. \tag{7.22}$$

The quasi-static solution of the vertical displacement on the surface is calculated when the wave number k_s tends to zero. For this purpose, $\breve{u}_z(r,0)$ is reduced to

$$\breve{u}_z(r,0) = \frac{p_0 r_0}{n(\lambda+2\mu)} \frac{1}{(1+i2\zeta)} \int_0^\infty \frac{J_1(\xi r_0) J_0(\xi r)}{\xi}\, d\xi. \tag{7.23}$$

The dynamic amplification factor $\breve{u}_z/\breve{u}_{zs}$ on the surface and the amplitude of quasi-static vertical displacement at the origin $\breve{u}_{zs}$ are defined as

$$\frac{\breve{u}_z}{\breve{u}_{zs}} = h \exp(i\omega t), \tag{7.24}$$

where

$$\breve{u}_{zs} = \frac{p_0 r_0}{n(\lambda+2\mu)} \frac{1}{(1+i2\zeta)}. \tag{7.25}$$

The factor $(1+i2\zeta)$ has been retained in this expression to allow the damping ratio to be described as a constant, even when the frequency tends to zero. The complex function $h = h_1 + ih_2$ is the response function of the surface, defined as

$$h = \frac{1}{(1+i2\zeta)} I(\alpha), \tag{7.26}$$

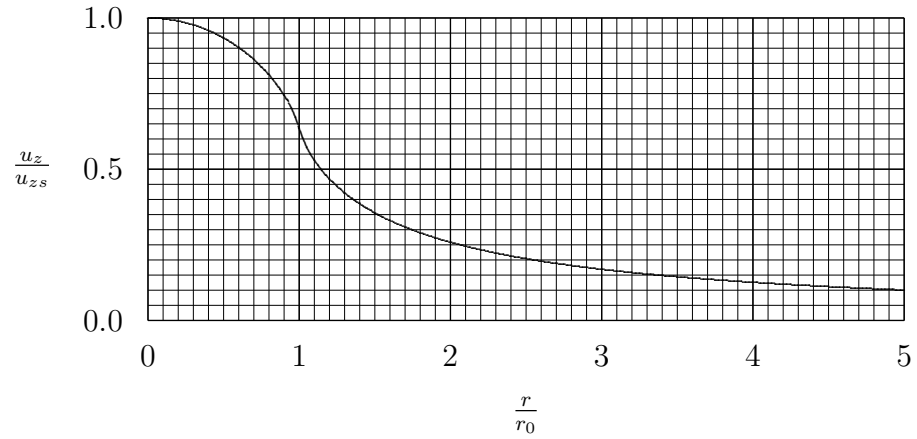

Figure 7.2: Quasi-static solution: $\nu = 0$, $\alpha = 0.01$, $\beta_{max} = 5000$.

with

$$I(\alpha) = \int_0^\infty \frac{J_1(\alpha\beta)J_0(d\alpha\beta)}{a_a}\, d\beta. \tag{7.27}$$

This integral can be evaluated numerically using Simpson's method.

As a first result the numerical evaluation for a very small value of the circular frequency is calculated. For this reason the value of α has been considered to be $\alpha = 0.01$. These results are depicted in Figure 7.2. The maximum number of divisions for the numerical integral β_{max} is equal to 5000.

The displacement at origin $d = 0$ is

$$\breve{u}_z(0,0) = \frac{p_0 r_0}{(\lambda + 2\mu)} \frac{1}{(1 + i2\zeta)} \int_0^\infty \frac{J_1(\alpha\beta)}{a_a}\, d\beta. \tag{7.28}$$

This can be also expressed as

$$\frac{\breve{u}_z}{\breve{u}_{zs}} = f \exp(i\omega t), \tag{7.29}$$

where $f = f_1 + if_2 = nI_0(\alpha)$ is the response function at the origin. The integral I_0 is

$$I_0(\alpha) = \int_0^\infty \frac{J_1(\alpha\beta)}{a_a}\, d\beta. \tag{7.30}$$

The value of the integral gives

$$I_0 = \frac{1 - \exp(-\alpha\kappa)}{n\alpha\kappa},$$

with

$$\kappa = i\frac{\exp(-i\iota)}{(1 + 4\zeta^2)^{1/4}} \quad \text{and} \quad \iota = \frac{1}{2}\arctan(2\zeta).$$

The angle ι is considered to be positive since the real part of a_a is positive and the radiation condition must be satisfied.

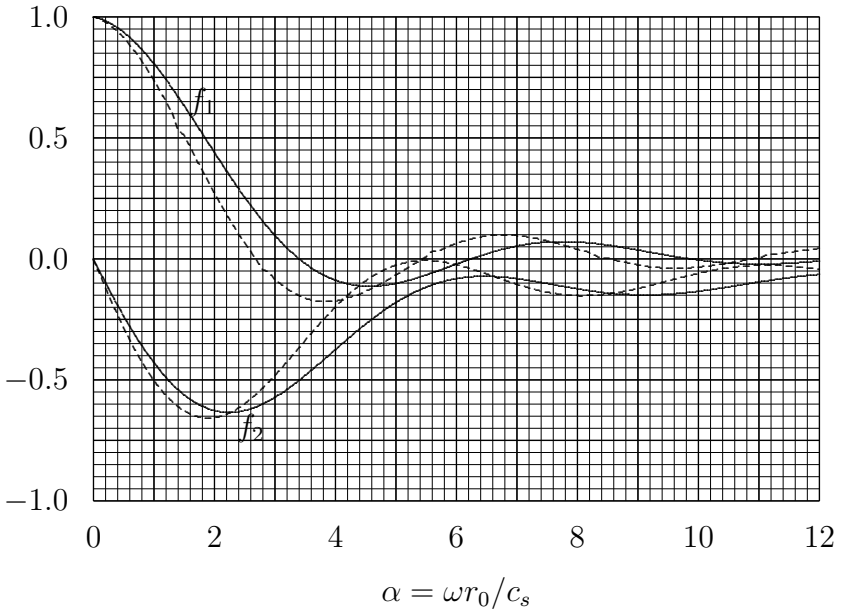

Figure 7.3: Real and imaginary values of the displacement at origin $d = 0$: $\nu = 1/3$, $\zeta = 0.1$, $\beta_{max} = 10000$.

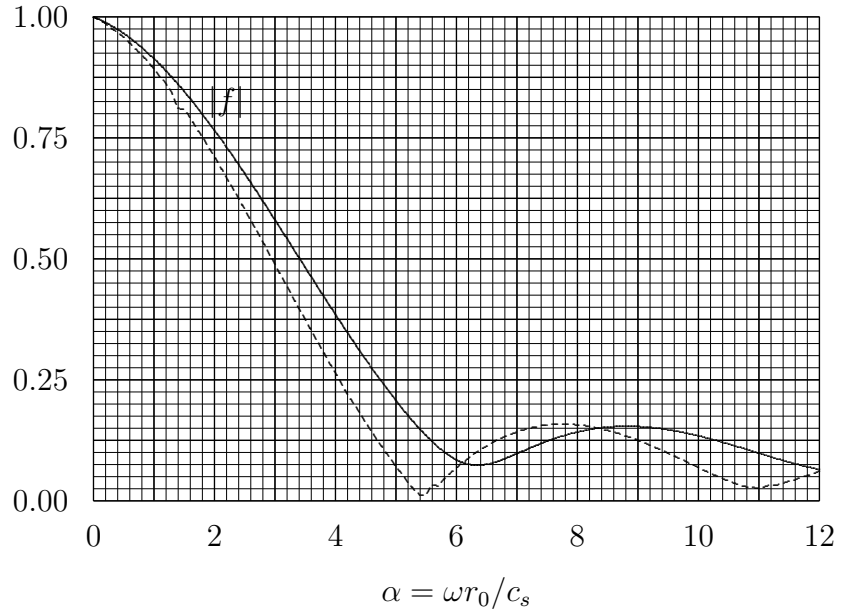

Figure 7.4: Absolute value of the displacement at origin $d = 0$: $\nu = 1/3$, $\zeta = 0.1$, $\beta_{max} = 10000$.

For the damping ratio $\zeta = 0.1$, Figure 7.3 shows the response functions of the displacement at the origin. It can be observed that results of Westergaard's solution give an acceptable approximation of the elastic solution, which is given by dashes. The absolute value $|f|$ is shown in Figure 7.4. The elastic solution is also depicted by dashes.

The average displacement at the origin is

$$\overline{u}_z(r,0) = \frac{1}{\pi r_0^2} \int_0^{2\pi} \int_0^{r_0} \breve{u}_z(r,0) r \, dr d\theta. \tag{7.31}$$

With the aid of the relation

$$\int_0^{r_0} J_0(\xi r) r \, dr = \frac{r_0}{\xi} J_1(\xi r_0),$$

and from (7.28), one obtains

$$\begin{aligned} \overline{u}_z(r,0) &= \frac{2p_0}{(\lambda+2\mu)} \frac{1}{(1+i2\zeta)} \int_0^{\infty} \frac{J_1^2(\xi r_0)}{\xi a} \, d\xi \\ &= \frac{2p_0}{(\lambda+2\mu)} \frac{1}{(1+i2\zeta)} \int_0^{\infty} \frac{J_1^2(\alpha\beta)}{k_s \beta a_a} \, d\beta. \end{aligned} \tag{7.32}$$

For the quasi-static case the amplitude of the average displacement $\overline{u}_{zs}$ is

$$\overline{u}_{zs} = \frac{8p_0 r_0}{3\pi n(\lambda+2\mu)} \frac{1}{(1+i2\zeta)}, \tag{7.33}$$

where the effect of the damping on the quasi-static response has been included in the factor $(1+i\zeta)$.

The dynamic amplification factor of the average displacement $\overline{u}_z/\overline{u}_{zs}$ is defined as

$$\frac{\overline{u}_z}{\overline{u}_{zs}} = \eta \exp(i\omega t), \tag{7.34}$$

where the complex function $\eta = \eta_1 + i\eta_2$ is the response function. This is given by

$$\eta = nN(\alpha), \tag{7.35}$$

with

$$N(\alpha) = \frac{3}{4\pi} \int_0^{\infty} \frac{J_1^2(\alpha\beta)}{\alpha\beta a_a} \, d\beta. \tag{7.36}$$

Figure 7.5 shows the response functions of the average displacement at the origin for the damping ratio $\zeta = 0.1$. The elastic solutions are again given by dashes. The absolute value $|\eta|$ is depicted in Figure 7.6. The elastic solution is also shown by dashes.

After comparing the exact elastic solution with Westergaard's solution it can be concluded that the Westergaard approximation can be applied to solve to the problem of a vibrating load on a half-space, in the vicinity of the load.

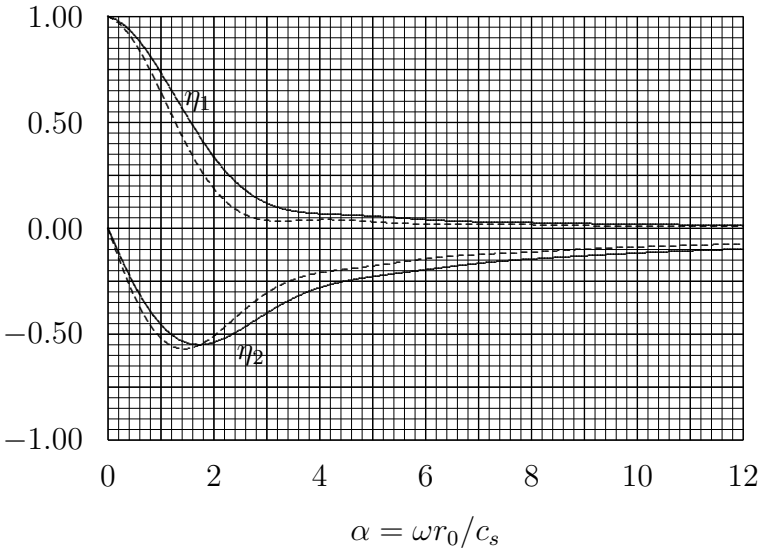

Figure 7.5: Real and imaginary values of the average displacement at origin $d = 0$: $\nu = 1/3$, $\zeta = 0.1$, $\beta_{max} = 10000$.

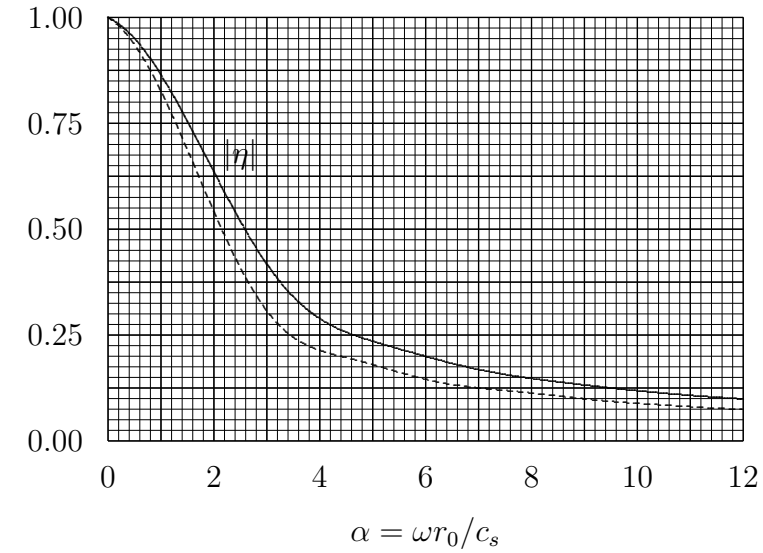

Figure 7.6: Absolute value of the average displacement at origin $d = 0$: $\zeta = 0.1$, $\beta_{max} = 10000$.

7.2 Moving loads on a half-plane

The basic equation of motion of the Westergaard approximation for a half-plane in the vertical direction is given by

$$\partial_x \sigma_{xz} + \partial_z \sigma_{zz} = \rho \partial_{tt}^2 u_z, \tag{7.37}$$

where $u_z = u_z(x, z, t)$ is the displacement in vertical direction. The stress components can be given as

$$\sigma_{xx} = \lambda \partial_z u_z + \lambda t_r \partial_t \partial_z u_z, \tag{7.38}$$

$$\sigma_{zz} = (\lambda + 2\mu) \partial_z u_z + (\lambda + 2\mu) t_r \partial_t \partial_z u_z, \tag{7.39}$$

$$\sigma_{xz} = \mu \partial_x u_z + \mu t_r \partial_t \partial_x u_z, \tag{7.40}$$

Introducing (7.39) - (7.40) into (7.37) leads to the partial differential equation

$$\partial_{xx}^2 u_z + m \partial_{zz}^2 u_z + t_r \partial_t \partial_{xx}^2 u_z + m t_r \partial_t \partial_{zz}^2 u_z = \frac{1}{c_s^2} \partial_{tt}^2 u_z, \tag{7.41}$$

where $m = 2(1-\nu)/(1-2\nu) = (\lambda + 2\mu)/\mu = c_p^2/c_s^2$ is a constant parameter.

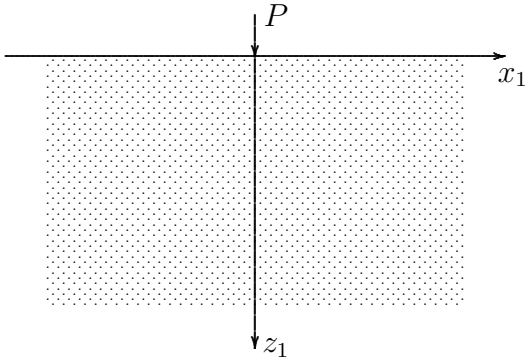

Figure 7.7: Moving load on a half-plane.

The case of a moving load at constant velocity v on the surface of a half-plane $z \geq 0$ is depicted in Figure 7.7. Introducing the moving coordinate system (x_1, z_1), with $-\infty < x_1 < \infty$ and $z_1 \geq 0$, defined as

$$x_1 = x - vt \quad \text{and} \quad z_1 = z, \tag{7.42}$$

the equation of motion (7.41) leads to

$$\partial_{x_1 x_1}^2 u_z + m \partial_{z_1 z_1}^2 u_z - v t_r \partial_{x_1} \partial_{x_1 x_1}^2 u_z - m v t_r \partial_{x_1} \partial_{zz}^2 u_z = M_s^2 \partial_{x_1 x_1}^2 u_z. \tag{7.43}$$

Similarly, the stress components can also be written as

$$\sigma_{xx} = \lambda \partial_{z_1} u_z - \lambda v t_r \partial_{x_1} \partial_{z_1} u_z, \tag{7.44}$$

$$\sigma_{zz} = (\lambda + 2\mu)\partial_{z_1} u_z - (\lambda + 2\mu) v t_r \partial_{x_1} \partial_{z_1} u_z, \tag{7.45}$$

$$\sigma_{xz} = \mu \partial_{x_1} u_z - \mu v t_r \partial_{x_1} \partial_{x_1} u_z. \tag{7.46}$$

Because the horizontal displacements are disregarded, in this case the Rayleigh waves will not be presented.

For a moving point load the only boundary condition is the vertical normal stress on the surface. This is given by

$$z = 0 \ : \ \sigma_{zz} = -P\delta(x - vt) = -P\delta(x_1), \tag{7.47}$$

where $\delta(x_1)$ is the Dirac function and P is the total force per unit length. In order to solve this problem the exponential Fourier transformation over the x_1 coordinate of the vertical displacement is used. This is defined as

$$\tilde{u}_z(k, z_1) = \int_{-\infty}^{\infty} u_z(x_1, z_1) \exp(-ikx_1)\, dx_1, \tag{7.48}$$

where k is the horizontal wave number. Substitution of (7.48) into (7.43), gives

$$\partial^2_{z_1 z_1} \tilde{u}_z - a^2 k^2 \tilde{u}_z = 0, \tag{7.49}$$

where the wave number a is given as

$$a^2 = \frac{1}{m}\left(1 - \frac{M_s^2}{1 - ivt_r k}\right). \tag{7.50}$$

Assuming that the solution of (7.49) can be expressed as

$$\tilde{u}_z(k, z_1) = A(k) \exp(-a|k|z_1), \tag{7.51}$$

where A is an arbitrary complex coefficient. The real part of a is assumed to be positive and the imaginary part is assumed to be negative, so that for $z_1 \to \infty$ the solution of $\tilde{u}_z$ must vanish. This effect describes the radiation condition. The wave number a can also be written as

$$a^2 = R^2 \exp(-i2\vartheta), \tag{7.52}$$

where R and the angle ϑ are defined by

$$R = \sqrt[4]{\frac{(1 - M_s^2 + (vt_r k)^2)^2 + (vt_r k M_s^2)^2}{m^2(1 + (vt_r k)^2)^2}}, \tag{7.53}$$

$$\vartheta = \frac{1}{2} \arctan\left(\frac{vt_r k M_s^2}{1 - M_s^2 + (vt_r k)^2}\right); \quad 0 \le \vartheta < \pi/2. \tag{7.54}$$

Because the propagation of waves only occurs in the positive vertical direction, the value of ϑ lies in the interval $[0, \pi/2)$.

Similarly, the transformed stress components (7.44) - (7.46) can be given as

$$\frac{\tilde{\sigma}_{xx}}{\mu} = (m-2)(1-ivt_r k)\partial_{z_1}\tilde{u}_z, \tag{7.55}$$

$$\frac{\tilde{\sigma}_{zz}}{\mu} = m(1-ivt_r k)\partial_{z_1}\tilde{u}_z, \tag{7.56}$$

$$\frac{\tilde{\sigma}_{xz}}{\mu} = ik(1-ivt_r k)\tilde{u}_z. \tag{7.57}$$

From the boundary condition (7.47) and using (7.56) for $z_1 = 0$, yields

$$m(1-ivt_r k)a|k|A = \frac{P}{\mu}. \tag{7.58}$$

The value of $\tilde{u}_z$ is

$$\tilde{u}_z = \frac{P}{m\mu(1-ivt_r k)}\frac{\exp(-a|k|z)}{a|k|}. \tag{7.59}$$

In order to represent the hysteretic damping the damping ratio ζ is introduced. This is defined as

$$\zeta = \frac{vt_r k}{2} sign(k), \tag{7.60}$$

where $|\zeta|$ is assumed to be constant and $sign(k)$ denotes the sign of k. The values of a, R and ϑ are rewritten as

$$a = R\exp(-i\vartheta) = p - iq, \tag{7.61}$$

$$R = \sqrt[4]{\frac{(1-M_s^2)^2 + 4\zeta^2}{m^2(1+4\zeta^2)}}, \tag{7.62}$$

$$\vartheta = \frac{1}{2}\arctan\left(\frac{2\zeta M_s^2}{1-M_s^2+4\zeta^2}\right); \quad 0 \le \vartheta < \pi/2. \tag{7.63}$$

Stress components

The stress components are found by using the respective exponential Fourier transformation in (7.59). It follows that

$$\sigma_{xx} = -\frac{(m-2)P}{m}\frac{1}{2\pi}\int_{-\infty}^{\infty}\exp(-a|k|z)\exp(ikx_1)\,dk, \tag{7.64}$$

$$\sigma_{zz} = -P\frac{1}{2\pi}\int_{-\infty}^{\infty} \exp(-a|k|z)\exp(ikx_1)\,dk, \tag{7.65}$$

$$\sigma_{xz} = i\frac{P}{m}\frac{1}{2\pi}\int_{-\infty}^{\infty} \frac{k\exp(-a|k|z)}{a|k|}\exp(ikx_1)\,dk. \tag{7.66}$$

The integrals are then calculated, yielding

$$\frac{\sigma_{xx}z_1}{P} = -\frac{(m-2)}{m\pi}\frac{p}{\left(\frac{x_1}{z_1}+q\right)^2+p^2}, \tag{7.67}$$

$$\frac{\sigma_{zz}z_1}{P} = -\frac{1}{\pi}\frac{p}{\left(\left(\frac{x_1}{z_1}+q\right)^2+p^2\right)}, \tag{7.68}$$

$$\frac{\sigma_{xz}z_1}{P} = -\frac{1}{m\pi}\frac{p\left(\frac{x_1}{z_1}+2q\right)}{(p^2+q^2)\left(\left(\frac{x_1}{z_1}+q\right)^2+p^2\right)}. \tag{7.69}$$

For different values of Poisson's ratios ν the vertical stress of the static Westergaard solution is illustrated in Figure 7.8. Results of the Flamant problem are given by dots.

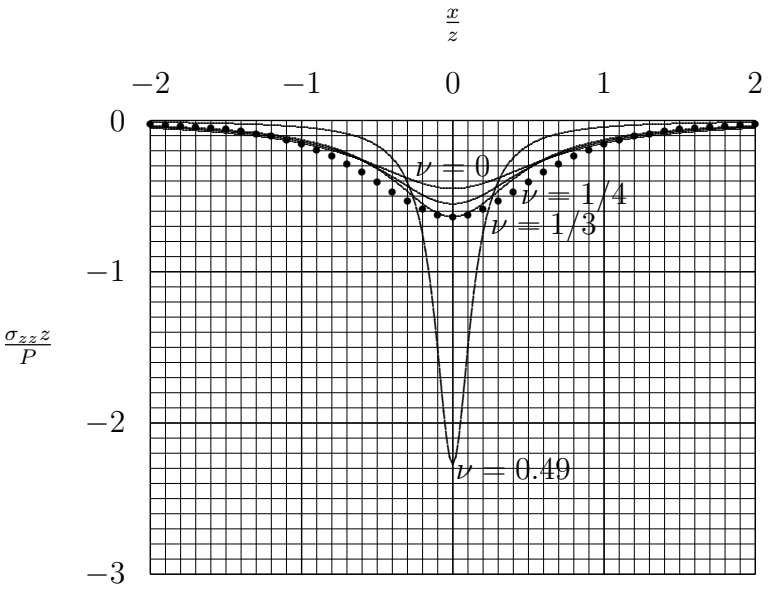

Figure 7.8: Vertical stress of the static Westergaard solution for different ν and Flamant's solution.

For Poisson's ratio $\nu = 0$, Fadum [1948] found the solution of the Westergaard problem for a line load of finite length. It also appears that for $\nu = 1/3$ the Westergaard problem gives a reasonable approximation of the Flamant problem, but for Poisson's

ratio $\nu = 0.49$ the Westergaard problem is to be inapplicable to the Flamant problem. It can also be verified that for $\nu < 0.4$, only the approximation can be applicable.

For the damping ratio $\zeta = 0.1$ and different values of M_s, the vertical stress of the Westergaard problem is shown in Figure 7.9. The elastic solution is depicted by dashes. It can be observed that for values of $M_s < 0.5$, the results of the Westergaard problem only give an acceptable approximation for the elastic solution.

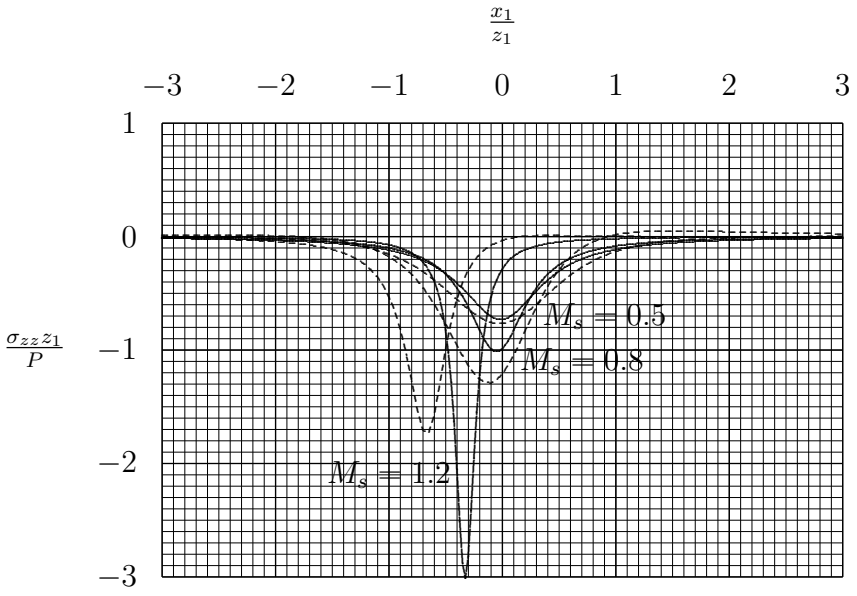

Figure 7.9: Vertical stress of Westergaard's solution and elastic solution for different M_s: $\nu = 1/3$, $\zeta = 0.1$.

Displacement

In order to obtain the displacement u_z the equation of motion (7.37) is expressed as

$$\partial_{x_1}\sigma_{xz} + \partial_{z_1}\sigma_{zz} = \rho v^2 \partial^2_{x_1 x_1} u_z. \tag{7.70}$$

Substitution of (7.68) and (7.69) into (7.70), and integrating with respect to x_1 twice gives

$$\begin{aligned}\frac{\pi m \mu}{P} M_s^2 u_z =& p\left(m - \frac{1}{(p^2+q^2)}\right)\log\sqrt{(x_1+qz_1)^2+(pz_1)^2} \\ &- q\left(m + \frac{1}{(p^2+q^2)}\right)\arctan\left(\frac{x_1+qz_1}{pz_1}\right) + K_z,\end{aligned} \tag{7.71}$$

or

$$\frac{\pi m \mu}{P} M_s^2 u_z = m\Re[a\log(\xi)] - \frac{1}{(p^2+q^2)}\Re[\overline{a}\log(\xi)] + K_z,$$

where $\overline{a}$ is the conjugate of a, K_z is an integration constant and $\xi = R_\xi \exp(-i\iota_\xi)$ with

$$R_\xi = \sqrt{(x_1+qz_1)^2+(pz_1)^2} \quad \text{and} \quad \iota_\xi = \arctan\left(\frac{x_1+qz_1}{pz_1}\right).$$

The static displacement on the surface u_{zs} can be obtained when the value of M_s tends to zero and the damping ratio $\zeta = 0$, yielding

$$\frac{\pi\mu}{P} u_z = -\frac{1}{\sqrt{m}} \log|x| + K_z. \tag{7.72}$$

The constant K_z can be eliminated by using the differential displacement Δu_z. This is defined as

$$\Delta u_z = u_z(x_1, z_1) - u_z(x_1 + l, z_1), \tag{7.73}$$

where l is a given non-zero length. Introducing (7.71) into (7.73), gives

$$\frac{\pi m\mu}{P} M_s^2 \Delta u_z = p\left(m - \frac{1}{(p^2+q^2)}\right) \log \sqrt{\frac{((x_1+qz_1)/l)^2 + (pz_1/l)^2}{((x_1+qz_1)/l+1)^2 + (pz_1/l)^2}}$$
$$+ q\left(m + \frac{1}{(p^2+q^2)}\right) \arctan\left(\frac{pz_1/l}{(pz/l)^2 + ((x_1+qz_1)/l + 1/2)^2 - 1/4}\right). \tag{7.74}$$

Figure 7.10 shows the differential displacement of the Westergaard problem for the damping ratio $\zeta = 0.01$ and $M_s = 0.5$. The elastic solution is depicted by dots. It

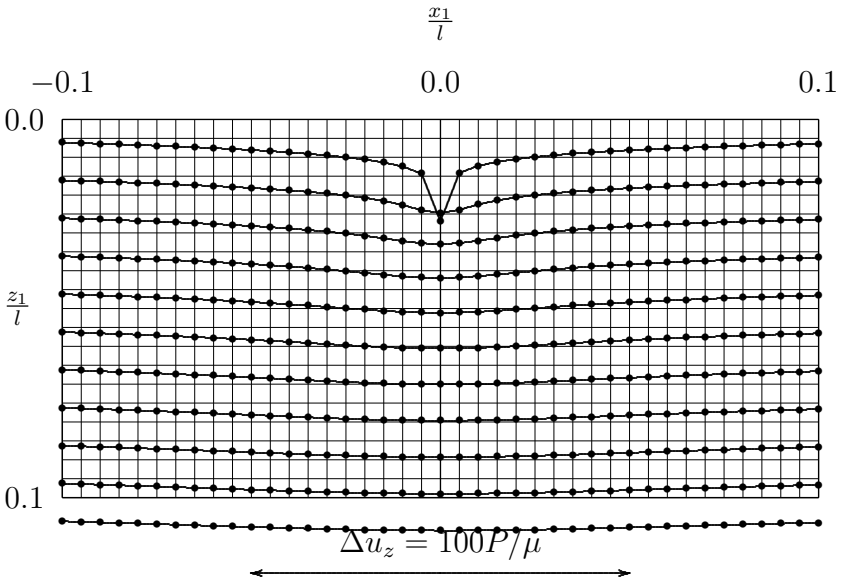

Figure 7.10: Differential displacement of the Westergaard problem: $M_s = 0.5$, $\nu = 1/3$, $\zeta = 0.01$.

appears that both results are very similar. The differential displacement on the surface is given by

$$\frac{\pi m\mu}{P} M_s^2 \Delta u_z = p\left(m - \frac{1}{(p^2+q^2)}\right) \log\left|\frac{x_1/l}{x_1/l+1}\right|. \tag{7.75}$$

Chapter 8

The Cagniard-de Hoop technique for a material with horizontal constraints

Analytical solutions to transient wave problems can be obtained by using integral transformation methods, especially Laplace and Fourier transformations. The mathematical problem is then reduced to the determination of the inverse transformation. For a variety of problems the inverse transformations can be performed conveniently by the Cagniard-de Hoop method (de Hoop [1960]). This method will be illustrated in this chapter for two problems. The first problem is a line load on the surface of a half-space and the second problem is a moving line load on the surface of a half-space. The equation of motion is solved in the transform domain, as a result of a Laplace transformation with respect to time (using a real, positive parameter of transformation) and Fourier transformation with respect to the spatial coordinate parallel to the surface.

In order to return to the space-time domain the Laplace and Fourier transformations must be inverted. For this purpose the Cagniard-de Hoop method is applied. In this method the path of integration of the inverse Fourier transformation in the complex plane is deformed, so that the integral resembles the forward Laplace transformation of a well-behaved function, with a real, positive parameter of integration defined along the deformed path of integration, which can then be identified with time.

Lamb [1904] studied the problem of the propagation of a pulse in a half-space, and also examined the problems of a line and point load at the surface and inside the half-space. The surface line source problem was also investigated by de Hoop [1970]. Various studies on the propagation of transient waves in a half-space due to a moving load on the surface have been presented by Payton [1967], Gakenheimer and Miklowitz [1969], Norwood [1969], Gakenheimer [1971], Kennedy and Herrmann [1973, 1974], Bakker *et al.* [1999], and Bakker [2000]. Transient wave problems for a material with horizontal constraints were examined by Barends [1971], de Hoop [2001] and Cornejo Córdova [2002].

The primary purpose of this chapter is to obtain a closed-form solution of the vertical displacement and the vertical stress to a normal impulsive load acting on the

surface of a half-space. For the case of a moving line load the problem is split into two parts: subsonic and supersonic surface load speeds. In this chapter it can also be seen that the inverse Fourier and Laplace transformations notably can be found in a simple way if the Cagniard-de Hoop method is used.

In a rectangular coordinate system, consider the half-plane $z > 0$ and $-\infty < x < \infty$, with bounding surface $z = 0$. For a two-dimensional problem, the governing scalar wave equation of motion of a material with horizontal constraints or Westergaard's equation of motion in vertical direction is (see Eq. 7.1)

$$\mu\partial_{xx}^2 u_z + (\lambda + 2\mu)\partial_{zz}^2 u_z = \rho\partial_{tt}^2 u_z, \tag{8.1}$$

where $u_z = u_z(x, z, t)$ is the vertical displacement. The essential approximation in this type of analysis, suggested by Westergaard [1938], is that horizontal deformations are neglected. Eq. (8.1) is rewritten as

$$c_s^2\partial_{xx}^2 u_z + c_p^2\partial_{zz}^2 u_z = \partial_{tt}^2 u_z, \tag{8.2}$$

where $c_s^2 = \mu/\rho$ and $c_p^2 = (\lambda + 2\mu)/\rho$. Eq. (8.2) indicates that the wave propagation in x- en z-direction take place with the shear wave speed c_s and the compressional wave speed c_p, respectively. This implies that the scalar wave Westergaard's equation manifests anisotropy in the propagation of its wave fronts. The corresponding vertical stress σ_{zz} is

$$\sigma_{zz} = (\lambda + 2\mu)\partial_z u_z. \tag{8.3}$$

The scalar wave equation will be solved for two types of boundary conditions.

8.1 Line pulse

Wave propagation in a half-space due to a line pulse is shown in Figure 8.1. The

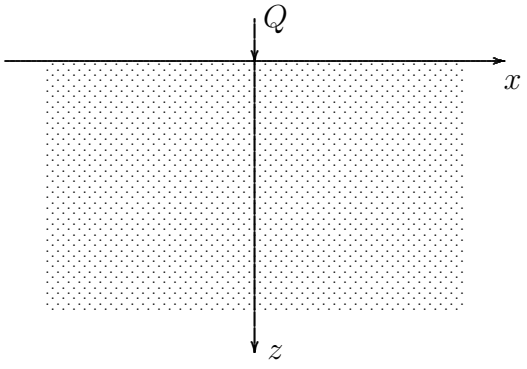

Figure 8.1: Line pulse.

boundary condition on the surface $z = 0$ is described by

$$z = 0 \ : \ \sigma_{zz} = -Q\delta(x)\delta(t), \tag{8.4}$$

where Q is a line force per unit of length multiplied by time, and $\delta(x)$ and $\delta(t)$ are the Dirac functions. It is assumed that the force is stationary prior to a certain instant $t = 0$ and it is then suddenly set into horizontal motion. The Laplace transformation with respect to time t is defined as

$$\hat{u}_z(x, z, s) = \int_{t=0}^{\infty} u_z(x, z, t) \exp(-st)\, dt, \tag{8.5}$$

where s is a real and positive parameter. From (8.2) and (8.4) it follows that

$$c_s^2 \partial_{xx}^2 \hat{u}_z + c_p^2 \partial_{zz}^2 \hat{u}_z = s^2 \hat{u}_z, \tag{8.6}$$

with the boundary condition

$$z = 0 \ : \ \hat{\sigma}_{zz} = -Q\delta(x), \tag{8.7}$$

where $\hat{\sigma}_{zz} = \hat{\sigma}_{zz}(x, z, s)$. The Fourier transformation of $\hat{u}(x, z, s)$ with respect to x

$$\tilde{u}_z(\alpha, z, s) = \int_{x=-\infty}^{\infty} \hat{u}_z(x, z, s) \exp(is\alpha x)\, dx, \tag{8.8}$$

is introduced. The factor s in the argument of the exponential function has been introduced to facilitate the solving of the problem. Substituting (8.8) in (8.6) and (8.7), gives

$$\partial_{zz}^2 \tilde{u}_z - s^2 \beta^2 \tilde{u}_z = 0, \tag{8.9}$$

with the boundary condition

$$z = 0 \ : \ \tilde{\sigma}_{zz} = -Q, \tag{8.10}$$

where $\tilde{\sigma}_{zz} = \tilde{\sigma}_{zz}(\alpha, z, s)$ and

$$\beta = \frac{c_s}{c_p}(\alpha^2 + c_s^{-2})^{1/2}; \quad \beta > 0. \tag{8.11}$$

The solution of (8.9) vanishing at infinity ($z \to \infty$) is

$$\tilde{u}_z(\alpha, z, s) = \tilde{A} \exp(-s\beta z), \tag{8.12}$$

where $\tilde{A}$ is a parameter. From (8.3), (8.10) and (8.12) it follows that

$$\tilde{A} = \frac{Q}{(\lambda + 2\mu)s\beta}.$$

Using the inverse of the Fourier transformation the solution of the problem is, expressed in the Laplace transformation

$$\hat{u}_z(x, z, s) = \frac{Q}{(\lambda + 2\mu)} \frac{1}{2\pi} \int_{\alpha=-\infty}^{\infty} \frac{\exp(-s\beta z)}{\beta} \exp(-is\alpha x)\, d\alpha. \tag{8.13}$$

Changing the parameter of integration with respect to α in (8.13) as an integration with respect to p, defined by

$$p = i\alpha$$

where p is considered to be a complex variable in the p-plane, gives

$$\hat{u}_z(x,z,s) = \frac{Q}{(\lambda+2\mu)}\frac{1}{2\pi i}\int_{p=-i\infty}^{i\infty}\frac{\exp(-s(px+\beta z))}{\beta}\,dp, \tag{8.14}$$

with

$$\beta = \frac{c_s}{c_p}(c_s^{-2}-p^2)^{1/2}; \quad \Re[\beta] > 0. \tag{8.15}$$

It appears that the singularities of the integrand of Eq. (8.14) are branch points at $p = 1/c_s$ and $p = -1/c_s$. Branch cuts can be introduced along the real axis, $\Im[p] = 0$ from $-\infty$ to $-1/c_s$ and from $1/c_s$ to ∞, see Figure 8.2. The basic step in the Cagniard-

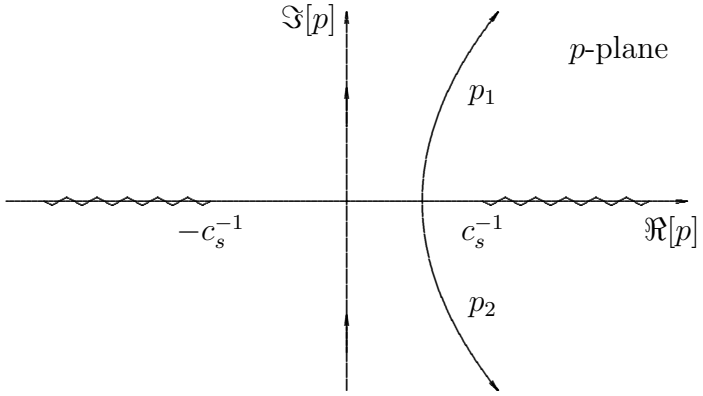

Figure 8.2: Line Pulse, the path of integration in the complex p-plane.

de Hoop method is now to replace by the path of integration in the p-plane, which originally is located along the imaginary axis $\Re[p] = 0$, to a curved path defined by

$$\chi = px + \beta z, \tag{8.16}$$

where χ is considered to be a real and positive parameter. From (8.16) and the definition (8.15) of β a quadratic expression for p can be obtained, with the solutions p_1 and p_2. The new path is assumed to consist of the two hyperbolic arcs p_1 and p_2, with

$$p_{1,2} = \frac{x}{r_n^2}\chi \pm i\frac{nz}{r_n^2}\sqrt{\chi^2 - \frac{r_n^2}{c_s^2}}; \quad r_n/c_s \le \chi < \infty, \tag{8.17}$$

where $n = c_s/c_p$ and $r_n = \sqrt{x^2+n^2z^2} > 0$.

The integration along the imaginary p-axis is replaced to an integration along the new path. The contributions of the arcs connecting the imaginary axis and the new

path vanish. Therefore, the integral along the imaginary p-axis, $\Re[p] = 0$ is equivalent to the integral along the hyperbolic arcs $p = p_1$ and $p = p_2$. Substitution of (8.17) into (8.16) leads to the following values of β along the two arcs

$$\beta_{1,2} = \frac{n^2 z}{r_n^2}\chi \mp i\frac{nx}{r_n^2}\sqrt{\chi^2 - \frac{r_n^2}{c_s^2}}. \tag{8.18}$$

Furthermore, it follows from (8.16) that

$$\partial_\chi p = \frac{1}{x} - \frac{z}{x}\partial_\chi \beta,$$

and then using (8.18) to evaluate $\partial_\chi \beta$ gives

$$\partial_\chi p = \pm i\frac{\beta}{n\sqrt{\chi^2 - r_n^2/c_s^2}}d\chi, \tag{8.19}$$

so that

$$\frac{1}{\beta}dp = \pm i\frac{1}{n\sqrt{\chi^2 - r_n^2/c_s^2}}d\chi.$$

Therefore, the expression (8.14) is transformed into

$$\hat{u}_z(x, z, s) = \frac{Q}{n(\lambda + 2\mu)}\frac{1}{\pi}\int_{\chi=r_n/c_s}^{\infty}\frac{\exp(-s\chi)}{\sqrt{\chi^2 - r_n^2/c_s^2}}\,d\chi. \tag{8.20}$$

The integral has now been brought into the form of a Laplace transformation, and the parameter χ can be identified with time t. It follows that

$$u_z(x, z, t) = \frac{Q}{\pi(\lambda + 2\mu)n}\frac{1}{\sqrt{t^2 - t_0^2}}H(t - t_0), \tag{8.21}$$

where $t_0 = r_n/c_s$ is the arrival time. The dimensionless vertical displacement u_z/u_q is shown in Figure 8.3, with

$$u_q = \frac{Q}{(\lambda + 2\mu)nt_0}.$$

The transformed vertical stress can also be found, using the transformed expression of (8.3) and the partial derivative of (8.14) with respect to z, yielding

$$\hat{\sigma}_{zz}(x, z, s) = -Q\frac{1}{2\pi i}\int_{p=-i\infty}^{i\infty} s\exp(-s(px + \beta z))\,dp. \tag{8.22}$$

Substituting $\chi = px + \beta z$ into (8.22) and using (8.17) - (8.19), it can be observed that the path of integration is again symmetric with respect to real axis. The transformed vertical stress is

$$\hat{\sigma}_{zz}(x, z, s) = -Q\frac{nz}{r_n^2}\frac{1}{\pi}\int_{\chi=r_n/c_s}^{\infty}\frac{s\chi}{\sqrt{\chi^2 - r_n^2/c_s^2}}\exp(-s\chi)\,d\chi. \tag{8.23}$$

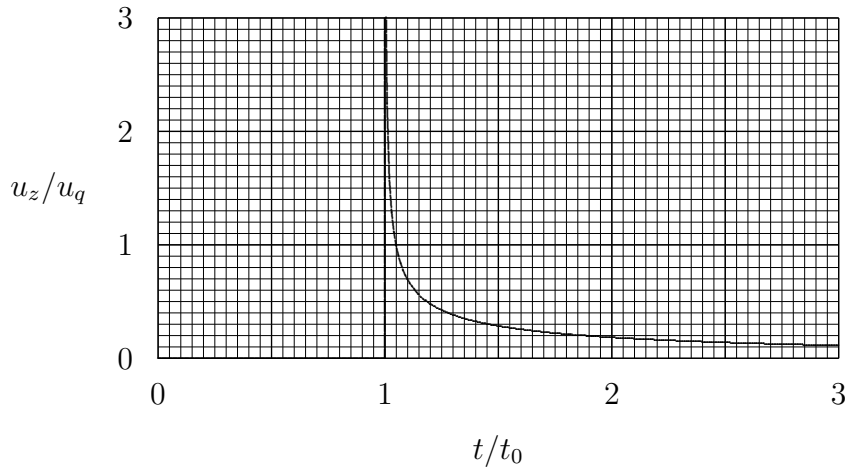

Figure 8.3: Line pulse, dimensionless vertical displacement u_z/u_q.

Applying the shift rule for Laplace transformation to the function $s\exp(-s\chi)$, yields

$$\sigma_{zz}(x,z,t) = -Q\frac{nz}{r_n^2}\frac{1}{\pi}\frac{d}{dt}\left(\frac{t}{\sqrt{t^2 - r_n^2/c_s^2}}\right)H(t - r_n/c_s). \tag{8.24}$$

The final expression for the vertical stress is

$$\sigma_{zz}(x,z,t) = \frac{Q}{\pi c_s^2}\frac{nz}{(t^2 - t_0^2)^{3/2}}H(t - t_0). \tag{8.25}$$

This result can also be obtained, of course, by using (8.3) and (8.21).

8.2 Moving line load

Wave motion in a half-space generated by a surface moving line load at constant speed v is depicted in Figure 8.4, see Cornejo Córdova [2002]. For this problem the boundary

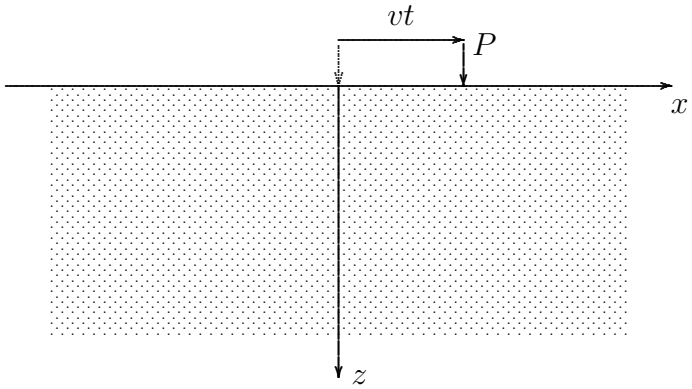

Figure 8.4: Moving line load.

condition on the surface $z = 0$ is represented by

$$z = 0 \;:\; \sigma_{zz} = -P\delta(x - vt)H(t); \quad v > 0, \tag{8.26}$$

where P is a line force per unit of length and $H(t)$ denotes the Heaviside unit step function. It is assumed that the force is stationary prior to a certain instant $t = 0$ and it is then suddenly set into horizontal motion.

Substituting the one-sided Laplace transformation with respect to time t (8.5) in (8.2), yields

$$c_s^2 \partial_{xx}^2 \hat{u}_z + c_p^2 \partial_{zz}^2 \hat{u}_z = s^2 \hat{u}_z, \tag{8.27}$$

With aid of the property

$$\delta(x - vt) = v^{-1} \delta(t - xv^{-1}), \tag{8.28}$$

and the Laplace transformation

$$\int_{t=0}^{\infty} \exp(-st) \delta(t - xv^{-1})\, dt = \exp(-sxv^{-1}) H(x), \tag{8.29}$$

the boundary condition (8.26) is, expressed in the Laplace domain,

$$z = 0 \;:\; \hat{\sigma}_{zz} = -Pv^{-1} \exp(-sxv^{-1}) H(x). \tag{8.30}$$

Introducing the Fourier transformation (8.8) in (8.6) and (8.30), gives

$$\partial_{zz}^2 \tilde{u}_z - s^2 \beta^2 \tilde{u}_z = 0, \tag{8.31}$$

where

$$\beta = \frac{c_s}{c_p} (\alpha^2 + c_s^{-2})^{1/2}; \quad \beta > 0, \tag{8.32}$$

with the boundary condition

$$z = 0 \;:\; \tilde{\sigma}_{zz} = P \frac{v^{-1}}{s(i\alpha - v^{-1})}. \tag{8.33}$$

The solution of (8.31) that remains bounded for $z \to \infty$ is

$$\tilde{u}_z(\alpha, z, s) = \tilde{A} \exp(-s\beta z), \tag{8.34}$$

where $\tilde{A}$ is a parameter. From (8.3), (8.33) and (8.34) it follows that

$$\tilde{A} = -\frac{P}{s^2(\lambda + 2\mu)\beta} \frac{v^{-1}}{(i\alpha - v^{-1})}. \tag{8.35}$$

Using the inverse of the Fourier transformation the solution of the problem is, expressed in the Laplace transformation,

$$\hat{u}_z(x, z, s) = -\frac{P}{s(\lambda + 2\mu)} \frac{1}{2\pi} \int_{\alpha=-\infty}^{\infty} \frac{\exp(-is\alpha x - s\beta z)}{\beta} \frac{v^{-1}}{(i\alpha - v^{-1})}\, d\alpha. \tag{8.36}$$

The parameter of integration with respect to α is replaced with the parameter of integration with respect to p, defined by

$$p = i\alpha,$$

yielding the following expression

$$\hat{u}_z(x,z,s) = -\frac{P}{s(\lambda+2\mu)}\frac{1}{2\pi i}\int_{p=-i\infty}^{i\infty}\frac{\exp(-s(px+\beta z))}{\beta}\frac{v^{-1}}{(p-v^{-1})}\,dp, \tag{8.37}$$

with

$$\beta = \frac{c_s}{c_p}(c_s^{-2}-p^2)^{1/2}; \quad \Re[\beta] > 0. \tag{8.38}$$

The integration with respect to p along the imaginary p-axis now is replaced with one along the curved path defined by

$$\chi = px + \beta z, \tag{8.39}$$

where χ is considered to be a real and positive parameter. The new path is assumed to consist of the two hyperbolic arcs p_1 and p_2, with

$$p_{1,2} = \frac{x}{r_n^2}\chi \pm i\frac{nz}{r_n^2}\sqrt{\chi^2 - r_n^2/c_s^2}; \quad r_n/c_s \leq \chi < \infty. \tag{8.40}$$

Substitution of (8.40) into (8.39) leads to the following values of β along the two arcs

$$\beta_{1,2} = \frac{n^2 z}{r_n^2}\chi \mp i\frac{nx}{r_n^2}\sqrt{\chi^2 - \frac{r_n^2}{c_s^2}}. \tag{8.41}$$

At this stage, the analysis of the complex p-plane is split into two parts: one, the velocity of the load being smaller than the velocity of S-waves ($v < c_s$) and two, for the case that the velocity of load is larger than the velocity of S-waves ($v > c_s$).

For $v < c_s$:

In the subsonic case ($v < c_s$), the new path of integration is depicted in Figure 8.5. The contributions of the arcs connecting the imaginary p-axis and the new path vanish. Therefore, the integral along the imaginary p-axis $\Re[p] = 0$ is equivalent to the integral along the hyperbolic arcs $p = p_1$ and $p = p_2$. Therefore, the expression (8.37) is transformed into

$$\hat{u}_z(x,z,s) = -\frac{P}{s\pi(\lambda+2\mu)}\int_{\chi=r_n/c_s}^{\infty}\exp(-s\chi)\Im\left[\frac{v^{-1}}{(p-v^{-1})}\frac{1}{\beta}\partial_\chi p\right]\,d\chi; \quad v < c_s. \tag{8.42}$$

This expression is only carried out for the case $v < c_s$ where the simple pole $p = v^{-1}$ is located to the right of the branch point $p = c_s^{-1}$. Because the region in the complex

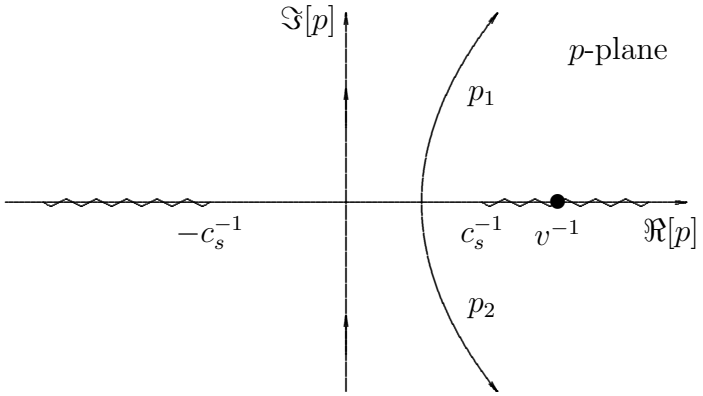

Figure 8.5: Moving line load, the path of integration in the complex p-plane: subsonic case ($v < c_s$).

p-plane in between the imaginary p-axis (the original path of integration) and the new path is free from singularities, then the integrand of Eq. (8.42) is not singular. In addition, branch cuts can be introduced along the real p-axis, from $-\infty$ to $-1/c_s$ and $1/c_s$ to ∞, as can be seen in Figure 8.5.

With the aid of the following expressions

$$\partial_\chi p = \pm i \frac{\beta}{n(\chi^2 - r_n^2/c_s^2)^{1/2}}, \tag{8.43}$$

$$\frac{v^{-1}}{p - v^{-1}} = v^{-1} r_n^2 \frac{((x\chi - v^{-1}r_n^2) \mp inz(\chi^2 - r_n^2/c_s^2)^{1/2})}{((x\chi - v^{-1}r_n^2)^2 + n^2 z^2(\chi^2 - r_n^2/c_s^2))}, \tag{8.44}$$

$$\frac{v^{-1}}{(p - v^{-1})} \frac{1}{\beta} \partial_\chi p = \frac{v^{-1} r_n^2}{n(\chi^2 - r_n^2/c_s^2)^{1/2}} \frac{(nz(\chi^2 - r_n^2/c_s^2)^{1/2} \pm i(x\chi - v^{-1}r_n^2))}{((x\chi - v^{-1}r_n^2)^2 + n^2 z^2(\chi^2 - r_n^2/c_s^2))}, \tag{8.45}$$

in which (8.45) is substituted into (8.42), and applying the shift rule for Laplace transformation to the function $\exp(-s\chi)/s$, the time-domain expression for the vertical displacement becomes

$$u_z(x,z,t) = -\frac{P}{\pi(\lambda + 2\mu)} \frac{v^{-1} r_n^2}{n} \int_{\chi = r_n/c_s}^{t} \frac{1}{(\chi^2 - r_n^2/c_s^2)^{1/2}} \times \frac{(x\chi - v^{-1}r_n^2)}{((x\chi - v^{-1}r_n^2)^2 + n^2 z^2(\chi^2 - r_n^2/c_s^2))} \, d\chi. \tag{8.46}$$

Changing the parameter of integration χ in (8.46), with the parameter of integration q defined as $\chi = q r_n/c_s$, gives

$$u_z(x,z,t) = \frac{P}{\pi(\lambda + 2\mu)n} \int_{q=1}^{t/t_0} \frac{(xC_1 + n^2 z^2)}{(C_1^2 + n^2 z^2(1 - v^2 c_s^{-2}))C_2} \, dq H(t - t_0); \quad v < c_s, \tag{8.47}$$

where $t_0 = r_n/c_s$ is the arrival time of the wave,

$$C_1 = x - r_n v c_s^{-1} q,$$

$$C_2 = (q^2 - 1)^{1/2}.$$

Consider the velocity of the line load tends to zero ($v \to 0$), then the vertical displacement gives

$$u_z(x,z,t) = \frac{P}{\pi(\lambda+2\mu)n} \ln(t/t_0 + (t^2/t_0^2 - 1)^{1/2}) H(t-t_0); \quad v \to 0. \tag{8.48}$$

Figure 8.6 shows the dimensionless vertical displacement u_z/u_p when $M_s \to 0$, with

$$u_p = \frac{P}{(\lambda+2\mu)n}.$$

It can be noted that when the dimensionless time t/t_0 in (8.48) tends to infinity then

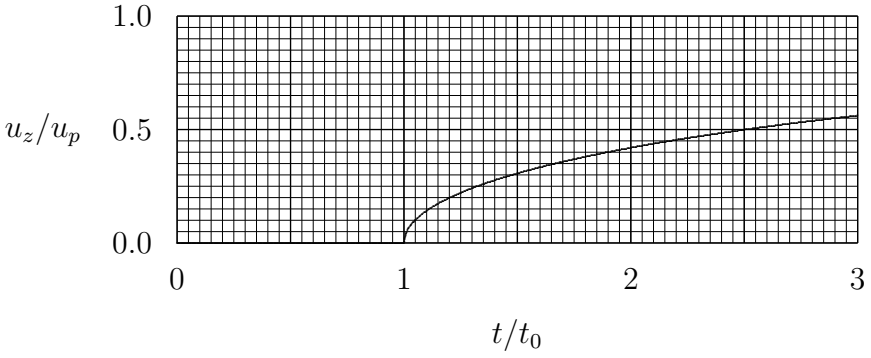

Figure 8.6: Dimensionless vertical displacement u_z/u_p: $M_s \to 0$.

u_z/u_p also tends to infinity.

For $z \to 0$ the vertical displacement (8.47) is

$$u_z(x,0,t) = \frac{P}{\pi(\lambda+2\mu)n} \int_{q=1}^{t/t_{0x}} \frac{1}{(1-M_s q)C_2}\, dq H(t-t_{0x}), \tag{8.49}$$

where $M_s = v/c_s$ and $t_{0x} = x/c_s$. Solving the integral, it is found that

$$\begin{aligned} u_z(x,0,t) =& \frac{P}{\pi(\lambda+2\mu)n} \frac{1}{\sqrt{1-M_s^2}} \ln\left(\frac{1-M_s+C_3\sqrt{1-M_s^2}}{1-M_s-C_3\sqrt{1-M_s^2}}\right) \\ & \times H(t-t_{0x}); \quad vt < x < c_s t, \end{aligned} \tag{8.50}$$

with

$$C_3 = \left(\frac{t/t_{0x}-1}{t/t_{0x}+1}\right)^{1/2}.$$

Figure 8.7 shows the dimensionless vertical displacement u_z/u_p for $z \to 0$ and $vt < x < c_s t$.

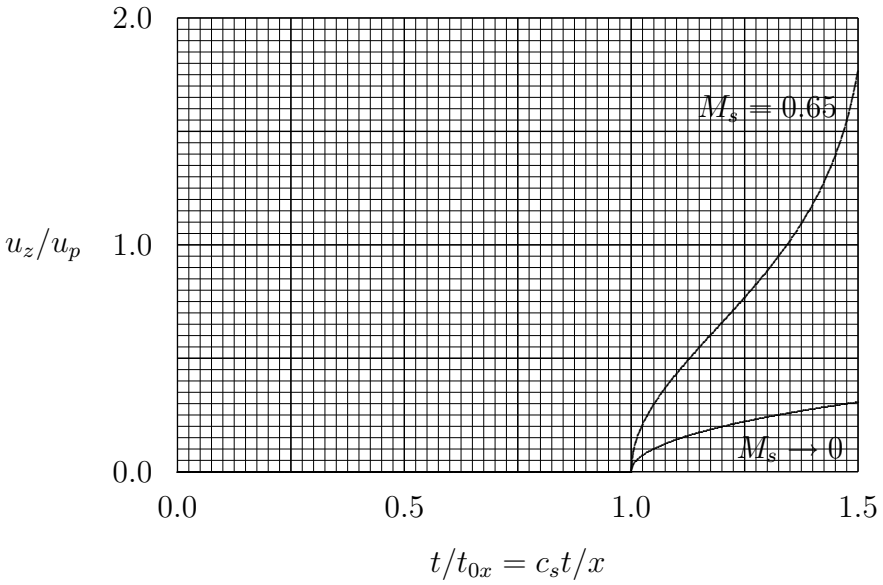

Figure 8.7: Dimensionless vertical displacement u_z/u_p: $z \to 0$ and $vt < x < c_s t$.

For $v > c_s$:

In order to calculate the supersonic case ($v > c_s$), the analysis of the complex p-plane is split into two possible cases.

In the first case, the contribution from the pole $p = v^{-1}$ is not required, as it is located outside the region in between the imaginary p-axis and the new path, depicted by the left hand side of Figure 8.8.

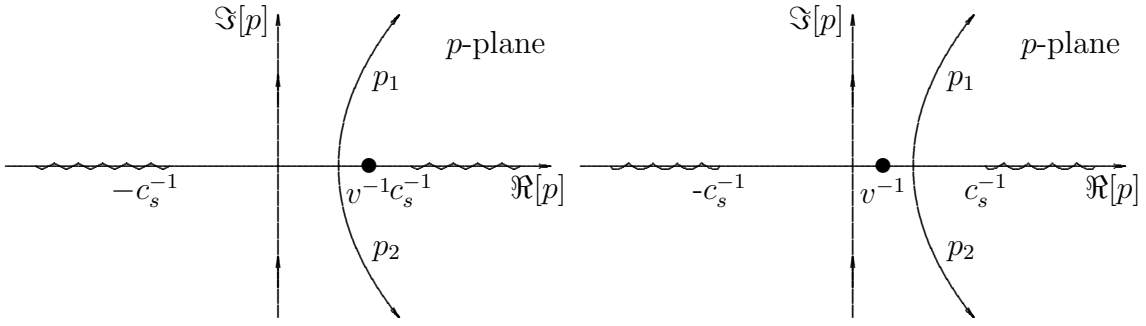

Figure 8.8: Moving line load, the path of integration in the complex p-plane: supersonic case ($v > c_s$).

In the second case, the process of path deformation requires a contribution from the pole $p = v^{-1}$, as in this case it is located within the region in between the imaginary p-axis and the new path, depicted by the right hand side of Figure 8.8. The point of intersection of the new path p for $r_n/c_s \leq \chi < \infty$ with the real p-axis is located to the right of the pole $p = v^{-1}$, that is, for $x^2(v^2/c_s^2 - 1) > n^2 z^2$.

The contributions of the arcs connecting the imaginary axis and the new path vanish. Therefore, the integral along the imaginary p-axis $\Re[p] = 0$ is equivalent to the

integral along the hyperbolic arcs $p = p_1$ and $p = p_2$. Applying the residue theorem to the integral on the right hand side of (8.37) the vertical displacement becomes, expressed in the Laplace transformation,

$$\begin{aligned}\hat{u}_z(x,z,s) =& \frac{P}{(\lambda+2\mu)}\frac{v^{-1}}{n(c_s^{-2}-v^{-2})^{1/2}}\frac{\exp(-s(xv^{-1}+n(c_s^{-2}-v^{-2})^{1/2}z))}{s}\\ &-\frac{P}{s\pi(\lambda+2\mu)}\int_{\chi=r_n/c_s}^{\infty}\exp(-s\chi)\Im\left[\frac{v^{-1}}{(p-v^{-1})}\frac{1}{\beta}\partial_\chi p\right]\,d\chi;\\ &v>c_s \quad \text{and} \quad x>nz/(v^2/c_s^2-1)^{1/2}. \end{aligned} \tag{8.51}$$

Substitution of (8.45) into (8.51) and applying the shift rule for Laplace transformation to the function $\exp(-s\chi)/s$, the vertical displacement becomes

$$\begin{aligned}u_z(x,z,t) =& \frac{P}{(\lambda+2\mu)n}\frac{1}{(v^2/c_s^2-1)^{1/2}}H(t-t_v)-\frac{P}{\pi(\lambda+2\mu)}\frac{v^{-1}r_n^2}{n}\\ &\times\int_{\chi=r_n/c_s}^{t}\frac{(x\chi-v^{-1}r_n^2)H(\chi-r_n/c_s)}{((x\chi-v^{-1}r_n^2)^2+n^2z^2(\chi^2-r_n^2/c_s^2))}\frac{1}{(\chi^2-r_n^2/c_s^2)^{1/2}}\,d\chi. \end{aligned} \tag{8.52}$$

with

$$t_v = x/v + n(c_s^{-2}-v^{-2})^{1/2}z; \quad t_v > 0.$$

Changing the parameter of integration χ in (8.52), with the parameter of integration q defined as $\chi = qr_n/c_s$, yields

$$\begin{aligned}u_z(x,z,t) =& \frac{P}{(\lambda+2\mu)n}\frac{1}{(v^2/c_s^2-1)^{1/2}}H(t-t_v)\\ &+\frac{P}{\pi(\lambda+2\mu)n}\int_{q=1}^{t/t_0}\frac{(xC_1+n^2z^2)}{(C_1^2+n^2z^2(1-v^2c_s^{-2}))C_2}H(t-t_0)\,dq;\\ &v>c_s \quad \text{and} \quad x>nz/(v^2/c_s^2-1)^{1/2}. \end{aligned} \tag{8.53}$$

The influence of the first factor on the right hand side of (8.53) is restricted to its spatial support $x > nz/(v^2/c_s^2-1)^{1/2}$. In this region, the wave associated with $t_v = x/v + n(c_s^{-2}-v^{-2})^{1/2}z$ arrives earlier than the one associated with $t_0 = r_n/c_s$.

The vertical displacement (8.53) for $z \to 0$ is

$$\begin{aligned}u_z(x,0,t) =& \frac{P}{(\lambda+2\mu)n}\frac{1}{(M_s^2-1)^{1/2}}H(t-x/v)\\ &+\frac{P}{\pi(\lambda+2\mu)n}\int_{q=1}^{t/t_{0x}}\frac{1}{(1-M_sq)C_2}\,dqH(t-t_{0x});\\ &v>c_s \quad \text{and} \quad x>0. \end{aligned} \tag{8.54}$$

Solving the integral, it is obtained that

$$u_z(x,0,t) = \frac{P}{(\lambda+2\mu)n}\frac{1}{(M_s^2-1)^{1/2}}H(t-x/v) + \frac{P}{\pi(\lambda+2\mu)n}\frac{1}{(M_s^2-1)^{1/2}}\arccos\left(\frac{M_s - t/t_{0x}}{M_s t/t_{0x}-1}\right)H(t-t_{0x}); \quad v > c_s \text{ and } x > 0. \tag{8.55}$$

Figure 8.9 shows the dimensionless vertical displacement u_z/u_p when $z \to 0$. The influence of the residue term can be observed at the arrival time $t = x/v = t_{0x}/M_s$. This means that a finite jump discontinuity occurs.

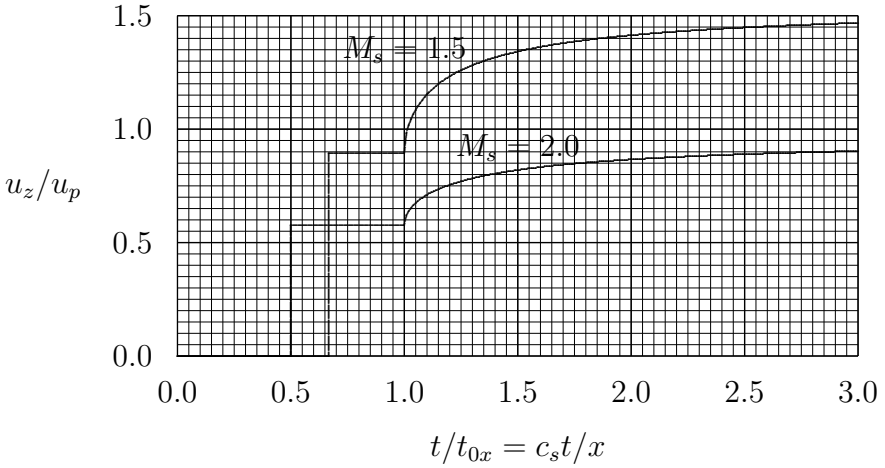

Figure 8.9: Dimensionless vertical displacement u_z/u_p: $z \to 0$, $v > c_s$ and $x > 0$.

8.2.1 Vertical stress

The expression of the transformed vertical stress $\hat{\sigma}_{zz}(x,z,s)$ can be obtained when the transformed vertical displacement $\hat{u}_z(x,z,s)$ in (8.37) is derived with respect to z and multiplied by the factor $(\lambda+2\mu)$. This leads to

$$\hat{\sigma}_{zz}(x,z,s) = P\frac{1}{2\pi i}\int_{p=-i\infty}^{i\infty}\exp(-s(px+\beta z))\frac{v^{-1}}{(p-v^{-1})}\,dp. \tag{8.56}$$

In order to find $\hat{\sigma}_{zz}(x,z,s)$ the procedure of integration in the complex p-plane is split into two possible cases.

For $v < c_s$:

Substituting the variable $\chi = px + \beta z$ in (8.56), yields

$$\hat{\sigma}_{zz}(x,z,s) = P\frac{1}{\pi}\int_{\chi=r_n/c_s}^{\infty}\exp(-s\chi)\Im\left[\frac{v^{-1}}{(p-v^{-1})}\partial_\chi p\right]\,d\chi; \quad v < c_s, \tag{8.57}$$

where χ is real and positive. It can be observed that the simple pole $p = v^{-1}$ is located to the right of the branch point $p = c_s^{-1}$ for $v < c_s$, depicted by Figure 8.5. In addition, the integrand of Eq. (8.57) is free from singularities for the part of the complex p-plane in between the imaginary p-axis and the new path. Using (8.41) and (8.45), yields

$$\frac{v^{-1}}{(p-v^{-1})}\partial_\chi p = \frac{((\chi^2 - r_n^2/c_s^2)^{1/2}(\chi v - x) \pm inz(xv/c_s^2 - \chi))}{((xv\chi - r_n^2)^2 + n^2z^2v^2(\chi^2 - r_n^2/c_s^2))} \times \frac{r_n^2}{(\chi^2 - r_n^2/c_s^2)^{1/2}}. \tag{8.58}$$

Substituting (8.58) in (8.57), gives

$$\hat{\sigma}_{zz}(x,z,s) = \frac{P}{\pi} nzr_n^2 \int_{\chi=r_n/c_s}^{\infty} \exp(-s\chi) \times \frac{1}{(\chi^2 - r_n^2/c_s^2)^{1/2}} \frac{(xv/c_s^2 - \chi)}{((xv\chi - r_n^2)^2 + n^2z^2v^2(\chi^2 - r_n^2/c_s^2))}\, d\chi. \tag{8.59}$$

The integral has now been brought into the form of a Laplace transformation, and the parameter χ can be identified with time t. It follows that the time-domain expression for the vertical stress is

$$\sigma_{zz}(x,z,t) = -\frac{P}{\pi} \frac{nz}{(t^2 - r_n^2/c_s^2)^{1/2}} \frac{(t - xv/c_s^2)}{((x-vt)^2 + n^2z^2(1 - v^2/c_s^2))} \times H(t - r_n/c_s); \quad v < c_s. \tag{8.60}$$

Consider the velocity of the load tends to zero ($v \to 0$), then the expression for the

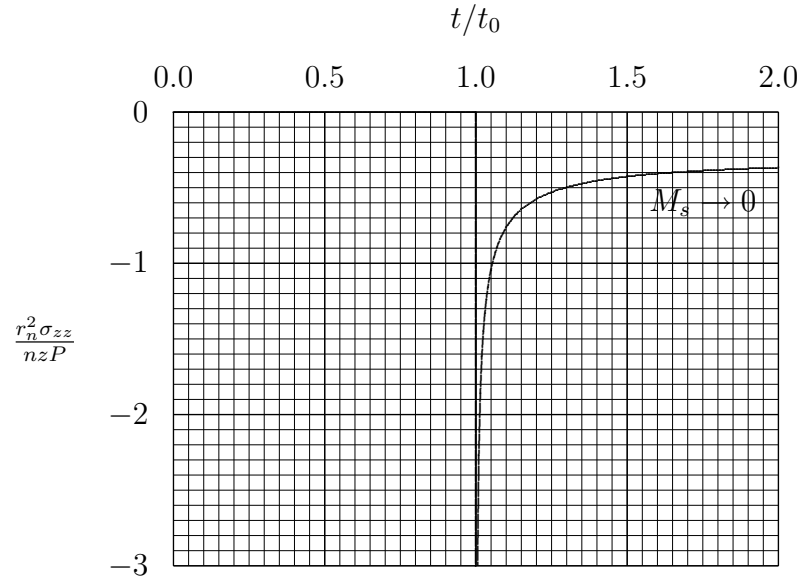

Figure 8.10: Vertical stress: $M_s \to 0$.

vertical stress is

$$\sigma_{zz}(x,z,t) = -\frac{P}{\pi} \frac{nzt/t_0}{r_n^2(t^2/t_0^2 - 1)^{1/2}} H(t - t_0); \quad v \to 0. \tag{8.61}$$

For $M_s \to 0$ results are given in Figure 8.10.

The vertical stress along the z-axis $x = 0$ is

$$\frac{\pi nz}{P}\sigma_{zz}(0,z,t) = -\frac{1}{(1+M_s^2(t^2/t_{0z}^2-1))}\frac{t/t_{0z}}{(t^2/t_{0z}^2-1)^{1/2}}H(t-t_{0z}), \tag{8.62}$$

with $t_{0z} = nz/c_s$. Figure 8.11 shows the vertical stress along the z-axis.

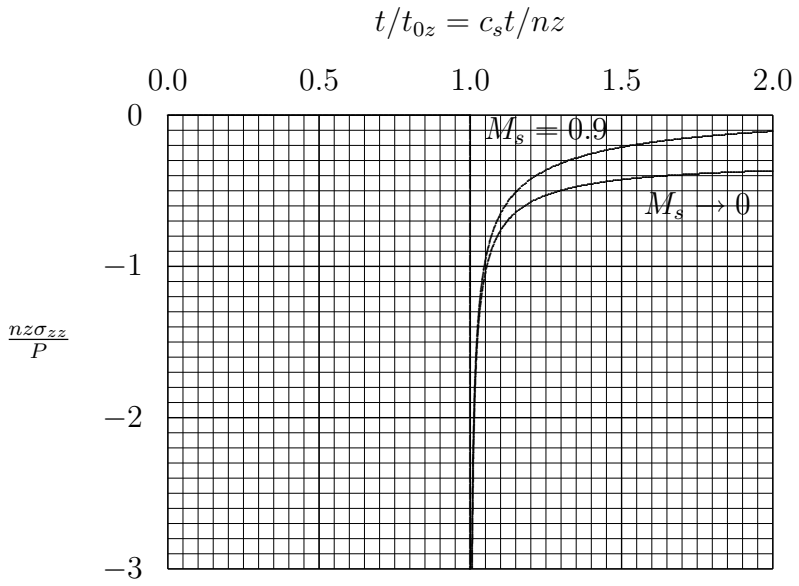

Figure 8.11: Vertical stress along the z-axis: $v < c_s$.

For $v > c_s$:

For the case $v > c_s$, the process of path deformation leads to a contribution from the pole $p = v^{-1}$ into the region, shown by Figure 8.8. The point of intersection of the new path p for $r_n/c_s \le \chi < \infty$ with the real p-axis is located to the right of $p = v^{-1}$, that is, for $x > nz/(v^2/c_s^2-1)^{1/2}$. Applying the residue theorem to the integral on the right hand side of (8.56) the vertical stress is, expressed in the Laplace transformation,

$$\begin{aligned}\hat{\sigma}_{zz}(x,z,s) =& -Pv^{-1}\exp(-s(xv^{-1}+n(c_s^{-2}-v^{-2})^{1/2}z)) \\ &+ P\frac{1}{\pi}\int_{\chi=r_n/c_s}^{\infty}\exp(-s\chi)\Im\left[\frac{v^{-1}}{(p-v^{-1})}\partial_\chi p\right]d\chi; \\ & v > c_s \ \text{ and } \ x > nz/(v^2/c_s^2-1)^{1/2}.\end{aligned} \tag{8.63}$$

Substituting (8.58) into (8.63), the time domain expression for the vertical stress is

$$\begin{aligned}\sigma_{zz}(x,z,t) =& -P\frac{1}{v}\delta(t-t_v) \\ &- \frac{P}{\pi}\frac{nz}{(t^2-r_n^2/c_s^2)^{1/2}}\frac{(t-xv/c_s^2)}{((x-vt)^2+n^2z^2(1-v^2/c_s^2))} \\ &\times H(t-r_n/c_s); \quad v > c_s \ \text{ and } \ x > nz/(v^2/c_s^2-1)^{1/2},\end{aligned} \tag{8.64}$$

where $t_v = xv^{-1} + n(c_s^{-2} - v^{-2})^{1/2}z > 0$ is the arrival time associated with the pole contribution. The first term of (8.64) generates an infinity jump for the results.

8.3 The inclusion of the Voigt viscosity mechanism

In order to describe dissipation mechanisms of a solid in a model, the Voigt viscosity mechanism is included in compliance relaxation function (Kolsky [1958], Hunter [1960], Flügge [1975], Findley *et al.* [1976] and de Hoop[1995]). A simple representation of the Voigt model is treated in Chapter 2.4. Several effects in viscoelastic wave propagation are presented by Christensen [1982].

Chapter 9

Determination of damping in soils

In the previous chapters it is shown that in many cases damping is relevant to find the solution of dynamic loaded systems. Therefore, it is important to gain an insight into the magnitude of the damping. The purpose of this chapter is to determine damping in sands by free vibration torsion tests.

9.1 Introduction

Simple physical models have been developed to estimate the material behaviour of soils under dynamic loads. A common way to determine dynamic properties of the soils is the resonant-column test method, where the soils are loaded harmonically. In this method the propagation of waves in cylindrical soil specimens is studied. Numerous publications on the dynamic properties of soils are known. Hardin and Drnevich [1972a, 1972b] carried out dynamic experiments in hollow cylinder torsional shear and resonant-column test devices. They also formulated equations for the calculation of the equivalent shear modulus and damping ratios. Drnevich *et al.* [1978] presented a broad description of the apparatus and testing procedures, including a computer program. Problems, solutions and limitations of the apparatus are provided in detail by Drnevich [1978]. Results and applications on this apparatus are also given in the texts of Richart *et al.* [1970], Das [1983] and Colindres [1993]. Based on the experimental results of Seed *et al.* [1986], procedures and suggestions were made to obtain the variation of shear modulus with shear strain and damping ratios for sandy soils. Li *et al.* [1998] and Li and Cai [1999] used a fixed-base column system in order to investigate the effects of loading history on the shear modulus and damping ratio of dry sand.

In many studies the analysis of the dynamic soil properties has been done under different constitutive models such as: the elastic-, Kelvin-Voigt- and Maxwell-model. Hall and Richart [1963], Hardin [1965], and Hardin and Scott [1966] have used the Kelvin-Voigt model to represent the behaviour of dry sand subjected to small cyclic vibration amplitudes, over a large frequency range. From steady state and free vibration in torsional and longitudinal form, experimental results have been found.

With the assumption that the ratio viscosity times frequency to shear modulus is constant with the frequency, Hardin [1965] suggested that within a large range of excitation frequencies, the damping behaviour of dry sand can be described by the

hysteretic damping. In the field of ground response analysis, in frequency domain, this concept has been applied and recognized by many researchers. Initially, frequency-independent structural damping was introduced by Theodorsen and Garrick [1940]. Later, the label of hysteretic damping was formulated by Bishop [1955]. Based on the suggestions by Hardin [1965], time analysis of generalized viscoelastic models have been examined by Makris [1995], Inaudi and Kelly [1995], and Makris and Zwang [2000].

Effects of frequency on shear modulus

Based on the experimental investigation, using the resonant column test, the influence of frequency on the shear wave velocity in dry sand was presented in detail by Hardin and Richart [1963]. Test results in the free-free apparatus showed that the frequency has small effect on the shear-wave velocity. The free-free apparatus was designed and developed by Hardin and Richart [1963]. In measurements of small-strain shear modulus, Hardin and Drnevich [1972b] observed that the frequency of loading is relatively unimportant in soils. The shear modulus and the damping ratio for sands were investigated by Seed and Idriss [1970] and by Hardin and Drnevich [1972b]. They studied the relative effects of various parameters such as: the amplitude of the shear strain, the void ratio and the number of loading cycles. Relationships between damping ratio and shear strain were also shown.

This chapter presents the results and the interpretation of an experimental investigation on the behaviour of Baskarp sand under small deformations. The experiments were performed by using a free vibration torsion apparatus. This apparatus could be of the fixed-free resonant-column type, where the bottom of the sample is fixed, and the top is in free vibration. The same procedure, for the determination of the shear modulus and the damping ratio, was also proposed by Zeevaert [1972] with the aid of the free torsion pendulum.

9.2 Testing procedure

Laboratory tests, using the free vibration torsion method, were performed to examine the damping in Baskarp sand specimens. The tests were carried out in the laboratory of GeoDelft, The Netherlands. The main objective of the laboratory tests was to quantify the magnitude of the damping in soils. Figure 9.1 shows a photo of the free vibration torsion equipment. The apparatus used to measure the damping of the specimen consists of a cylinder with its bottom fixed to a base. A bar rigidly connected to the top of the cylinder supports different weights. The polar moment of inertia of the bar varies according to the weights attached to the bar. A small rotation is given to the bar. Consequently, the cylinder is rotated with the maximum turn at the top and the minimum turn at the bottom. Finally, the bar is released, and the cylinder executes rotational vibrations. Tests were performed on solid cylindrical specimens of 145 mm in height and 65.8 mm in diameter. For the tests, two uniform confining pressures of 50 and 90 kPa were applied to the sand specimens with porosities of 40 and 35%, respectively. The amplitudes of shear strains were smaller than 5×10^{-4}.

9.3 Test results and interpretations

In Figure 9.2 and 9.3, the angular displacement u_θ of the top of the sand specimens,

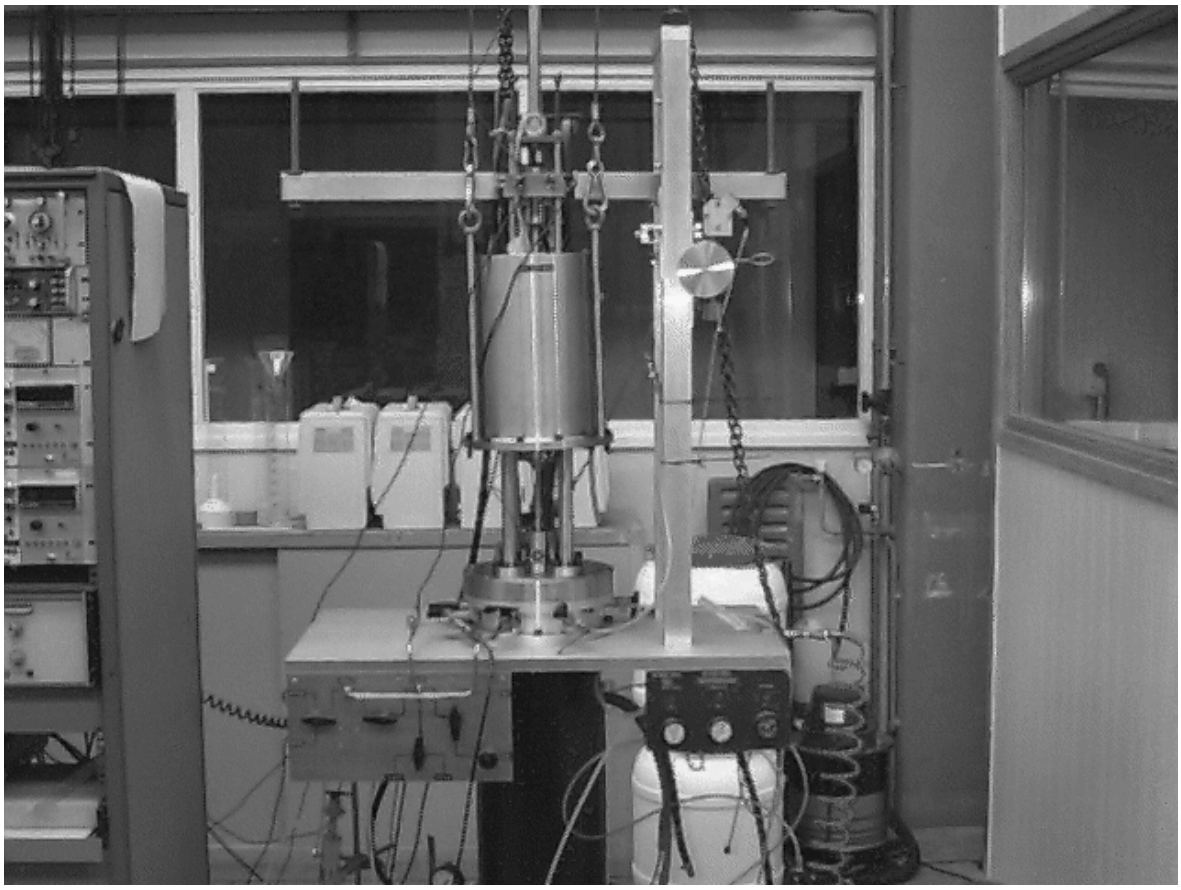

Figure 9.1: Free vibration torsion test equipment.

during free vibration, are shown as function of the time. It also appears that when the polar moment of inertia of the mass attached to the bar increases, the period of vibration also increases. The dissipative (energy loss) properties of sand have been investigated. This was done mainly by observing the gradual decrease of free vibration of the specimen-apparatus system. With the aid of the observed logarithmic decrement δ, defined according to the decay curve as:

$$\delta = \ln(A_n/A_{n+1}),$$

the free vibration decay of the sand specimens is determined. Herein are A_n and A_{n+1} the amplitudes of two successive cycles. For a group of cycles, each test has been represented by an equivalent damping ratio and a corresponding period of vibration. The first cycle of every test has been neglected. Furthermore, it is considered that the cycle counter starts at zero at the beginning of the second cycle.

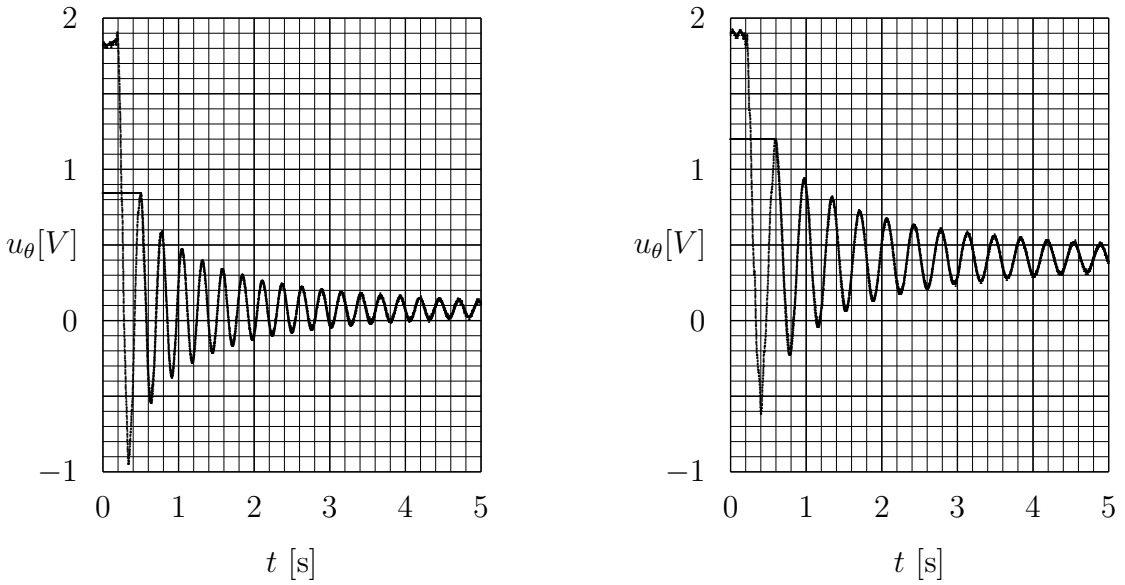

Figure 9.2: Decay of free vibration: $1V = 0.1$ mm. Left hand side: Test No. 15, mass $2 * 10$ kg. Right hand side: Test No. 17, mass $2 * 20$ kg.

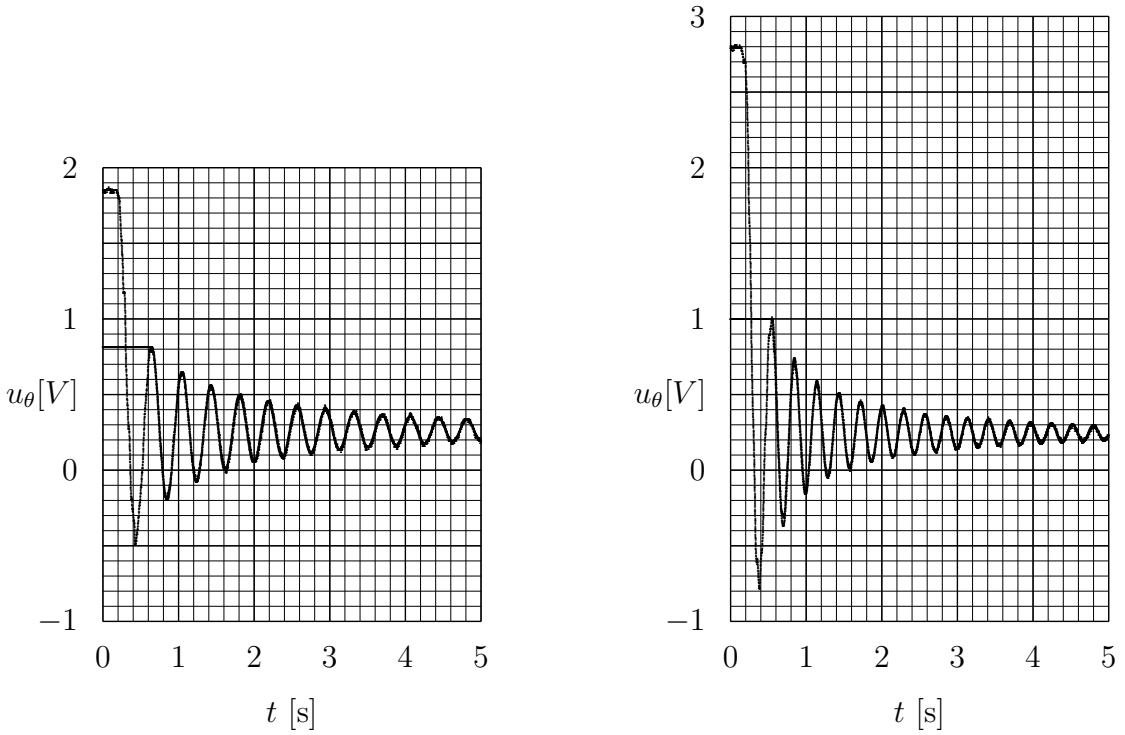

Figure 9.3: Decay of free vibration: $1V = 0.1$ mm. Left hand side: Test No. 42, mass $2 * 20$ kg. Right hand side: Test No. 46, mass $2 * 10$ kg.

For a Kelvin-Voigt material with a mass density ρ, shear modulus G and the relaxation time t_r, the field equation of the fixed-base system is as follows

$$G\partial^2_{zz}u_\theta + Gt_r\partial_t\partial^2_{zz}u_\theta = \rho\partial^2_{tt}u_\theta, \tag{9.1}$$

where $u_\theta(z,t)$ is the angular displacement, z is the longitudinal axis of the specimen, with $0 \leq z \leq h$. The hight of the specimen is h and t denotes time, with $t \geq 0$, see Hardin [1965]. Consider the solution of (9.1) to be of the form

$$u_\theta(z,t) = \sum_{j=1}^{\infty} A_n \exp(-\omega_j^2 t_r t/2)\cos(\omega_j(1-\omega_j^2 t_r^2/4)^{1/2}t - \vartheta_j)\sin(\omega_j z/c_s), \tag{9.2}$$

where ϑ_j and ω_j are the phase angles and the frequencies for the torsional vibration with fixed-free conditions, respectively. These are found from the expression

$$J_s/J_m = \alpha_j \tan(\alpha_j); \quad j = 1,2,3,..., \tag{9.3}$$

where J_s is the polar moment of inertia of the sand specimen, J_m is the polar moment of inertia of the attached mass and $\alpha_j = \omega_j h/c_s$ are the eigenvalues. In order to describe the angular displacement u_z, only the first eigenvalue α_1 is considered, since for the performed tests $J_s/J_m \ll 1$. Defining the hysteretic damping ratio as

$$\zeta = \omega_j t_r/2, \tag{9.4}$$

where ζ is considered to be constant, the motion at the top of the specimen $z = h$ is expressed in terms of ω_1, as follows

$$u_\theta(h,t) = A_1 \exp(-\omega_1\zeta t)\cos(\omega_1(1-\zeta^2)^{1/2}t - \vartheta_1). \tag{9.5}$$

Expression (9.4) can also be written as

$$\zeta = \upsilon_1 T_1/(4\pi^2 + \upsilon_1^2 T_1^2)^{1/2}, \tag{9.6}$$

where $\upsilon_1 = \omega_1^2 t_r/2 = \omega_1\zeta$ and $T_1 = 2\pi/(\omega_1(1-\zeta^2)^{1/2})$ are the time attenuation factors and the periods of vibration, respectively.

Figure 9.4 and 9.5 show the equivalent hysteretic damping ratios of the free vibration decay curves in the range of 2 to 5%. It appears that the damping ratio increases due to the increase in the amplitude of the angular displacement. This implies that the damping of the sand is mainly dependent of the shear strain. By varying the value of frequency f between 2 and 9 [Hz], it may be observed that the magnitude of the damping ratio at a given shear strain level remains almost unchanged. It can be concluded that by assuming the factor $\omega_1 t_r$ to be constant, the response of Baskarp sand can be closely described over frequencies between 2 and 9 [Hz]. This conclusion agrees well with those presented by Hardin [1965]. On the basis of a wide experimental program, Hardin formulated that a viscoelastic model can be used to describe the behaviour of sand if the viscosity is assumed to be inversely proportional to the frequency.

The results of each test also shows that the period of vibration T decreases and the shear modulus G increases with the decay of the free vibrations, see Table 9.1. Therefore, it can be concluded that the shear modulus is dependent on the frequency of vibration. For low frequencies the shear modulus remains nearly constant. For interpretation of the test results, Hölscher and den Haan [2001] also developed a model where hysteresis damping has been incorporated.

Test No.	11	15	16	17	20	42	45	46	49	50
increase $G\%$	15	14	20	17	21	14	20	11	26	22
decrease $T\%$	8	7	9	8	9	7	9	5	11	10

Table 9.1: Variation of the shear modulus with respect to the period of vibration.

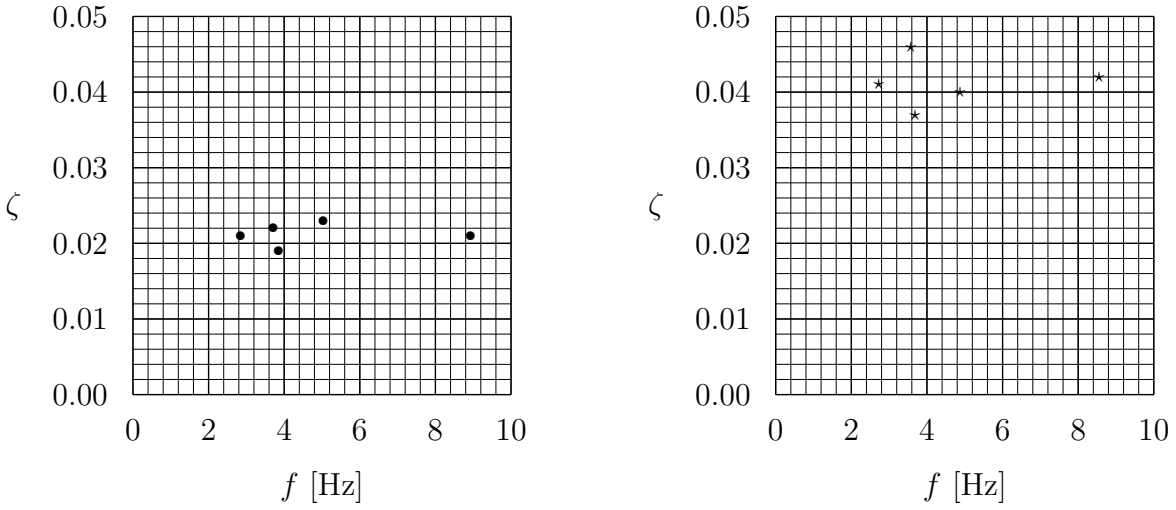

Figure 9.4: Damping ratio versus frequency: 50 kPa confining pressure and 40% porosity. Left hand side: shear strain $= 5 \times 10^{-5}$. Right hand side: shear strain $= 2 \times 10^{-4}$.

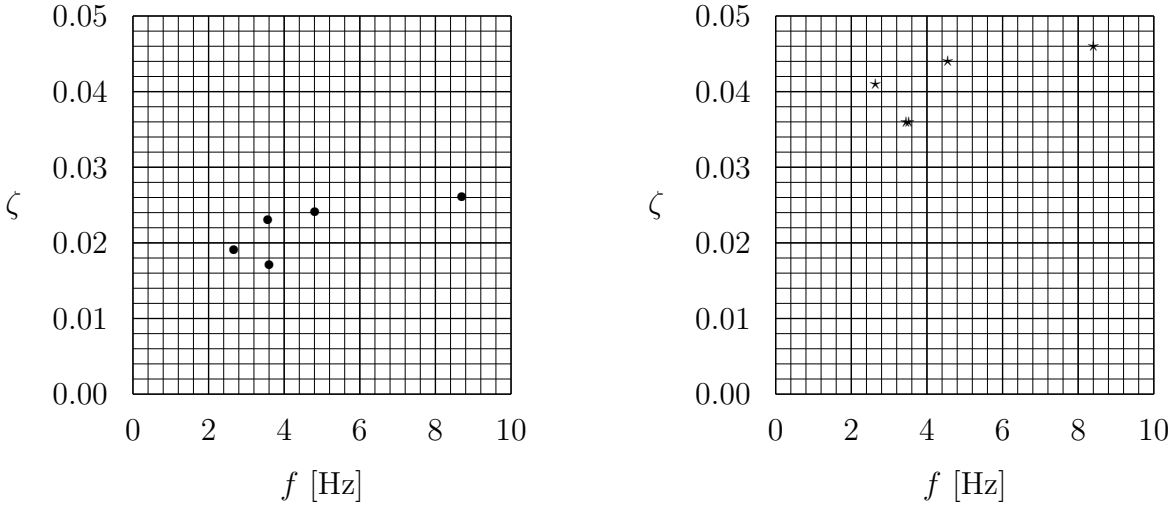

Figure 9.5: Damping ratio versus frequency: 90 kPa confining pressure and 35% porosity. Left hand side: shear strain $= 5 \times 10^{-5}$. Right hand side: shear strain $= 2 \times 10^{-4}$.

Chapter 10

Conclusions

Analytic methods have been presented for problems of the elastodynamic response of a loaded half-space and half-plane. The medium under consideration is taken to be linear elastic with hysteretic damping. Starting point is a constant hysteretic damping, which is a particular case of the Kelvin-Voigt damping with frequency dependent viscosity, suggested by Hardin [1965]. Based on an exhaustive laboratory investigation Hardin detected that the viscosity of the soil should diminish with the frequency so that the ratio, viscosity times frequency to the storage shear, is a constant independent of the frequency. Because dissipative stresses are not linearly proportional to frequency, describing the soil as linear viscoelastic material is not appropriate.

The behaviour of soils cannot be represented very well by linear elastic or ideal plastic models. Soils generally exhibit irreversible deformations produced by local plastic deformations which represent their non-linear behaviour of soils. For relatively small loads, such as loads on a soil body generated by machines and vehicles in motion, large plastic deformations are not usually considered, but cyclic irreversible deformations may be present. These effects, which may incorporate a notable loss of energy, are the aim of theoretical and experimental investigations. It is proposed in this study to represent this loss of energy by hysteretic damping.

In general, this study presents theoretical findings on the dynamic behaviour of an elastic half-space, half-plane, plane layer and single layer on a half-plane with hysteretic damping, which have been subjected to vibrating loads and have been perturbed by moving loads on its surface.

In Chapter 3, the problem of a uniform vibrating load over a circular area on the surface of an elastic half-space with hysteretic damping is solved by using the Hankel transformation. The displacement at the origin and the average displacement have been found. Results are compared to the solution by Reisser [1936] for an undamped material. The influence of the damping ratio on the average displacement is relatively small, and decreases monotonically with increasing frequency of the load. Furthermore, the problem of a vibrating point load over a half-plane has also been solved.

The solution for a moving load with a constant velocity on a half-plane with hysteretic damping is obtained in Chapter 4. The stresses and displacements have been calculated, and the expressions for the dynamic amplification factor have been found. This factor is defined as the ratio of the dynamic response to the static response. The

hysteretic damping is expressed in terms of the constant damping ratio ζ. The influence of the damping ratio on the magnitude of response has clearly been observed. For small values of the damping ratio, the maximum displacements, which occur if the velocity of the load is close to the Rayleigh wave velocity, have been shown to be inversely proportional to the damping ratio. For a load velocity higher than the compression wave velocity, the so called supersonic case, results have been illustrated for the case the damping ratio ζ is equal to 0.1 and 0.01.

In Chapter 5 and 6, the solution of moving load problems on the surface of a plane layer and on the surface of a single layer on a half-plane have been found. The dimensionless wavenumber in terms of the phase velocity is calculated. Results obtained demonstrate that propagation of waves in a plane layer and in a single layer on a half-plane, and the elastic-wave reflections are dependent on the values of the damping ratio. The expressions for the stresses and the displacements have been obtained. The vertical stresses are depicted for the case that the velocity of the load approaches the Rayleigh wave velocity.

The problem of a moving load on a half-plane and a vibrating load on a half-space have been solved in Chapter 7 by assuming that the horizontal displacements are disregarded, so that the only actual displacement is the vertical displacement, see Westergaard [1938]. For Poisson's ratios between 0 and 0.4, and after comparing the solution of Chapter 3 with the Westergaard solution, it can be concluded that the Westergaard approximation can be used as a good approximation for solving the problem of a vibrating load on a half-space, in the vicinity of the load.

In Chapter 8, closed-form time-domain expressions have been found for the vertical displacement and stress of the elastic wave motion generated by a moving line load on the surface of a half-space. In this transient wave problem, the approximate method of Chapter 7 has been used, but the hysteretic damping has not been incorporated. The solution has been constructed with the aid of the Cagniard-de Hoop method. The subsonic and supersonic cases have been examined.

In order to investigate the dynamical behaviour of soil in cyclic free torsion it is recommendable to perform dynamic torsion tests. Therefore, tests have been carried out in cooperation with GeoDelft. Using the free vibration torsion method results found for various tests are reported in Chapter 9. In this experimental study, the damping ratio of the tested material have been determined.

This study explains how the dynamic analysis of soils can be described adequately in terms of a constant hysteretic model and not with a viscoelastic model which tends to overdamp for higher frequencies of vibration in the majority of the cases. This thesis can also form part of the next phase in further studies in elastodynamic theory and its applications. The content of this thesis can be used for prediction of vibrations generated by high-speed lines. For a more complete and rigorous physical understanding of the rail-embankment-soil response caused by high-speed trains, measurements of ground response should also be performed for different train speeds. Naturally, an exhaustive and wide parametric ground analysis on the effects of train speed should be added to establish the magnitude of the material damping. Furthermore, some aspects of this thesis may be helpful for the numerical simulation of the response in a stratified soil due to vibrating loads.

Bibliography

[1] M. Abramowitz and I. A. Stegun. *Handbook of Mathematical Functions*. Dover Publications, Inc., New York, 1972.

[2] J. D. Achenbach. Response of a Layered Half-Space to a Moving Load. *J. of Appl. Mech., ASME*, pages 247–248, March 1967.

[3] J. D. Achenbach. *Wave Propagation in Elastic Solids*. North-Holland Publishing Company, Amsterdam, 1973.

[4] J. D. Achenbach and H. I. Epstein. Dynamic Interaction of a Layer and a Half-Space. *J. of Engng. Mech. Div., ASCE*, V. 93(No. EM5):pp. 27– 42, October 1967.

[5] J. D. Achenbach and S. P. Keshava. Free Waves in a Plate Supported by a Semi-Infinite Continuum. *J. of Appl. Mech., ASME*, pages 397–404, June 1967.

[6] J. D. Achenbach, S. P. Keshava, and G. Herrmann. Moving Load on a Plate Resting on a Elastic Half Space. *J. of Appl. Mech., ASME*, pages 910–914, December 1967.

[7] R. J. Apsel and J. E. Luco. On the Green's Functions for a Layered Half-Space. Part II. *Bulletin of the Seismological Society of America*, V. 73(No. 4):pp. 931–951, August 1983.

[8] R. J. Apsel and J. E. Luco. Impedance fuctions for foundations embedded in a layered medium: An integral equation approach. *Earth. Engng. Struct. Dynam.*, 15:213–231, 1987.

[9] Arcadis Trischler & Partner. No Recess Testfeld bei 's Gravendeel, Dynamische Tests mit DyStaFit. Technical Report N-125.541.99, Arcadis Trischler & Partner (German), 1999.

[10] R. N. Arnold, G. N. Bycroft, and G. B. Warburton. Forced Vibrations of a Body on an Infinite Elastic Solid. *J. of Appl. Mech., Trans. ASME*, V. 77:pp. 391–400, 1955.

[11] A. O. Awojobi. Approximate Solution of High-Frequency-Factor Vibrations of Rigid Bodies on Elastic Media. *J. of Appl. Mech., ASME*, pages 111–117, March 1971.

[12] A. O. Awojobi and P. Grootenhuis. Vibration of Rigid Bodies on Semi-Infinite Elastic Media. In *Proceedings of the Royal Society*, volume 287 of *A*, pages 27–63, London, Engeland, 1965.

[13] M. C. M. Bakker. *Non-Destructive Inspection Techniques Based on Elastodynamics: Development and Validation.* PhD thesis, Delft University of Technology, The Netherlands, 2000.

[14] M. C. M. Bakker, M. D. Verweij, B. J. Kooij, and H. A. Dieterman. The traveling point load revisited. *Wave Motion*, 29:pp. 119–135, 1999.

[15] F. B. J. Barends. Elasto-Dynamica Response of a half plane. Technical report, Departament of Civil Engineering, Delft University of Technology, Delft, The Netherlands, 1971.

[16] A. Ben-Menahem and S. J. Singh. *Seismic Waves and Sources.* Springer-Verlag, New York, 1981.

[17] R. E. D. Bishop. The treatment of damping forces in vibration theory. *J. Royal Aero. Soc.*, V. 59:pp. 738–742, 1955.

[18] D. R. Bland. *The Theory of Linear Viscoelasticity.* Oxford, Pergamon, London, 1960.

[19] J. Boussinesq. Application des Potentiels a l'Etude de l'Equilibre et du Mouvement des Solides Elastiques. Gauthier-Villars, Paris, 1885.

[20] J. F. J. Branderhorst. Modellen voor het Boeggolfprobleem bij Hogesnelheidstreinen. Master's thesis, Technische Universiteit Twente, Faculteit Civiele Techniek (Dutch), 1997.

[21] T. J. I'A. Bromwich. On the Influence of Gravity on Elastic Waves and, in Particular, on the Vibrations of an Elastic Globe. In *Proceedings of the London Mathematical Society*, volume 30, pages 98–120, London, England, 1899.

[22] G. Caviglia and A. Morro. *Inhomogeneous Waves in Solids and Fluids.* World Scientific Publishing Co. Pte. Ltd., Singapore, 1992.

[23] R. M. Christensen. *Theory of Viscoelasticity.* Academic Press, Inc., New York, 1982.

[24] J. Cole and J. Huth. Stresses Produced in a Half Plane by Moving Loads. *J. of Appl. Mech., ASME*, V. 25:pp. 433–436, December 1958.

[25] R. Colindres Selva. *Dinámica de Suelos y Estructuras.* Editorial Limusa, S.A. de C. V. Grupo Noriega Editores, México, 2da. edition, 1993.

[26] C. J. Cornejo Córdova. Moving Line Load on an Elastic Medium with Horizontal Constraints. In F. B. J. Barends and P. M. P. C. Steijger, editors, *Learned and Applied*, pages 137–142, Lisse, 2002. A. A. Balkema.

[27] C. Cornejo. Dynamish gedrag van slappe grondslag voor een hogesnelheidslijn (HSL). Master's thesis, Technische Universiteit Delft, Faculteit der Civiele Techniek, Geotechniek (Dutch), Nederland, September 1997.

[28] F. C. P. de Barros and J. E. Luco. Response of a layered viscoelastic half-space to a moving point load. *Wave Motion*, 19:pp. 189–210, 1994.

[29] F. C. P. de Barros and J. E. Luco. Dynamic response of a two-dimensional semi-circular foundation embedded in a layered viscoelastic half-space. *Soil Dyn. Earth. Engng.*, V. 14:pp. 45–57, 1995.

[30] A. T. de Hoop. A modification of Cagniard's method for solving seismic pulse problems. *Applied Sci. Res.*, B8m:pp. 349–356, 1960.

[31] A. T. de Hoop. The surface line source problem in elastodynamics. *De Ingenieur / Jrg. 82 / Nr. 5*, pages 19–21, 30 Januari 1970.

[32] A. T. de Hoop. *Similarity Analysis of the Elastic Wave Motion in a Dissipative Solid under a Global Relaxation Law.* J. L. Wegner and F. R. Norwood (eds.), Nonlinear Waves in Solids, IUTAM ASME Book No. AMR137, 1995.

[33] A. T. de Hoop. The moving-load problem in soil dynamics - The vertical displacements approximation. Technical Report ITS/EM 2001-04, Department of Electrical Engineering, Delft University of Technology, January 2001.

[34] F. C. de Nie. Verbetering van de Spoorbaan Oudewater-Gouda. Technical report, Spoor- en Tramwegen, 22e jaar, Nr.14, 14 juli 1949: pages 209-212 and Nr.15, 28 juli 1949: pages 227-230 (Dutch), 1949.

[35] G. Degrande and G. Lombaert. High-speed train induced free field vibrations: In situ measurements and numerical modelling. In A. A. Balkema, editor, *Proceedings of the International Workshop WAVE 2000 Bochum/Germany*, pages 29–41, Rotterdam, 2000.

[36] G. Degrande and L. Schillemans. Free field vibrations during the passage of a Thalys high-speed train at variable speed. *J. of Sound and Vibration*, V. 247(1):pp. 131–144, 2001.

[37] H. G. Dieterman. Aanleg van HSL duurder, 27 juli 1996. Interview by Algemeen Dagblad (Dutch newspaper).

[38] H. G. Dieterman and A. Metrikine. Critical Velocities of a Harmonic Load Moving Uniformly Along an Elastic Layer. *J. of Appl. Mech., ASME*, V. 64:pp. 596–600, 1997.

[39] V. P. Drnevich. Resonant-Column Testing–Problems and Solutions. *Dynamic Geotechnical Testing, ASTM STP 654, American Society for Testing and Materials*, pages 384–398, 1978.

[40] V. P. Drnevich, B. O. Hardin, and D. J. Shippy. Modulus and Damping of Soils by the Resonant-Column Method. *Dynamic Geotechnical Testing, ASTM STP 654, American Society for Testing and Materials*, pages 91–125, 1978.

[41] C. Esveld (Ed.). Kritische treinsnelheden. Technical Report 7-95-110-8, Technische Universiteit Delft, Faculteit der Civiele Techniek, Railbouwkunde (Dutch), 1995.

[42] K. E. Egorov. Distribution of Stress in Base of Rigid Strip Footing. Nauchn. Issled. Stantsiya Fundamentstroya, 1938. No. 9.

[43] A. A. Eijgenraam, W. Gardien, and H. G. Stuit. Meaured vertical displacements of the railway Amsterdam-Utrecht the Netherlands versus different model computations. In Publications Committee of the XV ICSMGE, editor, *Proceedings of the Fifteenth International Conference on Soil Mechanics and Geotechnical Engineering Istanbul*, volume 3, pages 2199–2202, The Netherlands, 2001. A. A. Balkema, a member of Swets and Zeitlinger Publishers.

[44] A. C. Eringen and E. S. Suhubi. *Elastodynamics Volume 2: Linear Theory*. Academic Press, New York, 1975.

[45] W. M. Ewing, W. S. Jardetzky, and F. Press. *Elastic Waves in Layered Media*. McGraw-Hill Book Company, Inc., New York, 1957.

[46] R. E. Fadum. Influence Values for Estimating Stressses in Elastic Foundations. In *Proceedings of the Second International Conference, Soil Mechanics and Foundation Engineering*, volume III, pages 77–84, Rotterdam, 1948.

[47] W. N. Finley, J. S. Lai, and K. Onaran. *Creep and Relaxation of Nonlinear Viscoelastic Materials*. North-Holland Publishing, Amsterdam, 1976.

[48] W. Flügge. *Viscoelasticity*. Springer-Verlag, Berlin, 2nd edition, 1975.

[49] L. Fox. Computations of traffic stresses in a simple road structure. In *Proc. 2nd Int. Conf. Soil Mechs. Fndn. Eng.*, volume 2, pages 236–246, 1948.

[50] L. J. Frýba. *Vibration of Solids and Structures under Moving Loads*. Noordhoff International Publishing, Groningen, 1972.

[51] Fugro Ingenieursbureau B.V. Monitoring No-Recess Hoeksche Waard te 's-Gravendeel. Technical Report N-0515, Fugro Ingenieursbureau B.V. (Dutch), 1999.

[52] Y. C. Fung. *Foundations of Solid Mechanics*. Prentice-Hall, Inc., Englewood Cliffs, New Jersey, 1965.

[53] D. C. Gakenheimer. Response of an Elastic Half Space to Expanding Surface Loads. *J. of Appl. Mech., ASME*, pages 99–110, March 1971.

[54] D. C. Gakenheimer and J. Miklowitz. Transient Excitation of an Elastic Half Space by a Point Load Traveling on the Surface. *J. of Appl. Mech., ASME*, pages 505–515, September 1969.

[55] H. G. Georgiadis and J. R. Barber. Steady-State Transonic Motion of a Line Load Over an Elastic Half-Space: The Corrected Cole/Huth Solution. *J. of Appl. Mech., ASME*, V. 60:pp. 772–774, 1993.

[56] H. Hao and T. C. Ang. Analytical Modeling of Traffic-Induced Ground Vibrations. *J. of Engrg. Mech., ASCE*, V. 124(No. 8):pp. 921–928, 1998.

[57] B. O. Hardin. The nature of damping in sands. *J. of the Soil Mech. and Found. Div., ASCE*, Vol. 91(No. SM1, Proc. Paper 4712):pp. 63–97, June 1965.

[58] B. O. Hardin and V. P. Drnevich. Shear Modulus and Damping in Soils: Design Equation and Curves. *J. of the Soil Mech. and Found. Div., ASCE*, V. 98(No. SM7):pp. 667–692, July 1972.

[59] B. O. Hardin and V. P. Drnevich. Shear Modulus and Damping in Soils: Measurement and Parameter Effects. *J. of the Soil Mech. and Found. Div., ASCE*, V. 98(No. SM6):pp. 603–624, June 1972.

[60] B. O. Hardin and G. D. Scott. Generalized Kelvin-Voigt Used in Soil Dynamics Study. *J. of the Engng. Mech. Div., ASCE*, V. 92(No. EM1):pp. 143–156, February 1966.

[61] B.O. Hardin and F. E. Richart Jr. Elastic Wave Velocities in Granular Soils. *J. of the Soil Mech. and Found. Div.*, V. 89(No. SM1):pp. 33–65, February 1963.

[62] M. E. Harr. *Foundations of Theoretical Soil Mechanics*. McGraw-Hill, Inc., New York, 1966.

[63] P. Hölscher and E. J. den Haan. Uitbreiding toepassingsmogelijkheden van het model voor hystereze demping. Technical Report No. 710203/11, GeoDelft (Dutch), Delft, November 2001.

[64] S. C. Hunter. *Progress in Solid Mechanics*, volume 1, chapter 1 Viscoelastic Waves, pages 1–57. North-Holland Publishing Company, Amsterdam, 1960.

[65] J. A. Inaudi and J. M. Kelly. Linear Hysteretic Damping and the Hilbert Transform. *J. of Engng. Mech., ASCE*, V. 121(No. 5):pp. 626–632, 1995.

[66] C. J. C. Jones, X. Sheng, and D. J. Thompson. Ground vibration from dynamic and quasi-static loads moving along a railway track on layered ground. In A. A. Balkema, editor, *Proceedings of the International Workshop WAVE 2000 Bochum/Germany*, pages 83–97, Rotterdam, 2000.

[67] J. R. Hall Jr. and F. E. Richart Jr. Dissipation of Elastic Wave Energy in Granular Soils. *J. of the Soil Mech. and Found. Div., ASCE*, V. 89(No. SM6):pp. 27–56, November 1963.

[68] K. Kanai. On the Group Velocity of Dispersive Surface Waves. *Bull. Earthquake Research Inst. (Tokio)*, V. 29:pp. 49–60, 1951.

[69] P. Karasudhi, L. M. Kerr, and S. L. Lee. Vibratory Motion of a Body on an Elastic Half Plane. *J. of Appl. Mech., ASME*, pages 697–705, December 1968.

[70] E. Kausel and G. Manolis. *Wave Motion in Earthquake Engineering*. WIT Press, Bath, UK, 2000.

[71] E. Kausel and J. M. Roësset. Dynamic Stiffness of Circular Foundations. *J. of Engng. Mech. Div., ASCE*, V. 101(No. EM6):pp. 771–785, December 1975.

[72] E. Kausel and J. M. Roësset. Stiffness Matrices for Layered Soils. *Bulletin of the Seismological Society of America*, V. 71(No. 6):pp. 1743–1761, December 1981.

[73] A. M. Kaynia. Measurement and prediction of ground vibration from railway traffic. In Publications Committee of the XV ICSMGE, editor, *Proceedings of the Fifteenth International Conference on Soil Mechanics and Geotechnical Engineering Istanbul*, volume 3, pages 2105–2109, The Netherlands, 2001. A. A. Balkema, a member of Swets and Zeitlinger Publishers.

[74] A. M. Kaynia, C. Madshus, and P. Zackrisson. Ground Vibration from High-Speed Trains: Prediction and Countermeasure. *J. of Geotech. and Geoenv. Engng.*, Vol. 126, No. 6:pp. 531–537, June 2000.

[75] T. C. Kennedy and G. Herrmann. Moving Load on a Fluid-Solid Interface: Supersonic Regime. *J. of Appl. Mech., ASME*, pages 137–142, March 1973.

[76] T. C. Kennedy and G. Herrmann. The Response of a Fluid-Solid Interface to a Moving Disturbance. *J. of Appl. Mech., ASME*, pages 287–288, March 1974.

[77] H. Kolsky. The Propagation of Stress Waves in Viscoelastic Solids. *Applied Mechnics Surveys*, pages 841–846, September 1958.

[78] H. Lamb. On the Propagation of Tremors Over the Surface of an Elastic Solid. *Phil. Trans. Roy. Soc. (London) A*, V. 203:pp. 1–42, 1904.

[79] H. Lamb. On Waves in an Elastic Plate. In *Proceedings of the Royal Society of London*, volume 93 of *A*, pages 114–128, England, 1917.

[80] G. Lefeuve-Mesgouez, D. Le Houédec, and A. T. Peplow. Ground vibration due to a high speed moving harmonic load. In A. A. Balkema, editor, *Proceedings of the Fourth European Conference on Structural Dynamics Eurodyn '99/Prague*, pages 963–968, Rotterdam, 1999.

[81] X. S. Li and Z. Y. Cai. Effects of Low-Number Previbration Cycles on Dynamic Properties of Dry Sand. *J. of Geotech. and Geoenv. Engng., ASCE*, V. 125(No.11):979–987, November 1999.

[82] X. S. Li, W. L. Yang, C. K. Shen, and W. C. Wang. Energy-Injecting Virtual Mass Resonant Column System. *J. of Geotech. and Geoenv. Engng., ASCE*, V. 124(No. 5):428–438, May 1998.

[83] G. Lombaert and G. Degrande. Experimental validation of a numerical prediction model for free field traffic induced vibrations by in situ experiments. *Soil Dynamics and Earthquake Engineering*, 21:pp. 485–497, 2001.

[84] A. E. H. Love. *Some Problems of Geodynamics*. Cambridge University Press, Cambridge, England, 1911.

[85] A. E. H. Love. *Some Problems of Geodynamics*. Cambridge University Press, London, 1911, 1926.

[86] A. E. H. Love. *A Treatise on the Mathematical Theory of Elasticity*. Dover, New York, 4th edition, 1944.

[87] J. E. Luco and R. J. Apsel. On the Green's Functions for a Layered Half-Space. Part I. *Bulletin of the Seismological Society of America*, V. 73(No. 4):pp. 909–929, August 1983.

[88] J. E. Luco and R. A. Westmann. Dynamic Response of Circular Footings. *J. of Engng. Mech. Div., ASCE*, Vol. 97(No. EM5):pp. 1381–1395, October 1971.

[89] J. E. Luco and H. L. Wong. Response of hemispherical foundations embedded in half-space. *J. Engng. Mech., ASCE*, V. 112(No. 12):pp. 1363–1374, 1986.

[90] J. Lysmer and F. E. Richart Jr. Dynamic Response of Footings to Vertical Loading. *J. of the Soil Mech. and Found. Div., ASCE*, Vol. 92(No. SM1, Proc. Paper 4592):pp. 65–91, January 1966.

[91] N. Makris. Time domain analysis of generalized viscoelastic models. *Soil Dynamics and Earthquake Engineering.*, V. 14:pp. 375–386, 1995.

[92] N. Makris. Causal Hysteretic Element. *J. of Engng. Mech., ASCE*, V. 123(No. 11):pp. 1209–1214, 1997.

[93] N. Makris and J. Zhang. Time-domain viscoelastic analysis of earth structures. *Earthquake Engng. Struct. Dyn.*, V. 29:pp. 745–768, 2000.

[94] K. Marguerre. Druckverteilung durch eine elastische Schicte auf starrer rauher Unterlage. *Ing. Archiv.*, V. 2, 1931.

[95] K. Marguerre. Spannungsverteilung und Wellenausbreitung in der Kontinuierlich gestützten Platte. *Ing. Archiv.*, V. 4(No. 4), 1933.

[96] A. V. Metrikine and H. A. Dieterman. Three-Dimensional Vibrations of a Beam on an Elastic Half-Space: Resonance Interaction of Vertical-Longitudinal and Lateral Beam Waves. *J. of Appl. Mech., ASME*, V. 64:pp. 951–956, 1997.

[97] A. V. Metrikine, A. V. Vostrukhov, and A. C. W. M. Vrouwenvelder. Drag experienced by a high-speed train due to excitation of ground vibrations. *Int. J. of Soils and Structures*, V. 38:pp. 8851–8868, 2001.

[98] A. V. Metrikine and A. C. W. M. Vrouwenvelder. Ground vibration induced by a high-speed train in a tunnel: Two-dimensional model. In A. A. Balkema, editor, *Proceedings of the International Workshop WAVE 2000 Bochum/Germany*, pages 111–120, Rotterdam, 2000.

[99] J. W. Miles. Response of a Layered Half-Space to a Moving Load. *J. of Appl. Mech., ASME*, pages 680–681, September 1966.

[100] G. F. Miller and H. Pursey. The Field and Radiation Impedance of Mechanical Radiators on the Free Surface of a Semi-Infinite Isotropic Solid. In *Proceedings Royal Society*, volume 223 of *A*, pages 521–541, 1954.

[101] G. F. Miller and H. Pursey. On the Partitition of Energy between Elastic Waves in a Semi-Infinite Solid. In *Proceedings Royal Society*, volume 233 of *A*, pages 55–69, 1955.

[102] R. D. Mindlin. Influence of Rotatory Inertia and Shear on Flexural Motions of Isotropic, Elastic Plates. *J. of Appl. Mech., ASME*, pages 31–38, March 1951.

[103] F. R. Norwood. Exact Transient Response of an Elastic Half Space Loaded Over a Rectangular Region of Its Surface. *J. of Appl. Mech., ASME*, pages 516–522, September 1969.

[104] R. G. Payton. Transient Motion of an Elastic Half-Space due to a Moving Surface Line Load. *Int. J. Engng. Sci.*, V. 5:pp. 49–79, 1967.

[105] C. L. Pekeris. Theory of Propagation of Explosive Sound in Shallow Water. *Geol. Soc. Amer. Mem.*, V. 27, 1948.

[106] H. G. Poulos and E. H. Davis. *Elastic Solutions for Soil and Rock Mechanics*. John Wiley & Sons, Inc., New York, 1974.

[107] J. W. S. Rayleigh. *The Theory of Sound*. reprinted by Dover Publications 1945, New York, 2nd edition, 1894.

[108] E. Reissner. Stationare, axialsymmetrische, durch, eine schüttelnde Masseerregte Schwingungen eines homogenen elastischen Halbraumes. *Ingenieur-Archiv. (German)*, V. 7 (Part 6):pp. 381–396, 1936.

[109] F. E. Richart Jr., J. R. Hall Jr., and R. D. Woods. *Vibrations of Soils and Foundations*. Prentice-Hall, Englewood Cliffs, 1970.

[110] J. L. Sackman. Uniformly Moving Load on a Layered Half Plane. *J. of Engng. Mech. Div., ASCE*, V. 87(No. EM4):pp. 75–89, August 1961.

[111] Y. Satô. Study on Surface Waves. II: Velocity of Surface Waves Propagated upon Elastic Plates. *Bull. Earthquake Research Inst. (Tokio)*, V. 29:pp. 223–262, 1951.

[112] H. B. Seed and I. M. Idriss. Soil moduli and damping factors for dynamic response analyses. Technical Report EER 70-10, Earthquake Engineering Research Center, Univ. of California, Berkeley, Calif., 1970.

[113] H. B. Seed, R. T. Wong, I. M. Idriss, and K. Tokimatsu. Moduli and Damping Factors for Dynamic Analyses of Cohesionless Soils. *J. of. Geotech. Engng.*, V. 112(No. 11):1016–1032, November 1986.

[114] K. Sezawa and K. Kanai. Discontinuity in the Dispersion Curves of Rayleigh Waves. *Bull. Earthquake Research Inst. (Tokio)*, V. 13:pp. 237–244, 1935.

[115] X. Sheng, C. J. C. Jones, and M. Petyt. Ground Vibration Generated by a Load Moving Along a Railway Track. *J. of Sound and Vibration*, V. 228(1):pp. 129–156, 1999.

[116] I. N. Sneddon. Stress Produced by a Pulse of Pressure Moving Along the Surface of a Semi-Infinite Solid. *Rendiconti Circolo Matematico di Palermo*, V. 2:pp. 57–62, January-April 1952.

[117] A. Sommerfeld. *Partial Differential Equations in Physics*. Academic Press, Inc., New York, 1949.

[118] L. Sun. Dynamic displacement response of beam-type structures to moving line loads. *Int. J. of Soils and Structures*, V. 38:pp. 8869–8878, 2001.

[119] T. Theodorsen and I. E. Garrick. Mechanism of flutter, a theoretical and experimental investigation of the flutter problem. Technical Report NACATR Rep. No. 685, Natl. Advisory Com. for Aeronautics, Washington, D.C., 1940.

[120] W. T. Thomson. Transmission of Elastic Waves through a Stratified Solid Medium. *J. of Appl. Phys.*, V. 21:pp. 89–93, February 1950.

[121] S. P. Timoshenko and J. N. Goodier. *Theory of Elasticity*. McGraw, New York, 2nd edition, 1951.

[122] TNO. Samenvatting en Analyse Metingen HSL, juni, september, oktober. Technical Report 97-CON-R1522, TNO Bouw (Dutch), 26 november 1997.

[123] I. Tolstoy and E. Usdin. Dispersive Properties of Stratified Elastic and Liquid Media: A Ray Theory. *Geophysics*, V. 18:pp. 884–870, 1953.

[124] A. Udías. *Principles of Seismology*. Cambridge University Press, Cambridge, 1999.

[125] A. Verruijt. *Soil Dynamics*. Delft University of Technology, The Netherlands, 1996.

[126] A. Verruijt. Dynamics of soils with hysteretic damping. In *Geotechnical Engineering for Transportation Infrastructure*, pages V. 1, pp. 3–14, Rotterdam, 1999. A. A. Balkema.

[127] A. Verruijt and C. Cornejo Córdova. Moving Loads on an Elastic Half-Plane With Hysteretic Damping. *J. of Appl. Mech., ASME*, V. 68:pp. 915–922, November 2001.

[128] I. A. Viktorov. *Rayleigh and Lamb Waves.* Cavitron Corporation, New York, 1967. Translated from Russian.

[129] G. N. Watson. *A Treatise on the Theory of Bessel Functions.* Cambridge University Press, London, 2nd edition, 1962.

[130] H. M. Westergaard. *A Problem of Elasticity Suggested by a Problem in Soil Mechanics: Soft Material Reinforced by Numerous Strong Horizontal Sheets.* The Macmillan Company, New York, 1938. Contributions to the Mechanics on Solids, Dedicated to S. Timoshenko by his Friends on the Occasion of his 60th Birthday Anniversary.

[131] R. F. Woldringh and B. M. New. Embankment design for high speed trains on soft soils. In *Geotechnical Engineering for Transportation Infrastructure*, volume V. 3, pages 1703–1712, Rotterdam, 1999. A. A. Balkema.

[132] J. P. Wolf. *Soil-Structure-Interaction Analysis in Time Domain.* Prentice-Hall, Inc., New Jersey, 1988.

[133] J. P. Wolf. *Foundation Vibration Analysis Using Simple Physical Models.* Prentice-Hall, Englewood Cliffs, 1994.

[134] P. C. Xu and A. K. Mal. Calculation of the Inplane Green's Functions for a Layered Viscoelastic Solid. *Bulletin of the Seismological Society of America*, V. 77(No. 5):pp. 1823–1837, October 1987.

[135] L. Zeevaert. *Foundation Engineering.* Van Nostrand Reinhold Company, New York, 1972.

Samenvatting

In onderhavig proefschrift is een studie verricht naar het gedrag van elastische golfbeweging in een dissiperend medium als gevolg van uitwendige krachten. De voornaamste eigenschap van het beschouwde medium in dit promotieonderzoek is dat de energiedissipatie als gevolg van dynamische belasting niet lineair evenredig is met de frequentie. Het doel van deze studie is het beschrijven van de dynamische analyses van de grond in relatie tot een linear elastisch medium met hystereze demping. Dit is een speciaal geval van de Kelvin-Voigt demping met frequentieafhankelijke viscositeit. Hystereze demping is beschreven door middel van de dempingsgetal ζ. Met behulp van de Fourier transformatie en de Hankel transformatie zijn de golfbewegingsvergelijkingen van het materiaal opgelost. Diverse gevallen zijn ontwikkeld om het gedrag van golven in een elastisch medium met hystereze demping te voorspellen. Deze gevallen kunnen toegepast worden ten behoeve van hoge snelheidstreinen en trillingen van funderingen.

In het algemeen zijn de oplossingen van deze problemen, beschouwd in dit onderzoek uitgedrukt in termen van het spanningsveld, de verplaatsingen en de dynamische vergrotingsfactor van de verticale verplaatsing. De invloed van de hystereze demping als functie van de dempingsfactor op de grote van de resultaten is bepaald.

Trillende belastingen op het oppervlak van een halfruimte en op het oppervlak van een halfvlak zijn eveneens onderzocht, inclusief het geval van een stijve cirkelvormige plaat op een halfruimte. De invloed van de frequentie van de trillende belasting op de respons is bepaald.

Een oplossing in gesloten vorm is gevonden voor het probleem van een halfvlak belast door een op zijn oppervlak bewegende belasting. Oplossingen van de gevallen subsonisch, transonisch en supersonisch zijn gevonden. De resultaten tonen aan dat voor kleine waarden van de demping, stel $\zeta < 0,1$, de verplaatsingen en spanningen, vergeleken met de elastostatische oplossing zeer groot zijn. Voor waarden van de snelheid van de bewegende belasting in de buurt van de Rayleigh snelheidsgolf worden de resultaten getoond. De respons van de bewegende belasting op een laag en op een gelaagde halfvlak zijn tevens gedetermineerd. Voor het geval van de dynamische interactie van een laag en een halfvlak is de invloed van de relatieve stijfheid van de laag en halfvlak gevonden. Voor zeer kleine waarden van het dempingsgetal is een eenvoudige benadering van de positie van de twee pieken veroorzaakt door een bewegende belasting bij supersonische snelheden bepaald.

Voor verticale belastingen op het oppervlak van een elastische halfruimte met hystereze demping is als oplossing ook een benaderingsmethode ontwikkeld. De methode is gebaseerd op de veronderstelling dat de horizontale verplaatsingen genegeerd zijn. Door gebruik te maken van deze methode zijn het trillende belastingsprobleem en het

bewegende belastingsprobleem tevens opgelost. De oplossingen van deze problemen zijn vergeleken met de elastische oplossingen. Voor de waarden van Poisson tussen 0 en $0,4$ geven de respons functies van de verplaatsingen, onder een uniforme trillende belasting op cirkelvormige oppervlak, een acceptabele benadering van de elastische oplossing.

Een bewegende transiente lijnbelasting op een halfruimte is onderzocht door gebruik te maken van een benaderingsmethode. In dit geval is de hystereze demping van het medium niet beschouwd. Met de bedoeling om analytische uitdrukkingen in gesloten vorm voor de verticale verplaatsingen en verticale spanningen te bepalen, is het probleem opgelost met behulp van de Cagniard-de Hoop methode. Zowel de subsonische als de supersonische gevallen zijn bestudeerd.

Voor kleine vervormingen zijn zandmonsters getest in vrij trillende torsie in het laboratorium van GeoDelft in Nederland. De testen zijn uitgevoerd om de grote van het dempingsgetal vast te stellen. Voor verschillende polar traagheidsmoment van de massa verbonden bovenaan het monster zijn verhoudingen tussen de schuifspanning en de schuifrek bepaald. Uit proefresultaten valt op te maken dat het dempingsgetal van de monsters matig varieerde met de grootte van de vervormingen.

C. J. Cornejo Córdova, Elastodynamics with Hysteretic Damping, Proefschrift, Technische Universiteit Delft, 2002.

Resumen

En la presente tesis se realiza un estudio del movimiento de ondas elásticas en un medio disipativo generado por fuerzas superficiales. La principal característica del medio considerado en esta tesis es que la disipación de energía causada por cargas dinámicas no es proporcional a la frecuencia. El propósito de este estudio es describir el análisis dinámico de suelos en un medio linear elástico con amortiguamiento histerético, el cual es un caso particular del amortiguamiento Kelvin-Voigt donde la viscosidad depende de la frecuencia. El amortiguamiento histerético se denota mediante la razón de amortiguamiento ζ. Por medio de la transformación de Fourier y de la transformación de Hankel, las ecuaciones gobernantes de movimiento de onda del material son resueltas. Varios casos son desarrollados para la predicción del comportamiento de ondas en un medio elástico con amortiguamiento histerético. Estos casos se pueden aplicar a líneas ferroviarias de trenes de alta velocidad y a la vibración de cimentaciones.

En general, la solución a los problemas considerados en esta tesis se plantean en términos de campos de esfuerzos, desplazamientos y del factor de amplificación dinámica del desplazamiento vertical. Además, se presenta la influencia en la magnitud de los resultados del amortiguamiento histerético como una función del factor de amortiguamiento.

Cargas de vibración sobre la superficie de un semiespacio y sobre la superficie de un semiplano son examinadas, incluyendo el caso de un disco circular rígido sobre el semiespacio. La influencia de la frecuencia de vibración de la carga sobre el resultado queda determinada.

Para el problema del semiplano cargado mediante una carga móvil sobre su superficie se ofrece una solución de tipo *close-form*. También se encuentran soluciones para los casos subsónico, transónico y supersónico. Los resultados indican que para valores pequeños de amortiguamiento, por ejemplo $\zeta < 0.1$, los desplazamientos y esfuerzos son muy grandes, comparados con la solución elastoestática. Para valores de la velocidad de la carga móvil cercanas a la velocidad de la onda Rayleigh, se muestran igualmente resultados. La respuesta de la carga móvil sobre una capa y un semiplano estratificado también es determinada. Para el caso de interacción dinámica de una capa y un semiplano, se obtiene la influencia de la rigidez relativa de la capa y del semiplano. Se ofrece también una aproximación simple de la posición de dos picos generados por una carga móvil a velocidades supersónicas.

Para cargas verticales en la superficie del semiespacio elástico con amortiguamiento histerético, se desarrolla un método de solución aproximado. Éste método se basa en la suposición de que los desplazamientos horizontales se pueden ignorar. Con la ayuda de éste método, se resuelven también los problemas de la carga de vibración y de la carga

móvil. Las soluciones a estos problemas se comparan con las soluciones elásticas. Para valores de Poisson entre 0 y 0.4 las funciones de respuesta de los desplazamientos por debajo de una carga uniforme de vibración sobre un area circular, dan una aproximación aceptable de la solución elástica.

Una carga lineal móvil transiente sobre un semiespacio es examinada usando el método aproximado. En este caso no se considera el amortiguamiento histerético del medio. Con el fín de obtener expresiones analíticas y de tipo *close-form* para los desplazamientos y esfuerzos verticales, el problema es resuelto con la ayuda del método Cagniard-de Hoop. Se estudian también los casos subsónico y supersónico.

Para pequeñas deformaciones muestras de arena han sido sometidas a torsión libre de vibración en el laboratorio de GeoDelft en Holanda con la finalidad de determinar la magnitud de la razón de amortiguamiento. Para diferentes momentos polares de inercia de la masa sujeta en la parte superior de la muestras, se presentan relaciones entre los esfuerzos y deformaciones unitarias de corte. En los resultados de las pruebas se observó que la razón de amortiguamiento de las muestras varió moderadamente junto con la magnitud de las deformaciones.

C. J. Cornejo Córdova, Elastodynamics with Hysteretic Damping, PhD Tesis, Universidad Tecnológica de Delft, 2002.

About the author

The author Carlos Cornejo was born in Lima, Perú, on Augustus 19, 1966. After his study at the *Pontificia Universidad Católica del Perú* in Lima the author began the study of Civil Engineering at the Technical College *HTS* in 's-Hertogenbosch in October 1992. From September 1993 to October 1997 the author continued his study of Civil Engineering at Delft University of Technology. His graduation project was on the subject of "Dynamic behaviour of soft soil for high-speed trains" at the Geotechnical Laboratory under supervision of Prof.Dr. A. Verruijt. In October 1997 the author started his doctoral research under supervision of Prof.Dr. A. Verruijt. The results of this research have been presented in this thesis.

During the period at the Geotechnical Laboratory the author gave lectures on Soil Dynamics to students of the Faculty of Civil Engineering. Furthermore, the author published papers and participated in several international conferences.